



ICOR 2023

Proceedings of
**3rd International
Conference on Rheology**

12-13 December, 2023

Iran Polymer and Petrochemical Institute (IPPI), Tehran, Iran



Contents

Scientific Committee	1
Organizing Committee	2
Executive Committee	2
Plenary Lectures	3
Keynote Lecturers	3
Organizers	4
Sponsors	4
Workshops	5
Plenary and Keynote Abstracts	6
Conference Articles	43

Scientific Committee

Name	Organization
Nazockdast H. (Chair)	Amirkabir University of Technology, nazdast@aut.ac.ir
Goharpey F. (Conf. President)	Amirkabir University of Technology, goharpey@aut.ac.ir
Abbassi F.	Sahand University of Technology, f.abbasi@sut.ac.ir
Abbassi Sourki F.	Iran Polymer and Petrochemical Institute, f.abbasi@ippi.ac.ir
Ahmadi S.	Iran Polymer and Petrochemical Institute, sh.ahmadi@ippi.ac.ir
Alavi S.M.Z.	University of Tehran, zia.alavi@ut.ac.ir
Babaei A.	Golestan University, a.babaei@gu.ac.ir
Dabir B.	Amirkabir University of Technology, drbdabir@aut.ac.ir
Foudazi R.	University of Oklahoma, rfoudazi@ou.edu
Ghafelebashi S.M.	Petrochemical Research and Technology Co.
Ghasemi I.	Iran Polymer and Petrochemical Institute, i.ghasemi@ippi.ac.ir
Golshan Ebrahimi N.	Tarbiat Modares University, ebrahmn@modares.ac.ir
Ghoreishy M.H.R.	Iran Polymer and Petrochemical Institute, m.h.r.Ghoreishy@ippi.ac.ir
Haghtalab A.	Tarbiat Modares University, haghtala@modares.ac.ir
Haririan I.	University of Tehran, haririan@tums.ac.ir
Hashemabadi S.H.	Iran University of Science and Technology, hashemabadi@iust.ac.ir
Kaffashi B.	University of Tehran, kaffashi@ut.ac.ir
Katbab A.A.	Amirkabir University of Technology, katbab@aut.ac.ir
Khademzadeh Yeganeh J.	Qom University of Technology, jkh.yeganeh@gmail.com
Khosrokhavar R.	Iranian Association of Polymer and Chemical Engineers, Ramin@khosrokhavar.com
Mehranpour M.	Islamic Azad University, m.mehranpour@srbiau.ac.ir
Mirzadeh H.	Amirkabir University of Technology, mirzadeh@aut.ac.ir
Moghimi E.	University of Crete, Greece, esmaeel@iesl.forth.gr
Moini Jazani O.	Isfahan University of Technology, o.moini@eng.ui.ac.ir
Mohammadi H.	Florida State University, hadi.moham@eng.famu.fsu.edu
Mohammadi N.	Amirkabir University of Technology, mohamadi@aut.ac.ir
Nazockdast E.	University of North Carolina, ehssan@email.unc.edu
Nekoomanesh Haghghi M.	Iran Polymer and Petrochemical Institute, m.nekoomanesh@ippi.ac.ir
Norouzi M.	Polymer Shahrood University of Technology, mnorouzi@shahroodut.ac.ir
Pircheraghi G.	Sharif University of Technology, pircheraghi@sharif.ir
Pishvaei M.	Institute of Color Science and Technology, pishvaei@icrc.ac.ir
Rafizadeh M.	Amirkabir University of Technology, mehdi@aut.ac.ir
Ramezani Saadat Abadi A.	Sharif University of Technology, ramazani@sharif.edu
Razavi M.A.	Ferdowsi University of Mashhad, s.razavi@um.ac.ir
Razavi Aghjeh M.K.	Amirkabir University of Technology, karimrazavi@sut.ac.ir
Razzaghi Kashani M.	Tarbiat Modares University, mehdi.razzaghi@modares.ac.ir
Sadeghi K.	University of Tehran, sadeghy@ut.ac.ir
Salami-Hosseini M.	Sahand University of Technology, salami@sut.ac.ir
Salehi Barmi M.	Research of Institute of Petroleum Industry, msalehibarmi@gmail.com
Shams Eshaghi K.	Isfahan University of Technology, k_shams@cc.iut.ac.ir
Sharif F.	Amirkabir University of Technology, sharif@aut.ac.ir

Organizing Committee

Name	Organization
Sodeifian G.H.	University of Kashan, sodeifian@kashanu.ac.ir
Goharpey F.	Amirkabir University of Technology, goharpey@aut.ac.ir
Ebrahimi M.	Amirkabir University of Technology, ebrahimi@aut.ac.ir
Ghasemi I.	Iran Polymer and Petrochemical Institute, i.ghasemi@ippi.ac.ir
Khosrokhavar R.	Iranian Association of Polymer and Chemical Engineers, Ramin@khosrokhavar.com
Mehranpour M.	Islamic Azad University, m.mehranpour@srbiau.ac.ir
Esfandeh M.	Iran Polymer and Petrochemical Institute, m.esfandeh@ippi.ac.ir
Nazockdast H.	Amirkabir University of Technology, nazdast@aut.ac.ir
Parian S.	Varesh Shimi Co., parian@vareshchimie.ir

Executive Committee

Name	Organization
Nazockdast H. (Scientific Chair)	Amirkabir University of Technology, nazdast@aut.ac.ir
Goharpey F. (Conf. President)	Amirkabir University of Technology, goharpey@aut.ac.ir
Ghasemi I. (Chair)	Iran Polymer and Petrochemical Institute, i.ghasemi@ippi.ac.ir
Salami M. (Chair)	Sahand University of Technology, salami@sut.ac.ir
Farhangzadeh S. (Conf. Office Manager)	Iran Polymer and Petrochemical Institute, s.farhangzadeh@ippi.ac.ir
Mehranpour M.	Islamic Azad University, m.mehranpour@srbiau.ac.ir
Khosrokhavar R.	Iranian Association of Polymer and Chemical Engineers, Ramin@khosrokhavar.com
Mirghasemi A.	Iranian Society of Rheology, mirghasemi.a@gmail.com
Alikhani S. (Site Administrator)	Islamic Azad University, sarveenaz.ali@gmail.com
Zabeti V.	Amirkabir University of Technology, vista_zabeti@aut.ac.ir

Plenary Lecturers

- ✿ Ronald G. Larson, University of Michigan
- ✿ Jan Vermant, ETH Zurich

Keynote Lecturers

Name	Organization
Foroud Abbasi	Iran Polymer and Petrochemical Institute, Iran
Shervin Ahmadi	Iran Polymer and Petrochemical Institute, Iran
Mohammad Zia Alavi	University of Tehran, Iran
Amir Babaei	Golestan University, Iran
Peter Fischer	ETH Zurich, Switzerland
Gerald Fuller	Stanford University, USA
Reza Foudazi	University of Oklahoma, USA
Hamid Garmabi	Amirkabir University of Technology, Iran
Alan J. Giacomin	Queen's University, Canada
Savvas G. Hatzikiriakos	University of British Columbia, Canada
Sarah Hormozi	Cornell University, USA
Safa Jamali	Northeastern University, USA
Sadhan C. Jana	University of Akron, USA
Fardin Khabaz	University of Akron, USA
Alex G. Kuchumov	Polytechnic University, Russia
Joao Maia	Case Western University, USA
Parisa Mirbod	University of Illinois, USA
Esmael Moghimi	Georgetown University, USA
Jeff Morris	City College of New York, USA
Mehdi Mostafaiyan	Leibniz Institute of Polymer Research, Germany
Ehssan Nazockdast	University of North Carolina, USA
M. Reza Nofar	Istanbul Technical University, Turkey
Mahmood Norouzi	Shahrood University of Technology, Iran
Rob Poole	University of Liverpool, UK
Ahmad Ramezani	Sharif University of Technology, Iran
Mehdi Razzaghi-Kashani	Tarbiat Modares University, Iran
Amir Rezvani-Moghaddam	Sahand University of Technology, Iran
Kayvan Sadeghy	University of Tehran, Iran
Mehdi Salami	Sahand University of Technology, Iran
Patrick Spicer	UNSW Sydney, Australia
S. Mohammad Taghavi	Laval University, Canada
Sachin Velankar	University of Pittsburg, USA
Dimitris Vlassopoulos	FORTH, University of Crete, Greece



Organizer

- ✿ Iranian Society of Rheology (ISR Co-organizers)
- ✿ Polymer Engineering and Color Technology, Amirkabir University of Technology (AUT)
- ✿ Iran Polymer Science and Technology Society (IPSTS)
- ✿ Iran Polymer and Petrochemical Institute (IPPI)

Sponsors

- ✿ The International Committee on Rheology
- ✿ Anton Paar Company
- ✿ Varesh Chimie Bahar Company
- ✿ Iranian Association of Polymer and Chemical Engineers
- ✿ Dana Polymer Holding
- ✿ Polymer Pishrafteh Dana Company
- ✿ University of Tehran
- ✿ Tarbiat Modares University
- ✿ Sharif University of Technology
- ✿ Sahand University of Technology
- ✿ Science and Research Branch of Islamic Azad University
- ✿ Qom University of Technology
- ✿ Pooya Polymer Tehran Company
- ✿ Petro Services Company
- ✿ Andisheh Bartar Miran Company
- ✿ DIDI Water Company
- ✿ Rangdaneh Sirjan Company
- ✿ Nazh Laboratory Equipment Supplier
- ✿ Parsa Polymer Sharif Company
- ✿ Iran National Industries Association



- ✿ Association of Polymer Machinery and Equipment Suppliers
- ✿ Baspar Chemi Sepidan Company
- ✿ Masterbatch and Compound Producers Association of Iran
- ✿ AVA Polymer Company
- ✿ Farnam Baspar
- ✿ Nekousaz Polymer Sanat Aria Company
- ✿ Baspar Magazine

Workshops

Title	Lecturer	Date
Course I: Rheology of Vitrimers	Fardin Khabaz	December 10
Course II: Rheology of Jammed Suspensions		
Dynamics of Particles in Viscous Films and Membranes	Ehssan Nazockdast	December 11



Plenary and Keynote Abstracts

Plenary Lecture

Multi-Scale Rheological Modeling of Polyethylene for Processing Flows

Ronald Larson^{1,2}

1. Department of Macromolecular Science and Engineering, University of Michigan, Ann Arbor, Michigan, 48109, USA
2. Department of Chemical Engineering, University of Michigan, Ann Arbor, Michigan, 48109, USA
rlarson@umich.edu

Abstract

Multi-scale simulation methods are described that can contribute to an old question: how molecular weight and short- and long-chain branching distributions affect rheology, processing, and crystallization, which, in turn, control the modulus and toughness of polyethylene film. In this talk, a practical method is presented to account for the effects of short- and long-chain branching on rheological properties of commercial polyethylene through use of an “optimal ensemble” of chains that can be used to predict chain orientation in a processing flow such as film blowing. Molecular dynamics simulations are used to determine rates of primary and secondary nucleation of polyethylene crystals including the influence of branching, which we find proceed through a nematic-like intermediate. These insights are aimed at the development of a film blowing model that includes new insights into both rheology and crystallization.

Plenary Lecture**Engineering Sustainable Multiphase Systems****Jan Vermant**Jan Vermant
Department of Materials, ETH Zürich, Switzerland
jan.vermant@mat.ethz.ch**Abstract**

Stable foams or emulsions that can resist disproportionation for extended periods of time have important applications in a wide range of technological and consumer materials. Yet, legislative initiatives limit the range of surface active materials that can be used, for environmental impact reasons. There is a need for technologies to efficiently produce multiphase materials using more eco-friendly components, such as particles, and for which traditional thermodynamics-based processing routes are not necessarily efficient enough. In this talk I will first discuss how the relationship between the structure and properties of these interfaces warrants a deeper look and forces us to think about the rheological modelling of these interfaces, with properties ranging from 2D fluids to (surprisingly) auxetic solids. The second aspect relates to novel strategies to produce ultrastable Pickering-Ramsden foams, with bubbles of micrometer-sized dimensions, through pressure-induced particle densification. Specifically, aqueous nanosilica-stabilized foams are produced by foaming a suspension at sub-atmospheric pressures, allowing for adsorption of the particles onto large bubbles. This is followed by an increase back to atmospheric pressure, which induces bubble shrinkage and compresses the adsorbed particle interface, forming a strong elasto-plastic network that provides mechanical resistance against disproportionation. The foam's interfacial mechanical properties are quantified to predict the range of processing conditions needed to produce permanently stable foams, and a general stability criterion is derived by considering the interfacial rheological properties under slow, unidirectional compression. Foams that are stable against disproportionation are characterized by interfaces whose mechanical resistance to compressive deformations can withstand their tendency to minimize the interfacial stress by reducing their surface area. Our ultrastable nanosilica foams are tested in real-life applications by introducing them into concrete, as an environmentally friendly air entrainer. The applicability of our stability criterion to other rheologically complex interfaces and the versatile nature of our foaming technology enables usage for a broad class of materials, beyond the construction industry.

Dynamics and Self-healing of Aminated Polyolefins

**B.M. Yavitt^{1,2}, Z. Zhang¹, N. Moradinik¹, N. Kuanr², D.J. Gilmour²,
E. van Ruymbeke³, L.L. Schafer², and S.G. Hatzikiriakos^{1*}**

1. Department of Chemical and Biological Engineering, University of British Columbia, Vancouver, B.C, Canada, V6T 1Z3
2. Department of Chemistry, University of British Columbia, Vancouver, B.C, Canada, V6T 1Z4
3. Bio-and Soft Matter, Institute of Condensed Matter and Nanosciences, Universite Catholique de Louvain, Croix du Sud 1, B-1348 Louvain-la-Neuve, Belgium
*savvas.hatzi@ubc.ca

Abstract

The rheological and self-healing behavior of a class of catalytically synthesized amine functionalized polyolefins is investigated. These materials possess tunable rheological properties depending on their molecular weight and display autonomous, fast self-healing. The linear viscoelastic properties are modelled using a tube-based model developed by Hawke *et al.*, (Journal of Rheology, 2016) to calculate several parameters that describe the individual chain dynamics. Their self-healing response is depicted reasonably well using theory developed by Stukalin *et al.*, (Macromolecules, 2013). These materials also exhibit excellent adhesive properties with low surface substrates such as polytetrafluoroethylene (PTFE) well known for its anti-stick properties.

Approaches to Re-evaluate Recycled Thermoplastics

M. Reza Nofar

Sustainable & Green Plastics Laboratory, Metallurgical & Materials Engineering Department, Faculty of
Chemical and Metallurgical Engineering, Istanbul Technical University,
Istanbul, 34469, Turkey
nofar@itu.edu.tr

Abstract

Two various approaches to re-evaluate recycled thermoplastics are discussed in this study. In the first part, recycled polyethylene terephthalate (rPET) and polybutylene terephthalate (PBT) were melt compounded using a twin-screw extruder with two different chain modifiers (i.e., epoxy-based chain extender Joncryl ADR 4468 and pyromellitic dianhydride PMDA). rPET, PBT and rPET/PBT with blend ratios of 75/25, 50/50 and 25/75 were reactively extruded with the addition of 0.5 and 1.0 wt% of each chain modifier. Melt properties were examined using small amplitude oscillatory shear (SAOS) rheological analysis to reveal the effect of mixed chain extender addition in all samples. Two chain extenders showed different reaction kinetics on enhancing the melt properties which was more time dependent. While Joncryl showed more serious improvements on melt properties of all systems during longer process times, PMDA showed significant enhancements during shorter times and the increase in processing time expedited the thermal degradation and dampened the overall effect of chain extension. The foaming behavior of the modified samples was consequently examined and the impact of melt properties improvements on the cell stability and foam expansion ratio was clearly observed. In the second approach, recycled polyethylene (rPE) based microfibrillar composites (MFCs) were developed while incorporating rPET and recycled polyamide6 (rPA) as the reinforcing fibrillar phases at a given weight ratio of 80 wt% (rPE)/20 wt% (rPET or rPA). The blends were first melt processed using a twin-screw extruder. The extrudates were then cold stretched at a drawing ratio of 2.5 to form rPET and rPA fibrillar structures. Next, the pelletized drawn samples were injection molded at the barrel temperatures below the melting temperatures of rPET and rPA. The tensile, three-point bending, impact strength, dynamic thermomechanical, and rheological properties of the fabricated MFCs were analyzed. The effects of injection molding barrel temperature (i.e., 150 °C and 190 °C) and extrusion melt processing temperature (i.e., 250 °C and 275 °C) on the generated fibrillar structure and the resultant properties were explored. A strong correlation between the fibrillar morphology and the mechanical properties with the extrusion and injection molding temperatures was observed. Moreover, the ethylene/n-butyl acrylate/glycidyl methacrylate (EnBAGMA) terpolymer and maleic anhydride grafted PE (MAH-g-PE) were, respectively, melt processed with rPE/rPET and rPE/rPA6 blends as compatibilizers. The compatibilizers refined the fibrillar structure and remarkably influenced mechanical properties, specifically the impact strength.

Rheology of Hybrid-Filler Rubber Compounds

Mehdi Razzaghi-Kashani

Polymer Engineering Department, Faculty of Chemical Engineering,
Tarbiat Modaress University, P.O.Box 14115-114, Tehran, Iran
mehdi.razzaghi@modares.ac.ir

Abstract

Energy dissipation in large-strain dynamic loadings is a concern in many rubber products, especially tires. This loss of energy is mainly due to breakage and reformation of filler secondary network in highly-filled rubber compounds, known as the Payne effect. Dispersion of reinforcing fillers in rubber compounds is an important factor determining this nonlinear viscoelastic property in rubber compounds. Nonlinear rheology can be used as a tool to assess the quality of filler dispersion and related characteristics of highly-filled rubber compounds. Other than common methods of improving filler dispersion, i.e. modification of filler surface or elastomer microstructure, application of hybrid fillers has been under attention by researchers. Using small concentrations of a secondary filler, with different chemistry, size, or shape than the primary filler, has been promising as an inexpensive method of obtaining morphological synergy and controlled nonlinear behavior in rubber compounds. In this talk, few hybrid-filler systems will be reviewed, and application of rheology in prediction of nonlinear viscoelasticity of rubber compounds will be discussed.

Evaluating the Processability and Rheological Behavior of Polypropylene Vitrimers

Hamid Garmabi* and Saba Taheri

Department of Polymer and Color Engineering, Amirkabir University of Technology, Tehran, Iran

*garmabi@aut.ac.ir

Abstract

Polypropylene (PP) vitrimers were prepared in two steps: First, glycidyl methacrylate (GMA) was melt grafted onto PP chains, and second, the crosslinked network was formed by reacting these active sites with dodecanedioic acid (DDDA) in the presence of zinc acetate as a catalyst. These chemically crosslinked networks are capable of undergoing transesterification exchange reactions with temperature, enabling rearrangement of network topology while maintaining a constant crosslink density. Rheological studies were conducted on samples containing various concentrations of grafting agents, and therefore, different crosslink densities, to evaluate their processability and flow behaviors. Rheological tests, including strain, time, and frequency sweeps, along with stress relaxation, show that increasing the functional groups on the polymer chains improves the melt strength and increase relaxation times in samples. Therefore, the flow and viscoelastic properties of vitrimer samples can be adjusted by the grafting agent concentration and temperature having a constant amount of catalyst.

Evaluating Effects of Storage Temperature and Duration on the Blending between Aged and Virgin Bitumen Binders through Rheological Measurements

Mohammad Zia Alavi

School of Civil Engineering, College of Engineering, University of Tehran, Tehran, Iran
zia.alavi@ut.ac.ir

Abstract

The use of Recycled Asphalt Pavement (RAP) for producing new asphalt mixtures has been widely acknowledged because of its environmental and engineering benefits. The main concern in producing asphalt mixtures containing a high amount of RAP is the interaction between the aged bitumen in RAP and the virgin bitumen. Blended aged and virgin binders affect the performance-related properties of asphalt mixtures, mainly the stiffness and the tensile strength. This study evaluated the effect of storage temperature and duration on the interaction and blending between aged and virgin bitumen binders using rheological parameters obtained by Dynamic Shear Rheometer (DSR) tests performed on the specially prepared test samples. The preliminary results showed that the mobilization of aged bitumen in RAP and the interaction between aged and virgin binders were highly influenced by temperature. At a specific effective temperature, the blending level between the two binders increased with time at a decaying rate. Complete blending between the aged and virgin binders was achieved after 60 min at 163 °C. The blended binder has higher stiffness and lower phase angle than the virgin binder. With increasing the portion of aged binder in the blended binder, the increase in stiffness and reduction in phase angle were observed, as expected. The proposed sample preparation and testing procedure could be effectively applied to understand the interaction between different binders and other additives, such as softeners and rejuvenating agents.

Keywords: Recycled Asphalt Pavement (RAP), Aging, Blending, Rheology, Storage

Investigation of the Effect of the Presence of MWCNT on Rheological Properties of In-situ Polymerized Nylon 12 During Reactive Extrusion

Shervin Ahmadi* and Mohammad Barmar

Department of Polymer Processing, Iran Polymer and Petrochemical Institute, Tehran, Iran

*sh.ahmadi@ippi.ac.ir

Abstract

In-situ ring opening anionic polymerization of Laurolactam towards polyamide 12 (PA12) was successfully performed via the melt polymerization of Laurolactam in the presence of MWCNT during reactive extrusion. This reaction takes place significantly faster and gives a narrower molecular weight distribution than those obtained with other techniques. The effects of various concentrations of nanoparticles on the rheological properties were determined. In order to characterize the synthesized samples, electrical properties analyses have been done. Also, the existence of amide groups was proved by ATR and XRD spectrums accordingly.

Keywords: ring opening anionic polymerization, polyamide12, MWCNT, reactive extrusion

Rheological Properties of Virgin Rubber/Modified Rubber Powder Blends

M. Jamilipoor, M.H.R. Ghoreishy, F. Abbasi-Sourki*, and M. Karrabi

Department of Rubber Processing, Faculty of Processing, Iran Polymer and Petrochemical Institute, P.O. Box
14975-112, Tehran, Iran
*f.abbasi@ippi.ac.ir

Abstract

Rubbers are a category of polymers which offer wide range of applications. Tires, as high technology rubbery materials, are produced in a large volume to address the today's society needs. Approximately, the same volume of waste tires is produced at the end of the product life. Therefore, the world is tolerating an undegradable waste crosslinked material with a life span more than several decades resulting in a continuous pollution of the environment. Various applications of waste tires may include; burning to benefit of its combustion energy, using in civil industry to replace a part of the cement, adding to bitumen to increase the bituminous products' life and blending with polymers as a powder or reclaimed rubber to decrease the product cost. In 2019, the major part of the waste tires produced in China was landfilled or stockpiled, while in Europe, US and particularly in India and Japan, the main part of the waste tires was recovered as reusable materials and energy recovery etc. The present work aims at the surface modification of the waste tire powder using various chemicals. The modified powder was then characterized to measure the extent and quality of surface modification. The modified powder, later used as a filler or a blend component in a virgin polar rubber. The mechanical, viscoelastic, and rheological properties of the blends were investigated in both cured and non-cured states. The results indicated no significant loss in properties for the blends of virgin rubber/modified rubber powder.

Rheology as a Powerful Tool to Discriminate the Contradictory Effects!

Amir Babaei

Polymer Engineering Department, Golestan University, Gorgan, Iran
a.babaei@gu.ac.ir

Abstract

In this talk, we describe the capability of rheology, and specifically, small amplitude oscillatory shear (SAOS) measurements to investigate the relationship between the microstructure and performance of polymeric blend including nanoparticles when some parameters are acting against each other. As a matter of fact, when all affecting parameters of a polymer mixture are acting in a same direction (for instance, decreasing or increasing the mechanical properties or elasticity or etc.) all of characterizations support and validate each other. What would happen if they acted against each other!? How we can differentiate which parameter is enhancing and which one is decreasing the determined properties or performance? We aim to have a talk about the potential of rheology for such sophisticated situations. For the case study some nanocomposites and polymer blends including nano-hybrids have been selected and would be discussed.

Keywords: SAOS, Rheology, Nano-hybrids, polymer blends

On the Use of Vibration for Controlling the Settling Dynamics of Heavy Particles in Viscoplastic Liquids

Keyvan Sadeghy

School of Mechanical Engineering, College of Engineering, University of Tehran, Tehran, Iran
sadeghy@ut.ac.ir

Abstract

Many industrial products exist in particulate form with the continuous phase being a viscoplastic liquid. These complex systems are usually designed in such a way that the particles are either stuck or settling with an exceedingly small velocity. During their transportation, however, it is often observed that the particles prematurely start settling in the liquid in an expedited fashion. This is an undesirable effect because any particle(s) settled in transit must be remixed before the product can be delivered to the customer. The main cause of early sedimentation is the vessel's vibration which induces an extra stress in the liquid surrounding the particles thereby reducing the liquid's apparent viscosity. In the present work, it is shown that vibration can be used as an effective means for controlling the dynamical behavior of particles immersed in viscoplastic fluids. Using a very small threshold velocity to decide whether a particle is stuck or unstuck, it is shown that stuck particles can be excited to fall in the BP liquid provided that, for any given frequency, the amplitude is larger than a minimum threshold. An increase in the size of the particle or its density is shown to reduce the threshold amplitude. In general, vibration is found to have an accelerating effect on particle settling in the BP liquid although the effect is non-monotonic. The accelerative effect of vibration is interpreted in terms of the yielded zone formed around the particle, which is enlarged when the vessel is vibrated. The general conclusion is that vibration is indeed a viable option for controlling the settling characteristics of heavy particles immersed in yield-stress fluids.

The Fluctuation Dynamics of a Filament in a Spherical Membrane

Ehssan Nazockdast

Department of Applied Physical Sciences, University of North Carolina, USA
ehssan@email.unc.edu

Abstract

Many of the biological cell membrane's vital functions, including molecular transport and signal transduction, are achieved by self-organization of its lipids and proteins. These structural variations coincide with changes in membrane mechanics. Microrheology has been extensively used for studying the mechanics of biological materials. Yet, the theoretical frameworks of microrheology need to be modified for applications to 2D membranes. Here, we outline the theoretical framework that relates the linear viscoelastic properties of a freely suspended and supported spherical membrane to the fluctuating dynamics of a semiflexible filament embedded in that membrane. By using filaments as probes one can simultaneously measure the membrane mechanics over multiple length scales. We begin by deriving the response function that computes the time-dependent filament shape, specifically the time-dependent amplitudes of different filament wavelengths, as a function of the external forces on the filament as well as membrane viscoelasticity, and the mechanics of 3D domains that surround the membrane. We, then, use Fluctuation-Dissipation theorem to express these shape amplitudes in terms of thermal forces and the response function. We show that the confined spherical geometry and the presence of rigid boundaries in supported membranes give rise to unique dynamical features in the relaxation behavior of the fluctuating filament that can be used to characterize the membrane rheology.

Impact of Rheology on Fabrication of Mesoporous Polymer Sheets and Films

Erin Farrell and Sadhan C. Jana*

School of Polymer Science and Polymer Engineering
University of Akron, Akron, OH 44325, USA

*janas@uakron.edu

Abstract

This talk discusses fabrication of polyimide aerogel foam sheets with embedded micrometer size voids (macrovoids) introduced via oil-in-oil (O/O) emulsion-templating of polyimide sol with silicone oil, followed by casting, gelation, and supercritical drying. The aerogel foam sheets contain significant fractions of mesopores (2-50 nm) inherent to polyimide aerogel and macrovoids introduced in the form of silicone oil droplets. An understanding is developed in this work to correlate sol casting conditions, sol composition, and transient viscosity growth with macrovoid size distribution, mesopore content, and the morphology of aerogel foam sheets. The study finds that the flow of sol in doctor's blade casting system induces coalescence of silicone oil droplets. The study also determines that the properties of the cast gel and aerogel sheet materials strongly depend on the time of sol casting, measured in terms of lead time (tlead) away from the gel point.

Keywords: Aerogel foam; gel casting; porous polymers; emulsion-templating; polyimide

Numerical Study on the Effect of Agglomerate Configuration on the Rheological Properties of Particulate Suspension Using Stokesian Dynamics

Mehdi Salami

Sahand University of Technology, Tabriz, Iran
salami@sut.ac.ir

Abstract

This research utilizes Stokesian Dynamics to investigate the influence of agglomerate arrangements on the rheological characteristics of particulate suspensions. Employing numerical simulations accounting for particle interactions, diverse agglomerate configurations are studied to discern their impact on suspension behavior. Our findings demonstrate a substantial correlation between agglomerate configurations, specifically in terms of fractal dimension, and the resultant viscosity of the system. Notably, agglomerates with higher fractal dimensions exhibited rheopectic behavior, while those with lower dimensions displayed thixotropic behavior. Moreover, systems composed of lower fractal dimension agglomerates exhibited higher viscosity compared to those with higher fractal dimensions, despite an identical particle count. Similarly, particles with greater fractal dimensions displayed elevated viscosity at equivalent gyration radii. Furthermore, this study observed that higher activity levels among particles corresponded to increased system viscosity compared to less active particles. These insights offer a nuanced understanding of how agglomerate configurations, characterized by fractal dimensions and particle activity, intricately influence suspension rheology, providing valuable implications for various industrial and natural systems.

Thermodynamic Description of the Stress Overshoot in Sheared Soft Particle Glasses

Nazanin Sadeghi¹, Hrishikesh Pable¹, and Fardin Khabaz^{1,2*}

1. School of Polymer Science and Polymer Engineering, The University of Akron,
Akron, OH, 78712, USA

2. Department of Chemical, Biomolecular, and Corrosion Engineering, The University of Akron, Akron, OH,
78712, USA

*fkhbaz@uakron.edu

Abstract

Particle dynamics simulations are used to study the start-up flow of jammed soft particle suspensions in shear flow from a thermodynamic perspective. This thermodynamic framework is established using the concept of the two-body excess entropy extracted from the pair distribution function and elastic energy of the particles. Results show that the evolution of the elastic energy in the system closely mimics the stress-strain behavior at different shear rates. Furthermore, the transient excess entropy of the suspensions at all volume fractions shows general behavior: the excess entropy at high shear rates increases as a function of the strain, shows a mild overshoot, and attains a steady state. On the other hand, it is nearly constant at shear rates close to the dynamic yield stress. Using the transient elastic energy and excess entropy, an effective temperature is defined to establish a relationship between thermodynamics and the static yield stress data. The magnitude of this effective temperature follows a direct relationship with the peak stress and shows universal behavior for suspensions with different volume fractions.

Nonlinear Rheology of Dense Non-Brownian Suspensions: What is the Role of Particle Shape?

Sarah Hormozi*, Enzo d'Ambrosio and Donald L. Koch

Robert Frederick Smith School of Chemical and Biomolecular Engineering, Cornell University,
Ithaca, NY 14853, USA
*hormozi@cornell.edu

Abstract

Suspensions of non-Brownian particles in viscous fluids are relevant in engineered processes and in natural phenomena. These suspensions typically consist of solid particles of nonspherical shape and often exhibit nonlinear behavior such as shear thinning and/or shear thickening even when the suspending fluid is Newtonian. This talk focuses on such nonlinear rheological behaviors and it is motivated by one central question: "What is the role of particle shape?". We will present our recent results concerning the rheology of two suspensions, which differ solely through the particle shapes. One suspension was made of spheres, and the other of globular faceted particles produced by crushing identical spheres. The suspension of crushed particles exhibited a higher viscosity than the suspension of spheres for the same volume fraction and applied stress and displayed a steeper shear thinning behavior. The results show that the stronger nonlinear rheology of crushed particles stems from a combination of stress-weakening sliding friction and extra resistance to rolling motion due to the angular shape of the crushed particles. We will use these recent findings to put forward a scaling analysis to systematically explore the nonlinear rheology of dense non-Brownian suspensions made of nonspherical particles of arbitrary shape with the interplay of shape with hydrodynamic, colloidal, and contact forces.

Dynamics of Viscoplastic Fluid Flow in Superhydrophobic Grooved Channels

S.M. Taghavi* and H. Rahmani

Department of Chemical Engineering, Université Laval, Québec, Quebec G1V 0A6, Canada

*seyed-mohammad.taghavi@gch.ulaval.ca

Abstract

The study examines the behavior of viscoplastic fluids within channels lined with grooved superhydrophobic surfaces, using both theoretical modeling and numerical simulation techniques. The research aims to elucidate the dynamics between the viscoplastic fluids and the superhydrophobic textures by assessing the influence of the groove's orientation relative to the flow direction. With groove angles ranging from parallel ($\theta = 0$) to perpendicular ($\theta = 90$) and angles in between, the fluid's interaction with the air trapped in the grooves (i.e., a state known as the Cassie state) is presumed to have a flat interface. This interface is modeled according to the Navier slip condition and the Bingham plasticity model. The study explores varying channel dimensions and flow characteristics such as the Bingham number, slip number, groove periodicity, slip area ratio, and groove angle. Through perturbation theory, semi-analytical solutions for the velocity fields in larger channels are derived, while the Papanastasiou regularization method is applied in numerical simulations for both wide and narrow channels. The research notably identifies the distinct behaviour of viscoplastic fluids in oblique grooves, compared to the predictable patterns of Newtonian fluids. The findings present exact formulas for the flow mobility and effective slip length, highlighting the pronounced impact of viscoplastic rheology. In addition, a linear stability analysis under a uniform slip condition reveals the potential for stabilizing or destabilizing effects in Poiseuille-Bingham flow, contingent on the orientation of the slip.

Particle Migration of Non-Colloidal, Non-Brownian Suspensions Over Permeable Structures

Parisa Mirbod

Mechanical and Industrial Engineering Department
University of Illinois at Chicago, USA
pmirbod@uic.edu

Abstract

Flows containing particle (suspension flows) are prevalent in both natural environments and industrial settings. Examples range from slit-laden water flowing in rivers to blood moving through a cell counting analyzer. While suspensions have been extensively examined in various complex geometries with smooth walls, as well as pure Newtonian flows over permeable surfaces, little is known about the integration of particle-laden flows with permeable structures. This seminar will present laboratory experimental analyses of suspension flows over permeable structures, utilizing Magnetic Resonance imaging (MRI), Particle Image Velocimetry (PIV), and Particle Tracking Velocimetry (PTV) techniques. Wherever possible, the pertinent numerical methods will be also introduced and the associated challenges will be characterized. The insights gained from these analyses are expected to yield innovative methods to control particles in the flow and near the wall. The implications of these findings extend to a broad spectrum of industries and technologies involved in the processing and transport of suspension flows.

Macromolecular Architecture Affects Colloidal Gelation

Dimitris Vlassopoulos

Foundation for Research and Technology Hellas (FORTH), Institute of Electronic Structure and Laser, and
University of Crete, Department of Materials Science and Technology,
Heraklion, Crete, Greece
dvlasso@iesl.forth.gr

Abstract

It is known that small non-adsorbing linear polymers act as depletants to colloidal particles, yielding gels due to entropic attraction. In this work, we provide experimental evidence that ring polymers are stronger depleting agents in colloidal suspensions than their linear counterparts. We use PMMA hard sphere colloidal suspensions and add linear or ring non-adsorbing polystyrene of the same molar mass or the same size. The experimental results reveal that in the presence of rings, gels are formed at smaller concentrations and possess a larger storage modulus and larger yield stress in comparison to those induced by the linear chains. These findings are in agreement with theoretical calculations. Finally, we also demonstrate the strong gelling action of star polymers. The overall emerging picture points to the crucial role of macromolecular architecture on the properties of colloidal gels.

This presentation reflects the work of E. Moghimi and P. Kiany (Crete), and collaboration with G. Sakellariou (Athens) and C. Likos (Vienna).

Structure, Flow and Large Strain Flows of Rough, Arrested Emulsion Gels

Patrick Spicer* and Maryam Hosseini

School of Chemical Engineering, University of New South Wales, Sydney, Australia

*p.spicer@unsw.edu.au

Abstract

The static structure and flow of aggregated systems like colloidal gels determines the rheology and performance of commercial products in numerous industries. Recent experimental and simulation studies have focused on the network connectivity of colloids and how it provides elasticity to a fluid before and after yielding occurs. We study here emulsions that form structures very similar to colloidal gels but with unique potential for deformation and capillary interactions at droplet length scales. Arrested coalescence of these emulsions occurs when droplets possess some form of elastic colloidal microstructure, like fat crystal networks in dairy emulsions, that balances interfacial tension and halts coalescence before its completion. While networks of arrested emulsion droplets resemble colloidal gels in many ways, they possess a number of unique elements that make them worth additional study. A simple example is the degree of interpenetration or overlap between droplets, providing a map of the local mechanical properties and strain in the network as well as the history of the network connectivity as it rearranges to accommodate stress. We use confocal microscopy imaging to understand the complex interactions of the solid and liquid components of waxy and fatty emulsions as they greatly influence the overall network connectivity and structure of emulsion gels. We also map the restructuring of these system in high-shear mixing flows and relate the properties to the droplet structures.

On the Astarita flowfield and Stress Responses in 2D Steady, Homogeneous Viscoelastic Flows

Rob Poole

School of Engineering, University of Liverpool, United Kingdom
Robpoole@liverpool.ac.uk

Abstract

The two-dimensional steady, homogeneous flowfield proposed by Astarita (1991, *Journal of Rheology*, 35(4), pp.687-689) is studied for a range of viscoelastic constitutive equations of differential form including the models due to Oldroyd (the upper and lower convected Maxwell) {UCM/LCM}, Phan-Thien and Tanner (simplified, linear form) {sPTT} and Giesekus. As the flow is steady and homogeneous, the sPTT model results also give the FENE-P model solutions via a simple transformation of parameters. The flowfield has the interesting feature that a scalar parameter may be used to vary the flow “type” continuously from solid-body rotation to simple shearing to planar extension whilst the rate of deformation tensor D remains constant (i.e. independent of flow-type). The response of the models is probed in order to determine how a scalar “viscosity” function may be rigorously constructed which includes flow-type dependence. We show that for most of these models – the Giesekus being the exception – the first and second invariants of the resulting extra stress tensor are linearly related, and for models based on the upper convected derivative, this link is simply via a material property viz. half the modulus. By defining a frame-invariant coordinate system with respect to the eigenvectors of D , we associate a “viscosity” for each of the flows to a deviatoric stress component and show how this quantity varies with the flow-type parameter. For elliptical motions rate-thinning is always observed and all models give essentially the UCM response. For strong flows, i.e. flow-types containing at least some extension, thickening occurs and only a small element of extension is required to remove any shear-thinning inherent in the model (e.g. as occurs in steady simple shearing for the sPTT/Giesekus models). Finally, a functional form of a viscosity equation which could incorporate flow-type, but be otherwise inelastic, the so-called GNFFTy (Generalized Newtonian Fluid incorporating Flow Type pronounced “nifty”) model, is proposed.

On the Origin of Saffman-Taylor Instability of Viscoelastic Fluids

Mahmood Norouzi

Faculty of Mechanical Engineering, Shahrood University of Technology, Shahrood, Iran
mnorouzi@shahroodut.ac.ir

Abstract

Saffman-Taylor instability (STI), or viscous fingering instability, is a crucial phenomenon observed in fluid displacement within porous media and Hele-Shaw cells. When a low-viscosity fluid displaces a high-viscosity one in porous media, the interface between them may become unstable, forming finger-like patterns in the flow field. This instability finds significant applications in separation processes, water resource contamination, and Enhanced Oil Recovery (EOR). Polymer flooding, an EOR technique, involves dissolving viscosifying polymers in injected water to mitigate STI's intensity by reducing the viscosity difference between the displaced and displacing fluids. Our investigation focuses on understanding the role and contribution of the first normal stress difference and elongational viscosity in STI for dilute polymeric solutions during viscoelastic-Newtonian displacement. We present results derived from experimental data, linear stability analysis, and Computational Fluid Dynamics (CFD) for both Hele-Shaw cell and porous media scenarios. We also propose a hyperbolic wavy topology for the Hele-Shaw cell, aligning the viscoelastic flows with those observed in regular porous media.

Investigation on Non-Einsteinian Rheological Behaviour of Oxidized Molybdenum Disulfide Nano-Sheet in Suspension of Microglass Beads in Polyethylene Glycol

Ahmad Ramezani Saadat-Abadi

Sharif University of Technology, Tehran, Iran
ramazani@sharif.edu

Abstract

Rheological behavior of bimodal size glass beads including transient, steady, and dynamic shear flow of suspensions of glass beads with different concentration in polyethylene glycol are investigated. The presented results show non-Newtonian behavior for these suspensions. To find a method to reduce viscosity and increase flow ability of such systems, oxidized nano sheet of MoS_2 are prepared and added to polyethylene glass bead suspension in different concentration. The presented results show that a very low concentration of this nano sheet could induce significant non-Entientnian effects with reduction in viscosity of the glass bead suspensions. So, it could be concluded that such nano particles could be an effective processing aids in process of concentrated suspension of microparticles.

Rheology Control: Tailoring Properties in Water-Based Coatings and Inks

Amir Rezvani-Moghaddam

Faculty of Polymer Engineering, Sahand University of Technology, Tabriz, Iran
arezvani@sut.ac.ir

Abstract

The shift towards environmentally friendly water-based formulations in coatings and inks has highlighted the critical role of rheology control in optimizing their properties. Rheology control plays a critical role in improving the performance and application characteristics of water-based coatings and inks. In this regard, appropriate additive selection can strongly affect the water-based coating performance such as leveling and sagging. Rheological properties can play an important role in obtaining preferred properties which will pave the way for commercializing water-based coating in different industrial applications. Besides, rheology as a tool which is the deformation study of the ink under an applied stress/strain can be useful to determine the behavior of water-based inks in the channel, nozzle, and on the substrate during the printing process and control the drop ejection properties in inkjet applications. In this talk, I will discuss different strategies for tailoring rheological profiles to optimize flow, leveling, and film-forming properties in coatings and inks, supported by case studies and recent advancements in rheological measurement techniques.

Application of FSI and CFD in Solution of Actual Cardiovascular Problems

Alex G. Kuchumov^{1,2}

1. Biofluids lab, Perm National Research Polytechnic University

2. Department of computational mathematics, mechanics and biomechanics, Perm National Research Polytechnic University, Russia
kuchymov@inbox.ru

Abstract

The development of non-invasive diagnostic methods in modern surgery, mathematical and computer models allows describing biomechanical processes occurring in the body with an increasing degree of accuracy. This fact increases the possibility of their use in the improvement of existing and development of new personalized methods of diagnosis and treatment prediction. Computational fluid dynamics is a dynamically developing tool in solving engineering and interdisciplinary problems. Medicine is one of the fields where the application of computational methods and technologies is essential. One of the important aspects is to consider the application of biomechanics and computational fluid dynamics methods. This paper presents the results of application of computational fluid dynamics methods in solving actual problems of cardiovascular surgery (assessment of hemodynamic parameters in the aortic valve in norm and pathology, modeling of blood flow during stenting).

Keywords: FSI, blood, aortic valve, stent

Introduction

The development of noninvasive diagnostic methods in modern surgery, mathematical and computer models allows describing biomechanical processes occurring in the body with an increasing degree of accuracy [1-3]. This fact increases the possibility of their use in improving the existing and developing new personalized methods of diagnosis and treatment prediction [4,5]. Computational fluid dynamics is a dynamically developing tool in solving engineering and interdisciplinary problems [6]. Medicine is one of the fields where the application of computational methods and technologies is necessary. One of the important aspects is to consider the application of biomechanics and computational fluid dynamics methods [7]. This paper presents the results of application of computational fluid dynamics methods in solving actual problems of cardiovascular surgery (assessment of hemodynamic parameters in the aortic valve in norm and pathology, modeling of blood flow during stenting).

Experimental/Theoretical

Evaluation of Hemodynamic Parameters in the Aortic Valve in Healthy State and Pathology

The problem was solved on three-dimensional geometry constructed on the basis of ultrasound images data and literature review. The problem was solved within the FSI approach using the COMSOL Multiphysics software package. Blood flow is modeled as an incompressible Newtonian fluid with constant density and viscosity.

To model the biomechanical behavior of the aortic valve leaflets in normality, the Holzapfel-Gasser-Ogden model of anisotropic hyperelasticity is used. The pathologic state of aortic valve leaflets is described by a linearly elastic model.

The mathematical formulation includes the Navier-Stokes equation with incompressibility condition, equations to describe turbulence models. The equation of motion for a solid body is also written. The system is closed by initial and boundary conditions, as well as conditions of coupling of fluid and solid bodies.

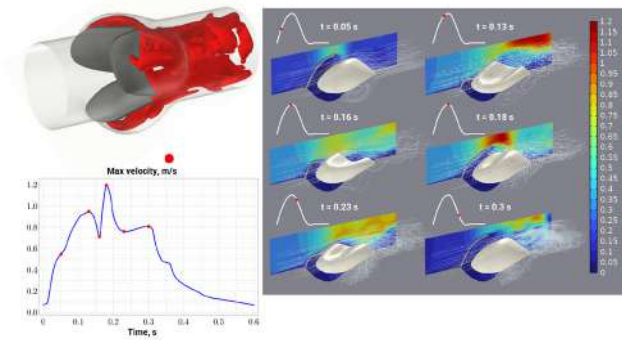


Fig. 1. Velocity distribution at different time of heart cycle.

A velocity profile is defined at the inlet of the computational domain. To determine the pressure at the outlet of the computational domain, the two-element Windkessel model is used.

Modeling of blood flow during stenting

The aim of this work is to evaluate the influence of mechanical parameters of the artery, plaque and stent on the effectiveness of stenting by analyzing the parameters of both stress-strain state and hemodynamics.

In this study an idealized model of the “artery - plaque - stent” system is considered. The geometrical model consists of several layers: adventitia - outer layer, media - middle layer, stent - stent.

The mechanical parameters of the artery layers were described using the using the three-parameter Ogden model.

Results and Discussion

Evaluation of Hemodynamic Parameters in the Aortic Valve in Healthy State and Pathology

The obtained results describe the changes in the main hemodynamic indices: velocity, pressure, wall shear stress and oscillatory shear index. The results for the

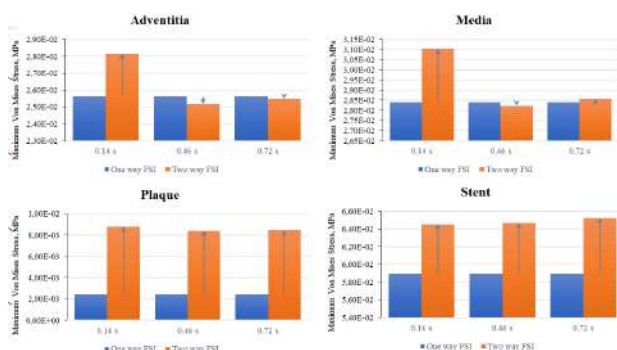


Fig. 2. Von Mises stress distribution in artery layers.

values of kinetic and turbulent kinetic energy between two models of turbulence and the state in normal and pathology were also compared.

Modeling of Blood Flow During Stenting

As a result of realization of 1-way and 2-way FSI, the distributions of hemodynamic parameters were obtained. Stress-strain distribution in all layers was found.

Conclusion

It was shown that FSI has been a useful tool in cardiovascular engineering. This systematic review looks at FSI's applicability in both cardiovascular engineering and medicine. FSI techniques enable the development of patient-specific models from MRI or CT imaging data by applying them to geometries of interest. Nowadays, one or more patient-specific geometries are used to perform cardiovascular FSI research. These techniques are widely used in cardiovascular CFD and are being used to develop FSI models that are more physiologically correct. Additionally, physical phenomena that are difficult to quantify but have an impact on the development, progression, diagnosis, or course of therapy of a disease can be studied thanks to FSI.

Acknowledgements

The results were obtained by grant of the state assignment of the Ministry of Science and Higher Education of the Russian Federation for fundamental scientific research (project FSNM-2023-0003).

References

- Kuchumov A.G., Doroshenko O.V., Golub M.V., Rakisheva, I.O., Shekhmametyev R.M. *Mathematics*, 2023, **11**(13), 2871
- Taghilou B., Sadeghy K., Pourjafar-Chelikdani M., Taghavi S.M., Nejad A.M., Kuchumov A., *Journal of Non-Newtonian Fluid Mechanics*, **306**, 2022.
- Sabir Q., Kuchumov A.G., Nguyen-Quang, T. *Russian Journal of Biomechanics*, 2023, **27**(1), 74–86.
- Pil, N., Kuchumov, A.G., Kadyraliev, B., Arutunyan, V. *Mathematics*, 2023, **11**(2), 428.
- Kuchumov A.G., Khairulin A., Shmurak M., Porodikov A., Merzlyakov A. *Materials*. **26**, 2022.

Physics-Discovery through Machine Learning for Complex Fluids and Soft Matter

Safa Jamali

Northeastern University, USA
s.jamali@northeastern.edu

Abstract

The ability to concisely describe the dynamical behavior of soft materials through closed form constitutive relations holds the key to accelerated and informed design of materials and processes. The conventional approach is to construct constitutive relations through simplifying assumptions and approximating the time- and rate-dependent stress response of a complex fluid to an imposed deformation. While traditional frameworks have been foundational to our current understanding of soft materials, they often face a two-fold existential limitation: (i) constructed on ideal and generalized assumptions, precise recovery of material-specific details is usually serendipitous, if possible, and (ii) inherent biases that are involved by making those assumptions commonly come at the cost of new physical insight. This work introduces a novel approach by leveraging recent advances in scientific machine learning methodologies to discover the governing constitutive equation from experimental data for complex fluids. Our Rheology-informed Neural Network (RhiNN) framework is found capable of learning the hidden rheology of a complex fluid through a limited number of experiments. This is followed by construction of an unbiased material-specific constitutive relation that accurately describes a wide range of bulk dynamical behavior of the material. While extremely efficient in closed-form model discovery for a real-world complex system, the model also provides new insight into the underpinning physics of the material.

The Moving Least-Squares Aided Finite Element Method (MLS-FEM) as a Means to Accurate Calculation of Flow Field Parameters

Mehdi Mostafaiyan

Leibniz Institute of Polymer Research, Germany
mostafaiyan@ipfdd.de

Abstract

Computation rheology is a scientific field that can help us better understand theoretical and experimental tasks of rheology or study the phenomenon we can not observe during fluid flow. However, these calculations comprise some difficulties, such as dealing with spurious or parasite-like currents, which appear in flow fields containing more than one phase. In this research, we would like to present the moving least-squares aided finite element method (MLS-FEM), which considerably reduces the magnitude of the spurious currents in multi-phase flow systems and provides more accurate results. The employed mesh or sub-domains of the MLS-FEM is independent of the second phase deformation, as it is with the extended FEM, the cut-FEM, and the meshless FEM. However, the MLS-FEM has some advantages compared to the stated methods: It does not introduce any new unknown parameter to the finite element simulation and retains the stiffness matrix's symmetrical shape in finite element formulation. Also, the MLS-FEM maintains the Kronecker- δ properties for the interpolation functions.

Slime for Defense–Rheological Design Principles in a Marine Environment

Peter Fischer

ETH Zurich, Institute of Food, Nutrition and Health, 8092 Zurich, Switzerland
peter.fischer@hest.ethz.ch

Abstract

Hagfish are genetically one of the oldest living creatures on earth. Neither charming in appearance or task they brought their defense mechanism to perfection during the last 150 million years. When attacked by predators, hagfish excrete a concentrated mucin–protein fiber solution, which forms within milliseconds a large body of slime [1,2]. Although the slime consists out of vast amounts of water, the diluted mucin and fibers span a cohesive network eventually clogging mouth or gills of the predators and enabling the hagfish to escape. Here, we present both the rheological properties of the slime in defense and escape situations as well as the biophysical principles of slime formation in the saline marine environment. We show that the different rheological responses of the slime under shear and elongational flow lead to strain hardening under attack but shear thinning during escape, promoting the survival chances of the hagfish [2]. Considering the slime as a complex polyelectrolyte, a fine-tuned interaction with the different ions present in seawater must be given to employ the full defense capability of the slime, i.e. the rapid unraveling and network formation of both mucins and skeins under charge screening conditions [3-6]. By elucidating the molecular and biophysical design principles and their consequences on the rheological properties of the slime, we are able to provide guidelines for tailoring mechanical properties of other mucin-like polyelectrolyte systems.

- [1] L. Böni, P.A. Rühs, P. Fischer, S. Kuster: Gelation of soy milk with hagfish exudate creates a flocculated and fibrous emulsion- and particle gel, PLoS ONE 11 (2016) e0147022
- [2] L. Böni, P. Fischer, L. Böcker, S. Kuster, P.A. Rühs: Hagfish slime and mucin flow properties and their implications for defense, Scientific Reports 6 (2016) 30371
- [3] L. Böni, R. Zurfluh, M. Widmer, P. Fischer, E.J. Windhab, P.A. Rühs, S. Kuster: Hagfish slime exudate stabilization and its effect on slime formation and functionality, Biology Open 6 (2017) 1115-1122
- [4] L.J. Böni, A. Sanchez-Ferrer, M. Widmer, M.D. Biviano, R. Mezzenga, E.J. Windhab, R.R. Dagastine, P. Fischer: Structure and nanomechanics of dry and hydrated intermediate filament films and fibers produced from hagfish slime fibers, ACS Appl. Mater. Interfaces 10 (2018) 40460-40473
- [5] L.J. Böni, R. Zurfluh, M.E. Baumgartner, E.J. Windhab, P. Fischer, S. Kuster, P.A. Rühs: Effect of ionic strength and seawater cations on hagfish slime formation, Scientific Reports 8 (2018) e9867
- [6] K. Rementzi, L.J. Böni, J. Adamcik, P. Fischer, D. Vlassopoulos: Structure and dynamics of hagfish mucin in different saline environments, Soft Matter 15 (2019) 8627

Stress, Velocity and Density Fluctuations in a Shear-thickening Suspension

Esmael Moghimi

University of Crete, Greece
esmaeel@iesl.forth.gr

Abstract

Dense particulate suspensions demonstrate a significant increase in average viscosity beyond a material-specific critical shear stress. Utilizing direct measurements of spatially resolved boundary stresses during the thickening phase in a suspension of monodisperse silica microspheres, we observe the presence of regions of well-defined dynamic localized high-stress which intermittently manifest at stress levels exceeding the critical threshold. When subjected to higher applied stresses, a persistent cluster of localized high-stress regions develops, propagating in the direction of flow at a velocity nearly half that of the top boundary. These prominent localized stress fluctuations coincide with a rapid increase in particle speed, the loss of positional order, and a decrease in particle concentration near the boundary. Notably, we observe that particles' speed during these events is independent of depth, suggesting collective motion as a shear-jammed aggregate. However, between consecutive high-speed regions, particle velocities exhibit nearly affine flow, indicating that these jammed regions propagate as density waves with continual particle exchange and only modest non-affine particle transport.

Correlation between Cluster Rigidity and Shear Thickening in Dense Suspensions

Jeffrey F. Morris^{1*}, Michel Orsi¹, Aritra Santra^{1,2}, and Bulbul Chakraborty³

1. Benjamin Levich Institute and Department of Chemical Engineering,
CUNY City College of New York, NY, USA

2. Department of Chemical Engineering, Indian Institute of Technology (ISM) Dhanbad, Jharkhand, India

3. Martin Fisher School of Physics, Brandeis University, Waltham, MA, USA

*morris@ccny.cuny.edu

Abstract

Shear thickening in dense suspensions is a well-known phenomenon. Recently, the relationship of shear thickening to shear jamming – which implies rigid structures – has been considered. Although many studies have been carried out to understand the continuous (CST) and discontinuous (DST) shear thickening in dense suspensions using analytical theory, experiments and numerical simulations, the evolution of rigidity in contact networks developed during the CST to DST transition and at shear jamming is not understood. Specifically, there is a lack of understanding on how particle contacts at local level lead to the appearance of large-scale rigid structure near the shear jamming transition. In this work we have studied the evolution of network structure in 2D dense suspensions as they undergo transition from CST to DST using LF-DEM (lubrication flow-discrete element methods) simulations. Evolution of rigidity in the contact network is investigated by computing the degree of particle coordination (Z) and rigid cluster size distribution by implementing a (3,3) pebble game algorithm. A distinct correlation has been observed between the DST onset and appearance of rigid clusters. Furthermore, using a phenomenological argument we show that the maximum size of rigid clusters as a function of mean contact per particle (Z) follows a universal curve.

A Novel Approach to the Recycling of PET/PE Blends and Laminates: Rheology-Driven Continuous In-Melt Separation

J. Maia^{*}, S. Vecchi, M. Lu, L. Hampton, H. Ghassemi, and D. Schiraldi

Department of Macromolecular Science and Engineering, Case Western Reserve University,
2100 Adelbert Rd, Cleveland, OH 44106, USA

*joao.maia@case.edu

Abstract

Multilayer, multicomponent films are widely used for their barrier properties, with more than 40 million tons of all plastic being produced annually being composed of multilayer polymer systems. This creates an enormous challenge as recycling of these multilayer systems is not technically feasible at large scales. In fact, the component plastics often have differing recycling pathways which prevents these films from being recycled. This work is aimed at presenting a novel chemical-mechanical approach that leads to achieving in-process melt separation of polyethylene/polyethylene terephthalate (PE/PET) blends in twin-screw extrusion for posterior individual recycling. Herein, we pursue two strategies to achieve this goal. In the first, pyromellitic dianhydride (PMDA) is used as a PET chain extender. The corresponding increase in PET viscosity induces coalescence of the PET droplets, which can then be mechanically filtered out of the main PE melt stream. Alternatively, ethylene glycol (EG) is used to depolymerize PET. The corresponding decrease in PET molecular weight allows for it to be extractable with the aid of SC CO₂. This work further studies the effect EG%, time, temperature, screw design, feed rate, and screw speed have on the depolymerization in a twin-screw extruder.

Recent Advances in Polymer Viscoelasticity from General Rigid Bead-Rod Theory

Alan Jeffrey Giacomini^{1*} and Mona A. Kanso²

1. Mechanical Engineering Department, University of Nevada, Reno,
Nevada 89557-0312, USA
2. Chemical Engineering Department, Massachusetts Institute of Technology,
Cambridge, Massachusetts 02139, USA
*giacomini@unr.edu

Abstract

One good way to explain the elasticity of a polymeric liquid, is to just consider the orientation distribution of the macromolecules. When exploring how macromolecular architecture affects the elasticity of a polymeric liquid, we find general rigid bead-rod theory to be both versatile and accurate. This theory sculpts macromolecules using beads and rods. Whereas beads represent points of Stokes flow resistances, the rods represent rigid separations. In this way, how the shape of the macromolecule affects its rheological behavior in suspension is determined. Our work shows the recent advances in polymer viscoelasticity using general rigid bead-rod theory, including advances applied on different viruses, including coronavirus. We calculate the rotational diffusivity of the viral suspensions, from first principles, using general rigid bead-rod theory. We do so by beading the spherical polymer, and then also by replacing each of its bulbous spikes with a single bead. We use energy minimization for the spreading and positioning of the spikes, charged identically, over the oblate or prolate capsids. We use general rigid bead-rod theory to explore the role of ellipticity on its rotational diffusivity, the transport property around which its cell attachment revolves.

Keywords: Rotational diffusivity, general rigid bead-rod model, complex viscosity, viscoelasticity, orientation

References

- [1] M.A. Kanso, M. Naime, V. Chaurasia, K. Tontiwattanakul, E. Fried, and A.J. Giacomini, "Coronavirus Pleomorphism," *Phys. Fluids*, 34(6), 063101, 2022.
- [2] M.A. Kanso, J.H. Piette, J.A. Hanna, and A.J. Giacomini, "Coronavirus rotational diffusivity," *Physics of Fluids*, 32(11), 113101 (2020).

Live Cell Rheometry Applied to Airway Mucus

Gerald G. Fuller

Chemical Engineering, Stanford University, Stanford, CA 94305, USA
ggf@stanford.edu

Abstract

Human tissue is in the category of “soft matter” and its rheological properties are of interest to understanding many problems in human health. A rheometer, a device to establish the relationship between stress and deformation, has been developed for the purpose of interrogating the dynamic response of living cells under a variety of conditions. In this presentation, the application of the live cell rheometer (LCR) to the viscoelasticity of the mucus layer produced above bronchial epithelial cells is described. Mucus that lines the lungs acts as the primary defense against inhaled foreign particles and infectious agents. Effective mucus clearance, and thus removal of the trapped invaders, is vital for healthy airway function. Asthma is a chronic inflammatory disorder associated with the inflammatory cytokine IL-13 that results in mucus hypersecretion of MUC5AC. The LCR is used to measure the creep compliance of mucus layers in the absence and presence of IL-13. It is found that inflammatory conditions transition the mucus from a viscoelastic liquid response to a viscoelastic solid. With this method, we demonstrate the ability to study mucus rheology in a physiologically relevant environment, examine phenotypic differences in mucus rheology, and rapidly test drugs on mucociliary mechanics.

Rheological Study of Nanoemulsions with Repulsive and Attractive Interdroplet Interactions

Zahra Abbasian Chaleshtari and Reza Foudazi*

School of Sustainable Chemical, Biological and Materials Engineering,
University of Oklahoma, Norman, OK 73019, USA

*rfoudazi@ou.edu

Abstract

The rheology of concentrated nanoemulsions is critical for their formulation in various applications, such as pharmaceuticals, foods, cosmetics, and templating advanced materials. The rheological properties of nanoemulsions depend on interdroplet interactions, Laplace pressure, dispersed phase volume fraction, and continuous phase properties. The interdroplet forces can be tuned by background electrolytes (i.e., charge screening), surfactant type, the excess surfactant micelle concentration, and depletant molecules such as polymer chains. In this research, we study model concentrated nanoemulsions which are stabilized by sodium dodecyl sulfate (SDS). To prepare samples in different structural states, semi-dilute nanoemulsions are prepared, after which evaporating the continuous phase at room temperature leads to concentrated nanoemulsions up to 60% volume fraction. Surfactant concentration is also tuned to induce different interdroplet interactions so that concentrated nanoemulsions in repulsive glass, attractive glass, and gel states are achieved. Rheological properties of nanoemulsions with different structural states are comprehensively studied over a volume fraction range. Utilizing the existing predictive models for (nano)emulsion rheology reveals a more satisfactory prediction for repulsive systems than systems with attractive interactions. In addition, a master curve is constructed for storage and loss moduli of nanoemulsions with different interdroplet interactions.

Short Bio

Dr. Reza Foudazi is an Associate Professor in the School of Sustainable Chemical, Biological and Materials Engineering (SCBME) at the University of Oklahoma (OU). His research is focused on porous polymers, self-assembly, complex fluids, and colloid and interface science. Before joining SCBME at OU in 2021, he was a tenured Associate Professor at New Mexico State University (NMSU). Dr. Foudazi has authored more than 70 publications in ISI peer-reviewed journals and is inventor of 7 intellectual properties. He received the Early Career Award from NMSU Research Council in 2016, Polymer Processing Society Early Career Award in 2019, ACS PMSE Young Investigator Award in 2020, and NMSU Intellectual Property Award in 2021.

Material Instabilities in Tension and Compression: Viscoelastic Creasing and Plastic Necking

Sachin Velankar

Department of Chemical Engineering, University of Pittsburgh, USA
velankar@pitt.edu

Abstract

Non-Newtonian materials can show instabilities, even when subject to simple flows or deformations. We will first discuss the creasing instability of a viscoelastic material under uniaxial compression. It has been known for many decades that when the free surface of an elastic material such as a block of rubber experiences severe compression, its surface develops sharp cusp-like creases. We show that a viscoelastic liquid undergoes a similar, but rate-dependent, surface-creasing instability. Experiments on a well-entangled molten polymer compressed at a controlled rate show that the strain required for creasing increases as rate decreases. A model is developed wherein the creasing criterion known previously for neo-Hookean elastic solids is applied to the elastic portion of the deformation of a viscoelastic liquid. Using the upper-convected Maxwell model, we derive an analytical criterion for viscoelastic creasing which is in good agreement with experiments. It predicts that the strain for creasing increases with decreasing Weissenberg number, and creasing is not possible below a critical Weissenberg number. The drawing instability of an elastoplastic material will also be explored briefly. Under uniaxial tension, many polymers show necking and drawing where a highly-stretched region coexists with a less stretched region. Such behavior occurs due to a combination of yielding and strain hardening. We will examine how the drawing instability disappears when an elastoplastic material is combined with a hyperelastic material. We will draw an elegant analogy between the mechanics of such elastic-plastic composites and second-order phase transitions from thermodynamics.

12-13 December 2023, IPPI, Tehran, Iran

3rd International
Conference on Rheology (ICOR 2023)



ICOR 2023

Conference Articles

(In order of code number)

Transporting Viscoplastic Biofluids by Off-Center Rotating Cylinders

Alireza Abdollahi¹, Soheil Almasi¹, Mohammad Pourjafar², and Kayvan Sadeghy¹

1. University of Tehran, College of Engineering School of Mechanical Engineering, Tehran, Iran

2. Department of Mechanical Engineering, University of Tehran, Rezvanshahr, Iran

Abstract

Physiological fluids such as blood are known to be viscoplastic and their yield stress may affect the performance of micropumps used to transport them in microfluidic channels. In the present work, the effect of a fluid's yield stress is studied on the performance of a typical rotor-pump having assumed that the fluid obeys the bi-viscous rheological model. The device works on the premise that a cylinder rotating in a channel can give rise to a net flow provided that it is placed in an off-center position. Numerical results obtained using the finite-element method over a wide range of Bingham numbers suggest that a fluid's yield stress has a negative effect on the performance of viscous micropumps. The drop in performance depends on the Bn number. At very high Bingham numbers, the flow rate becomes independent of the aspect ratio making the device attractive for use in microfluidic systems and also for drug-delivery implants.

Keywords: viscous micropump, bi-viscous model, bingham number, drug delivery, viscoplastic fluid

Introduction

Pumping biofluids through microfluidic systems is a huge challenge [1]. A major problem is the small length scales involved so that the flow normally occurs under creeping conditions. As such, viscous forces are dominant force, and so the use of conventional centrifugal pumps has to be ruled out. Over the years a variety of mechanisms have been developed for fluid transport in microfluidic devices, with some of them working better the larger the viscous forces. One can particularly mention the so-called "viscous micropump". The pump features a rotor (usually in the form of a cylinder) positioned across a channel with its axis situated normal to the flow direction [2]. The above works were concerned with Newtonian fluids. Most biofluids are known to exhibit a variety of non-Newtonian behavior. From the limited works published in the past, one can conclude that the device is not best suited for the transport of non-Newtonian fluids exhibiting shear-thinning or viscoelasticity [3]. In a recent numerical work [4], using the lattice Boltzmann method (LBM) it has been shown that the device is applicable for yield-stress fluids obeying the Bingham-Papanastasiou model [5]. But due to the limitation of LBM and the rheological model, it was not possible to obtain results for Bingham numbers larger than 10. In the present work, we have relied on the finite-element method (FEM) and a less demanding viscoplastic fluid model (called bi-viscous model) to obtain numerical results at Bingham numbers as large as 500. We will show that the performance of viscous micropump indeed drops the larger the Bingham number. At very high Bingham number, however, it delivers a constant flow rate (typical of drug-delivery implants) which is independent of the aspect ratio making the device a viable option in such applications.

Theory

Fig. 1 shows the flow geometry used for this study. The

geometry comprises two fixed parallel plates of infinite width with the gap between them occupied by the liquid of interest. The channel is seen to incorporate a rigid cylinder of diameter D with its axis oriented in the z -direction, which is the neutral direction. The distance between the center of the cylinder and the axis of the channel has been denoted by y_c and for any $y_c \neq 0$, rotation of the cylinder generates a net flow, from left to right for the configuration depicted in Fig. 1. The geometry is similar to that used in the previous works [1]. The equations governing the flow are:

$$\rho \frac{Du}{Dt} = -\frac{\partial p}{\partial x} + \frac{\partial \tau_{xx}}{\partial x} + \frac{\partial \tau_{yx}}{\partial y}, \quad (1)$$

$$\rho \frac{Dv}{Dt} = -\frac{\partial p}{\partial y} + \frac{\partial \tau_{xx}}{\partial x} + \frac{\partial \tau_{yx}}{\partial y}, \quad (2)$$

$$\frac{\partial u}{\partial x} + \frac{\partial v}{\partial y} = 0, \quad (3)$$

where D/Dt is the material derivative. For shear-dependent fluids obeying the power-law model, the stress terms can be related to the velocity terms as:

$$\tau_{ij} = m |\Pi_{2d}|^{(n-1)/2} (2d_{ij}), \quad (4)$$

where τ_{ij} is the deviatoric stress tensor, and d_{ij} is the rate-of-deformation tensor with Π_{2d} being its second invariant. In this rheological model, m is the consistency index and n is the exponent signifying the degree of shear-thinning or shear-thickening of the fluid. For $n < 1$, the fluid is shear-thinning whereas for $n > 1$, it is shear-thickening. The model

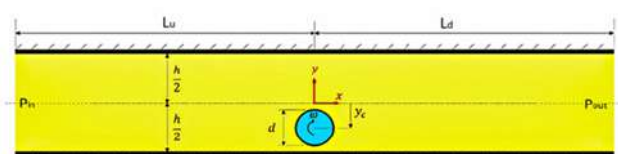


Fig. 1. Schematic showing the flow configuration.

reduces to Newtonian fluids by simply setting $n=1$.

Numerical Method

We have relied on the finite-element software package, COMSOL. Mesh-independent results have been obtained using 10,000 elements. We are primarily interested in reporting the flow rate for different power-law index (n) with the focus laid mostly on $n < 1$, results, i.e., the shear-thinning fluids. The parameter study involves two dimensionless geometrical parameters, i.e., the aspect ratio $S=h/d$, and the eccentricity $e=2yc/(h-d)$. The rotational speed is the independent parameter, which is made dimensionless as: $\Omega = \rho \omega d^2 / 2\mu_{ref}$, where μ_{ref} is the reference viscosity (say, viscosity of water considered as the infinite-shear viscosity of the solution). As the velocity boundary conditions, on the rotor and also the upper/lower walls, we impose no-slip and no-penetration conditions. For the upper-wall, however, a no-slip condition is released at some point to investigate its effect on the average velocity (U). The pressures at the inlet and outlet sections are assumed to be the same. Results will be presented in terms of U , normalized by the rotor surface velocity.

Results and Discussion

For the simulations, we fix the density and infinite-shear viscosity of the viscoplastic fluid at $\rho=1000$ (kg/m³) and $\mu_{\infty} = 0.05$ Pa.s, respectively. The angular velocity is determined by knowing the Reynolds number and the radius of the cylinder (which is set equal to unity). The increase in the torque coefficient is not surprising because the apparent viscosity of the fluid is larger than, which is the viscosity for $B_n=0$. The torque needed to rotate the cylinder is increased by an increase in the material's yield stress and also an increase in wall shear stress. Fig. 2 shows the transient response of the viscous micropump ($\Delta t=0.5$ s) and also the effect of aspect ratio on the average velocity. As is seen in this figure by an increase in the B_n number the time needed by the fluid to reach a steady state is reduced. As can be seen in this figure, by an increase in the B_n number the flow rate drops. This figure shows that although the device is still capable of transporting viscoplastic fluids at

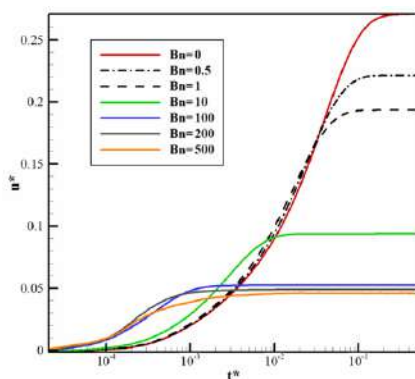


Fig. 2. Variation of the average velocity with time obtained for $S=2.5$.

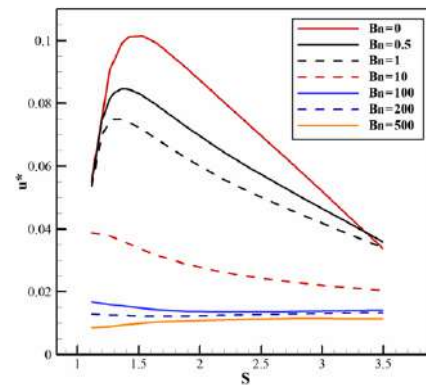


Fig. 3. Variation of the average velocity with time obtained for aspect ratio under steady conditions.

B_n numbers as large as 500, the flow rate is too small. The effect of the yield stress on system performance saturates at exceedingly large B_n numbers. Fig. 3 shows the effect of Bingham number on the averaged velocity over a wide range of aspect ratios. This figure shows the strong effect of the channel's height (which is how S is varied) on the flow rate of the pump, as previously noted for Newtonian fluids. Actually, this figure also includes results for Newtonian fluids ($B_n=0$) for comparison purposes.

Conclusion

The obtained numerical results suggest that by an increase in the Bingham number the flow rate of viscous micropumps is indeed reduced while the torque needed to rotate the cylinder is increased. Efficiency of the pump is also reduced the higher the Bingham number.

References

- [1] K.M. Bataineh and M.A. Al-Nimr, "2D Navier–Stokes simulations of microscale viscous pump with slip flow", *J. Fluid. Eng.*, **131**, 51105-51107, 2009.
- [2] A.K. da Silva, M.H. Kobayashi, and C.F.M. Coimbra, "Optimal design of non-Newtonian micro-scale viscous pumps for biomedical devices", *Biotechnol. Bioeng.*, **96**, 37-47, 2007.
- [3] B. Zhang, X. Liu, and J. Sun, "Topology optimization design of non-Newtonian roller type viscous micropumps", *Struct. Multidiscip. Optim.*, **53**, 409-424 2016.
- [4] B. Taghilou, S.M.J. Sobhani, M. Pourjafar-Chelikdani, A. Mahdavi Nejad, M.R. Ghoroghi, and K. Sadeghy, "On the use of viscous micropumps for transporting viscoelastic fluids in channel flows: A numerical study", *J. Non-Newton. Fluid Mech.*, **291**, 104528, 2021.
- [5] T.C. Papanastasiou, "Flow of materials with yield", *J. Rheol.*, **31**, 385-404, 1987.

The Effect of Initial PDMS Viscosity on the Rheological Properties of PBDMS Gels and Its Compatibility with Rheological Models

Hamid Reza Shadman, Masoud Tavakoli Dare, Amirhosein Mohammadpour, and Seyed Reza ghaffarian*
Amirkabir University of Technology (Polytechnic of Tehran), polymers and paints department, Tehran, Iran

*sr_ghaffarian@aut.ac.ir

Abstract

PBDMS represents a form of synthetic substance, generated through the interaction between PDMS and boric acid, or its related compounds. Belonging to the shear stiffening gel (SSG) category, this material thwarts the transmission of energy to lower levels during high-speed and immediate impacts by intensifying the dissipation or reflection of energy. Consequently, it has garnered attention within the protective materials sector. Investigating the rheological characteristics of this material under force application (distinct from sudden impacts) holds significance, as it aids in estimating and strategizing component longevity, optimal composite production methods, and more. Recognizing this significance, this article delves into the rheological conduct of this substance under standard temperatures, employing five rheological models to forecast such behavior. The Power law model emerges as the closest match to the material's behavior under test conditions, effectively elucidating this conduct.

Keywords: poly borodimethyl siloxane (PBDMS), rheological behavior, ambient temperature, power law model, Bingham model, Herschel-Bulkley model, Newton model, casson model

Introduction

Certain substances exhibit shear thickening characteristics, which can be broadly categorized into two main groups: those involving particles and those without particles. The initial category mainly encompasses polymer and particle suspensions, such as the case of nano-silica within an ethylene glycol base. The second group comprises substances featuring distinct intermolecular bonds in their composition. An illustration of this is poly boro dimethyl siloxane (PBDMS) [1]. The source of energy absorption during impacts in these systems arises from the mobility of the polymer segments connected to the glass transition temperature (T_g) and the unique intermolecular bonds within the system [1]:

1. As the shear stress intensity increases, the duration for stress relaxation decreases, which is linked to the glass transition temperature (T_g). Consequently, the material transitions from a rubbery state to a more solid-like state.
2. This phenomenon is evident in cases where hydrogen bonds and coordinated bonds are present, and it occurs when the energy from bonds matches the thermal energy.

Within pure PBDMS, the chains are interconnected, giving rise to a three-dimensional framework due to the presence of hydrogen bonds and coordination bonds between oxygen and boron. In cases where this structure undergoes extended stress, these bonds experience an opening effect (without breaking the covalent bonds), causing the material to exhibit a flowing behavior. However, when the material experiences abrupt stress, the bonds do not have sufficient time to open, resulting in a quasi-solid behavior [2-6].

Given the outlined structure and mechanisms, along with the versatility of these materials for various applications, such as their utilization in creating force-resistant fibers, it becomes imperative to delve into the study of their rheological behavior [7-9]. By examining their rheological characteristics and forecasting their rheological properties, it becomes feasible to devise an appropriate model for predicting these properties. This predictive capability can then be harnessed for formulating composite manufacturing methods and even estimating the durability of these composites under diverse conditions.

It is pertinent to investigate the rheological properties of these materials at room temperature, which can facilitate the development of a cold molding technique for the composites. Furthermore, exploring the rheological behaviors of these substances at varying temperatures can provide insights into the establishment of hot molding methodologies for composite fabrication.

Experimental

PDMS is available for purchase from the Gelest company in varying viscosities such as 150, 750, and 1000 cSt. Boric acid can be acquired from Sigma-Aldrich. The synthesis of PBDMS involves a reaction between boric acid and PDMS at 150 °C for approximately 1.5 h, followed by a reaction at 200 °C for about 1 h. To conduct rheological characterization, samples were shaped into tablets with a diameter of 25 mm and a thickness of 1 mm. The rheological testing was carried out using the Anton Paar MCR 350 instrument at room temperature.

Results and Discussion

As depicted in Fig. 1, an elevation in polymer viscosity (molecular

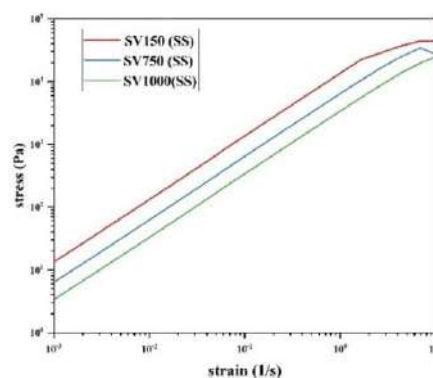


Fig. 1. Experimental result of shear stress diagram according to shear rate for V 150 (red), V 750 (blue) and V 1000 (green) samples.

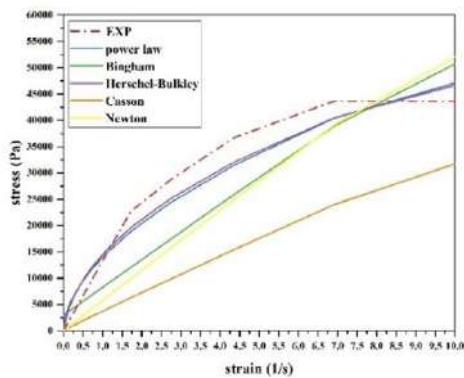


Fig. 2. Curve fitting of Rheological Model on experimental data of V150 sample.

weight) corresponds to a reduction in shear stress within the system. Moreover, when dealing with samples featuring higher initial material viscosity, an increase in shear rate results in elevated stress levels characterized by a shallower slope. This phenomenon emerges due to the chosen initial polymers falling within a range below the entanglement threshold. Consequently, the dominant factor influencing stress in this system is the presence of reversible bonds formed within it. These bonds exhibit behavior akin to the physical entanglements observed in rheology. As the initial material's molecular weight decreases and a stoichiometric reaction takes place, the initial polymer contains a greater number of functional groups, thereby enhancing the likelihood of forming reversible bonds. The heightened count of these bond types mirrors the impact of physical entanglements, augmenting shear resistance. Additionally, as illustrated in Fig. 1, an augmentation in initial material viscosity among these samples leads to an approach towards Newtonian behavior. Consequently, the degree of shear thinning decreases, accompanied by a reduction in slope alterations. This outcome arises due to a decrease in the count of entanglements results in reduced resistance factors against fluid flow, leading to a fluid behavior more closely aligned with Newtonian characteristics. To comprehensively explore and accurately characterize the rheological properties of these fluids, as well as the impact of their initial molecular weight on these properties, this study employed five distinct numerical models: Power Law, Bingham, Herschel-Bulkley, Casson, and Newton

Table I. The result of curve fitting of 5 Rheological Model in 3 samples.

Model name	Equation	V150	V750	V1000
Power Law	$\tau = k\dot{\gamma}^n$	$k = 14170$ $n = 0.55$ $R^2 = 0.962$	$k = 7023$ $n = 0.84$ $R^2 = 0.997$	$k = 3991$ $n = 0.81$ $R^2 = 0.996$
Bingham	$\tau = \tau_y + \eta_B \dot{\gamma}$	$\tau_y = 2971$ $\eta_B = 5415$ $R^2 = 0.854$	$\tau_y = 340$ $\eta_B = 5380$ $R^2 = 0.988$	$\tau_y = 387$ $\eta_B = 2653$ $R^2 = 0.983$
Herschel-Bulkley	$\tau = \tau_y + k\dot{\gamma}^n$	$\tau_y = -2321$ $k = 17030$ $n = 0.49$ $R^2 = 0.97$	$\tau_y = -273$ $k = 7341$ $n = 0.82$ $R^2 = 0.997$	$\tau_y = -243$ $k = 4235$ $n = 0.79$ $R^2 = 0.996$
Casson	$\sqrt{\tau} = \sqrt{\tau_0} + \sqrt{\eta_p \dot{\gamma}}$	$\tau_0 = 6.83$ $\eta_p = 3493$ $R^2 = 0.91$	$\tau_0 = 3.626$ $\eta_p = 4608$ $R^2 = 0.993$	$\tau_0 = 3.75$ $\eta_p = 2181$ $R^2 = 0.991$
Newton	$\tau = \eta \dot{\gamma}$	$\eta = 5896$ $R^2 = 0.82$	$\eta = 5477$ $R^2 = 0.987$	$\eta = 2693$ $R^2 = 0.981$

models (e.g., Fig. 2 illustrates the fitting of these 5 models to the V150 sample). The outcomes derived from fitting these models to the experimental behavior of the samples have been documented in Table I. Based on the findings, both the Power Law and Herschel-Bulkley models demonstrate a superior alignment with the experimental data. However, it is worth noting that, despite its favorable numerical fit, the Herschel-Bulkley model yields a negative yield stress value, which contradicts logical expectations. Furthermore, it is evident that the parameter 'n' exhibits variation across different samples. Samples characterized by lower initial polymer molecular weights showcase a more pronounced departure from Newtonian behavior ($n_{150} < n_{750} < n_{1000}$). Conversely, samples with higher molecular weights tend to exhibit a closer fit to Newtonian behavior.

Conclusion

The outcomes derived from this research indicate a clear trend: as the viscosity of the initial polymer increases, the rheological characteristics of the material tend to align more closely with Newtonian behavior. Moreover, samples containing a greater abundance of reversible bonds exhibit heightened fluid stress compared to their counterparts. Furthermore, the findings pertaining to the investigation of rheological models corroborate this observation. Among the various models studied, the Power Law model emerges as the most effective in predicting the rheological behavior of this material.

References

- [1] J. Ding, P.J. Tracey, W. Li, G. Peng, and P.G. Whitten, "Review on shear thickening fluids and applications", *Text. Light Ind. Sci. Technol.*, **2**, 161–173, 2013.
- [2] M. Song, C. Zhang, Z.Y. Song, N. Yan, and S.Z. Wu, "Study on the structure and properties of novel impact resistance fabric composites", *Appl. Mech. Mater.*, **182-183**, 153-157, 2012.
- [3] D.J. Plant, "The optimisation of flexible impact-protection systems for varying strain rates and energies", 2014.
- [4] S. Zhao, M.Y. Zhang, Y.N. Ren, W. Yang, and S.Z. Wu, "Impact resistance of shear thickening fluid (STF)/Kevlar composites for body armor application", *Adv. Mater. Res.*, **834-836**, 241-245, 2013.
- [5] D. Xu, J.L. Hawk, D.M. Loveless, S.L. Jeon, and S.L. Craig, "Mechanism of shear thickening in reversibly cross-linked supramolecular polymer networks", *Macromolecules*, **43**, 3556-3565, 2010.
- [6] "Silly Putty", 2009. [Online]. Available: soft-matter.seas.harvard.edu/index.php/Rheological_behavior.
- [7] C. Xu et al., "Anti-impact response of Kevlar sandwich structure with silly putty core", *Compos. Sci. Technol.*, **153**, 168-177, 2017.
- [8] C. Zhao, Y. Wang, S. Cao, S. Xuan, W. Jiang, and X. Gong, "Conductive shear thickening gel/Kevlar wearable fabrics: A flexible body armor with mechano-electric coupling ballistic performance", *Compos. Sci. Technol.*, **182**, 107782, 2019.
- [9] Q. He, S. Cao, Y. Wang, S. Xuan, P. Wang, and X. Gong, "Impact resistance of shear thickening fluid/Kevlar composite treated with shear-stiffening gel", *Compos. Part A Appl. Sci. Manuf.*, **106**, 82-90, 2018.

Rheological Study of an Epoxy/Microcapsule System During Cure

Sayed Morteza Mozaffari*

Department of Engineering and Technology, University of Mazandaran, Babolsar, Iran

*m.mozafari@umz.ac.ir

Abstract

The encapsulation of the curing agent is a method for preparing latent curing agents for epoxy resins. These curing agents have been used in one-part epoxy systems. In this study, viscoelastic properties of the epoxy resin (diglycidyl ether bisphenol A) containing microcapsule (1-methylimidazole capsulated by solid epoxy) were investigated by the dynamic shear parallel-plate rheometer, at 120 °C. The storage modulus, loss modulus, and complex modulus of the epoxy resin system containing 20 Phr microcapsules (latent curing agent) are used for determining the curing behavior of this epoxy resin system. The results showed that at different times, three different regions are observed in the viscoelastic behavior of the epoxy resin/microcapsule system at 120 °C. Also, in the presence of microcapsules in these three stages, the storage module is more than the loss module. Fourier transform infrared spectroscopy and Differential scanning calorimetry test also confirmed this curing reaction.

Keywords: epoxy, microcapsule, latent curing agent, parallel, plate rheometer, viscoelastic

Introduction

Epoxy resins are used in adhesives, composites, coatings, and others. Due to their unique thermo-mechanical properties, they are applied in high-performance lightweight systems, such as cars, airplanes, and wind energy plants. Also, epoxies are expected to play an important role in manufacturing smart products in the future. In order to fully understanding the potential of epoxy applications, requires a thorough analysis of the epoxy viscoelastic properties [1]. The study on the curing behavior of epoxy resin adds an extra dimension to its use and characterization. During the curing reaction, hardeners like anhydrides or amines, solids the epoxy through the ring opening of the epoxy group. 1-methylimidazole as an anionic curing agent at a relatively low concentration could react with diglycidyl ether bisphenol A up to a high degree of conversion. Encapsulation of imidazole has been suggested as an easy and economical procedure for deactivating this curing agent [1–3].

From an engineering view, the main phase transitions to be considered during cure is gelation time. Viscoelastic properties are a reliable method to monitor the cure. A parallel-plate rheometer was originally conceived for measurements of viscous fluids. The sinusoidal shear torque can be used to calculate the storage modulus, loss modulus, and complex modulus of epoxy resin [1].

In this study, the viscoelastic properties of the epoxy resin containing microcapsule (1-methylimidazole curing agent as core, solid epoxy as shell) were investigated by the dynamic shear rheometer, at 120 °C.

Experimental

Materials

The prepared microcapsule containing 1-methylimidazole

(DY 070, Huntsman, Germany) and solid epoxy resin (NPES-903, Nan Ya epoxy resin, Japan) was used as a curing agent [4]. Epoxy diglycidyl ether bisphenol A resin (DGEBA, Epikote 828) was purchased from (Momentive Co., USA) and used as the liquid resin.

Characterization

The rheological behavior of the epoxy resin systems containing 20 phr microcapsules was investigated using a dynamic shear rheological analyzer (Physica MCR 300, Anton Paar GmbH, Austria), at 120 °C, with plate/plate geometry (gap 1 mm, diameter 5 cm). A parallel plate viscometer test was performed at amplitude at the frequency 1 Hz, strain 1%, and according to ASTM D 4473.

Results and Discussion

Fig. 1 shows the changes in the storage modulus, loss

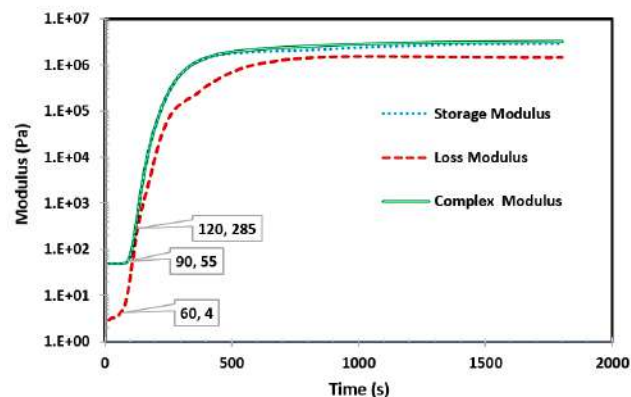


Fig. 1. The storage modulus, loss modulus, and complex modulus of the diglycidyl ether bisphenol a epoxy resin system containing 20 phr microcapsules at 120 °C over cure time.



modulus, and complex modulus of the diglycidyl ether bisphenol A epoxy resin system containing 20 phr microcapsules (latent curing agent) at 120 °C over cure time.

According to these curves, three stages are observed: the stage before the start of the curing reaction, the stage of the curing reaction, and the stage after the curing reaction. In the stage before the start of the curing reaction, the complex modulus is low and constant. By performing the curing reaction, the complex modulus increases, and in the stage after the curing reaction, the complex modulus is high and constant. Before the curing reaction, the system is in the form of a suspension (solid microcapsule particles in liquid epoxy resin). Microcapsule with a solid epoxy shell is compatible with liquid epoxy. This compatibility prevents the movement of liquid epoxy resin chains, and the storage modulus is greater than the loss modulus. With the increase of time at a constant temperature of 120, both storage and loss modules increase. With the increase of time, due to the release of the curing agent from the microcapsule and the curing reaction and creating a chemical connection between the liquid epoxy chains, the storage modulus increases [5]. However, due to the increase in time at 120 °C and the increase in the movement of the chains in short-range fluctuations, the loss modulus increases. The increase of the loss modulus (chain movements in short-range fluctuations) occurs in a shorter time (60 s) than the increase of the storage modulus (creating crosslink) (90 s). This indicates that the reaction needs more time than chain movements. In the stage of the curing reaction, the cross-linking density increases, and as a result, the storage modulus increases. Also, when the time of the epoxy resin system is increased at 120 °C, the short-range movements are more, and the loss modulus increases. However, during the curing reaction of the epoxy resin system by encapsulated 1-methylimidazole, the storage modulus changes are more than the loss modulus changes. In the time of 120 s, the two curves will have the closest distance to each other, this time can be considered as the gelation time of this epoxy resin system. After the curing stage, both the storage modulus and the loss modulus will have constant values. After the curing stage, the density of the crosslink does not change, and as a result, the storage modulus is constant. On the other hand, when the crosslink density reaches the maximum, time does not affect the short-range movements of the polymer chain and the loss modulus remains constant.

Conclusion

The encapsulation of the curing agent is a promising method to form a latent curing agent for epoxy resins. The rheological properties of the epoxy-microcapsule system were investigated by the dynamic shear rheological analyzer, at 120 °C. Time

sweep is a rheological technique used for determining

the curing behavior of this epoxy resin system. According to this rheological test, three different regions are observed in the viscoelastic behavior of the epoxy resin/microcapsule system at 120 °C at different times. At first, it is a suspension system and at the end it is solid. In these two stages, the storage modulus and loss modulus are constant. In the first stage, both modules are low and at the end, both modules are high. In the stage between these two areas, as the curing reaction takes place, both modules increase. On the other hand, despite the fact that the change process of both modules is the same, in these three stages, the storage module is more than the loss module.

References

- [1] Müller-Pabel M., Agudo J.A.R., and Gude M., *Polym. Test*, **114**, 107701-107731, 2022.
- [2] Mozaffari S.M., Beheshty M.H., and Mirabedini S.M., *Iran. Polym. J.*, **25**, 385-394, 2016.
- [3] Rafie M, Mozaffari SM and Kenari HS, *Technol. Sci. Polym. J. Iran*, **34**, 532-523, 2022.
- [4] Mozaffari S.M. and Beheshty M.H., *Polym. Bull.*, **78**, 3103-3115, 2021.
- [5] Chillakuru T.R., Khan W.S., Uddin M.N., Ibrahim M. Alarifi and Asmatulu R., *Academ. J. Polym. sci.*, **5**, 1-10, 2021

Effect of Conductive Filler Content and Process Time on Electrical and Rheological Conductivity Properties of Conductive Composites

Hadi Veisi¹ and Mohammad-Javad Hafezi^{2*}

1. Amirkabir University of Technology, Mahshar Campus, Mahshahr, Iran

2. Department of Polymer Engineering and Color Technology, Amirkabir University of Technology, Tehran, Iran

*hafezi@aut.ac.ir

Abstract

Two important factors on the conductivity and rheological properties of conductive composites, filler content, and process time were investigated. Polymer composites based on carbon black and polypropylene were prepared in different percentages of fillers and samples were obtained from the mixer at different times of the process. Both groups of samples were subjected to electrical conductivity and strain sweep tests. According to the results obtained by increasing the amount of carbon black in the composite, the solid behavior of the composite is strengthened at low frequencies. We also saw an increase in compound viscosity at low frequencies. As the time of the compounding process increases, the dispersion improves and causes the filler aggregates to break, which acts in the opposite direction of conductivity. At low frequencies, as the processing time increases, the behavior of the composite moves away from the solid-like.

Keywords: conductive composites, process time, strain sweep, dispersion, solid-like

Introduction

Polymers are often used as electrical insulators due to their electrical resistance. However, researchers are interested in adding conductive particles such as intrinsically conductive polymers, carbon black (CB), carbon nanotubes, graphene, or metal particles to the polymer matrix to give it conductivity [1]. The electrical resistance of conductive polymers by conductive particles can be in the range of resistance of metals (10-7 $\Omega.m$) to the resistance of insulating materials (1015 $\Omega.m$) [2] which can find their applications in many fields such as floor heating elements, electronic equipment [4,5], important strategic materials such as electromagnetic interference (EMI) shielding [6], apart from the conventional application of semi-conducting materials for dissipation of static electricity [7]. Polymeric conductive composites have been used for sensing components [8,9]. Compared with metallic conductors, conductive polymer composites have the advantages of ease of shaping, low density, and a wide range of electrical conductivities and corrosion resistance [10]. Due to the spherical structure of the particles and their tendency to form conductive networks, carbon black is one of the best and most common additives used in the production of conductive polymers today. By adding conductive particles of carbon black to the polymer matrix, the change in the properties of the polymer begins with a change in its color until the final product becomes conductive with the increase in the amounts of additive particles and the formation of a conductive network [11]. Process parameters, especially those involving significant shearing of the polymer/filler mixture, profoundly affect the conductivity properties of the final conductive polymer composite. Since two opposing effects must be balanced when mixing conductive polymer composites. (1) To ensure the dispersion of the conductive fillers uniformly throughout the polymer matrix, the composites must be sufficiently stirred, which means that vigorous and long-term stirring has a positive effect on the conductivity improvement. (2) On the other hand, however, this intense mixing condition creates more shear forces and leads to severe breakage of carbon black aggregates, which

decreases their tendency to create conductive paths in polymer matrices and as a result, the resistance will increase [12-15]. In this study, we intend to deal with the rheological behavior of the conductive composite in values close to the critical additive limit.

Experimental

The polymer matrix that was used to make the composite was polypropylene (PP) ($T_m=165$ °C) with a melt flow index of 6) g/10min (and was obtained from Navid Zar Chimi Industrial Company. The carbon black used as a conductive additive was from Degussa company with the brand name Printex 60. It also has a surface area of 115 m^2/g and an average particle size of 21 nm. First, in a 60 mL internal mixer made by Brabender, made in Germany, polymer, and additives with five different mass percentages of 5, 7.5, 10, 12.5, and 15% of carbon black were mixed for 10 min at 30 rpm (the time of 10 min starts after the complete gradual addition of carbon black to the device). Also, for the 12.5% sample, samples were taken from the mixer at 3, 13, and 30 min. To study dynamic rheological behavior, the composites were melted and compressed into a round sample with a thickness of 2.0 mm and a diameter of 25 mm. The measurements were performed on a Modular Compact Rheometer (MCR302) with frequency sweeps between 0.1 and 628 rad/s and a strain of 1% at temperatures of 240 °C. The device used in this study to calculate the conductivity of the composite was Diligent Waveforms Impedance Analyzer Trace located in the Faculty of Electrical Engineering of Amirkabir University of Technology.

Results and Discussion

The conductivity diagram for different percentages of carbon black is given in Fig. 1a. At 10% by weight, this conductive network is still forming. At 12.5% by weight, this network is formed and at 15%, only the number of its particles increases. In Fig. 2a, the storage modulus (G') for three percentages of 10, 12.5, and 15% can be seen that at low frequencies the conductive particles hold the polymer chains and cause the formation of a solid-like behavior. As mentioned, the reason is that conductive particles

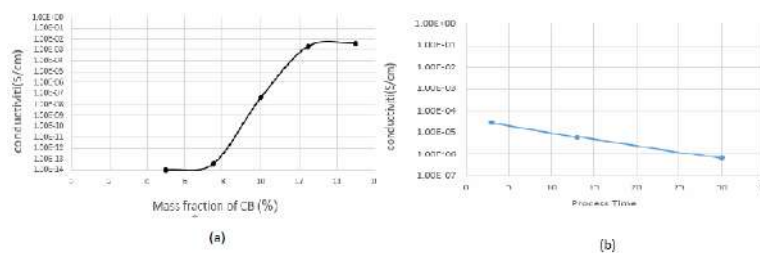


Fig. 1. The dependence of conductivity on the CB loading (a) and mixing time (b).

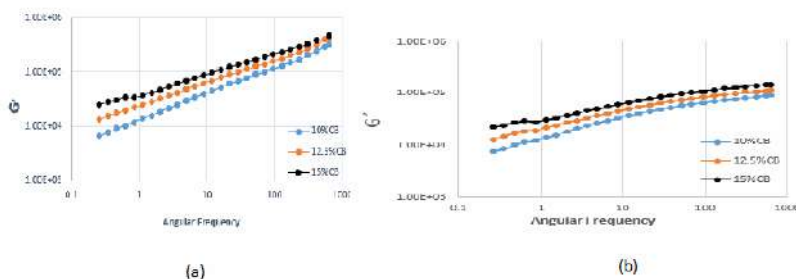


Fig. 2. The dependence of storage modulus (a) and loss modulus (b) on the CB loading.

form a network that can restrain polymer chains. As a result, in Fig. 2, the low-frequency dependence of loss modulus (G'') shows a similar trend. However, the corresponding increase in the loss modulus is much lower than that in the storage modulus at a fixed CB content, by comparing Fig. 2a with Fig. 2b. According to Fig. 1b, it can be seen that as the time increases, the conduction path becomes disturbed. In

Fact, with time, the amount of dispersion improves, this dispersion causes the failure of conductive aggregates and causes disturbances in the conduction path. The same event also affects the rheological properties of the composite, and as seen in Fig. 3, when the conductive network remains strong, the composite shows relatively more solid behavior. With the passage of time and the increase of dispersion, the solid-like behavior of composite decreases, and with moving toward complete dispersion, no noticeable change is observed in rheology diagrams and the graphs of 13 and 30 min are approximately the same. According to the conductivity data in Fig. 5, the conductivity of the composite of 15% by mass of conductive additive in 30 min is almost equal to.

Conclusion

Samples of conductive composite with different percentages of carbon black as a conductive additive were prepared. Also, samples were taken for 12.5 carbon black masses during the process at different times. The electrical and rheological properties were investigated under the influence of the above two factors (additive amount and process time). It was observed that with the increase in the amounts of additives in the composite, we saw a more solid

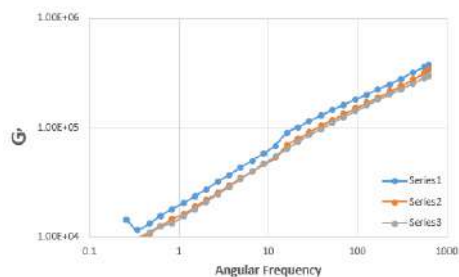


Fig. 3. Influence of mixing time on storage modulus.

response for G' and G'' at low frequencies. Also, at low frequencies, the viscosity of the complex increased with the increase in the amount of carbon black. At high frequencies, the rheological behavior is determined by the matrix, so we mostly saw liquid behavior. As the processing time increases, the dispersion improves, which causes the additive aggregates to break and disrupt the conduction path, which leads to a decrease in conductivity with an increase in the processing time. Also, an increase in the processing time causes the rheological behavior of the composite to deviate from the solid-like behavior at low frequencies.

References

- [1] M. Narkis, M. Zilberman, and A. Siegmann, *Polym. Adv. Technol.*, **8**, 525, 1997.
- [2] E. Frydman, UK Patent 604695, 8, 1948.
- [3] R.M. Scarisbrick, *J. Phys. D. Appl. Phys.*, **6**, 2098, 1973.
- [4] A.Y. Xiao, Q.K. Tong, A.C. Savoca, and H. Van Oosten, *IEEE Trans Compon. Pack Technol.*, **24**, 445, 2001.
- [5] T. Fujitani (Osaka) and K. Matsuoka (Tondabayashi), US4258100, Mar. 24, 1981.
- [6] S.K. De and J.R. White, *Short Fibre-Polymer Composites*, Woodhead Publishing Limited, Cambridge England, 1996, pp. 182.
- [7] R.H. Norman, *Conductive Rubbers and Plastics*, Elsevier Publishing Company Limited, Amsterdam, 1970, pp. 224.
- [8] L. Flandin, Y. Brechet, and J.Y. Cavaille, *Compos. Sci. Technol.*, **61**, 895, 2001.
- [9] X. Wang and D.D.L. Chung, *Sensor Actuator A*, **71**, 208, 1998.
- [10] R.H. Norman, *Conductive Rubbers and Plastics*, Elsevier Publishing Company Limited, Amsterdam, 1970, pp. 3.
- [11] I. Medalia, *Rubber Chem. Technol.*, **59**, 432-454 1985.
- [12] K.P. Sau, T.K. Chaki, and D. Khastagir, *Polymer*, **39**, 6461, 1998.
- [13] P.K. Pramanik, D. Khastagir, S.K. De, and T.N. Saha, *J. Mater. Sci.*, **25**, 3848, 1990.
- [14] P.K. Pramanik, D. Khastagir, S.K. De, T.N. Saha, *Plast. Rubber Compos. Proc. Appl.*, **15**, 189, 1991.
- [15] P.K. Pramanik and D. Khastagir, *J. Mater. Sci.*, **28**, 3539, 1993.

Rheological Behavior of PBAT/Recycled PLA

Mohammad Heidari and Hamid Garmabi

Department Color and Polymer Engineering, Amirkabir University of Technology, Tehran, Iran

Abstract

Polymer blends of poly(butylene adipate-co-terephthalate) (PBAT) and Recycled polylactide (PLA) have potential for additive manufacturing, which makes them attractive to researchers. Recycled PLA demonstrates low toughness and weak melt strength. In this study, PBAT and Recycled PLA were melt-blended by an internal mixer in a range of ratios from 15 wt% to 25 wt% PBAT. Dynamic rheological measurements were performed in the linear viscoelastic region. The complex viscosity of blends shows increased shear thinning behavior. Melt elasticity of the blends increased with the concentration of PBAT at low frequency. Despite the use of a significant amount of PBAT, the loss modulus did not show any significant change.

Keywords: PLA, PBAT, blend, miscibility, processing, rheology

Introduction

Enhancements in the performance of plastics can be achieved by designing specific polymer structures and blends. A new sustainable material with complementary properties can be created by blending PBAT and PLA in a cost-effective manner [1]. The primary objective of this study is to analyze the miscibility of PBAT/PLA blends.

PLA possesses a high modulus (3 GPa) and strength (50-70 MPa), making it comparable to many petroleum-based plastics. However, its low toughness and physical aging pose challenges for applications in medical devices and consumer products [2].

Experimental/Theoretical

Material. The main component of prepared blends was recycled PLA with 0.5% filler. PBAT was used as second component of the blend.

PLA/PBAT Preparation. In order to eliminate the influence of moisture on the properties of the obtained mixtures, the pellets were dried in an oven. The PLA and PBAT pellets were dried in a cabinet drier at 80 °C for 10 h. The total sample weight in the mixing chamber was 48 g and the mixing process was carried out at 190 °C for 10 min at a rotor speed of 50 rpm.

Dynamic Rheological Analysis. The rheological properties are analyzed using a rheometer (MCR 302, Anton Paar GmbH, Graz, Austria) with a parallel-plate measuring system. The diameter of the upper and lower plates is 25 mm, respectively. The test specimens are stamped out of panels (diameter: 25 mm, thickness: 0.8 mm) and then pre-dried before use. The programming and recording are accomplished using the software RheoCompass provided by the manufacturer. Frequency sweeps are carried out at a frequency range of 0.1–700 Hz, at 190 °C. After reaching 190 °C with a tolerance of 0.1%, each sample is heated for 2 min.

Results and Discussion

Melt Rheology

The complex viscosities of both PLA and PBAT were measured using capillary rheometry at 190 °C. Fig. 1 illustrates the variation in the complex viscosities of PLA and PBAT with increasing frequency. It is evident from Fig. 1 that the melts of both PLA and PBAT exhibit shear-thinning behavior.

At 190 °C, the complex viscosity of pure polymers decreases with increasing angular frequency, indicating shear-thinning behavior. This behavior is more pronounced in blends. Interestingly, PLA exhibited a longer Newtonian region than PBAT, and the addition of PBAT reduced the Newtonian region of the blends. This observation suggests that PLA/PBAT blends have partial compatibility. The storage modulus plot (Fig. 3) supports this by showing an increase in storage modulus at low frequency, indicating that the structure was prepared. The capillary number suggests that the dispersion of PBAT in Recycled PLA will occur more effectively due to the lower viscosity of the

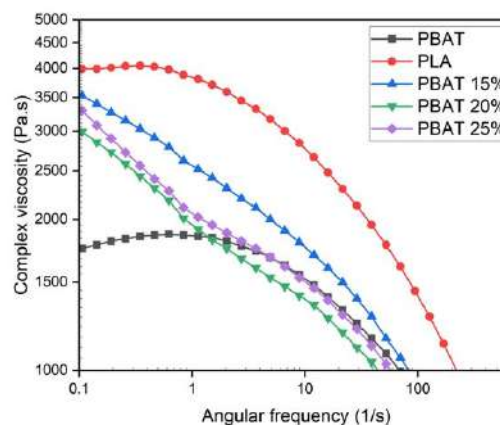


Fig. 1. Complex viscosity as function of angular frequency for PLA, PBAT, and PLA/PBAT blends.

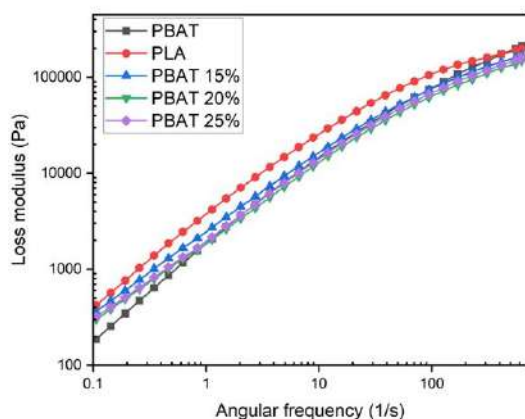


Fig. 2. Loss modulus as function of angular frequency for PLA, PBAT, and PLA/PBAT.

dispersed phase, implying potential miscibility of both components [1].

The complex viscosity of PLA/PBAT blends decreases more dramatically with increasing frequency, possibly due to the loss of physical entanglement at higher frequencies at 190 °C.

It's worth noting that the melting point of PBAT is significantly lower (120 °C) compared to that of PLA (150 °C). [3]

The higher complex viscosity of PLA compared to PBAT could be attributed to additional filler in PLA. However, adding PBAT increases elasticity and shear thinning. As the proportion of PBAT increases, the complex viscosity decreases, although at 25%, this trend reverses due to agglomeration.

PBAT, with its long and flexible molecular chains, is thought to result in elastic deformation due to molecular entanglement [2]. Furthermore, the presence of filler inhibits the movement of the polymer chains, inducing stiffness and a solid-like state in the molten polymer, especially at low frequencies (Fig. 3).

In Fig. 2, the blends appear to remain largely unaffected by the variation in PBAT content, as the loss modulus of the

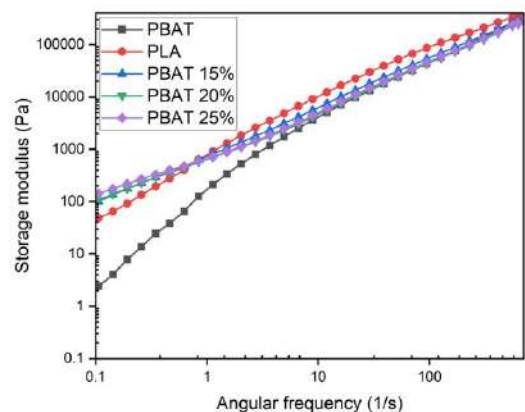


Fig. 3. Storage modulus as function of angular frequency for PLA, PBAT, and PLA/PBAT.

blends is similar. However, for pure PLA, the loss modulus is higher due to the inhibition of mobility caused by the presence of the filler.

Conclusion

Based on the complex viscosity and storage modulus plots, limited miscibility is observed between recycled PLA and PBAT, despite PLA and PBAT being immiscible at room temperature. A similar result was achieved with the pure PLA/PBAT blend, making this approach more cost-effective. Looking ahead, we can consider using recycled PLA as a substitute for PLA, offering both environmental and economic benefits.

References

- [1] S. Su, R. Kopitzky, and C. Berrenrath, "Experimental determination of molecular weight-dependent miscibility of PBAT/PLA blends", *Polymers (Basel)*, **13**, 3686, 2021.
- [2] L. Jiang, M.P. Wolcott, and J. Zhang, "Study of biodegradable polylactide/poly(butylene adipate-co-terephthalate) blends", *Biomacromolecules*, **7**, 199-207, 2006.
- [3] W. Prasong, P. Muanchan, A. Ishigami, S. Thumsorn, T. Kurose, and H. Ito, "Properties of 3D printable poly(lactic acid)/poly(butylene adipate-co-terephthalate) blends and nano talc composites", *J. Nanomater.*, **2020**, 2020.

Rheological Behavior of Polylactic Acid (PLA): The Effect of Chain Extender and Graphene Oxide Nanoplatelets (GO)

Ali Rastegar¹, Parvin Ehsani Namin², and Ismaeil Ghasemi^{3*}

1. Faculty of Polymer and Color Engineering, Amirkabir University, Tehran, Iran

2. Faculty of Chemistry, Tehran North Branch, Islamic Azad University, Tehran, Iran

3. Faculty of Processing, Department of Plastic Processing and Engineering, Iran Polymer and Petrochemical Institute, P.O. Box 14965/115, Tehran, Iran

Abstract

To improve the melt strength, thermal stability and mechanical properties of polylactic acid (PLA), a multifunctional styrene-acrylic oligomeric chain extender and graphene oxide nanoplatelets (GO) were incorporated into PLA. Melt flow index (MFI) and rheometric mechanical spectrometer (RMS) tests were examined to study the rheological behavior. The results showed that the chain extension reactions lead to an increase in the storage modulus, complex viscosity, and molecular weight. On the other hand, Joncryl helped to have better dispersion and distribution of GO. Nevertheless, GO hindered the reaction between epoxy groups of Joncryl and carboxyl groups of PLA.

Keywords: polylactic acid, chain extender, graphene oxide, nanocomposite, rheological behavior

Introduction

Since petroleum-based polymers are harmful to nature, biodegradable polymers have gained special attention due to their compatibility with nature and their wide applications [1]. One of these biocompatible polymers is polylactic acid. Polylactic acid belongs to linear polyesters, which are derived from natural sources such as sugar cane, corn starch and other biodegradable sources [2,3]. Despite its biocompatibility with nature, high modulus and strength, this polymer has low thermal stability, low toughness, inherent brittleness and low melt strength which reduce its applications [4]. To compensate these drawbacks, different kinds of materials were blended with PLA. In this work, we use a multifunctional chain extender (Joncryl) which contains epoxy groups for increasing molecular weight and melt strength of PLA. In addition, graphene oxide nanoplatelets was used to improve mechanical properties and thermal stability.

Experimental

Materials and Preparation of Chain-Extended Nanocomposites

The polylactic acid (PLA) used in this study was purchased from NatureWorks Co, USA, grade 8052D. The chain extender, Joncryl ADR-4468 was supplied from BASF, Germany. Additionally, graphene oxide nanoplatelets was purchased from US research nanomaterials Co, USA. Before processing, PLA was dried at 75 °C for 3 h and Joncryl at 30 °C for 1 h. Melt blending of PLA, chain extender and nanoplatelets were carried out in an internal mixer (Brabender Plasticorder) with a mixing chamber

volume of 60 mL, at 190 °C, using a rotation speed of 60 rpm for 10 min. First, PLA was melted in the internal mixer for 2 min, and then, Joncryl and GO were added at the same time. In this study, chain extended PLA nanocomposites named Int-P, sample 1 (P/0.5J), sample 4 (P/0.5J/1.5G), sample 6 (P/1J/1G), sample 8 (P/1.5J/0.5G) and sample 10 (P/1.5J/1.5G). P means PLA, J means Joncryl, G means graphene oxide and numbers in the nomination of the samples depict the weight percentage of Joncryl and graphene oxide.

Results and Discussion

Rheological Behaviors

The MFI of selected samples are depicted in Fig. 1. First, weak melt strength of Int-P is about 400 g/10min. According to Fig. 1, in sample 1, we saw an increase in

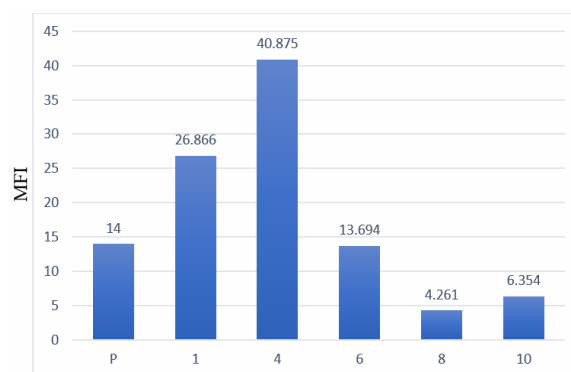


Fig. 1. MFI values of virgin PLA and PLA nanocomposites containing chain extender. 1) P/0.5J, 4) P/0.5J/0.5G, 6) P/1J/1G, 8) P/1.5J/0.5G, 10) P/1.5J/1.5G.

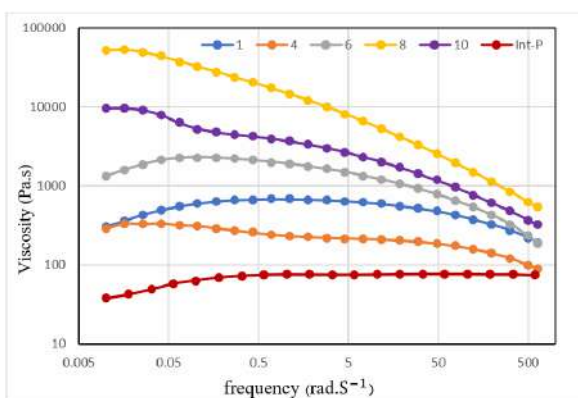


Fig. 2. Viscosity complex of Int-P and chain extended PLA nanocomposites. 1) P/0.5J, 4) P/0.5J/1.5G, 6) P/1J/1G, 8) P/1.5J/0.5G, 10) P/1.5J/1.5G.

MFI. By adding 1.5 wt% GO, it reached 40.875 g/10min (sample 4). However, MFI decreased to 13.694 g/10min by adding 1 wt% Joncryl and GO. After that, sample 8 has the least MFI between samples. Finally, by increasing GO up to 1.5 wt%, MFI faced to a little increasing (6.354 g/10min). In fact, by the creation of long branched structure by adding wt% Joncryl, melt strength increases, so MFI decreases. Fig. 2 shows the variation of viscosity versus angular frequency. As seen, all samples show Newtonians behavior approximately. Int-P shows the lowest viscosity (38 Pa.s). The highest viscosity is observed in sample 8 reaching 52000 Pa.s. In spite of the highest wt% of Joncryl and GO in sample 10 (9710 Pa.s), it places under sample 8 in the graph. High modulus of GO causes concentration

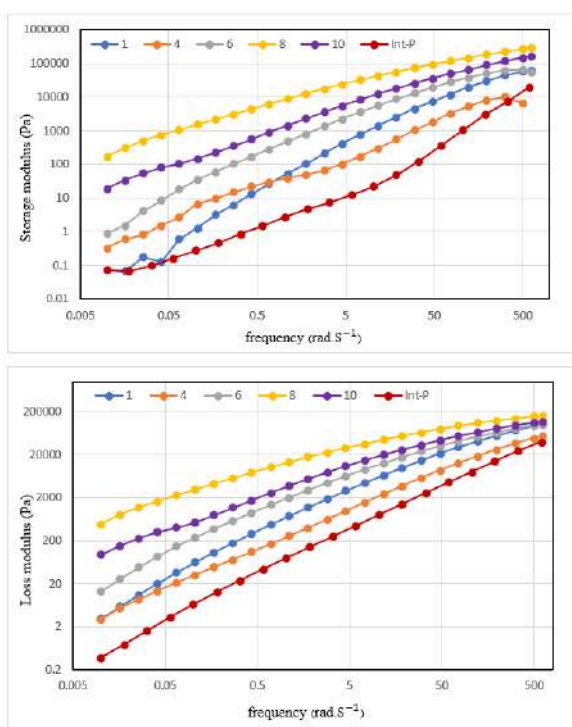


Fig. 3. Storage and loss modulus of pure and modified PLA. 1) P/0.5J, 4) P/0.5J/1.5G, 6) P/1J/1G, 8) P/1.5J/0.5G, 10) P/1.5J/1.5G.

and prevents increasing viscosity. Also, carboxyl groups of graphene oxide react with carboxyl groups of PLA and epoxy groups of Joncryl. As a matter of fact, high wt% of GO prevents the reaction between PLA and Joncryl. Fig. 3 depicts the storage and loss modulus of the samples. The storage modulus was increased by the increase of chain extender and GO. Increment of storage modulus is related to increase of molecular weight and develop of branching structure by the presence of chain extender. On the other hand, the interaction between GO and PLA causes to higher storage modulus.

Conclusion

The following results can be drawn from this study:

- The simultaneous presence of chain extender and GO could affect on rheological properties.
- MFI were decreased by addition of chain extender and GO.
- Rheological properties such as viscosity, loss and storage modulus were affected by addition of chain extender and GO due to developing of molecular weight and branching structure of PLA.

References

- [1] Z. Liu et al., "Effect of epoxy chain extender on the properties of polylactic acid", *J. Appl. Mater. Sci. Eng. Res.*, **2**, 1-7, 2019.
- [2] L. Avérous, "Chapter 21-polylactic acid: synthesis, properties and applications", *Monomers Polym. Compos. Renew. Resour.*, 433-450, 2008.
- [3] D. Garlotta, "A literature review of poly(lactic acid)", *J. Polym. Environ.*, 63-84, 2001.
- [4] X. Liu et al., "Improving melt strength of polylactic acid", *Int. Polym. Process.*, **28**, 64-71, 2013.

Effect of Solvent Viscosity on Swelling and Swelling Stress on NBR

Mohadese Mohammadi, Mohammad-Reza Pourhossaini*, Mahmoud Razavizadeh, and Mohammad Khabiri

Department of Materials Science and Manufacturing Technology, Malek-Ashtar University of Technology,

P. O. Box 15875-1774, Tehran, Iran

*mr_pourhossainy@yahoo.com

Abstract

The mechanism of penetration of solvent molecules into the material is called swelling. Diffusion of solvent molecules in the concentration gradient continues until reaching the chemical energy balance between the polymer and the solvent. The knowledge of swelling of network polymers was completed by Flory-Renner. One of the effective factors of swelling is the viscosity of the solvent as a penetrating agent. Solvent viscosity is an internal resistance to the change of state of matter and is related to of solvents. We used NBR (ACN 34%) with several solvents. The swelling decreases with the reduction of viscosity difference between polymer and solvent. By reducing the difference between the viscosity of the solvent and the NBR, the rubber's resistance to changing its state to accept the solvent decreases. Therefore, solvent molecules need less energy to penetrate the rubber, it enters the free volume of the tire with more energy and causes more swelling and causes more swelling tension.

Keywords: swelling, viscosity, swelling stress, treloar equation, NBR

Introduction

The mechanism of penetration of solvent molecules into the material system (provided that it is not dissolved) is called swelling [1]. Inflation is an incomplete dissolution. Dissolution takes place due to the chemical potential difference between the polymer and the solvent (concentration difference type). Diffusion of solvent molecules in the concentration gradient continues until reaching the chemical energy balance between the polymer and the solvent ($\Delta\mu_p = \Delta\mu_s$) [2,3]. The process of permeation and by passing through the surface of the material, the solvent molecules enter the mass of the material and spread throughout the material [2]. One of the physical phenomena in network polymers is swelling. The presence of solvent exposed to a network rubber leads to changes in weight and dimensions [4]. In network tires, the swelling does not exceed the first stage of dissolution and the equilibrium swelling is the maximum swelling [2]. Because, the osmotic pressure (chemical potential difference between the solvent and polymer molecules, which is the origin of the movement of the fluid flow towards the polymer) on the polymer from the solvent side is less than the forces preventing the penetration, and the chains will not be allowed to release due to the presence of crosslinks [5,6]. The basic knowledge in the field of swelling of network polymers was completed by Flory-Renner. Based on this, the amount of swelling is a function of the density of crosslinks and polymer-solvent interaction, and the equilibrium point has the lowest gradient of the energy level [5]. One of the effective factors in the field of swelling is the viscosity of the solvent as a penetrating agent. In fact, solvent viscosity is an internal resistance to the change of state of matter and is related to the kinetic energy of molecules (change of state in motion or conditions) [7-10]. With the entrance of solvent molecules, polymer chains and crosslinks are stretched into the system of a network rubber [6]. Therefore, from the mechanical point of view, swelling is a three-dimensional dynamic stress and the amount of swelling is heterogeneous in three dimensions of the material. Liquid absorption is related to the three-dimensional expansion

of the polymer structure. Swelling is a three-dimensional dynamic stress and leads to stretching of chains and crosslinks [11]. Calculation of inflation strain, the result of Flory-Renner researches in the field of inflation. For the first time, Treloar, by studying the statistical results of Florey-Renner in the field of volume inflation of tires and the theory of rubber elasticity (assuming chain tension and transverse links in the inflation process), realized the simulation of one-dimensional tension from the inflation stress [2,12].

Experimental/ Theoretical

Nitrile rubber (NBR, acrylonitrile content 34% made in France), zinc oxide (ZnO) produced by Merck, Germany, stearic acid (St.Ac) made by Uinichema, Malaysia, accelerator including (CBS) produced in China and sulfur as an agent Pukht was procured from TESDOK Iran. All solvents used were purchased from Merck. The NBR was prepared using the formulations as presented in Table I. To investigate the effect of solvent and swelling stress, the swelling test according to the international standard ASTM D471 was used. Eq. (1) is related to the weight changes of the inflated tire sample:

$$Q = \frac{W_2 - W_1}{W_1} \times 100 \quad (1)$$

In Eq. (1), parameter Q is related to inflation percentage, W_1 is primary weight and W_2 is secondary weight [13]. Eq. (2) is related to Treloar swelling stress:

$$\sigma_{sw} = \left[\frac{RT}{V} \right] \left[F(Q) + \left(\frac{AL^*}{Q} \right) \right] \quad (2)$$

In Eq. (3), parameter T is the absolute temperature, R is the global gas constant, V is the molar volume of the solvent, L^* is the change ratio, Q is the degree of swelling, F(Q) is

Table I. The NBR was prepared using the formulations.

Material (phr)	NBR	ZnO	AS	S	CBS
	100	5	1	1.8	1.8

Table II. Solvent viscosity and absorbed solvent weight.

Material	Viscosity (mN/m)	$\Delta\mu$	W_s (g)
NBR*	42	-----	-----
DMF	0.802	41.198	0.861
TOL	0.552	41.448	0.592
ACT	0.302	41.698	0.491
n-Hexane	0.294	41.706	0.0114

*[14]

the swelling function, and A is the network resistance; which is calculated from Eqs. (3) and (4) respectively:

$$F(Q) = \ln \left[1 - \frac{1}{Q} \right] + \frac{1}{Q} + \frac{\chi}{Q^2} \quad (3)$$

$$A = \frac{\rho V}{M_c} \quad (4)$$

In Eqs. (3) and (4), the parameter ρ is the volumetric mass of the solvent, V is the molar volume of the solvent [12], M_c is the average molecular mass between two crosslinks:

$$M_c = \frac{-\rho V_s \left(\frac{1}{\phi^2} - \frac{\phi}{2} \right)}{\ln(1-\phi) + \phi + \chi \phi^2} \quad (5)$$

In Eq. (5), the parameter ρ is the volumetric mass of the polymer, V_s is the molar volume of the solvent, χ is the polymer-solvent interaction, and ϕ is the volume fraction of the polymer in the swollen state:

$$\chi = \frac{V_s}{RT} (\delta_s - \delta_p)^2 + \beta \quad (6)$$

In Eq. (6), the parameter V_s is the molar volume of the solvent, R is the universal gas constant, T is the absolute temperature, δ_p and δ_s are the solubility parameter of the polymer and the solvent [13].

Results and Discussion

According to Table II, the swelling decreases with the reduction of viscosity difference between polymer and solvent. By reducing the difference between the viscosity of the solvent and the nitrile rubber, the rubber's resistance to changing its state to accept the solvent decreases. Therefore, solvent molecules need less energy to penetrate the rubber; So, it enters the free volume of the tire with more energy and causes more swelling and causes more swelling tension. Swelling stress is shown in Fig. 1.

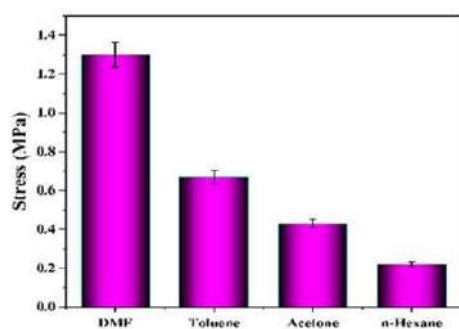


Fig. 1. Swelling stress of solvents.

Conclusion

In this research, by measuring the difference in viscosity, the amount of swelling stress caused by the introduction of solvent was measured for nitrile rubber. The swelling decreases with the reduction of viscosity difference between polymer and solvent. By reducing the difference between the viscosity of the solvent and the nitrile rubber, the rubber's resistance to changing its state to accept the solvent decreases.

References

- [1] S. Sadeghnejad, M. Ashrafzadeh, and M. Nourani, "Improved oil recovery by gel technology: Water shutoff and conformance control", in *Chemical Methods*, Elsevier, 2022, pp. 249-312.
- [2] M. Liu et al., "Anisotropic swelling of elastomers filled with aligned 2D materials", *2D Materials*, **7**, 025031, 2020.
- [3] S.P. Danielsen et al., "Molecular characterization of polymer networks", *Chem. Rev.*, **121**, 5042-5092, 2021.
- [4] X. Jiang et al., "Influence of aviation hydraulic oil swelling on the mechanical properties of HNBR/EPDM vulcanizates reinforced by carbon black", *J. Appl. Polym. Sci.*, **140**, e53549, 2023.
- [5] U.W. Gedde and M.S. Hedenqvist, *Fundamental Polymer Science*, Springer, 2019, vol. 2.
- [6] Y. Guo et al., "Hydrogels and hydrogel-derived materials for energy and water sustainability", *Chem. Rev.*, **120**, 7642-7707, 2020.
- [7] T. Klein et al., "Liquid viscosity and surface tension of n-hexane, n-octane, n-decane, and n-hexadecane up to 573 K by surface light scattering", *J. Chem. Eng. Data*, **64**, 4116-4131, 2019.
- [8] J. Merchiers et al., "Fiber engineering trifecta of spinnability, morphology, and properties: centrifugally spun versus electrospun fibers", *ACS Appl. Polym. Mater.*, **4**, 2022-2035, 2022.
- [9] A. Koochakzadeh et al., "Review on using pH-sensitive microgels as enhanced oil recovery and water shutoff agents: Concepts, recent developments, and future challenges", *Geoenergy Sci. Eng.*, **211477**, 2023.
- [10] N. Kumar et al., "Fundamental aspects, mechanisms and emerging possibilities of CO₂ miscible flooding in enhanced oil recovery: A review", *Fuel*, **330**, 125633, 2022.
- [11] B. Yang et al., "Molecular dynamics study on the reinforcing effect of incorporation of graphene/carbon nanotubes on the mechanical properties of swelling rubber", *Polym. Test.*, **102**, 107337, 2021.
- [12] C. Nah et al., "Swelling of rubber under nonuniform stresses and internal migration of swelling liquid when the stresses are removed", *Macromolecules*, **44**, 1610-1614, 2011.
- [13] G. Liu et al., "Investigation of the swelling response and quantitative prediction for hydrogenated nitrile rubber", *Polym. Test.*, **34**, 72-77, 2014.
- [14] Y.S. Lee and K. Ha, "Effects of acrylonitrile content on thermal characteristics and thermal aging properties of carbon black-filled NBR composite", *J. Elastom. Plast.*, **53**, 402-416, 2021.

How Does Long-Chain Silane Grafted on the Silica Control Rheology, Crystallinity and Mechanical Properties of Polyamide- Reclaimed Rubber Blend

Ali Nazari¹, Mohammad Alimardani^{1*}, and Mohammad Tavakol²

1. Polymer Engineering Department, Faculty of Chemical Engineering, Tarbiat Modares University, P.O. Box 14115-114, Tehran, Iran
 2. Shamim Polymer Company, P.O. Box 3136993781, Tehran, Iran
- *alinazari4869@gmail.com

Abstract

Development of recycling technologies for waste tires has always been of significant importance to address environmental concerns and to bring economic benefits. The use of Reclaimed Tire Rubber (RTR) as a rubber toughener for engineering plastics such as Polyamide 6 (PA) may be a promising recycling route, and it is essential to find out how silica nanoparticles contribute to modification of the blend properties. Evaluating the effect of hydrophilicity/hydrophobicity of silica particles on the rheological and mechanical properties of the PA/RTR blend is the main purpose of the present study. Silica nanoparticles were surface modified at three levels (low, medium, and high) using a long-chain 16-carbon silane (hexamethyltrimethoxysilane). The surface modification was confirmed using the infrared spectroscopy (IR) and a furnace-based gravimetric test. The contact angle measurements were employed on all the components to assess the hydrophilicity of the surfaces, and also to predict the state of silica dispersion, the interfacial strength, and the filler-localization. Results indicated that regardless of the hydrophilicity character of silica, the presence of long chain silane grafted on the silica surface remarkably controls linear and non-linear rheological properties of the blend, and a higher elastic modulus is expected for high level of silane treatment. A model of mechanical engagement between the silica particles and silica-PA components resulting from the long chain of silane was proposed to explain the rheological properties. Based on the DSC, it is shown that the level of such rheological modification has been severe enough to significantly reduce the polyamide crystallinity, and to conceal the other positive aspects that silica may impose on mechanical properties of the blend.

Keywords: reclaimed tire rubber (RTR), polyamide 6 (PA), silica, rheology, mechanical properties

Introduction

Nowadays, because of the environmental concerns and economic considerations, special attention has been devoted to the subject of rubber recycling, and one of the recycling routes is the toughening of plastics by rubber. This is while the incompatibility between the recycled rubber toward other polymers not only prevents any improvement in performance, but also it could deteriorates the mechanical and impact properties [1]. The use of nanoparticles as a compatibilizer in polymer systems is a promising approach to tackle this challenge. The compatibilizing role of the nanoparticles is greatly influenced by the status of its localization in blend. In a research by Christian Boudoin *et al.*, the effect of nanoparticles (carbon nanotubes) as modifiers for the morphological stability in polyamide (PA)/ethylene methyl acrylate (EA) blends was studied using electron microscopy techniques. It was shown that by placing nanoparticles at the interface of two phases, the size of the dispersed phase decreases because of two reasons; First, the viscosity of the layers being close to the interface increases, which could by itself suppress the coalescence of dispersed phase. Second, presence of nanoparticle at the interface lowers the interfacial tension between the components. Localization at the interface also finds immense importance when improvement in

impact properties is pursued. This is because presence of nanoparticle at the rubbery phase is undesirable as it prevents cavitation and limits the absorption of impact energy [2]. Use of particles may also positively address the challenge of “stiffness-toughness balance” commonly observed in rubber-toughened thermoplastics. Nanoparticles have a general reinforcing feature to prevent the loss in stiffness and tensile strength offered by the presence of rubber phase.

This research was built on a recent experimental observation that silica particles at a particular loading level was not capable of positively enhancing the mechanical properties of the RTR/PA blend. It will be shown that based on the DSC, this behavior is deeply connected to the PA crystallinity. Rheological evidence thoroughly supports this claim, and it describes how mechanical engagement offered by the long chain of silane modifiers controls the rheology, crystallinity and mechanical properties of the blend.

Experimental

Reclaimed rubber (RTR) were supplied from Qom Rubber Industry (Mooney Viscosity 35±5). Pristine silica Ultrasil VN3 and the long chain silane Hexadecyltrimethoxysilane were obtained from Evonic Co. In the first step, silica was

modified by the silane in different stoichiometric ratios (i.e. low, medium and high) to the hydroxyl groups of silica. Unmodified silica is named as S and the three other modified ones are referred to as S1, S2, and S3, where higher number of the subscript represents a higher degree of hydrophobicity. PA6 and TMQ antioxidant first fed into the internal mixer (Haake Buchler Rheomix 750 at the temperature of 230 °C). Then, silica particle and RTR were added after 2.5 and 5 min, respectively and the mixing process continued for another 5 min (total mixing time=10 min). Rheological frequency sweep tests were carried out at a fixed strain amplitude of $\gamma_0=0.05$ to acquire linear rheological properties under small amplitude oscillatory shear (SAOS) flow. Nonlinear rheological responses were obtained through strain sweep tests under the large amplitude oscillatory shear (LAOS) flow with increasing strain amplitude from $\gamma_0=0.01$ to 100 at a fixed frequency of 1 rad/s.

Results and Discussion

Fig. 1 illustrates the results of tensile strength as a representative of mechanical properties on PA and other blend systems. Although by addition of reclaim rubber, the tensile strength is expectedly shrunk, a compensating improvement in mechanical properties cannot be observed by the presence of reinforcing silica. Hydrophilic silica shows the best performance and by increasing the degree of silane grafting, the tensile strength and a number of other properties including impact strength (not shown here) are almost monotonically reduced.

These findings could not be fully explained by the available thermodynamic predictions that was made for the filler localization and dispersion. DSC was then employed to help elucidate the behavior. As reflected in Fig. 2, presence of both rubber and silica disturbs the crystallization behavior of PA, and the restriction is intensified by the increasing the level of grafting of long chain silane. It seems that PA crystallinity is dramatically reduced in the presence of modified silica.

To find more support for this claim, SAOS and LAOS

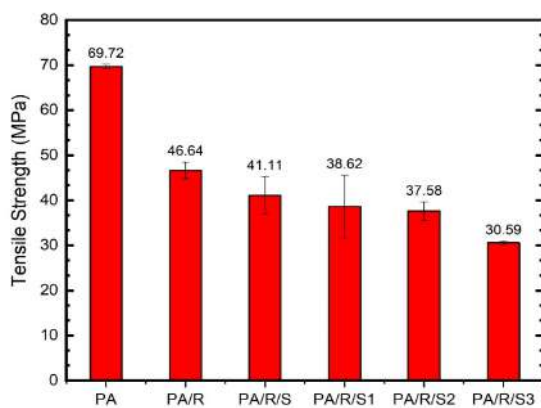


Fig. 1. Tensile strength results for various systems.

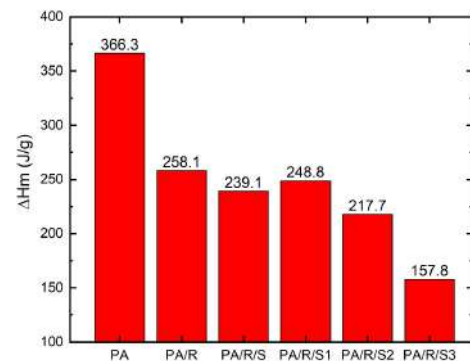


Fig. 2. Melting enthalpy of various systems obtained by DSC.

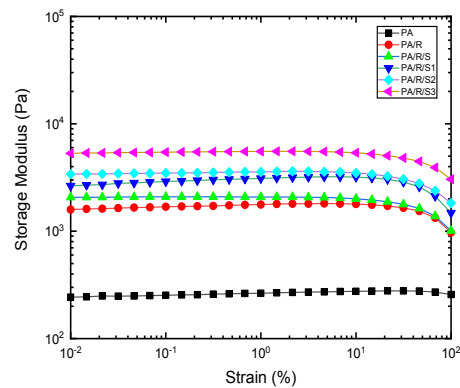


Fig. 3. LAOS rheological experiment on samples.

rheological experiments were conducted on the prepared blends. For brevity, the results of SAOS test has been presented in Fig. 3. As mentioned earlier, highly modified silica particles strongly influence the rheological behavior of the polymer matrix by forming a network of particles. Filler-filler mechanical engagement resulting from the interpenetration of long chain silane grafted on the silica prevails the roles played by the loss in filler-filler energetic interaction induced by silica treatment. Such a restriction in flow of the PA is responsible for a significant change in PA crystallinity and it can meaningfully explain the trend previously observed for the mechanical properties.

Conclusion

LAOS rheological test clearly explained how flow-restriction offered by the long chain silane leads to a immature crystallinity and a loss of mechanical properties in PA/RTR blends.

References

- [1] I. Kelnar et al., "Effect of graphene oxide on structure and properties of impact-modified polyamide 6", *Polym. Plast. Technol. Eng.*, **57**, 827-835, 2018.
- [2] A.-C. Baudouin, C. Bailly, and J. Devaux, "Interface localization of carbon nanotubes in blends of two copolymers", *Polym. Degrad. Stab.*, **95**, 389-398, 2010.

Investigate Establishing Long Chain on Nylon-6 by Styrene Maleic Anhydride (SMA) Via Reactive Extrusion

Mohammadamin Nejadhaji, Shervin Ahmadi*, and Ghasem Naderi

Iran Polymer and Petrochemical Institute, Postal Code 14977-13115, Tehran, Iran

*sh.ahmadi@ippi.ac.ir

Abstract

Long chain branched nylon-6 has been fabricated by styrene maleic anhydride (SMA) as a chain extender during the reactive extrusion. The small amplitude oscillatory shear (SAOS) dynamical rheological test has been investigated to determine the effect of chain extender on the rheological properties of nylon-6. Shown that the sample that contained the 0.5 weight percent of different SMA in addition to 0.25 weight percent of accelerator had the highest zero shear viscosity and more Shear thinning in comparison to the pure sample, as a result of improving melt strength, due to the sequence of increasing of molecular weight, the raising of entanglement density and increment of melt viscosity respectively.

Keywords: long chain branched polyamide 6, small amplitude oscillation shear, relaxation time, shear thinning behavior, melt strength

Introduction

Nylon-6 belongs to aliphatic polyamides that due to its desired properties such as high dimensional stability or low coefficient of friction could be used in various industries such as in fiber, film, and packaging production [1].

However, one of its main problems is its low structure entanglement which limits its uses in polymer processing like fiber or foam production. To fix this limitation, researchers have found that creating long chain on polymer's backbone, could fix this limitation, so they suggested 4 approaches to creating long chain on polymer's backbone: 1) solid state polymerization [1].

2) Use multi-functional comonomer [2];

3) Use powerful irradiation [3];

4) Use chain extender (Reactive extrusion) [4].

Chain extender is a multifunctional material that creates free radicals in the polymer processing temperature, and could create connections between itself and any part of the backbone.

Among these approaches the last one is the best; because the amount of entanglement could be easily controlled by changing the dose of adding a chain extender [1].

Hence, the effect of adding Styrene Maleic Anhydride (SMA) with the Oxirane contain accelerator on the complex viscosity has been investigated with Rheological Mechanical Spectroscopy (RMS) in the linear viscoelasticity region (LVE).

Experimental

First of all, all the materials were heated at 90 °C for two hours in the oven, based on the formulation (listed in

Table I. Formulation of sample preparation.

Sample code	Nylon-6	SMA 1	SMA 2	Accelerator
Virgin	50	0	0	0
221	48.75	0.5	0.5	0.25
220	49	0.5	0.5	0

Table I) they extruded in a micro-compounder at 250 °C at 50 rpm speed, for preparing the rheometric samples, they were pressed at 250 °C for 10 min.

Rheological properties have been investigated by MCR 501S in the presence of nitrogen gas at 250 °C at the period of 0.03-628 rad/s with the 1 strain amplitude.

Results and Discussion

The melt complex viscosity of various content of chain extender and accelerator is shown in Figure, by using the Carreau model (Eq. (1)), some valuable parameters such as Zero shear viscosity, Relaxation time, and Power law index could be extrapolated. and the effect of changing of polymer's structure could be investigated by these parameters.

Obviously, the chain extender and accelerator had a synergism effect, but the accelerator had more effect on the change of Nylon structure.

Zero shear viscosity (η_0) is related to weight average molecular weight (M_w), so the sample with chain extender and accelerator (221), has increased approximately 4.28 times more than the neat sample; which showed increasing molecular weight, on the other side the sample without accelerator (220), shown lower η_0 (about 2.68 times lower) than the neat sample. (Table II-Fig. 1). Another parameter that could be related to the effect of molecular weight on

Table II. Driven data from Carreau model.

Sample code	η_0 (Pa.S)	λ	Power law index	Deborah number
Virgin	408.64	$\frac{27.7}{7}$	0.22	0.15
221	1747.00	$\frac{46.7}{7}$	0.19	0.26
220	152.66	4.42	0.13	0.02

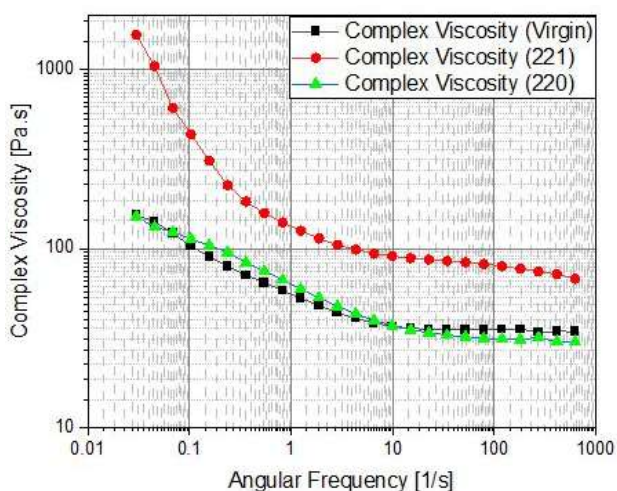


Fig. 1. Complex viscosity of sample with different content of chain extenders and accelerator.

the rheological properties of polymers, is relaxation time (λ). Shown the sample with chain extender and accelerator (221), had the longest relaxation among the other samples. Deborah number (De) is a nondimensional parameter that shows the behavior of polymer in terms of relaxation and processing time. According to obtained data from the Carreau model (Table II), sample 221 shows more elastic behavior than the other samples.

The power law index is a Criterion of polymer behavior in terms of different shear rates. Sample 221 shows the lowest Power law index, which means the slope of its decreed is the most than others. The above proved that the elastic portion of the polymer increased.

$$\eta(\dot{\gamma}) = [1 + (\lambda\dot{\gamma})^a]^{\frac{(n-1)}{a}} \times (\eta_0 - \eta_\infty) + \eta_\infty \quad (1)$$

Conclusion

Test results show the syncretistic effect of SMA and accelerator on chain branching of nylon 6. The polymer structure shift toward creating Long Chain Branching (LCB) on the polymer backbone, which caused increasing Zero shear viscosity (η_0), longest Relaxation time (λ), and Deborah number, on the other side power law index, decreased. Which could be concluded that the elastic portion of the polymer increased.

References

- [1] M. Xu, H. Yan, Q. He, C. Wan, T. Liu, L. Zhao, and C.B. Park, "Chain extension of polyamide 6 using multifunctional chain extenders and reactive extrusion for melt foaming", *Eur. Polym. J.*, **96**, 210-220, 2017.
- [2] Z. Osváth, A. Szöke, S. Pásztor, G. Szarka, L.B. Závoczki, and B. Iván, "Post-polymerization heat effect in the production of polyamide 6 by bulk quasiling anionic ring-opening polymerization of ϵ -caprolactam with industrial components: A green processing technique", *Processes*, **8**, 1-13, 2020.
- [3] X. Han, Y. Hu, M. Tang, H. Fang, Q. Wu, and Z. Wang, "Preparation and characterization of long chain branched polycarbonates with significantly enhanced environmental stress cracking behavior through gamma radiation with the addition of difunctional monomer", *Polym. Chem.*, **7**, 3551-3561, 2016.
- [4] J. Benz and C. Bonten, "Reactive extrusion of PA6-Different ways to increase the viscosity", *AIP Conf. Procc.*, **2055**, 6-11, 2019.

Experimental Investigation and simulation of a Drag Reducing Agent on the Pressure Drop and Heat Transfer of Gasoline

Vahid Oroujpour^{1*}, Ahamd Ramezani S.A², Smaeil Valizadeh³, and Mojtaba Matloub Moghaddam²

1. Tehran University, Tehran, Iran

2. Sharif University of Technology, Tehran, Iran

3. Khaje Nasir University of Technology, Tehran, Iran

*nksgostareazar@gmail.com

Abstract

In the present research, firstly, the laboratory module containing coil and long copper tube, pump, flowmeter, pressure gauge and temperature sensors was installed and the circuit was set up and it has been validated with water. In the continuation the effect of increasing a polymer with high molecular weight on the pressure drop of gasoline, as well as the simulation results of the pressure drop and heat transfer of these fluids with Ansys CFX software are presented. The results show that the concentration of 100 ppm of dodecylbenzene sulfonate as a surfactant in gasoline and the dissolution of 30-40 PPM of polyisobutylene with a molecular mass of 0.1 million did not cause a significant decrease in pressure drop, which is probably related to their low molecular mass, but the dissolution of 30-40 PPM of poly Isobutylene with a molecular mass of 1.2 million shows a 15% reduction in gasoline with a molecular mass of 1.2 million.

Keywords: non Newtonian fluid, drag reducing agent, CFD simulation, pressure drop, hat transfer

Introduction

Drag is a mechanical force that arises as a result of the reaction between a solid body and a moving fluid or vice versa. The problem of reducing the resistance force against the movement of objects inside a fluid, and as a result, the possibility of reaching higher speeds and also reducing fuel consumption, or the energy resources needed for the movement of the object, has been the concern of researchers for a long time [1]. On the other hand, the reduction of resistance or drag, in addition to the above, leads to the possibility of traveling longer distances for less frequent refueling, less pollution of the environment, as well as increasing the service life of the equipment.

Theoretical

The actual mechanism of reducing the friction of the fluid inside the pipe to which the friction reducer is added is still not fully understood, but what is known is that the addition of the friction reducing agent to the fluid appears to change the turbulence regime of the fluid inside the pipe. Masses of fluid separate from one area and go to another area are called strike. When these striks move from under the smooth viscous layer towards the buffer layer, they begin to form a vortex and oscillate in this area. These vortices are finally broken and thrown into the core of the flow, causing the turbulence of the turbulent fluid to become more advanced [1]. Reducing drag means reducing the surface friction coefficient, which improves the speed profile and shear stress distribution in the boundary layer. The concept of drag reduction in crude oil transmission lines has been successfully applied for the first time in

Alaska and Norway. Adding polymer causes the following changes [2]:

1. The thickness of the resistant layer increases and covers the logarithmic area.
2. The slope of the velocity profile increases almost in the logarithmic region at low Reynolds numbers.

Mechanism of Action of DRA

In recent years, many articles have discussed about the theoretical, numerical and experimental aspects of the effect of polymer additives on reducing drag in turbulent flows, all of which support the reduction of turbulence and turbulence in such flows if a small amount of polymer is used (Fig. 1). In fact, due to being heavy, these polymers move towards the wall, which has a lower speed, and due to the low coefficient of friction of polymers, friction and hydraulic pressure drop are also reduced [2].

Experimental

At first, the electric valve is started so that the fluid moves from the storage tank to the bed by the pump and in this phase, data collection of hydraulic pressure drop is done for cold conditions. After 1 s, the electric heater is turned on so that the substrate is heated (about 5 s) and ready for data

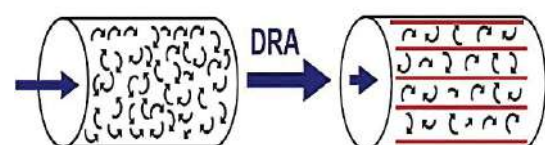


Fig. 1. Schematic of the mechanism of operation of DRA [1].

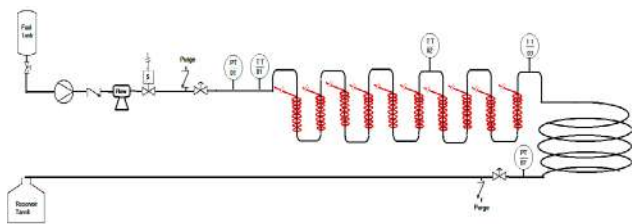


Fig. 2. Schematic of heat transfer and fuel pressure drop test.

collection for the heated state. After calibrating the measuring equipment, by adjusting the pressure of the environment and the tube to be tested, heat flux that enters the tube is adjusted by an electric heater, and then the amount of refrigerant flow that passes through the tube is determined. The conditions are also measured with the temperature and pressure sensor of the coolant before and after passing. Due to the lack of the desired additive, the maximum total test time is 15 s (Fig. 2).

Results and Discussion

In this test, a polymer with a molecular mass of 1.5 million was used as a friction reducing agent with a concentration of 50 ppm. At first, the test was done with pure fuel, which is needed for comparison with DRA + fuel test. In order to ensure the repeatability of these results, each of the tests was performed twice, and the result showed that there is complete repeatability. In the Fig. 3, the results related to the input and output pressure for pure fuel and also the results related to fuel + DRA are shown. The pressure fluctuations are acceptable at around 0.3 bar, which is caused by the pump's natural oscillation. The results of pressure drop for pure fuel and fuel + DRA can be seen in the figure below, which has reached from 8.15 bar pressure drop for pure fuel to 6.85 bar for DRA + fuel, which shows a 15% reduction in pressure drop. This result is in good agreement with the results of scientific authorities, and with the increase of the molecular sanctuary to about 3 million to 4 million, there is hope for a reduction of up to 30%.

Simulation

CFD was done with Ansys CFX 16 for 2 situation of with and without DRA (conductivity of fluid= decrease, friction factor of fluid=decrease, Viscosity of fluide=pawerlaw

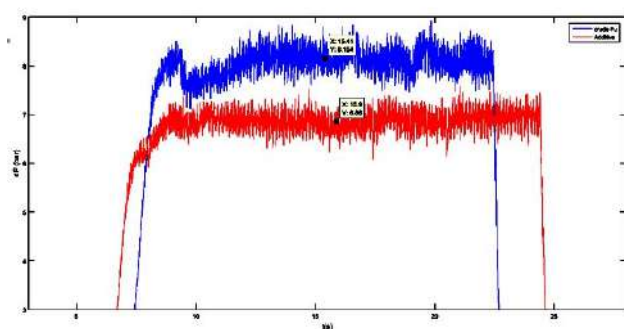


Fig. 3. Pressure drop for With (up) and without (down) DRA.

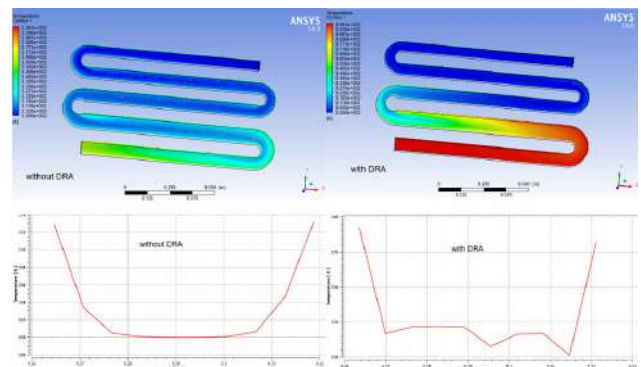


Fig. 4. Temperature profile.

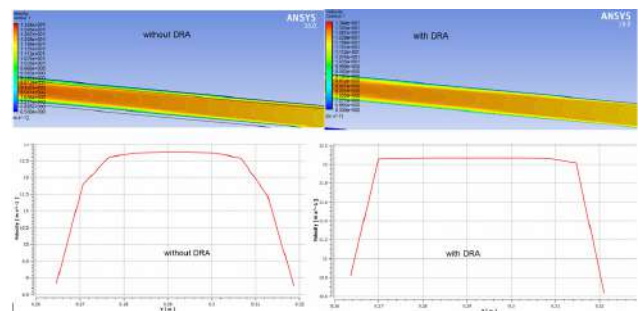


Fig. 5. Velocity profile.

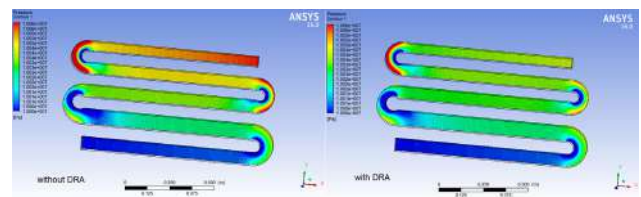


Fig. 6. Pressure profile.

[4]). Results show that pressure drop reduced 30% and haet transfer increased 28% (Figs. 4, 5, and 6).

References

- [1] M.J. Od Dinoil, "Soloube drag reducing polymers", *J. Polym. Mater.*, 1994.
- [2] K.B. Konovalov, V.D. Gaponov, and V.N. Manzhai, "Drag reduction in jet engines fuel supply systems", *Int. J. Adv. Sci. Eng. Technol.*, 2014.
- [3] M. Baou, M. Norouzi, and A. Jabari-Moghadam, "Numerical investigation of hydrodynamic and thermal Falkner–Skan boundary layer of viscoelastic fluids", *Modares Mech. Eng.*, **16**, 69-78, 2016.
- [4] Z. Lalehgani and A. Ramazani S.A, "Emulsion polymerization of triple monomers of acrylamide, maleic anhydride, and styrene to achieve highly hydrophilic–hydrophobic modified polyacrylamide", *J. Appl. Polym. Sci.*, 2019.



On the Relaxation Spectra of Ionically Cross-linked and Unmodified Polypropylene Blends

Hussain Namvar Maroofy and Mohammad-Javad Hafezi*

Department of Polymer Engineering and Color Technology, Amirkabir University of Technology, Tehran, Iran

*hafezi@aut.ac.ir

Abstract

In this research, we study the morphology-dependent rheology of a novel blend comprising ionically cross-linked polypropylene (icPP) and unmodified PP. Employing a batch melt-mixing process, we prepare samples with four different concentrations of the cross-linked PP counterpart. Surprisingly, the sample with 57.5 wt% icPP content shows synergistic properties in the high angular frequency range of complex viscosity and exhibits a characteristic relaxation peak in its relaxation spectrum; it can be attributed to the morphological transition from a co-continuous structure to a three-dimensional network of percolated cross-linked PP particles interconnected via ligaments. This alteration in morphology leads to the observed changes in rheological properties, promising new opportunities for material design and applications.

Keywords: polypropylene, ionic cross-linking, relaxation spectra, TPV, polymer blend

Introduction

Among the most widely used plastics, PP plays a significant role in various industries. However, its environmental impact has raised concerns, prompting a pressing need for effective recycling strategies. Recycled polypropylenes exhibit inferior properties compared to pristine materials due to their degradation mechanisms. Cross-linking is an effective strategy for enhancing the processing and mechanical properties of recycled plastics but is not reversible in general approaches. Ionic cross-linking as a thermally reversible procedure to overcome this problem provides re-processibility for the cross-linked systems [1]. On the other hand, blending virgin polymers with recycled plastics is a common method for making use of recycled plastics in the line of production. In this work, we have studied the ionic cross-linking of polypropylene and then blended it with virgin polypropylene. The rheological properties of the blends have been investigated. Based on the rheological experiments, the relaxation spectra of the samples have been studied to further understand the morphologies. A hypothesis is proposed to shed light on the mechanisms controlling the observed synergism in one of the samples.

Experimental

Materials. Two grades of polypropylene, Jampilen RP120L (terpolymer, MFI=6 g/10min, Vicat softening point=118 °C) and Jampilen HP510L (homopolymer, MFI=6 g/10min, Vicat softening point=152 °C) were used for ionic cross-linking and blending, respectively. Dicumyl peroxide (DCP), maleic anhydride (MAH), Irganox 1010, and Irgafos 168 as antioxidants and stearic acid were used without further purification. Zinc oxide (ZnO, Pharma 950, 99.91% purity) was kindly provided by Sepid Oxide

Shokuhie.

Sample Preparation. Ionic cross-linking of RP120L was conducted in an internal mixer; melt mixing of the PP with 4 wt% DCP, 4 wt% MAH, and 0.4 wt% of each of the antioxidants was performed at 150 °C and 30 rpm for 7 min to graft MAH groups. Subsequently, the temperature was raised to 180 °C at the rate of 10 °C/min and 5 phr of ZnO and 7.5 phr of stearic acid were added to cross-link the PP; the mixing continued until a plateau torque was obtained. Finally, to prepare the blends, icPP was mixed with HP510L for 5 min at 180 °C and 30 rpm in four concentrations: 82.5, 70, 57.5, and 45 wt%.

Dynamic viscoelasticity. Frequency sweep testing (Anton Paar MCR 302) was performed on the samples with a parallel-plate geometry to obtain the dynamic data in oscillatory shear mode over the angular frequency range of 0.1 rad/s to 628 rad/s, strain amplitude of 0.5%, at 180 °C, and under N₂ atmosphere.

Results and Discussion

Fig. 1 shows the complex viscosity of the samples; in the low-frequency region, blended samples exhibit a linear relationship in viscosity with the concentration of icPP. However, in the high-frequency region, all samples, save for the sample with 57.5 wt% icPP (namely B3 as of here), have similar viscosities.

B3 behaves out of the ordinary and exhibits a pseudo-plateau in the mid-frequencies, and also a considerably higher viscosity in the high-frequency region. This is an indication that a different relaxation mechanism is at work for this sample in the mid-and high-frequency region than other samples. RepTate rheology software was used to obtain the relaxation spectra of the samples from the dynamic viscoelastic data [2,3]. Fig. 2 shows the relaxation

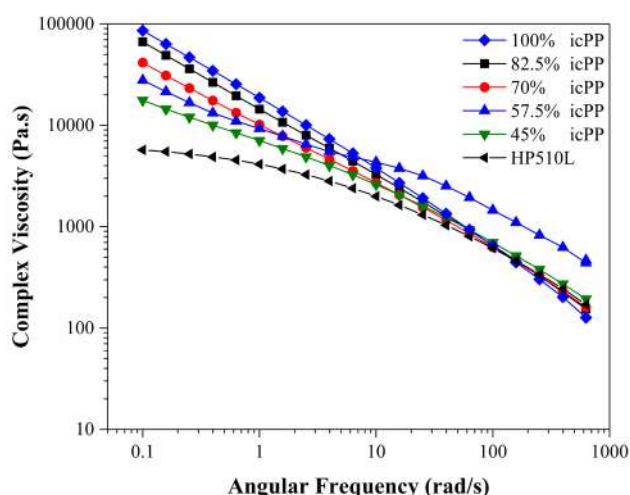


Fig. 1. Complex viscosity of cross-linked (100% icPP), unmodified (HP510L), and blended (82.5, 70, 57.5, and 45 wt% icPP) samples.

spectra of the samples. A prominent new peak can be observed for B3 in the $\lambda=0.01-0.1$ s region which is weakly present for other blend compositions. The peak at circa 10 s, characteristic of samples with higher icPP content, has faded away completely for B3 and lower concentrations. Goharpey *et al.* have reported a similar behavior in the relaxation spectrum of PP/EPDM blends at a critical concentration and attributed this to the percolation of cross-linked rubber particles [4]. Saha *et al.* have reported synergism in the dynamic viscoelastic properties of PVDF/HNBR blends for a specific concentration range and attributed this phenomenon to the rubber particles' percolation too; in contrast to our results, the synergism is reported for the low-frequency region. They also reported that the percolated rubber particles are interconnected via ligaments at these concentrations [5]. Based on these results, it can be hypothesized that the mentioned peak in B3 is due to the formation of a network that is median in nature; a miscible blend comprising both phases and connecting the

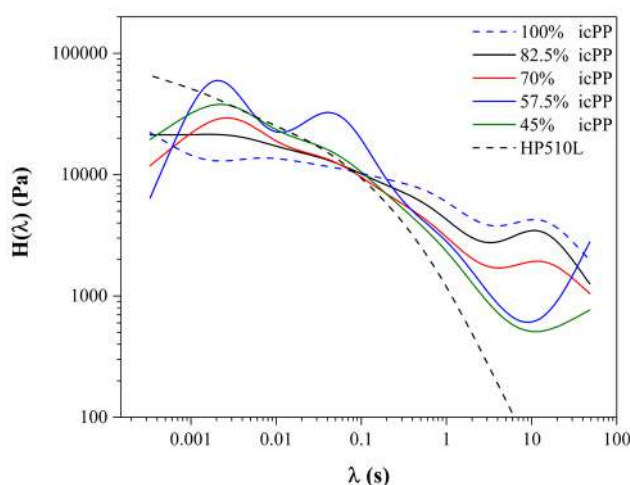


Fig. 2. Relaxation spectrum of cross-linked (100% icPP), unmodified (HP510L), and blended (82.5, 70, 57.5, and 45 wt% icPP) samples.

icPP particles as ligaments. With increasing the HP510L content, at a critical concentration, the icPP phase becomes the dispersed phase; while the concentration of icPP is high, the particles are closely dispersed in the system giving a chance for the interphases around the particles to connect and form ligaments. These ligaments perform as rubber bands connecting the icPP particles, exhibiting higher elasticity with increasing deformation rate (higher frequency) and explaining the observed behavior for the B3 sample.

Conclusion

Our investigation of blends of icPP and unmodified PP has concluded that synergism in the rheological properties of these blends can be observed in specific concentrations, relatable to the formation of a percolated structure of icPP particles interconnected with ligaments. This enhanced elasticity with higher deformation rates offers insights into the intricate behavior of the blend, shedding light on potential applications and underlying mechanisms.

References

- [1] S.-S. Choi, H.-M. Kwon, Y. Kim, J.W. Bae, and J.-S. Kim, "Characterization of maleic anhydride-grafted ethylene-propylene-diene terpolymer (MAH-g-EPDM) based thermoplastic elastomers by formation of zinc ionomer", *J. Ind. Eng. Chem.*, **19**, 1990-1995, 2013.
- [2] V.A.H. Boudara, D.J. Read, and J. Ramirez, "RepTate rheology software: Toolkit for the analysis of theories and experiments", *J. Rheol. (N. Y. N. Y.)*, **64**, 709-722, 2020.
- [3] A. Takeh and S. Shanbhag, "A computer program to extract the continuous and discrete relaxation spectra from dynamic viscoelastic measurements", *Appl. Rheol.*, **23**, 24628, 2013.
- [4] F. Goharpey, H. Nazockdast, and A.A. Katbab, "Relationship between the rheology and morphology of dynamically vulcanized thermoplastic elastomers based on EPDM/PP", *Polym. Eng. Sci.*, **45**, 84-94, 2005.
- [5] S. Saha and A.K. Bhowmick, "Effect of structure development on the rheological properties of PVDF/HNBR-based thermoplastic elastomer and its vulcanizates", *J. Appl. Polym. Sci.*, **137**, 48758, 2020.

Effect of Organoclay on the Rheology and Morphology of Poly(lactic acid) and Natural Rubber Blend

Mohammad Hesam Alemi and Azam Jalali-Arani*

Department of Polymer Engineering and Color Technology, Amirkabir University of Technology, Tehran, Iran

*ajalali@aut.ac.ir

Abstract

In this study, samples of polylactic acid and natural rubber (PLA/NR; 90/10) containing different amounts of nanoclay were prepared by melt mixing method. The rheology and morphology of the samples were investigated. The obtained results showed that the terminal slope for storage moduli rapidly decreased with the clay content and was almost constant above 3 wt%. The droplet size of the dispersed phase of NR in the presence of nanoparticles first decreased and then remained constant with increasing clay. The critical concentration of the clay was found to be between 3 wt% to 5 wt%. In addition, the distribution of dispersed phase (polydispersity index, PI) is almost constant, suggesting a stable morphology of dispersed phase, regardless of the clay content.

Keywords: polylactic acid, biodegradable, morphology, polymer blend, melt mixing

Introduction

The potential of poly(lactic acid) (PLA) as an ecofriendly alternative to non-biodegradable plastics is evident due to its biodegradability, biocompatibility, thermal stability, and processability. However, PLA faces challenges such as brittleness, slow degradation, and low melt strength that limit its industrial applications [1]. To address these limitations, blending of PLA with the flexible elastomer, natural rubber (NR) is a solution, however, blending PLA with an elastomer reduces its modulus, therefore a nanoparticle can be used to partially compensate for the modulus reduction [2]. Clay is a mineral that has a silicate layered structure and is found abundantly in nature. The surface modification of clay layers with organic materials makes it possible to use organic clay as a reinforcement in polymers. Modification of clay increases its compatibility with polymer materials. Past studies have explored the impact of organoclays on various properties of PLA and natural rubber blends, including mechanical strength, barrier properties, crystallinity, and thermal stability. Despite these researchs, there is no comprehensive understanding of the mechanisms behind the structural changes and morphological development caused by this nanoparticles. This knowledge is very important to control the blending process and achieve the desired properties for practical applications. In essence, the blending PLA with natural rubber and the use of organoclay as a compatibilizer provide solutions to enhance the performance of PLA-based materials. Further investigation is needed to uncover the precise mechanisms driving the improvements observed in these blends [3]. In this research, with the aim of achieving a better understanding of how clay affects the compatibility and properties of PLA/NR, the rheology of this mixture has

been investigated in the presence of closite 30B.

Experimental

Ingeo PLA 4032D biopolymer was purchased from NatureWorks (Minnesota, USA). Natural rubber (Thailand) and organoclay (Closite 30B) from Southern clay product (USA) were used. All samples were dried in a vacuum oven for 12 h at 70 °C. Melt compounding was carried out with an internal mixer (RheoSense, Iran) for 12 min at 160 °C. Linear rheological properties were measured with a 25 mm parallel plate fixture at 180 °C, using a rheometric spectrometer MCR 302 model (Anton paar, Austria). A scanning electron microscope (SEM) (AIS2100, South Korea) was employed to study the morphology of the cryogenically fractured surface of the samples. Average number (D_n), average volume-to-surface diameter (D_{vs}) and polydispersity index (PI) were measured for at least 150 droplets using ImageJ software; as follows:

$$D_n = \frac{\sum n_i D_i}{\sum n_i} \quad (1)$$

$$D_{vs} = \frac{\sum n_i D_i^3}{\sum n_i D_i^2} \quad (2)$$

$$PI = D_{vs} / D_n \quad (3)$$

Results and Discussion

Fig. 1a shows the storage modulus of the blend and nanocomposites (PNCs) containing C30B. The storage modulus of the blend gradually increased as the clay content increased. The terminal slope for storage moduli rapidly decreased with the clay content and became almost constant above 3 wt%, displaying a certain transitional

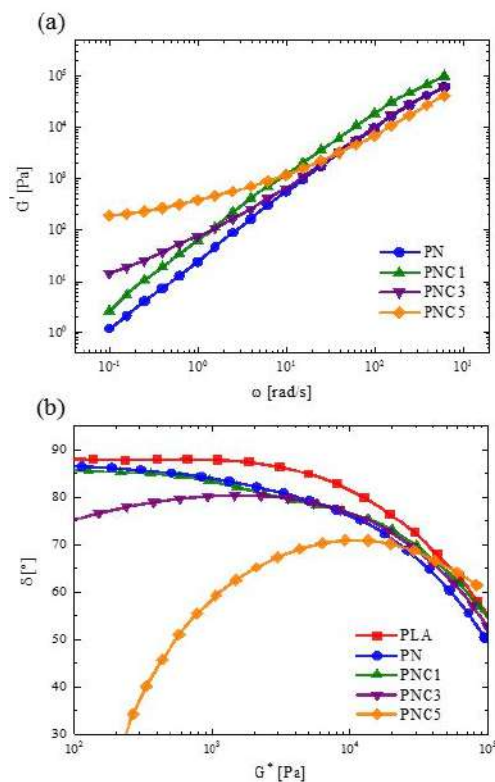


Fig. 1. The variation of storage modulus against frequency (a) and Van Gurp-Palmen plots (b) of neat blend and its nanocomposites.

behavior (as known as liquid-like to solid-like transition) of the PLA/NR blends depending on the clay content. In general, the increase in the moduli of the complex system (i.e., polymer nanocomposites, polymer blends, particulate suspension, etc.) in terminal region strongly reflects the network formation between the components. This liquid-solid transition can be determined from the Van Gurp-Palmen plots of the nanocomposites. The Van Gurp-Palmen plot relates the absolute value of the

complex modulus (G^*) to the loss angle (δ), where the liquid-like behavior of melt is indicated by $\lim_{G^* \rightarrow 0} \delta = 90^\circ$ while for a solid-like behavior, δ drops towards zero when approaching the plateau modulus G_0 at low frequencies. As the C30B loading is increased, δ deviates from 90° in the low modulus region. This deviation becomes more pronounced for the blend with 5 wt% C30B (PNC5). Therefore, the C30B percolation threshold in PLA/NR

Table I. D_n , D_{vs} , and PI of the neat blend and its nanocomposites with various content of C30B (1, 3, and 5 wt%).

Sample	D_n (μm)	D_{vs} (μm)	PI
PN	1.62	2.26	1.39
PNC1	1.23	1.59	1.29
PNC3	0.76	0.98	1.29
PNC5	0.75	0.99	1.31

blend is between 3 wt% to 5 wt%. The droplet size of the dispersed NR phase (D_n) initially decreased and then remained constant as the clay content increased, however the distribution of dispersed phase (Polydispersity index, PI) presented in Table I, is almost constant, regardless of clay content, indicating a stable morphology of the dispersed phase [4].

Conclusion

The rheological and morphological study of PLA/NR (90/10) blend filled with various amounts of organoclay showed that solid-like behavior occurs at a concentration higher than 3 wt% of organoclay and the percolation threshold was between 3 wt% to 5 wt% of organoclay. The presence of nanoclay decreased the size of dispersed phase droplets. In addition, the polydispersity index decreased but remained constant with increasing organoclay content.

References

- [1] E. Castro-Aguirre, F. Iñiguez-Franco, H. Samsudin, X. Fang, and R. Auras, *Adv. Drug Deliv. Rev.*, **107**, 333–366, 2016.
- [2] N. Bitinis et al., *Appl. Clay Sci.*, **93-94**, 78-84, 2014.
- [3] S. Cho, J.S. Hong, S.J. Lee, K.H. Ahn, J.A. Covas, and J.M. Maia, *Macromol. Mater. Eng.*, **296**, 341-348, 2011.
- [4] H.G. Ock, K.H. Ahn, S.J. Lee, and K. Hyun, *Macromolecules*, **49**, pp. 2832-2842, 2016.

Evaluation of Rheological and Mechanical Properties of SR/EPDM Blend in the Presence of Graphene

Zahra Kheirabadi, Azam Jalali-Arani*, and Hamid Garmabi
Amirkabir University of Technology, Tehran, Iran

*ajalali@aut.ac.ir

Abstract

In this study, blends of silicone rubber (SR) and Ethylene propylene diene monomer rubber (EPDM) in the presence different amounts of graphene nanosheets (GNS) were prepared in an internal mixer and the effects of GNS loading on the rheological and mechanical properties of SR/EPDM (50/50) were studied. The obtained results showed an increase in the complex viscosity and storage modulus of the compound by introduction of GNS and increasing its amount. It was attributed to the GNS-polymer interaction. However, the use of GNS caused the reduction of tensile strength of the vulcanized samples. Which might be related to the effect of GNS on crosslinking density of the vulcanized compound.

Keywords: silicone rubber, EPDM rubber, blend, graphene nanosheets, rheological properties

Introduction

Nanofillers have been received exceptional interest in the fabrication of polymer composites due to their high surface area providing much more favorable interactions with the matrix, and thereby giving rise to much-enhanced properties. Among nano fillers, Graphene nanosheets (GNS) have recently generated tremendous excitement due to its unique structure. The introduction of GNS into elastomeric matrix has generated enormous activities in many fields of science and engineering, as it provides a significant improvement in the physical and mechanical properties of various host matrixes such as silicone rubber [1]. SR or polydimethylsiloxane (PDMS), as a well-known high temperature-resistance synthetic elastomer, has been widely used in various industrial fields due to its superb properties including nontoxicity, biocompatibility, flexibility, ease of fabrication, thermal stability, low-temperature toughness, and electrical insulating [2]. However, large-scale implementation of silicone rubber is restricted because of its poor mechanical properties including stiffness and tensile strength, therefore it is usually blended with other polymers such as EPDM rubber or reinforced with fillers to overcome these deficiencies [3]. Electrically conductive silicone rubbers are generally used in flexible electronics and sensors [4]. In this work blends of (SR/EPDM, 50/50) reinforced with GNS and the effect of GNS on the rheological and mechanical properties of the blend was investigated.

Experimental Materials

Materials including silicone rubber (DJ Silicone, NE 7180),

EPDM rubber (kep 270) ethylene contents: 56.5 ± 3.5 wt% – ENB contents: 4.5 ± 1 wt%, GNS (thickness: 5-10 nm), dicumil peroxide (98%) as a curing agent and silane (si-69) as a coupling agent were used in this work.

Preparation and Characterization

The composite samples were prepared in a laboratory-size internal mixer. Various amounts of graphene (0, 0.1, 1, and 1.78 wt%) were used in the samples. Table I shows the formulation of the samples. To achieve a uniform dispersion of GNSs in the matrix, it was added into the masticated SR at 130 °C and then the coupling agent was added. EPDM rubber introduced to the compound in the final stage. A laboratory-size two-roll mill was employed to mix DCP as the curing agent with the compound. The obtained compound cured in a hot press at a temperature of 155 °C for 20 min.

Rheological measurements were performed using Rheometric mechanical spectroscopy (RMS) at 160 °C. The tensile properties of the samples were measured by a Universal Tensile Testing machine at a speed of 500 mm/min according to the ASTM D412 standard test method.

Table I. Formulation of the prepared samples.

Sample code	SR/EPDM	GNS*	Silane*	DCP*
SR50/G0	50/50	0	0	2.5
SR50/G0.1si	50/50	0.1	0.1	2.5
SR50/G1si	50/50	1	0.1	2.5
SR50/G1.78si	50/50	1.78	0.1	2.5

*Phr

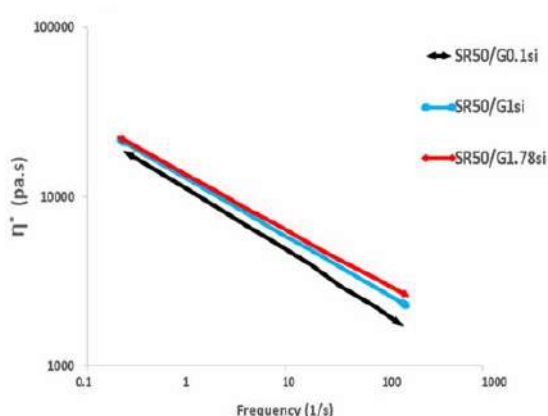


Fig. 1. Angular frequency dependence of complex viscosity (η^*) of the SR/EPDM nanocomposite samples at 160 °C.

Results and Discussion

Rheological Properties

The complex viscosity (η^*) variation of the samples is depicted in Fig. 1. It is observed that the η^* at low frequencies increases with graphene loading, it can be attributed to the rubber-graphene and graphene-graphene interactions, restricting the segmental chain mobility of rubber matrix. At high frequencies, all samples show a shear thinning behavior. The variations of storage modulus (G') and loss modulus (G'') are presented in Fig. 2. The changes of G' are more noticeable than G'' , due to its greater sensitivity to frequency. G' values increased significantly in the entire frequency range with the rise of GNS loading; however, the effect of GNS content is more substantial at low frequencies. This observation is stemmed from graphene, having higher modulus compared to rubber matrix. While the increase in G'' is lower than G' , a similar trend is observed for G'' values, which can be attributed to the formation of an inter-connected graphene network in the polymer matrix that restrains the long-range motion of polymer chains.

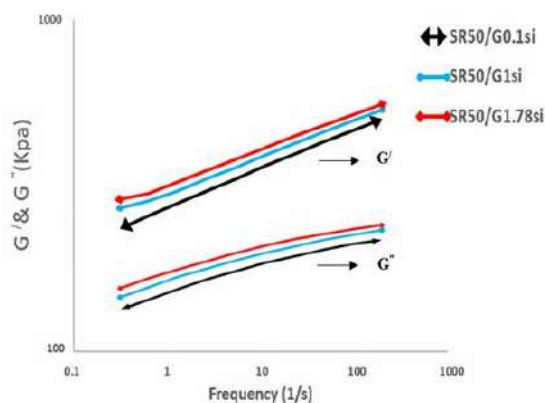


Fig. 2. Angular frequency dependence of storage modulus (G') and loss modulus (G'') of SR/EPDM nanocomposite samples at 160 °C.

Table II. Tensile strength of samples.

Sample code	Tensile strength (N/mm ²)
SR50/G0.1si	4.88
SR50/G1si	4.67
SR50/G1.78si	3.82

Tensile Properties

The results of tensile strength of the samples are illustrated in Table II. As it is obvious from the table, tensile strength (TS) monotonically decreased with the GNS content in the samples. This reduction might be related to the effect of GNS on the crosslinking density of the compound which was observed in the curing rheometry test (not reported here).

Conclusion

The influence of graphene nanosheets on properties of SR/EPDM blends was investigated. Rheological results showed that owing to the interaction between nanofiller and polymer chain, the segmental mobility of rubber matrix was restricted, and therefore the complex viscosity and storage modulus increased. It was also found that in the presence of GNS, the tensile strength of the samples decreased; due to the effect of GNS upon crosslinking density of the compound.

References

- [1] E. Esmizade et al., "Preparation and characterization of silicone rubber/graphene nanosheets nanocomposites by in-situ loading of the coupling agent", *J. Compos. Mater.*, **53**, 2019.
- [2] B. Pradhan et al., "Synergistic effect of three-dimensional multi-walled carbon nanotube-graphene nanofiller in enhancing the mechanical and thermal properties of high-performance silicone rubber", *Polym. Int.*, **63**, 2014
- [3] S. Azizi et al., "Performance improvement of EPDM and EPDM/Silicone rubber composites using modified fumed silica, titanium dioxide and graphene additives", *Polym. Test.*, **84**, 2019
- [4] Z. Qianqian et al., "Effects of graphene on various properties and applications of silicone rubber and silicone resin", *Compos. Part A*, **142**, 2021.

Simulation of Temperature Profile and Its Effect on Warpage in Fused Deposition Modeling Method

Nastaran Mosleh, Soheil Dariushi*, and Masoud Esfandeh

Composites Department, Iran Polymer and Petrochemical Institute, Pazhoohesh Blvd., 149771311, Tehran, Iran

*s.dariushi@ippi.ac.ir

Abstract

Acrylonitrile butadiene styrene, abbreviated as ABS, is a common thermoplastic filament used in fused filament fabrication (FFF) 3D printing method. Unfortunately, the printed object with this material tends to warp from the build plate during printing because of a large variation in specific volume with a temperature change. In this paper, the FFF 3D printing process and the temperature profile with and without heated bed were simulated with COMSOL Multiphysics software and the warpage phenomenon was investigated. For this purpose, the momentum and level set equations were used to model flow behavior and energy balance was also applied to obtain temperature profile in printed strand.

Keywords: Simulation, fused filament fabrication, 3D printing, warpage, temperature profile

Introduction

FFF is a common 3D printing method that makes parts by adding molten thermoplastic polymer layer by layer. ABS is one of the thermoplastic filaments with good thermal resistance and high strength. The disadvantage of this material (during printing) is warpage and peel off the build plate. The warpage problem occurs because of expansion and contraction of polymer in a molten and solid-state, respectively (Fig. 1). In fact, the specific volume in amorphous polymer changes sharply in glass transition temperature. In the case of a semi-crystalline polymer, the expansion and contraction occur more significantly than amorphous polymer because of the considerable shrinkage related to crystallization phenomena. In recent years, some researches have been done to model temperature profile and crystallization in 3D printed parts. Verma *et al.* [1] simulated flow behavior, heat transfer, and solidification of the deposited strand with CFD software. Kumar *et al.* [2] presented a model for heat transfer in the heat sink (before nozzle) in the filament transfer zone. Balani *et al.* [3] presented a model for coalescence and diffusion of printed PLA and PEEK strands with increasing the temperature

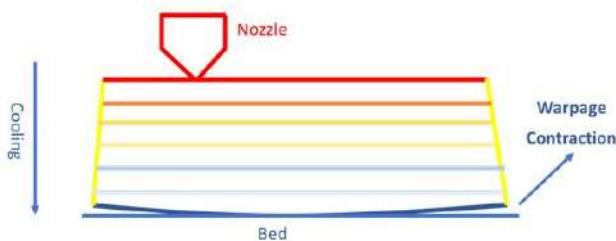


Fig. 1. Warpage phenomena.

in the FFF method. Brenken *et al.* [4] predicted residual stress related to the thermal history and crystallization phenomena of printed parts and showed that the results have good agreement with the obtained experimental data. In this paper, the flow behavior and temperature profile of molten ABS during printing were simulated by COMSOL Multiphysics software, and the effect of different heat bed temperatures on warpage phenomena was investigated.

Experimental/Theoretical

To evaluate the fluid flow in the FDM process, Eq. of motion (1) and continuity Eq. (2) inside the nozzle and in the gap between the nozzle and build platform were considered:

$$\rho \frac{\partial u}{\partial t} + \rho (u \cdot \nabla u) = -\nabla(pI + \mu(\nabla u + (\nabla u)^T)) + \rho g \quad (1)$$

$$\nabla \cdot u = 0 \quad (2)$$

In addition, it is necessary to use the coupling of the level set function (3) with the obtained velocity field to predict the front flow interface:

$$\frac{\partial \phi}{\partial t} + u \cdot \nabla \phi = \gamma \nabla \cdot (\epsilon \nabla \phi - \phi (1 - \phi) \frac{\nabla \phi}{|\nabla \phi|}) \quad (3)$$

The energy balance in nozzle and gap between the nozzle and bed is considered (Eq. (4)):

$$\rho C_p \frac{\partial T}{\partial t} + \rho C_p u \cdot \nabla T - k \nabla \cdot T = Q \quad (4)$$

Boundary conditions and process conditions are shown in Fig. 2. The material properties and the print condition were summarized in Table I.

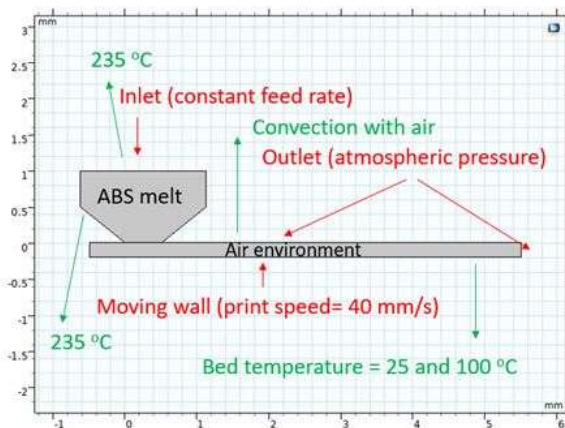


Fig. 2. Boundary conditions and process conditions.

Table I. The material properties and the print conditions.

Print condition	Value
Layer height	0.2 mm
Print speed	40 mm/s
Nozzle temperature	235 °C
Bed temperature	25 °C
ABS density	1154 kg/m ³
ABS thermal conductivity	0.128 W/m.K
ABS heat capacity	1600 J/kg.K
ABS viscosity	817 Pa.s

Results and Discussion

As can be seen in Table I, all process conditions including temperature, the gap between the nozzle and the build plate, and feed rate are constant and the only variable is the bed temperature. Results are considered for a printed strand with 4 mm length. Therefore, 0.2 s is required to print this strand for 40 mm/s print speed. As can be seen in Fig. 3, the different bed temperature (25 and 100 °C) causes the different temperature profiles. In high bed temperature, the minimum temperature is 99.8 °C and close to the glass transition temperature of ABS, but in low bed temperature, the deposited strand cools quickly and the minimum temperature in the domain is 25 °C that leads to warpage because of the fast contraction of the material.

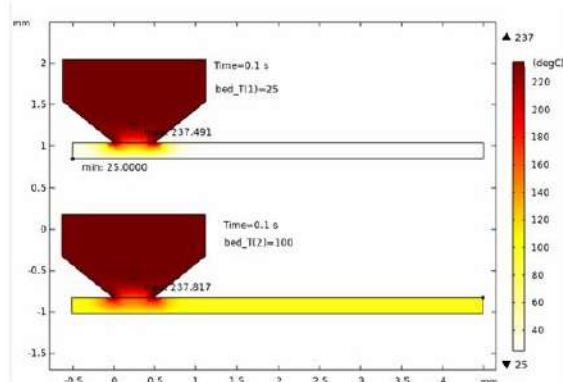


Fig. 3. The temperature profile in the gap between nozzle and bed.

Conclusion

In this study, the temperature profile of ABS in the nozzle and its deposition on the build platform in the FFF method were simulated. For modeling, the coupling of the equation of motion, the level set function, and energy balance were used. The simulation results showed that the increase of bed temperature reduces the warpage probability deposited strand because suitable strand temperature (above ABS glass transition temperature) prevents fast cooling and strand contraction. To overcome warpage problem and successful 3D printing, a heated bed over ABS glass transition temperature is recommended.

Acknowledgment

The authors would like to appreciate from Iran national science foundation (INSF) for its financial support. (Fund number: 99019781)

References

- [1]A. Verma et al., "Numerical simulation of extrusion additive manufacturing: fused deposition modeling", *Eng. Mater. Sci.*, **2018**, 118-121, 2018.
- [2]K.S.V. Munna Kumar and S.K. Nagpure, "Numerical simulation of rep-rap 3D printer liquefier to determine the thermal behavior of heat sink", *IJSRD-Int. J. Sci. Res. Dev.*, 92-101, 2017.
- [3]B.B. Shahriar et al., *Toward Improvement of the Properties of Parts Manufactured by FFF (Fused Filament Fabrication) through Understanding the Influence of Temperature and Rheological Behaviour on the Coalescence Phenomenon*, in AIP Conference Proceedings, AIP, 2017.
- [4]B. Brenken et al., "Development and validation of extrusion deposition additive manufacturing process simulations", *Addit. Manuf.*, **25**, 218-226, 2019.

On the Use of Non-Stick Coatings for Improving the Performance of Viscous Micropumps in Transporting Shear-Thinning Fluids

Mohammad Younes Heidari^{1*}, Saba Barghaman¹, Alireza Abdollahi¹, Mohammad Pourjafar²,
and Kayvan Sadeghy¹

1. University of Tehran, College of Engineering School of Mechanical Engineering, Tehran, Iran

2. Department of Mechanical Engineering, University of Tehran, Rezvanshahr, Iran

*myounesheydari@ut.ac.ir

Abstract

A cylinder rotating in a microchannel filled with a highly viscous fluid is known to generate a net flow provided it is placed in an off-center position across the channel. The mechanism works well for Newtonian fluids under creeping-flow conditions. For non-Newtonian fluids, however, a drop in performance has been reported in the literature. For shear-thinning fluids, for example, it is a well-established fact that the flow rate of the device is smaller than its Newtonian counterpart with its severity depending on the power-law index. In the present work, we numerically show that for shear-thinning fluids obeying the Power-Law model, the flow rate can be enhanced through coating the upper wall of the channel with a non-stick material. The effect is attributed to a dramatic change in flow structure. Specifically, the side vortices adjacent to the rotor are completely eliminated by this technique causing the flow rate to increase by twofold.

Keywords: viscous micropump, shear-thinning, power-law, slip

Introduction

It is a well-established fact that a cylinder rotating in an off-center position across a channel can be used as a viable option for the transport of Newtonian fluids [1-3]. The device is called “viscous micropump” and has the potential to be incorporated in micro-reactors for the production of new chemical compounds and/or in microfluidic systems dealing with physiological fluids. Studies carried out in the past have shown that the performance of the device is reduced for shear-thinning fluids [4], which is the dominant effect amongst non-Newtonian fluids. In the present work, we numerically show that for fluids exhibiting shear-thinning, it is possible to enhance the device performance, by coating the upper wall of the channel (i.e., the wall far from the rotor) with a non-stick coating so that the fluid slips at this wall. It is shown that this idea dramatically affects the size of the side vortices, thereby significantly increasing the flow rate.

Theory

Fig. 1 shows the flow geometry used for this study. The geometry comprises two fixed parallel plates of infinite

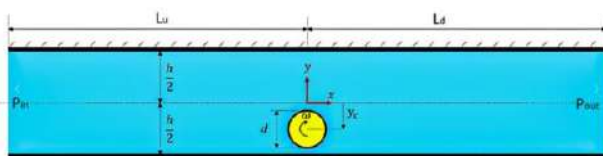


Fig. 1. Schematic showing the flow configuration.

width with the gap between them occupied by the liquid of interest. The channel is seen to incorporate a rigid cylinder of diameter D with its axis oriented in the z -direction, which is the neutral direction. The distance between the center of the cylinder and the axis of the channel has been denoted by y_c and for any $y_c \neq 0$, rotation of the cylinder generates a net flow, from left to right for the configuration depicted in Fig. 1. The geometry is similar to that used in the previous works [1]. The equations governing the flow are:

$$\rho \frac{Du}{Dt} = -\frac{\partial p}{\partial x} + \frac{\partial \tau_{xx}}{\partial x} + \frac{\partial \tau_{yx}}{\partial y}, \quad (1)$$

$$\rho \frac{Dv}{Dt} = -\frac{\partial p}{\partial x} + \frac{\partial \tau_{xx}}{\partial x} + \frac{\partial \tau_{yx}}{\partial y}, \quad (2)$$

$$\frac{\partial u}{\partial x} + \frac{\partial v}{\partial y} = 0, \quad (3)$$

where D/Dt is the material derivative. For shear-dependent fluids obeying the power-law model, the stress terms can be related to the velocity terms as:

$$\tau_{ij} = m |\Pi_{2d}|^{(n-1)/2} (2d_{ij}), \quad (4)$$

where τ_{ij} is the deviatoric stress tensor, and d_{ij} is the rate-of-deformation tensor with Π_{2d} being its second invariant. In this rheological model, m is the consistency index and n is the exponent signifying the degree of shear-thinning or shear-thickening of the fluid. For $n < 1$, the fluid is shear-

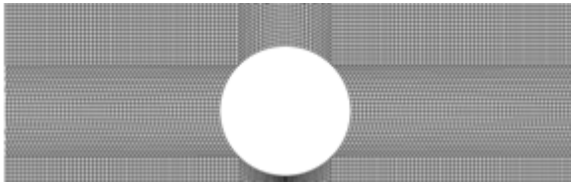


Fig. 2. A typical mesh used for the simulations ($S=3.5$).

thinning whereas for $n>1$, it is shear-thickening. The model reduces to Newtonian fluids by simply setting $n=1$.

Numerical Method

We have relied on the finite-element software package, COMSOL, for the simulations. Fig. 2 shows a typical mesh used for discretizing the domain. Mesh-independent results have been obtained using 10,000 elements. We are primarily interested in reporting the flow rate for different power-law index (n) with the focus laid mostly on $n<1$, results, i.e., the shear-thinning fluids. The parameter study involves two dimensionless geometrical parameters, i.e., the aspect ratio $S=h/d$, and the eccentricity $e=2y_c/(h-d)$. The rotational speed is the independent parameter, which is made dimensionless as: $\Omega = \rho\omega d^2/2\mu_{ref}$, where μ_{ref} is the reference viscosity (say, viscosity of water considered as the infinite-shear viscosity of the solution). As the velocity boundary conditions, on the rotor and also the upper/lower walls, we impose no-slip and no-penetration conditions. For the upper-wall, however, the no-slip condition is released at some point to investigate its effect on the average velocity (U). The pressures at inlet and outlet sections are assumed to be the same. Results will be presented in terms of U , normalized by the rotor surface velocity. We assume that the flow is occurring under creeping conditions, i.e., all convective inertial terms are dropped from the equations of motion.

Results and Discussion

Fig. 3 shows mesh-independent results for the average velocity covering a wide range of shear-thinning cases up to

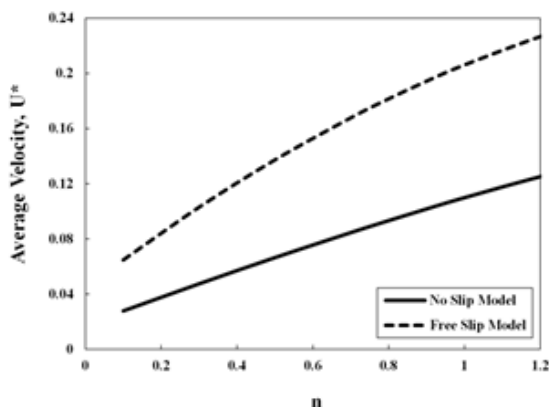


Fig. 3. Effect of slip boundary condition on the dimensionless average velocity (U^*) over a wide range of power-law index, n ($S=1.5$, $\epsilon=0.95$, $\Omega=1$, and $\Delta p^*=0$).

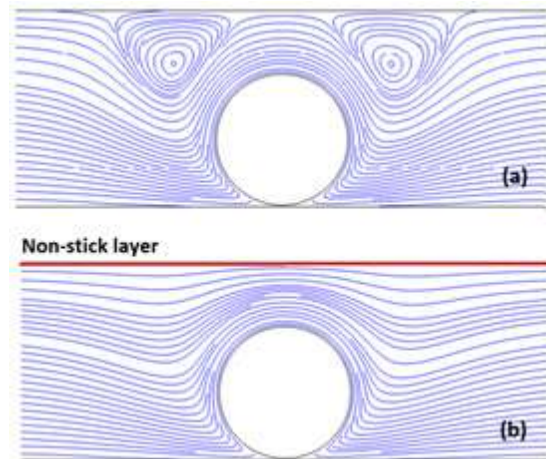


Fig. 4. Effect of the non-stick coating on the vortex structure this figure shows that by making the upper wall non-stick (cf. a with b), the side vortices are completely removed thereby increasing the flow rate ($n=0.5$, $S=1.5$, $\epsilon=0.95$, and $\Omega=1$).

$n=0.1$. According to this figure, by increasing n from $n=0.1$ to $n=1$ (i.e., the Newtonian case) the flow rate is increased. In other words, shear-thinning has a negative effect on the performance of viscous micropumps. On the other hand, if we go above $n=1$, so that the fluid becomes progressively more shear-thickening, the flow rate is increased. According to this figure, by coating the upper wall with a non-stick material, the two side vortices are completely eliminated. And this is the main reason why coating the upper wall with a non-stick material gives rise to a dramatic rise in the average velocity, or, equivalently, the flow rate.

Conclusion

Non-stick coatings can be used as an effective means to passively control the flow rate of viscous micropumps for transporting shear-thinning fluids.

References

- [1] M. Sen, D. Wajerski, and M. Gad-el-Hak, *J. Fluid. Eng.*, **118**, 624-627, 1996.
- [2] B. Taghilou et al., *J. Non-Newton. Fluid Mech.*, **291**, 104528, 2021.
- [3] M. Pourjafar et al., *J. Non-Newton. Fluid Mech.*, **308**, 104894, 2022.
- [4] B. Zhang, X. Liu, and J. Sun, *Struct. Multidiscip. Optim.*, **53**, 409-424, 2016.

Rheological Approach to Scaling Relations of Suspension Contains Anisotropic 2D Nanoparticles as Macromolecules

Atefeh Alimadadi¹, Mohamad Ali Sanjari Shahrezaei², and Seyed Hamed Aboutalebi^{2*}

1. Department of Polymer and Color Engineering, Amirkabir University of technology, Tehran, Iran
2. Condensed Matter National Laboratory, Institute for Research in Fundamental Sciences (IPM), Tehran, Iran

*hamed.aboutalebi@gmail.com

Abstract

The dimension (aspect ratio) of anisotropic nanoparticles is an important parameter that defines the liquid crystalline behavior of their suspensions. There are some models that correlate the intrinsic viscosity with the dimension of the particles. The usual method for measuring the intrinsic viscosity is the Ubbelohde viscometer. However, this method has some limitations, because the shear rate in the capillary is in the medium to high range. We suggest that the rheological data of non-Newtonian flow at low shear rates is more appropriate for calculating the intrinsic viscosity and provides a realistic estimation of the nanoparticle dimension.

Keywords: 2D nanoparticles, rheological measurements, suspension, viscometry, aspect ratio

Introduction

The viscosity of a polymer solution increases with the concentration and the molecular weight of the polymer. In the dilute regime, the viscosity of the solution is influenced by the hydrodynamic interactions and the excluded volume effects of the polymer chains. The molecular weight of the polymer chains can be estimated by measuring the intrinsic viscosity, according to the Mark-Houwink-Sakurada (MHS) equation. The molecular weight of a soluble polymer in the dilute regime is related to the intrinsic viscosity according to the MHS equation $[\eta] = KM_v^\alpha$ [1].

There are some assumptions for calculating the molecular weight using the MHS equation. To measure the intrinsic viscosity, the concentration of the solution must be very low ($c < c^*$) to ensure that there is no contact between the polymer molecules and that the hypothetical spheres that surround the coil-shaped polymer molecules can move and rotate freely and only have hydrodynamic effects on the solvent flow. In this case, the molecules do not interact with each other and the rheological behavior of the solution is independent of the shear rate. The range of shear rate in the Ubbelohde viscometer (0C code, which is usually used for polymer solutions) varies between 50–200 s^{-1} [2]. This is in the medium to high shear rate range. For systems with Newtonian behavior in this shear rate range, there is no problem in using the solution. However, for systems that depend on the shear rate, it is important to choose the appropriate viscosity for calculating the intrinsic viscosity. The zero shear viscosities, which are determined in the low shear or first Newtonian regions of the flow curves, should be used to find the intrinsic viscosity in the Huggins plots [3].

Results and Discussion

Liquid crystalline structures have been observed in a wide range of materials. One group of these materials is suspensions containing anisotropic (rod-like or plate-like) nanoparticles. In this category, the aspect ratio [the higher length divided by the smallest dimension (diameter or thickness)] is an important parameter for characterization. There is a relation between the rheological behavior and the dimension of the nanoparticles [4]. Recently, some models have been used to estimate the aspect ratio of anisotropic nanoparticles according to the variation of intrinsic viscosity. The intrinsic viscosity in capillary viscometer is a parameter that must be measured for these models. They assumed that the nanoparticles are macromolecules and used the Mark-Houwink-Sakurada (MHS) equation. For anisotropic nanoparticles with high aspect ratio, high shear thinning behavior was observed even at very dilute regions. Here, we aim to significantly advance our

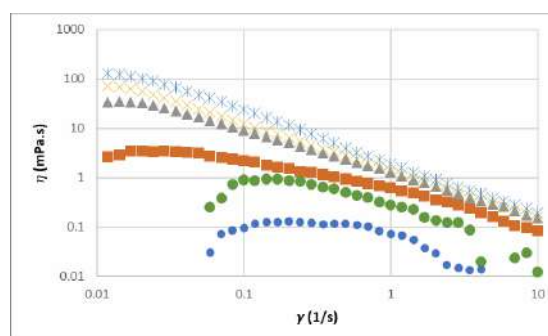


Fig. 1. The flow curve of GO in isotropic region. Carreau-Yasuda model was used to calculate the $\eta(\dot{\gamma}) = \frac{\eta_0}{(1 + (\lambda\dot{\gamma})^a)^{\frac{n-1}{a}}}$.

Table I. Rheometric data of GO suspension. The intrinsic viscosity calculated by $[\eta] = \lim_{c \rightarrow 0} \frac{\eta - \eta_s}{c\eta_s}$. The η_s (water viscosity) was assumed as 1 mPa.s.

c (mg/mL)	η_0 (Pa.s)	$(\eta - \eta_s)/\eta_s$	$(\eta - \eta_s)/c\eta_s$
0.001	0.12	120	120.000
0.005	0.9	900	180.000
0.01	2.25	2250	225.000
0.05	25	25000	500.000
0.1	73	73000	730.000

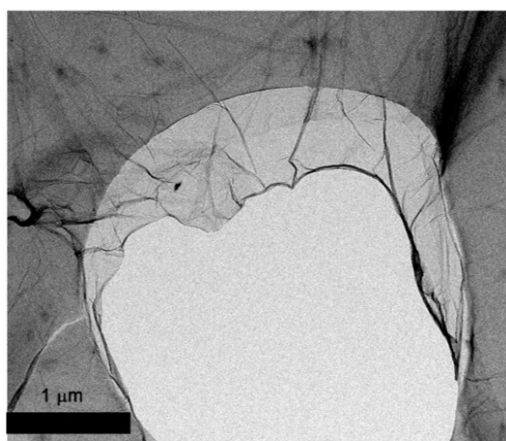


Fig. 2. SEM micrograph of GO sheet.

understanding about the measurement of intrinsic viscosity of non-Newtonian suspensions that are used in the MHS equation or models that are used to predict the molecular weight or aspect ratio of graphene oxide. For this purpose, the hypotheses for intrinsic viscosity measurements must be provided. For calculating the intrinsic viscosity, an important assumption is to be in the dilute regime.

According to Fig. 1, the zero shear viscosity was calculated by using the Carreau-Yasuda model. The intrinsic viscosity data were calculated at different concentrations, which are shown in Table I. The intrinsic viscosity was about 120000 (mL/mg).

According to the Kuhn and Kuhn model, which was proposed for monodisperse disk-like particles ($[\eta] = 32/15\pi r_p$), the calculated aspect ratio was $r_p \approx 170000$. The image processing of SEM (Fig. 2) showed that the mean GO sheet size was $\sim 80 \mu\text{m}$ and the lateral sheet thickness was $\sim 0.8 \text{ nm}$. The calculated aspect ratio was about ~ 100000 . This was a good estimation for the aspect ratio by using this measurement.

Conclusion

The dimension of 2D nanoparticles was estimated by calculating the intrinsic viscosity in the very low shear rate region. For this purpose, rheological measurements were used to find the zero-shear viscosity. Due to the high shear thinning behavior of high aspect ratio nanoplate suspensions, very dilute suspensions had to be used.

References

- [1] K. Catherine, G. Simon, and B. Lorenzo, *Nature*, **11**, 2425, 2020.
- [2] L. Peng et al., *Macromolecules*, **53**, 10421-10430, 2020.
- [3] Y. Lu, L. An, and Z.-G. Wa, *Macromolecules*, **46**, 5731-5740, 2013.
- [4] R. Jalili et al., *Adv. Funct. Mater.*, **43**, 5345-5354, 2013.

The Effect of Octaisobutyl Silsesquioxane Nanostructures on the Chemorheology of Polyurethane Formation Based on HTPB-DDI

Abolfazl Moein* and Abbas Kebritchi

Chemical Engineering Department, Imam Hossein Comprehensive University, Tehran, Iran

*fazl_moein@ihu.ac.ir

Abstract

This study investigated the effect of non-reactive POSS nanostructures (Octa isobutyl silsesquioxane (OIBS)) on polyurethane (PU) from hydroxyl-terminated polybutadiene resin (HTPB) and curing agents (Dimethyl-diisocyanate (DDI)). Chemo-rheological method and Arrhenius and Eyring equations were used to determine PU synthesis reaction kinetics. It was found that POSS nanostructures modulate the reaction kinetics between isocyanate and diol depending on the curing agent and POSS type. For example, POSS reduced the reaction speed in DDI systems. By increasing the concentration of POSS in PU, this decrease in speed became more noticeable. These results were explained by considering the interactions between POSS nanostructures and PU components. A plausible mechanism for the role of non-reactive POSS in PU synthesis kinetics was proposed.

Keywords: POSS, rheokinetic, brookfield viscometer, HTPB, DDI

Introduction

The kinetics of polyurethane (PU) network formation depends on various factors. These factors can affect the reaction speed, degree of polymerization, cross-linking, chemical structure, and physical and mechanical properties of PU. A change in any of the effective parameters can change the final properties of PU. This feature allows the use of PU in various industries. Additives can change the reaction kinetics. Additives can have different sizes, from nano to macro scale. Nanostructures, such as Polyhedral oligomeric silsesquioxane (POSS), have a high surface-to-volume (S/V) ratio, which makes them more effective than macro additives [1]. POSS is a new type of nanostructure that consists of a silicon-oxygen cage with organic groups linked to it. Depending on the type of organic groups, POSS can be reactive or non-reactive. Reactive POSS has functional groups that can participate in the polymerization reaction of the polymer matrix. For example, Honarkar *et al.* studied the effect of reactive POSS with two hydroxyl groups on the kinetics of PU formation. They found that this POSS reacts with the isocyanate to form urethane bonds, speeding up the reaction and changing the structure of the polymer [2]. Non-reactive POSS have non-reactive groups that do not react with the polymer matrix but can still affect its properties through physical interactions [3]. However, research on non-reactive POSS in PU is limited. This study investigates how non-reactive POSS, Octa isobutyl-POSS (OIBS), affect the formation of a PU network based on Hydroxyl-terminal polybutadiene (HTPB) resin. The chemo-rheological method, which tracks the rheological properties of polymers during curing, is used to investigate

Table I. PU formulation.

PU	Catalyst (wt%)	POSS	wt%	T (C°)	R
HTPB DDI	DBTDL (0.003)	OIBS	0	50	0.81
			1	55	
			5	60	
			10	50	
			15		

the kinetics of HTPB-PU network formation.

Experimental

According to Table I, the formulation was prepared. Before starting the work, the material was removed from water vapor using a vacuum oven. First, HTPB is mixed with POSS using a double-blade mixer in a water bath. Then the curing agent is added and mixed for 30 s at 1000 rpm. Brookfield viscometer model dv2t and spindle number 93 were used to measure changes in viscosity during urethane network formation. During the curing process, the system's temperature was kept constant using a hot water jacket. The system's viscosity was calculated up to 70 Pa.s, considered pot-life in this work.

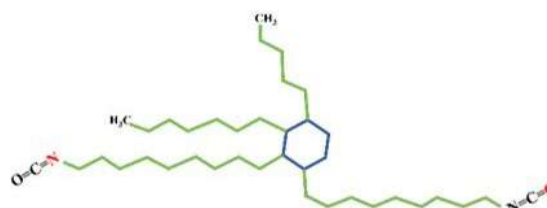


Fig. 1. DDI structure.

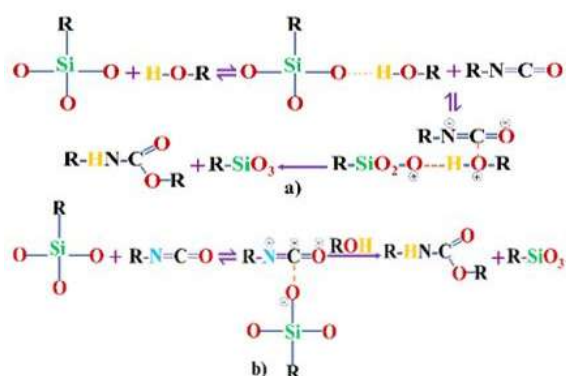


Fig. 2. Mechanisms of urethane formation by Siloxane core.

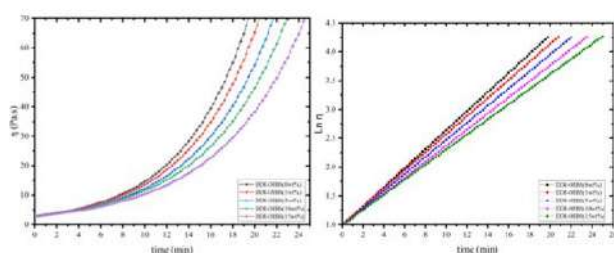


Fig. 3. Viscosity-time plot for HTPB-OIBS/DDI system.

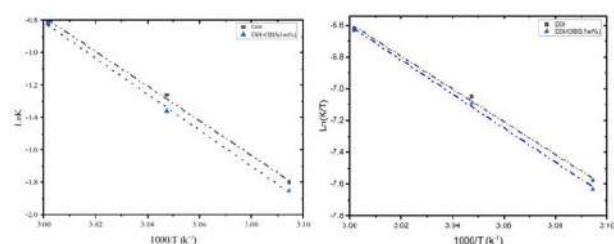


Fig. 4. Arrhenius and Eyring diagram for the curing reaction of the HTPB-DDI/POSS

Results and Discussion

The chemical structure of DDI consists of two isocyanate groups linked to a cycloaliphatic ring and are classified as cycloaliphatic isocyanates. DDI has low activity due to its high molecular weight and bulky structure (Fig. 1) The high molecular weight of DDI makes the viscosity changes over time substantial. The reactivity of the two isocyanate groups on its six-carbon ring is identical, So the reaction of DDI with HTPB follows first-order kinetics, and the reaction rate increases linearly with time (Fig. 3). POSS in the HTPB/DDI system increases pot life and slows polymerization (Fig. 3). It was found that this effect is more evident with higher concentrations of nanostructures in the HTPB matrix. A possible explanation for this phenomenon is that POSS becomes an active site for the reaction between isocyanate and hydroxyl due to its nanometer size and high surface-to-volume ratio, as well as the presence of highly polar oxygen groups in its structure (Fig. 2). Therefore, DDI cannot optimally interact with POSS active sites due to its

Table II. Rate constants and pot-life for the curing process of HTPB-DDI/POSS.

PU/POSS	POSS (wt%)	Pot-life	K
DDI	0	19.5	0.16551
DDI/OIBS	1	20.46	0.1441
	5	21.7	0.14842
	10	22.9	0.13976
	15	24.57	0.13103

Table III. Thermodynamic parameters for the curing reaction of the HTPB-DDI/POSS.

PU/POSS (1 wt%)	ΔE	A	ΔH‡	ΔS‡
DDI	88.63	e ^{31.21}	85.72	4.74
DDI/OIB	92.20	e ^{32.44}	89.13	14.88

large structure. As a result, POSS nanostructures prevent the formation of active complexes (HO-NCOO). These results are summarized in Table II. The thermodynamic constants extracted from Fig. 4 are compiled in Table III. The results show that with increasing concentration of nanostructures in HTPB matrix, Ea and ΔS‡ increase. These data justify the reduction of the reaction rate thermodynamically.

Conclusion

The results of this study showed that POSS nanostructures can interact with isocyanate and HTPB due to their special structure. These interactions make POSS affect the kinetics of HTPB-DDI formation. This effect on the DDI curing agent increases the pot life of the system and decreases the reaction rate constant.

References

- [1] Z. Li, J. Hu, L. Yang, X. Zhang et al., "Integrated POSS-dendrimer nanohybrid materials: Current status and future perspective", *Nanoscale*, **12**, 11395-11415, 2020.
- [2] H. Honarkar, M. Barmar, M. Barikani, and P. Shokrollahi, "Synthesis and characterization of polyhedral oligomeric silsesquioxane-based waterborne polyurethane nanocomposites", *Korean J. Chem. Eng.*, **33**, 319-329, 2016.
- [3] R. Shankar, L.K. Kemp, N.A. Smith, J.A. Cross et al., "POSS-induced rheological and dielectric modification of polyethersulfone", *J. Appl. Polym. Sci.*, **138**, 50537, 2021.

Dynamic of Gas Bubbles Surrounded by Thixo-Elastic Fluids Obeying DSM Rheological Model

Ali Masoudi¹, Mohammad Pourjafar², and Keyvan Sadeghy^{1*}

1. School of Mechanical Engineering, College of Engineering, University of Tehran, Tehran, Iran

2. Department of Mechanical Engineering, University of Tehran, Rezvanshahr, Iran

*sadeghy@ut.ac.ir

Abstract

When it comes to understanding the behavior of fluids, the field of rheology plays a crucial role. Among the diverse range of fluids, non-Newtonian fluids exhibit unique characteristics that challenge traditional fluid dynamics theories. One intriguing subset of non-Newtonian fluids is thixotropic fluids. In this article, we delve into the captivating world of bubble dynamics within the well-known De Souza Mendes thixotropic non-Newtonian fluids, exploring their properties, thixotropic and elastic behavior, and significance in various applications. To determine the integral-differential equation governing bubble dynamics, a numerical method based on Gauss-Laguerre quadrature is implemented. The numerical results show that the bubble response is significantly affected by the thixotropic properties of the surrounding fluid.

Keywords: Rayleigh, plesset equation, bubble dynamics, thixotropic fluid, de Souza Mendes model

Introduction

Bubble dynamics has long been the focus and interest of researchers due to its importance in the cavitation phenomenon. In recent years, the importance of investigating bubble dynamics has doubled due to its new applications. One of them can mention the injection of spherical air bubbles into the blood to increase the clarity of images in ultrasound operations. In most of the research, the assumption of the fluid being Newtonian has been used. While most physiological fluids such as blood are “complex fluids” and a variety of non-Newtonian behaviors such as viscoelastic behavior, thixotropic behavior and viscoplastic behavior usually occur simultaneously or under special conditions. A complex thixotropic model called Dullaert-Mewis was presented by Dullaert *et al.* is more interesting since it represents the level of microstructures remaining in the fluid system by a scalar called structural parameter. Ahmedpour *et al.* have studied the simultaneous effect of thixoeastic-viscoplastic fluid behavior on the dynamics of spherical gas bubbles using the Dullaert-Mewis rheological model in 2012 [1]. Unfortunately, in recent years, it has been found that Dullaert-Mewis rheological model is not very realistic too [2], and as a result, there are doubts about the effectiveness of the results presented in the abovementioned article. An advanced model that has recently been proposed to explain the aforesaid complex behavior is the de-Souza Mendes model that was presented by de Souza *et al.* in 2009 [3], which has not been comprehensively investigated on bubble dynamics in the acoustic pressure field before.

In this research, it is intended to investigate the effect of the fluid behavior on bubble dynamics by using this recently mentioned advanced model. Numerical method

in MATLAB software is adopted for solving the integral-differential equation.

Theoretical

A spherical gas bubble surrounded by an infinite surrounding fluid that the flow is incompressible, laminar, and isothermal is assumed. The oscillation of the bubble is forced by an external acoustic sinusoidal pressure source. Therefore, according to the continuity equation and the momentum equation in the radial direction of spherical coordinate, we will lead to integral-differential equation in spherical coordinate that is called the general Rayleigh-Plesset (RP) equation which describes the motion of a spherical bubble in any incompressible liquid whether Newtonian or non-Newtonian [4].

To calculate the integral value created in the general Rayleigh-Plesset equation, stress values are needed. So, we need constitutive equations. For this propose we used system of equation of de Souza Mendes fluid [3]. When dealing with bubble dynamics in a de Souza Mendes fluid, one prominent issue lies in accurately tracking the bubble's ever-changing boundary. To conquer this challenge, a Lagrangian coordinate transformation $y=r^3-R^3(t)$ comes to the rescue [5]. This ingenious technique swaps out material derivatives (D/Dt) for simpler time derivatives (d/dt), significantly simplifying the problem at hand. We confront the task of executing numerical integration for the last two terms in general Rayleigh-Plesset Equation. This demands a meticulous approach to ensure the accuracy and reliability of the solution. Here, the Gauss-Laguerre (GL) quadrature method steps onto the stage. The normalized system of differential equation can be written as below that

can be solved by numerical method in MATLAB software:

$$\ddot{R} = -\frac{3\dot{R}^2}{2R} + \frac{C_p}{R}(1+We)\left(\frac{1}{R}\right)^{3\kappa} - \frac{C_p}{R}(1+\delta \sin \omega t) - \frac{C_p We}{R} + \frac{2\sqrt{C_p}}{3R} \sum_{k=1}^N w_k e^{y_k} \frac{\tau_{rr}^{(k)} - \tau_{\theta\theta}^{(k)}}{y_k + R^3} \quad (1)$$

$$\frac{d\lambda_k}{dt} = \frac{1}{Tx} \left[-\left(1 - \lambda_{ss}^{(k)}\right)^a \left(\frac{\lambda_k}{\lambda_{ss}^{(k)}}\right)^b \left(\frac{\tau^{(k)}}{\eta_r \lambda_{ss}^{(k)} \dot{\gamma}_k}\right)^c \right] \quad (2)$$

$$\frac{d\tau_{rr}^{(k)}}{dt} = -\left(\frac{4R^2U}{y_k + R^3} + \frac{\lambda_k^{-m} \eta_r^{-\lambda_k}}{De}\right) \tau_{rr}^{(k)} - \frac{\lambda_k^{-m}}{De \sqrt{C_p}} \left(\frac{4R^2U}{y_k + R^3}\right) \quad (3)$$

$$\frac{d\tau_{\theta\theta}^{(k)}}{dt} = \left(\frac{2R^2U}{y_k + R^3} - \frac{\lambda_k^{-m} \eta_r^{-\lambda_k}}{De}\right) \tau_{\theta\theta}^{(k)} + \frac{\lambda_k^{-m}}{De \sqrt{C_p}} \left(\frac{2R^2U}{y_k + R^3}\right) \quad (4)$$

Results and Discussion

Decreasing the thixotropic number (Tx) leads to an increase in the range of bubble fluctuations. Secondary oscillations appear in bubble behavior with increasing thixotropic number (Fig. 1).

At high Reynolds (Re), the bubble demonstrates non-linear phenomena, including irregular changes in bubble radius fluctuation. At low Reynolds, strong viscosity curbs excessive expansion and contraction of the bubble environment, leading to oscillatory behavior (Fig. 2).

Higher pressure coefficients (Cp) correlate with increased bubble radius fluctuations. Small coefficients exhibit simple oscillatory responses, while larger ones

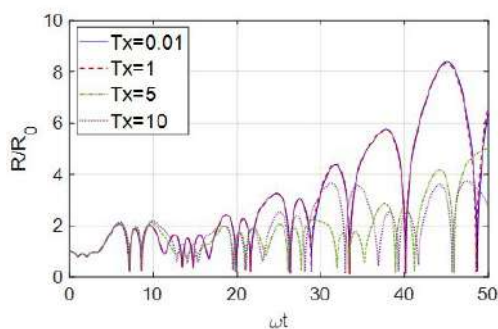


Fig. 1. Effect of Thixotropy number on bubble dynamic.

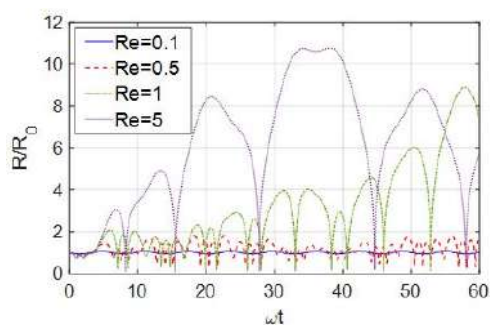


Fig. 2. Effect of Reynolds number on bubble dynamic.

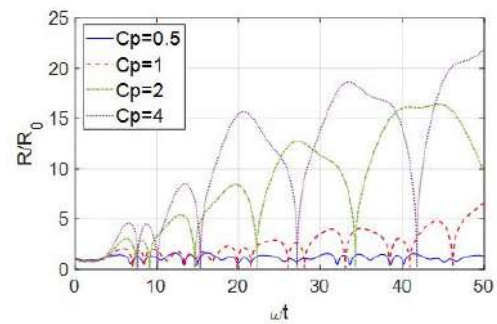


Fig. 3. Effect of pressure coefficient on bubble dynamic.

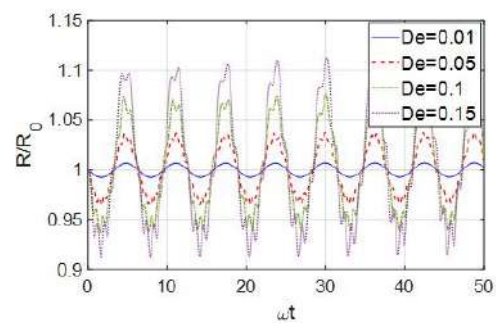


Fig. 4. Effect of Deborah number on bubble dynamic.

introduce secondary oscillations in addition to the primary oscillations (Fig. 3).

The increase of Deborah (De) greatly increases the fluctuation range of the bubble radius. In low Deborah, the oscillations are completely harmonic. With the increase of Deborah, secondary fluctuations also become unstable (Fig. 4).

Conclusion

Based on results obtained in this work, a competition between fluid's elasticity and thixotropy might give rise to second harmonics in bubble response that is significantly affected by the thixotropic properties of the surrounding fluid.

References

- [1] A. Ahmadpour, H. Amini-kafiabad, and K. Sadeghy, "Dynamic of gas bubbles surrounded by a dullaert-mewis thixotropic fluid", *Nihon Reorogi Gakkaishi*, **41**, 309-318, 2012.
- [2] P.R. de Souza Mendes and R.L. Thompson, "A critical overview of elasto-viscoplastic thixotropic modeling", *J. Non-Newton. Fluid Mech.*, **8-15**, 187-188, 2012.
- [3] P.R. de Souza Mendes, "Modeling the thixotropic behavior of structured fluids", *J. Non-Newton. Fluid Mech.*, **164**, 66-75, 2009.
- [4] J.S. Allen and R.A. Roy, *J. Acoust. Soc. Am.*, **108**, 1640, 2000.
- [5] E. Zana, L.G. Leal, *Int. J. Multiph. Flow*, **4**, 237 1978.

Effect of Hydrogenation on the Rheological Properties of HTPB-Based Polyurethanes

Ali Chanaani and Yasin Kaykha*

Chemical Engineering Department, Imam Hossein University, Tehran, Iran

*ykaykha@ihu.ac.ir

Abstract

Hydrogenation as a method to modify the properties of unsaturated polymers is of particular importance. Since hydrogenation reduces the mobility of hydroxyl-terminated polybutadiene (HTPB) chains, it probably affects the rheological properties, especially viscosity, so it seems necessary to investigate the effect of hydrogenation on viscosity. By performing chemical modifications through hydrogenation and properly understanding how this process affects the properties of HTPB, a wide range of physical and chemical properties can be achieved. In this article, the effect of hydrogenation on the viscosity of HTPB and polyurethanes based on this prepolymer has been tried to be expressed in a simple way. The results show that hydrogenation of HTPB can affect viscosity depending on the vinyl content.

Keywords: HTPB, HHTPB, viscosity, polyurethanes, hydrogenation

Introduction

Polyurethanes are a special group of polymer materials that have many applications in various fields such as paint, liquid coating, elastomer, insulation, elastic materials, and foam due to their versatility and suitability for replacing rare materials [1]. Polyurethane is a network polymer formed by the addition reaction between alcohols (diols or polyols) and isocyanates (diisocyanate or polyisocyanate). One of the most widely used polyols in the synthesis of polyurethanes is hydroxyl-terminated polybutadiene (HTPB). Processability of HTPB It is one of the factors that determine the properties and performance of polyurethanes based on this prepolymer [2]. On the other hand, rheological parameters such as viscosity strongly affect the processability of HTPB. The viscosity of the HTPB-based polyurethanes mainly depends on the viscosity of the HTPB, such that the viscosity of the polyurethane increases more slowly with the increase of the viscosity of the HTPB during curing [3,4]. Since hydrogenation reduces the mobility of HTPB chains, it seems to have an effect on viscosity, so it is necessary to investigate the effect of hydrogenation on viscosity [5]. In the following sections, the effects of hydrogenation on viscosity and processability are simply stated.

Effect of Hydrogenation on Viscosity

Hydrogenation affects viscosity by affecting the mobility and flexibility of polymer chains. The viscosity of a polymer is influenced by its molecular weight and structural factors such as branching [5]. In polybutadienes, branching refers to the vinyl content. Considering that the rotational barrier of the vinyl microstructure is much higher than that of the cis and trans microstructures. Therefore, more energy is

required for the mobility of polybutadienes chains with high vinyl content, which leads to an increase in viscosity [6]. Fig. 1 shows the effect of the degree of hydrogenation on the viscosity of 3 different polybutadiene samples [7].

Increasing the vinyl content from 15% to 60% doubles the viscosity. It should be noted that the molecular weight of the sample with lower vinyl content is two times higher. Hydrogenation of polybutadienes with high cis and trans content causes a slight increase in viscosity. But hydrogenation of polybutadienes with high vinyl content, especially in lower degrees, greatly increases viscosity. The reason can be the difference in the rotational barrier of ethyl and ethylene groups. At higher degrees of hydrogenation, the increase in viscosity is less observed. The increase in viscosity for higher degrees of hydrogenation can be explained by the increase in chain stiffness. It seems that

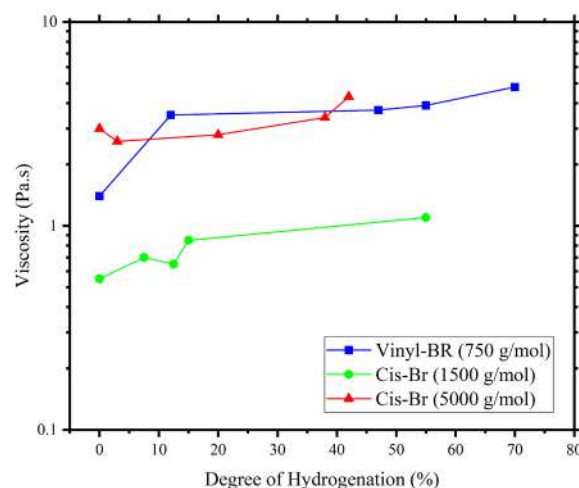


Fig. 1. Polybutadiene viscosity according to the degree of hydrogenation.

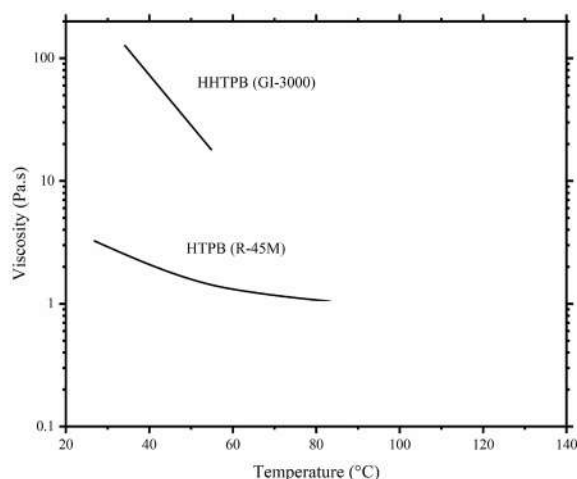


Fig. 2. Comparison of HTPB and HHTPB viscosity.

the effect of hydrogenation on viscosity varies depending on the vinyl content and degree of hydrogenation [7]. The viscosity of polybutadiene with a molecular weight between 1700 and 4350 g/mol strongly depends on the microstructure of polybutadiene [8]. Also, the minimum viscosity in molecular weight is observed when the amount of vinyl is between 30 and 70% [9].

Effect of Hydrogenation on Processability

The viscosity of HTPB increases after hydrogenation due to the decrease in chain mobility compared to the unsaturated sample. But the presence of a vinyl pendant group in vinyl-HTPB maintains the fluidity of this prepolymer. Therefore, the saturation of double bonds in HTPB is not expected to increase the viscosity to such an extent that it becomes difficult to process and directly cast the polyurethane. According to diagram in (Fig. 2), the viscosity of hydrogenated HTPB (HHTPB) is much higher than that of the unsaturated sample, but the remarkable thing is that the slope of the viscosity reduction with increasing temperature, is very high, therefore, according to this graph, the viscosity of HHTPB at higher temperatures does not cause a problem in processability [10].

Conclusion

Viscosity values (η) are very important in polymer processability and applications. Hydrogenation of polybutadienes with high cis and trans content causes a slight increase in viscosity. But, in polybutadienes with high vinyl content, hydrogenation at lower degrees strongly increases the viscosity. At higher degrees of hydrogenation, the increase in viscosity is less observed. It seems that the effect of hydrogenation on viscosity varies depending on the vinyl content and degree of hydrogenation. The decrease in viscosity with increasing temperature in HHTPB is very large, so the viscosity of HHTPB at Higher temperatures does not cause a problem in processability.

References

- [1] J.O. Akindoyo, M. Beg, S. Ghazali, M. Islam, N. Jeyaratnam, and A. Yuvaraj, "Polyurethane types, synthesis and applications—a review", *Rsc Adv.*, **6**, 114453-114482, 2016.
- [2] J. Guo et al., "Kinetic research on the curing reaction of hydroxyl-terminated polybutadiene based polyurethane binder system via FT-IR measurements", *Coatings*, **8**, 175, 2018.
- [3] C.Y. Chen, L.L. Gao, and X.F. Wang, "Effects of HTPB with different molecular weight on mechanical properties of HTPB/TDI system", *Adv. Mater. Res.*, **811**, 19-22, 2013.
- [4] V. Sekkar, A.S. Alex, V. Kumar, and G. Bandyopadhyay, "Pot life extension of hydroxyl terminated polybutadiene based solid propellant binder system by tailoring the binder polymer microstructure", *J. Macromol. Sci. Part A*, **54**, 171-175, 2017.
- [5] D.S. Pearson, L.J. Fetters, W.W. Graessley, G. Ver Strate, and E. von Meerwall, "Viscosity and self-diffusion coefficient of hydrogenated polybutadiene", *Macromolecules*, **27**, 711-719, 1994.
- [6] A. Miller, "Polymer-melt viscosity and the glass transition: An evaluation of the adam-gibbs and the free-volume models", *J. Chem. Phys.*, **49**, 1393-1397, 1968.
- [7] J.C. Uther, "Partly hydrogenated and functionalized polybutadiene rubber", Staats-und Universitätsbibliothek Hamburg Carl von Ossietzky, 2018.
- [8] J.-P. Dilcher, H. Jürgens, and G.A. Luinstra, "Sequential post-modifications of polybutadiene for industrial applications", *Multi-compon. Sequ. React. Polym. Synth.*, 163-201, 2015.
- [9] D.L. Handlin Jr et al., "Butadiene polymers having terminal functional groups", ed: Google Patents, 1995.
- [10] V. Sekkar, V. Krishnamurthy, and S. Jain, "Mechanical and Swelling Properties of Copolyurethanes based on Hydroxy-Terminated Polybutadiene and its hydrogenated analog", *Propellant. Explos. Pyrotech.*, **22**, 289-295, 1997.

Effect of Salt on the Rheological Properties of the Hydrophobically Modified Polyacrylamides Synthesized Via Micellar Polymerization

Zeinab Shirband and Mahdi Abdollahi*

Polymer Reaction Engineering Department, Faculty of Chemical Engineering, Tarbiat Modares University, P.O. Box 14115-114, Tehran, Iran

*abdollahim@modares.ac.ir

Abstract

Nowadays, the use of synthetic polymers such as polyacrylamide and its modified species has been highly regarded as a substitute for natural polymers used in drilling fluid. This project aims to synthesize polymer based on acrylamide (AM) modified with hydrophobic groups, including N-4-ethylphenylacrylamide (E ϕ AM). To obtain a polymer with the desired properties, the terpolymer of AM, 2-acrylamido-2-methyl-1-propane sulfonic acid (AMPS), and hydrophobic monomer was synthesized by micellar free radical copolymerization technique. Polymer structure was determined by the elemental analysis and FTIR spectroscopy. Then, the rheological properties of the samples in different situation were investigated. We observed that the formation of hydrophobic aggregates and the creation of a physical network that prevents the drop in viscosity against salt.

Keywords: micellar polymerization, hydrophobically modified polyacrylamide, rheology, N-4-ethylphenylacrylamide

Introduction

Thickening agents have attracted a lot of attention due to industrial applications like enhanced oil recovery, and drilling fluid [1]. Water soluble copolymers such as polyacrylamides modified with a low amount of hydrophobic monomers, called hydrophobically modified polyacrylamide (HMPAM), are one of the most important rheology modifiers due to the formation of hydrophobic physical networks [1]. The well-known method for HMPAMs synthesis is a micellar technique, where micelles of the surfactant molecules create an appropriate place for association of the hydrophobic comonomer [2,3]. Depending on the emulsifier and hydrophobic comonomer concentrations, hydrophobic blocks with different lengths can be formed by penetration of radicals into the micelles, resulting in a multi-block copolymer microstructure with different hydrophobic block lengths [1,2]. On the other hand, incorporation of the ionic monomers such as 2-acrylamido-2-methyl-1-propane sulfonic acid (AMPS) into the polymer backbone chain (typically acrylamide chain) forms polyelectrolytes with a significant improvement in thickening properties, temperature and salt resistance [2,3].

Experimental/Theoretical

The micellar method was used for the synthesis of hydrophobically modified polyelectrolyte via terpolymerization of AM/AMPS/hydrophobic monomer, where sodium dodecyl sulfate (SDS) and potassium persulfate (KPS) were employed as emulsifier and initiator, respectively. A 50 mL ampoule containing 40 mL deionized

water, as an aqueous phase, was employed as a reaction chamber. Predefined amounts of AM, AMPS, E ϕ AM, and SDS were dissolved in the aqueous phase. To remove air, the reaction mixture was immersed in a water/ice bath, followed by purging with nitrogen for at least 30 min, and then a predefined amount of KPS was added. The reaction chamber was immersed in a 50 °C water bath for 8 h. Terpolymer was precipitated by adding an excess amount of acetone, the precipitated product was again dissolved in the water, then precipitated using the excess acetone and dried. The length of the hydrophobic group is considered 8 for terpolymer [3].

Results and Discussion

FTIR spectroscopy was used for the characterization of the structure and functional groups of the synthesized

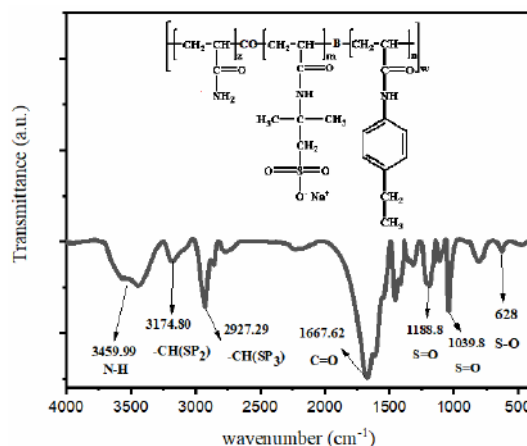


Fig. 1. FTIR spectra recorded for sample AM/AMPS/E ϕ AM.

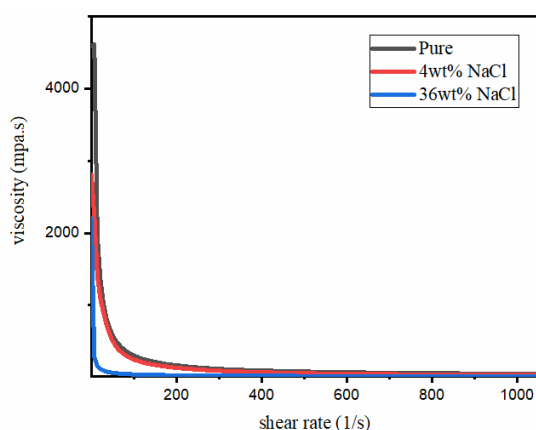


Fig. 2. Aqueous solution viscosity as a function of shear rate at a constant polymer concentration (0.7 wt%) in the deionized water containing salt at 60 °C.

terpolymer [2,3]. The characteristic FTIR absorption peaks of terpolymer are as follows in Fig. 1. A strong absorption peak at wavelength of 1667 cm^{-1} can be observed in the spectrum corresponding to the stretching vibration of the carbonyl group. The observed peaks at wavelengths of 2927 and 3174 cm^{-1} account for stretching vibrations of the -CH bond present in the AM and E ϕ AM. The stretching vibration of the amide bond (NH) that emerged around a wavelength of 3459 cm^{-1} and the peak around a wavelength of 1451 cm^{-1} are related to the bending vibration of the -CH_2 . A strong absorption band at wavelengths of 1039 and 1188 cm^{-1} can be observed due to the stretching vibration of the -S=O bond in the AMPS structure. According to the results, the desired polymer has been synthesized successfully [4]. As seen in Fig. 2, a decreasing trend in viscosity is observed with increasing shear rate in pure sample, which is due to the collapse of intermolecular aggregates as a result of increasing shear rate. Also In the absence of salt, repulsion forces originating from sulfonate groups prevent intermolecular hydrophobic interactions in the polyelectrolyte. A significant reduction of

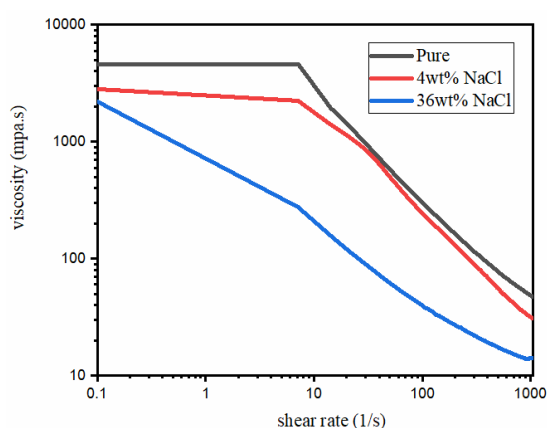


Fig. 3. Logarithmic plot of viscosity in terms of shear rate at a constant polymer concentration (0.7 wt%) in the deionized water containing salt at 60 °C.

terpolymer viscosity by adding salt to the medium was observed (Figs. 2 and 3). This behavior can be attributed to the rupture of extended chains of polyelectrolyte via partially neutralization of sulfonate anionic charges by salt molecules. In other words, intra-anionic electrostatic repulsion decreases significantly in the presence of salt. Decrease in the viscosity of solution can also be attributed to the ionic strength decline among the polyelectrolyte chains. In the presence of high concentration of NaCl, anionic polyelectrolyte shows non-electrolyte behavior.

Results and Discussion

Terpolymer of AM/ AMPS/ hydrophobic monomer as HMPAM was successfully synthesized through the micellar polymerization method. Hydrophobic block length (NH) with a suitable value showed the water solubility. The results presented in this paper show the shear thinning behavior. At low shear rates, the molecules are connected to each other through intermolecular bonds and show high viscosity. As the shear rate increases, aggregations and intermolecular interactions are broken and viscosity decreases. We also observed that the viscosity decreased with the addition of salt due to the neutralization of AMPS monomer charges, but the formed hydrophobic aggregates prevented a large drop in viscosity. Molecular weight, copolymer composition and distribution of the hydrophobic comonomer in the copolymer chain are key microstructure-related parameters with significant effects on the rheological properties and associative behavior of hydrophobic groups. By synthesizing a polymer with a higher molecular weight followed by the formation of a strong physical network, a higher viscosity can be achieved in the presence of salt even higher than its pure state.

References

- [1] D. Wever, F. Picchioni, and A. Broekhuis, *Prog. Polym. Sci.*, **36**, 1558-1628, 2011.
- [2] C. Zhong, R. Huang, X. Zhang, and H. Dai, *J. Appl. Polym. Sci.*, **103**, 4027-4038, 2007.
- [3] H. Khakpour and M. Abdollahi, *Polym.-Plast. Technol. Mater.*, doi/10.1080/25740881.2019.1669645
- [4] H. Khakpour, M. Abdollahi, and A. Nasiri, *J. Polym. Res.*, **22**, 189, 2015.

Effect of Crosslinking on Linear Viscoelastic and Nonlinear Large-Strain Properties of Poly(n-butyl acrylate) Latex Film

Ali Ahmadi-Dehnoei and Somayeh Ghasemirad*

Polymer Engineering Department, Faculty of Chemical Engineering, Tarbiat Modares University,
P.O. Box 14115-114, Tehran, Iran

*ghasemirad@modares.ac.ir

Abstract

The effect of crosslinking on linear viscoelastic and nonlinear large strain properties of poly(n-butyl acrylate) (PBA) latex films containing 0.05-0.25 wt% methacryloxypropyltrimethoxysilane as a self-crosslinking monomer (SCM) was systematically investigated using small amplitude oscillatory shear (SAOS) and uniaxial tension tests, respectively. These analyses revealed that the addition of 0.05 and 0.1 wt% SCM resulted in an increase in the storage modulus, complex viscosity, and tensile strength of the films. In addition to the formation of chemical crosslinks, this was attributed to the interdiffusion of polymer chains between neighboring particles and the formation of entanglements between them during the film formation process. However, at the SCM content of 0.25 wt%, the storage modulus, complex viscosity, and tensile strength of the film decreased, which was a consequence of increase in the crosslink density within the polymer latex particles. This prevented the interdiffusion of polymer chains between neighboring particles and the formation of entanglements during the film formation stage.

Keywords: crosslinking, linear viscoelastic, nonlinear large-strain properties, latex film

Introduction

Latexes are stable dispersions of polymer particles in water, which can be prepared by emulsion polymerization. Latexes are extensively used in coating and adhesive industries, owing to their environmental benefits regarding reduction in the emission of volatile organic compounds. The film formation process of latex particles includes evaporation of water to concentrate the particles, deformation of particles into space-filling polyhedral, and finally, interdiffusion of the polymer chains to eliminate the particle boundaries and to build up cohesion through the formation of entanglements [1]. Despite their exceptional performance in numerous applications, latex films typically possess lower tensile strength compared to their solvent-based counterparts [2]. The introduction of chemical crosslinks into a latex film may enhance its tensile strength [2]. Crosslinking may occur during the film formation process by introducing chemical functionalities in the latex particles or it may happen within the latex particles using multifunctional monomers [3]. Preparation of polymer latexes able to undergo chemical crosslinking reaction, both during the synthesis within the latex particles and during film formation after interdiffusion of the polymer chains between the latex particles, appears to lead to substantial enhancement in cohesion strength of the latex film. For this purpose, herein, a series of self-crosslinking latex nanoparticles were synthesized by emulsion copolymerization of butyl acrylate, BA, with different low contents of methacryloxypropyltrimethoxysilane (MAPTS) as a self-crosslinking monomer (SCM). The effect of the addition of different SCM contents on the linear viscoelastic

properties and also on the nonlinear large-strain properties of the PBA latex film was systematically investigated.

Experimental

To produce self-crosslinking latex particles, required amounts of sodium dodecyl sulfate and potassium persulfate solutions were poured into a flask equipped with a mechanical stirrer, condenser, and nitrogen inlet, in an oil bath at 80 °C. After the addition of BA, 0.05-0.25 wt% of MAPTS was added dropwise to the system and the reaction continued for 3.5 h. The formulations containing SCM were named as PBS_x, where x stands for the weight percentage of SCM with respect to BA. The gel content of the specimens were determined by a Soxhlet extraction in boiling tetrahydrofuran for 24 h. The linear viscoelastic and nonlinear large-strain properties of the latex films were evaluated by performing small-amplitude oscillatory shear (SAOS) and uniaxial tension tests, respectively.

Results and Discussion

The gel content of PBA, PBS_{0.05}, PBS_{0.1}, and PBS_{0.25} latex films was measured to be 80.2, 89.55, 94.62, and 94.32%, respectively. The observed increase in the measured gel content confirmed the participation of the SCM in the polymerization reaction, as well as the occurrence of the crosslinking reaction between adjacent chains in the latex particles.

Fig. 1 illustrates the measured storage modulus, G' , and complex viscosity, η^* , of the uncrosslinked PBA film and PBA films containing various amounts of SCM as a function of angular frequency. The G' and η^* increased at

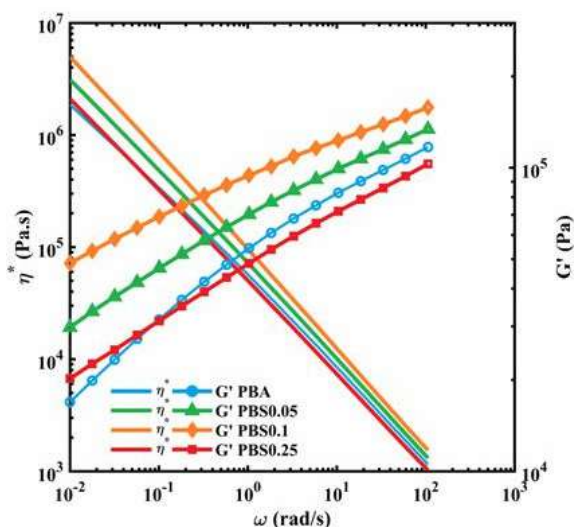


Fig. 1. Complex viscosity and storage modulus of PBA and PBSx.

all frequencies with an increase in the SCM content from 0 wt% to 0.1 wt%. However, with the increase in the SCM content to 0.25 wt%, the G' and η^* decreased to the values lower than those of PBA at most frequencies.

The measured nonlinear large-strain properties of the films are shown in Fig. 2. The tensile strength, σ , of PBA increased from 58 kPa to 274 and 467 kPa by the addition of 0.05 and 0.1 wt% of SCM, respectively. However, with the addition of 0.25 wt% of SCM, σ decreased. The fracture energy or toughness, W_B , was also calculated to be 1.48, 1.82, 1.66, and 0.58 mJ/mm^3 for PBA, PBS0.05, PBS0.1, and PBS0.25, respectively, Fig. 2. The trend of changes in the nonlinear large-strain properties was in agreement with the trends of changes observed in the linear viscoelastic properties, Fig. 1.

During the film formation process of PBA, the cohesive strength is only achieved as a result of the interdiffusion of polymer chains between neighboring particles and thus the formation of entanglements between them. By adding small amounts of SCM, 0.05 and 0.1 wt%, and

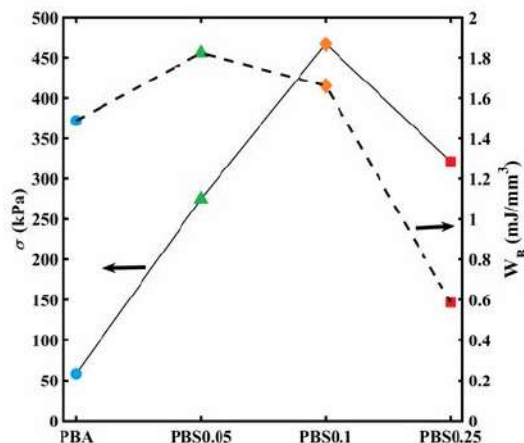


Fig. 2. Tensile strength and toughness of PBA and PBSx films.

occurrence of chemical crosslinking within the polymer latex particles during the synthesis, in addition to the ability of polymer chains in a latex particle to interdiffuse and entangle with the chains in the neighboring particles, the creation of chemical crosslinks between polymer particles after the interdiffusion of chains is highly probable. This results in an enhancement in the cohesion of the film, leading to higher storage modulus, complex viscosity, and tensile strength compared to PBA. However, the reduction in storage modulus and tensile strength upon the increase in the SCM content to 0.25 wt% may be attributed to two phenomena occurring during the film formation process. Firstly, the increase in the crosslink density may cause a reduction in the deformability of the polymer particles, and secondly, it may cause a reduction in the effective interdiffusion of polymer chains between the neighboring particles and thus preventing the formation of entanglements between polymer chains. Given that addition of SCM did not affect the glass transition temperature (T_g) of the latex films ($-46\text{ }^\circ\text{C}$, measured by differential scanning calorimetry) and considering the fact that the film formation temperature ($25\text{ }^\circ\text{C}$) was $70\text{ }^\circ\text{C}$ higher than the polymer T_g , it can be assumed that the addition of SCM had negligible effect on the deformability of polymer particles during the film formation process. Tamai *et al.* [2] also showed that utilizing a low amount of multifunctional monomers for crosslinking latex particles during emulsion polymerization had minimal effect on the deformability of polymer particles in the film formation process. Therefore, it can be deduced that the diminished storage modulus, complex viscosity, and tensile strength of the PBAS0.25 result from the decreased interpenetration depth of polymer chains between the adjacent particles and the diminished formation of entanglements between them.

Conclusion

The addition of SCM led to an increase in the gel content of the PBA films due to the formation of chemical crosslinks. The results showed that in order to improve the cohesion and tensile strength of PBA latex films, there should be a balance between the crosslink density within the polymer particles and the interdiffusion of polymer chains between the neighboring particles.

References

- [1] R. Shiri, A. Ahmadi-Dehnoei, and S. Ghasemirad, *J. Adhes.*, 1-29, 2023.
- [2] T. Tamai, P. Pinenq, and M.A. Winnik, *Macromolecules*, **32**, 6102-6110, 1999.
- [3] A. Zosel and G. Ley, *Macromolecules*, **26**, 2222-2227, 1993.



Preparation of Poly(acrylamide-co-Acrylic acid) Hydrogels in Presence of Graphene: Rheological Properties

Zahra Mohammadi and Fatemeh Goharpey*

Department of Polymer Engineering and Color Technology, Amirkabir University of Technology, 158754413, Tehran, Iran

*goharpey@aut.ac.ir

Abstract

In this research, by dealing with the synthesis methods of hydrogels, an attempt was made to improve the rheological properties of hydrogels based on acrylamide-co-acrylic acid copolymer by using graphene oxide nanoparticles and iron metal ions and prepare them for use in various fields. Based on this, using the experimental design, firstly, the optimal state of materials for synthesizing basic hydrogel without ions and nanoparticles was obtained, and then using it, the effect of the presence of ions and nanoparticles was studied. It was found that the presence of nanoparticles and metal ions in alignment decreased the area of the hydrogel's linear rheological behavior and increased the storage modulus up to 0.49 MPa and the loss modulus up to 0.12 MPa. Also, the presence of these two factors caused the tendency of the rheological behavior of the hydrogel towards viscoelastic solids. It kept the gelling temperature and time within the range of medical and pharmaceutical applications.

Keywords: hydrogel, acrylamide, acrylic acid, graphene oxide, metal ion Fe

Introduction

Hydrogel, an insoluble polymer, may swell and retain a lot of water. Agriculture, food science, drug delivery, tissue engineering, biosensors, and shape memory materials utilize this tridimensional substance. Surface absorption, biodegradability, hydrophilicity, and environmental reactions make it flexible. Hydrogels' softness, flexibility, wetness, and poor rheological properties limit their usage. Synthetic polymer hydrogels are popular because of their exceptional characteristics. Hydrogels exceed natural polymers in chemical, water, and durability. Their mechanical properties reduce wear and boost durability. Hydrogels are customizable [1].

Hydrogels are stable in aqueous solutions because hydrophilic chains crosslink chemically and physically. The iron (III) ion coordinates with the acetic acid group on acrylamide-co-acrylic acid polymer chains to crosslink double cross-linked hydrogels. A coordination complex and ionic attraction will improve the rheological properties of the polymer chain hydrogel, stimulating investigation into further crosslinking agents. These chemicals are explored to improve hydrogel rheological characteristics and stability. For medicine administration and tissue engineering, the hydrogel should be antimicrobial, electrically conductive, and biocompatible [2]. Took Nano graphene oxide's absorption into the hydrogel matrix and ability to crosslink via hydrogen bonding, van der Waals, and π - π electron interactions was the secondary crosslinking factor [3]. This study optimizes process and material variables to synthesize a system. The synthesized system's optimal rheology is also studied. Investigations will evaluate each physical crosslinking ingredient.

Experimental

Understanding material and process variables helps improve hydrogel manufacturing and industrial output. This study cannot regulate temperature. This study will employ previous limit states for each of these criteria. One must understand how acrylic acid and acrylamide monomers, catalyst and initiator levels, nanoparticle numbers, and iron metal ion concentration interact to achieve ideal circumstances. This study altered the amide monomer-acidic monomer-catalyst-initiator ratio.

These changes formed a hydrogel with stable physical cross-links from hydrogen bonding between polymer chains' amide and acidic groups. In a following experiment, nanoparticles and metal ions were tested under the most optimized situation. Thus, Qualitek-4 employed Taguchi design to find the best configuration for the first three variables' five levels. The second experiment employed two variables with four levels and the same methodology. Previous testing showed 2.55% acrylic acid monomer in the hydrogel specimen. Literature and sources examined variable ranges. The early experimental design materials were evaluated on their ability to generate hydrogel at macroscopic and microscopic scales and maintain structural integrity for 72 h.

Results and Discussion

The preliminary test design and stability tests showed that the best hydrogel is synthesized using a molar ratio of amide to acid of 6, a catalyst of 0.3% by mass, and an initiator of 0.07% (A6T3S7).

Fig. 1 (N25F6 lead to Hydrogel contains 0/25 w/w% nanoparticles and 0/06 w/w% ion metal) shows that for

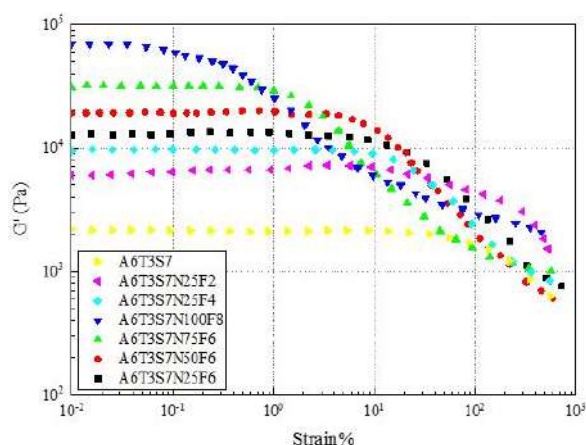


Fig. 1. Diagram of storage modulus in terms of strain percentage for synthesized hydrogel samples.

all selected samples of the second test design, storage modulus was independent of applied strain up to a certain strain percentage. Viscoelastic substances behave like this. After a specific strain, each sample's storage modulus drops significantly, suggesting the hydrogels' phase change from quasi-solid to quasi-liquid. As illustrated in Fig. 1, introducing nanoparticles or metal ions and increasing their concentrations lowers the storage modulus at lower strains. In this circumstance, samples become harder and less deformable. Due to hydrogen bonding or electrostatic interactions, these two chemicals boost transverse connection density.

Fig. 2 shows that for most samples, storage modulus is independent of applied frequency, indicating viscoelastic solids. These two figures show that nanoparticles and metal ions improve storage and loss modulus. Fig. 1 shows that the storage modulus increases with these two, the density of transverse connections, and the nanoparticle's reinforcing property. Electrostatic interactions of the metal ion with groups on polymer chains or nanoparticle plates that can be destroyed and reformed increase the loss modulus. As

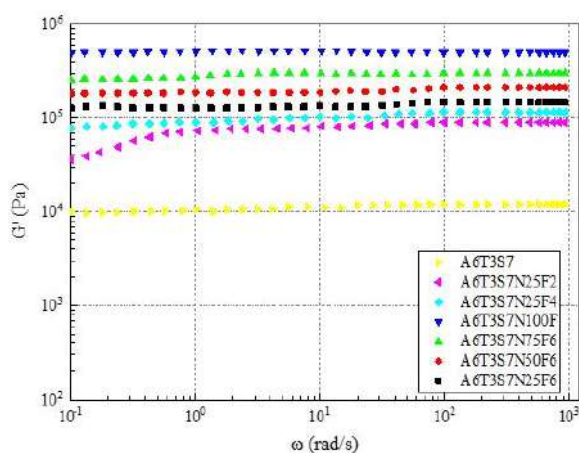


Fig. 2. Diagram of storage modulus by frequency for synthesized hydrogel samples.

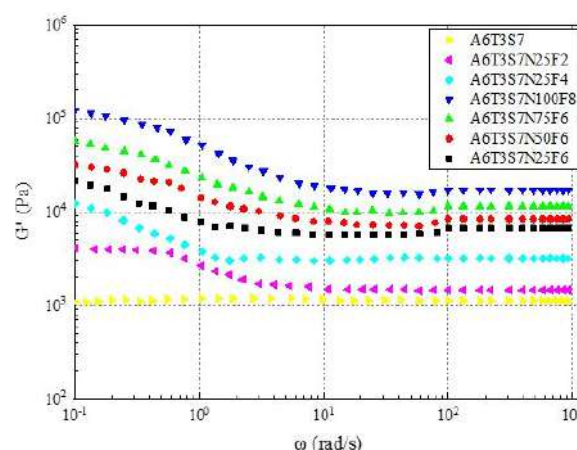


Fig. 3. Loss modulus diagram in terms of frequency for synthesized hydrogel samples.

frequency increases, time decreases, and the loss module decreases, as shown in Fig. 3. Also, in the temperature and time sweep tests, the gelation time was 1.2 min and the gelation temperature was 37 °C for the optimal sample (A6T3S7N5F6).

Conclusion

At first, in order to achieve the optimum material conditions for the synthesis of hydrogel-based copolymer, the design of the primary experiment was carried out by the Taguchi method, and by using the results of this design, it was tried to design the secondary experiment by varying the amount of nanoparticles and metal ions in the hydrogel system. Therefore, by using a network of double hydrogel joints with the ability to adjust rheological properties, it has a maximum storage modulus of 0.49 MPa and a loss modulus of 0.12 MPa, with the ability to form a structure at 37 °C in a period of 72 s, and it is introduced as a suitable option for medical and pharmaceutical users.

References

- [1] Y. Guo, J. Bae, Z. Fang, P. Li, F. Zhao, and G. Yu, "Hydrogels and hydrogel-derived materials for energy and water sustainability", *Chem. Rev.*, **120**, 7642-7707, 2020.
- [2] X. Lin, X. Zhao, C. Xu, L. Wang, and Y. Xia, "Progress in the mechanical enhancement of hydrogels: Fabrication strategies and underlying mechanisms", *J. Polym. Sci.*, **60**, 2525-2542, 2022.
- [3] U.S.K. Madduma-Bandarage and S.V. Madihally, "Synthetic hydrogels: Synthesis, novel trends, and applications", *J. Appl. Polym. Sci.*, **138**, 50376, 2021.

Study on the Effect of Processing Condition on TPV Microstructure and Its Relationship with Electrical Conductivity of Thermoplastic Vulcanized Nanocomposites Based on PP/EPDM/CNTs

Amirreza Khayati, Hossein Nazockdast*, and Ali Asghar Katbab

Department of Polymer Engineering and Color Technology, Amirkabir University of Technology, Tehran, Iran

*nazdast@aut.ac.ir

Abstract

In this study, nanocomposites based on dynamically vulcanized polypropylene (PP)/ethylene-propylene-diene rubber (EPDM) thermoplastic elastomer and multi wall carbon nanotube (MWCNT) were fabricated in different processing conditions via melt mixing process. The effects of CNT content, processing conditions and TPV microstructure on electrical conductivity has been investigated. Linear viscoelastic properties and electrical conductivity of TPV nanocomposites indicate that increasing processing speed results in formation of a more suitable 3-D network between rubber particles; also, dispersion and distribution of nanoparticles has been improved, which results in enhancement of electrical conductivity, and linear viscoelastic properties of the nanocomposites.

Keywords: electrical conductivity, polymer nanocomposites, thermoplastic vulcanized, carbon nanotubes

Introduction

The tire is one of the most important components of the car Electrically Conductive Polymer Nanocomposites (ECPNCs) incorporating carbon nanotubes (CNTs) have attracted significant attention for their easy production, processing flexibility, tunable properties, and diverse applications. Increasing nanoparticle concentration forms a 3-D network, vastly enhancing electrical conductivity and shifting the composite from insulator to conductor, known as Electrical Percolation Threshold (EPc). EPc is an essential requirement for achieving an acceptable electrical conductivity, and the main target in ECPNCs is achieving low EPc in order to maintain processability and mechanical properties and reduce production cost [1].

Thermoplastic vulcanizates (TPVs) as a matrix for producing ECPNCs has gain a lot of attention in recent years. TPVs, as a kind of high-performance thermoplastic elastomers, composed of a high content (>50 wt%) vulcanized rubber as dispersed phase, and low content of thermoplastic as the continuous phase, are prepared by dynamic vulcanization reaction. Due to the combination of the good processability and recyclability of the thermoplastic phase and the elasticity of the cured rubber phase, TPVs have gained a lot of attention recently. In this study, we investigate the effect of CNT content, processing condition, and TPV microstructure on electrical conductivity of thermoplastic vulcanized nanocomposites based on PP/EPDM/MWCNTs [1,2]

Experimental

Materials

Injection grade of PP with the trade name of Jampilen

EP440L (Jam Polypropylene Co, Iran, MFI=6 g/10min (230 °C, 2.16 kg)), EPDM with the trade name of KEP270 having Mooney viscosity of ML (1+4, 125 °C)=77, and multiwall carbon nanotubes (MWCNTs) with the trade name of NC7000 with 90% purity were used to prepare TPV samples. Zinc oxide (ZnO), Stearic acid, Sulfur (S), MBTS, and TMTD were used as cross-linking agents.

Sample Preparation

The blending process involved sequential steps: introducing PP into a Rheocord 90 internal mixer at 175 °C and 80 rpm, followed by EPDM after 3 min, crosslinking agents added after 5 min, and dynamic vulcanization continued for another 2 min. It should be noted that the blends were dynamically cured using a vulcanizing system reported elsewhere [2]. Different MWCNTs ratios were introduced to the mixer, and the mixing continued for another 8 min. TPVs with varying MWCNTs levels were denoted as TPV-x, indicating the volume content of MWCNTs. Also, the TPV-2-ref with a rotor speed of 120 rpm was fabricated with the same procedure for comparison. The resulting nanocomposites were compression molded into 1mm thick sheets at 200 °C and 50 bar after preheating. The PP to EPDM weight ratio remained constant at 50/50 across all samples.

Characterization

The rheological behavior and melt viscoelastic properties of the nanocomposites were studied using a rheometric mechanical spectrometer (Paar Physica USD200) with a parallel plate (diameter=2.5 cm; gap=1 mm) at a temperature of 220 °C, frequency range of 0.01–

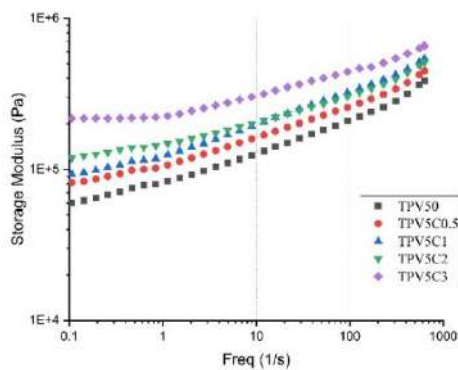


Fig. 1. The storage modulus of TPV nanocomposites containing CNTs in different concentrations prepared in processing speed of 80 rpm.

1000 s^{-1} , and strain amplitude of 1%. Volume electrical resistivity was measured on compression-molded plaques with dimensions of 100 3 100 3 1 mm, using a Keithley electrometer model 6517B equipped with a high-resistance test fixture.

Results and Discussion

Fig. 1 shows storage modulus (G') versus frequency of TPV nanocomposites in different CNTs concentrations. Increasing nanoparticles concentration results in a much stronger nonterminal behavior of storage modulus at low frequency range compared to unfilled TPV sample. Selective localization of nanoparticles in PP matrix and on the interface of two phase can results in reinforcement of rubber network and/or formation of 3-D network between particle-particle and particle-matrix.

Fig. 2 shows storage modulus versus frequency of filled and unfilled TPVs in different processing conditions. Clearly, increasing processing speed decreases the size of rubber particles and the rubber agglomerates. Also, enhances morphology development in TPV nanocomposites. This phenomena, improves the interaction between PP's chains and rubber particles, which increases the PP's relaxation

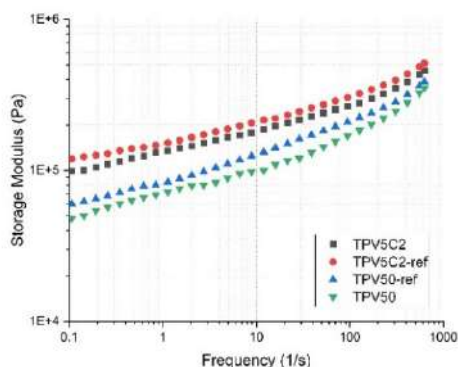


Fig. 2. The storage modulus filled and unfilled TPV nanocomposites prepared in processing speed of 80 and 120 rpm.

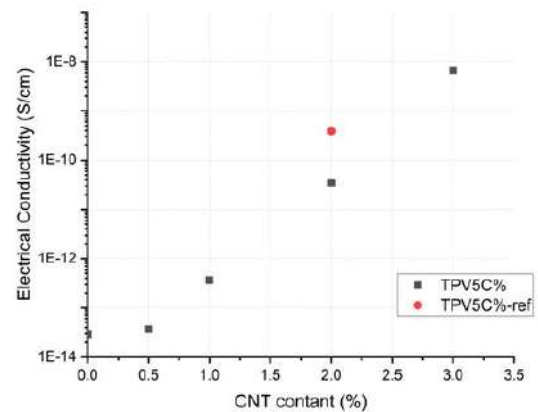


Fig. 3. DC electrical conductivity of different TPV nanocomposites in different CNT concentration prepared in different processing speeds.

time, and a more pronounced nonterminal behavior of storage modulus at low frequencies.

Fig. 3 shows DC electrical conductivity of different TPV and PP nanocomposites in different CNTs concentration. Clearly, increasing CNT concentration results in enhancement of electrical conductivity. Moreover, increasing processing speed causes better dispersion of nanoparticles, and improves microstructure development in TPVs, which results in increase in electrical conductivity compared to filled TPVs prepared in lower processing speed.

Conclusion

In this study, TPV nanocomposites based on PP/EPDM (50:50) and CNT were prepared and the effect of CNT content, processing condition and TPV microstructure on linear viscoelastic behavior, morphology development and electrical conductivity were investigated. Increasing CNTs content, enhances electrical conductivity, and linear viscoelastic properties. Furthermore, increasing processing fostered a more favorable microstructure in TPV nanocomposites, which is obvious from linear viscoelastic properties and electrical conductivity.

References

- [1] W. Zhang, A.A. Dehghani-Sani, and R.S. Blackburn, *J. Mater. Sci.*, **42**, 3408-3418, 2007.
- [2] F. Goharpey, A.A. Katbab, and H. Nazockdast, *Rubber Chem. Technol.*, **76**, 239-252, 2003.

Study on Microstructure and Its Relationship with Electrical Conductivity of Thermoplastic Vulcanized Nanocomposites Based on PP/EPDM/CNTs

Amirreza Khayati, Hossein Nazockdast*, and Ali Asghar Katbab

Department of Polymer Engineering and Color Technology, Amirkabir University of Technology, Tehran, Iran

*nazdast@aut.ac.ir

Abstract

In this study, nanocomposites based on Polypropylene and dynamically vulcanized PP/ethylene-propylene-diene rubber (EPDM) thermoplastic elastomer and multi wall carbon nanotube (MWCNT), were fabricated in melt mixing process. The effect of TPV microstructure on electrical conductivity has been investigated. Linear viscoelastic properties and electrical conductivity of PP and TPV nanocomposites indicate that three-dimensional network between rubber particles in TPVs, have hindered the formation of a 3-D network between CNTs, and high degree dispersion of nanoparticles. In other word, the final properties, especially electrical conductivity, were highly affected by nanoparticles dispersion, which was controlled by TPV microstructure.

Keywords: electrical conductivity, polymer nanocomposites, thermoplastic vulcanized, carbon nanotubes

Introduction

The incorporation of conductive nanofillers, like carbon nanotubes (CNTs), into an insulating polymer matrix to produce new multifunctional polymer nanocomposites with diverse application, and remarkable mechanical, electrical, and thermal properties, have gained considerable attention from researchers. However, increasing nanoparticles concentration to achieve acceptable electrical conductivity will rise number of challenges. Hence, among the proposed strategies to overcome these challenges and lowering the electrical percolation threshold, simultaneously taking the advantage of both reinforcements of nanoparticles and polymers blending techniques has drawn a significant attention in last decade.

Thermoplastic vulcanizates, a special class of immiscible polymer blends, are composed of a high content of dynamically cross-linked rubber as dispersed phase, and low content of a thermoplastic as continuous phase. It has shown that, the selective localization of nanoparticles in one of the phases or at the interface of two phases of TPVs significantly increases nanoparticles effective concentration, and results in the formation of a conductive path at lower nanoparticles concentration. As a result, in this study, we investigate the effect of TPV microstructure on the dispersion of nanoparticles and its relationship with electrical conductivity of TPV nanocomposites based on PP/EPDM/MWCNTs [1,2].

Experimental

Materials

Injection grade of PP with the trade name of Jampilen EP440L (Jam Polypropylene Co, Iran, MFI =6 g/10min (230 °C, 2.16 kg)), EPDM with the trade name of KEP270 having Mooney viscosity of ML (1+4, 125 °C)=77, and multiwall carbon nanotubes (MWCNTs) with the trade

name of NC7000 with 90% purity were used to prepare TPV samples. Zinc oxide (ZnO), Stearic acid, Sulfur (S), MBTS, and TMTD were used as cross-linking agents.

Sample Preparation

The process of producing thermoplastic vulcanizates nanocomposites involved sequential steps: introducing PP into a Rheocord 90 internal mixer at 175 °C and 80 rpm, followed by EPDM after 3 min, crosslinking agents added after 5 min, and dynamic vulcanization continued for another 2 min. It should be noted that the blends were dynamically cured using a vulcanizing system reported elsewhere [2] Then, 3 wt % were introduced to the mixer, and the mixing continued for another 6 minutes. TPVs with varying MWCNTs levels were denoted as TPV5Cx, where 'x' indicating the volume content of MWCNTs. In order to study the effect of TPV microstructure on dispersion of nanoparticles, and electrical properties, nanocomposites based on PP/CNTs (97:3) were produced by introducing PP into the internal mixer at the same processing condition, and then CNTs were added to mixer after 3 min and mixing continued for another 6 min. The resulting nanocomposites were compression molded into 1mm thick sheets at 200 °C and 50 bar after preheating. The PP to EPDM weight ratio remained constant at 50/50 across all samples.

Characterization

The rheological behavior and melt viscoelastic properties of the nanocomposites were studied using a rheometric mechanical spectrometer (Paar Physica USD200) with a parallel plate (diameter=2.5 cm; gap=1 mm) at a temperature of 220 °C, frequency range of 0.01–1000 s⁻¹, and strain amplitude of 1%. Volume electrical resistivity was measured on compression-molded plaques with dimensions of 100 × 100 × 1 mm, using a Keithley

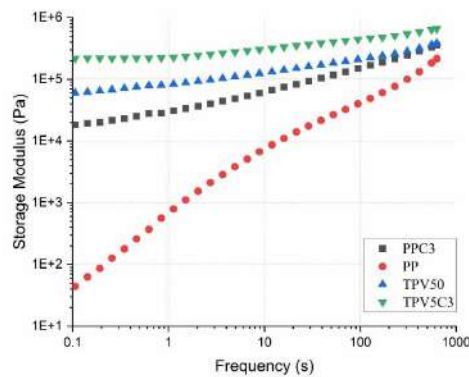


Fig. 1. Storage modulus (G') versus frequency of TPV, PP, and their nanocomposites containing 3 wt% MWCNTs.

electrometer model 6517B equipped with a high-resistance test fixture.

Results and Discussion

Fig. 1 shows storage modulus (G') versus frequency of TPV, PP and their nanocomposites containing 3 wt% MWCNTs. Addition of nanoparticles increased the storage modulus of both samples, and resulted in a much more stronger nonterminal behavior of storage modulus, especially in PP nanocomposites. Moreover, the slope of G' in low frequencies tend to zero with addition of nanoparticles, which is an indication of the formation of three-dimensional network between nanoparticles. In addition, because of the chosen feeding sequence in TPV samples, the selective localization of nanoparticles in PP matrix and on the interface of two phase can results in reinforcement of rubber network and/or formation of 3-D network between particle-particle and particle-matrix.

Fig. 2 presents storage modulus versus frequency of filled TPVs and PP relative to the storage modulus of their corresponding neat Polymers. Introducing MWCNTs increased the storage modulus of both polymers, but the trend is much more significant in the PP samples,

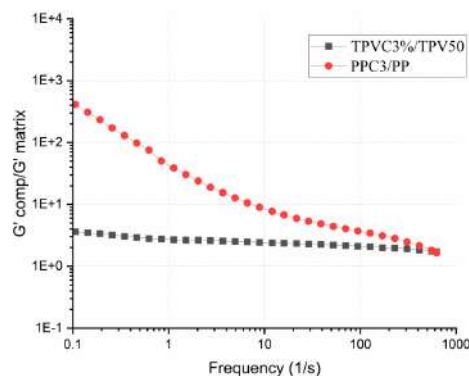


Fig. 2. Variation of relative storage modulus of PA6 and PP nanocomposites.

Table I. DC electrical conductivity of different TPV and PP nanocomposites containing 3 wt% MWCNTs.

Sample	CNTs Wt%	Electrical conductivity (S/cm)
TPV5C3	3	8.9E-9
PPC3	3	3.15E-5

especially at low frequencies. This behavior indicates that nanoparticles could form a better 3-D network in PP, compared to TPVs. In TPVs, the dispersion and distribution of nanoparticles are controlled by their microstructure, and the strong 3-D network between rubber particles hindered the dispersion of nanoparticles.

Table I shows DC electrical conductivity of different TPV and PP nanocomposites. Clearly, the electrical conductivity enhances significantly in PP nanocomposites. This could be the result of the TPV microstructure because the 3-D network between rubber particles have hindered the distribution of nanoparticles, so CNTs could not form an effective conductive path. Moreover, the rubber particles act as insulating phase, and this would also result in lower electrical conductivity in these samples.

Conclusion

In this study, TPV and PP nanocomposites containing 3 wt% CNTs were prepared and TPV microstructure on nanoparticles dispersion, and its relationship with linear viscoelastic properties, and electrical conductivity were investigated. The results indicated that the 3-D network between cured-rubber particles hindered a high degree dispersion of nanoparticles, and CNTs could not form a 3-D network in PP phase in TPVs, which was consistent with the rheological and electrical conductivity results.

References

- [1] W. Zhang, A.A. Dehghani-Sani, and R.S. Blackburn, *J. Mater. Sci.*, **42**, 3408-3418, 2007.
- [2] F. Goharpey, A.A. Katbab, and H. Nazockdast, *Rubber Chem. Technol.*, **76**, 239-252, 2003.

Spontaneous Imbibition of Viscoelastic Fluids in Paper-Based Rapid Diagnostic Kits

Farid Amjadizadeh¹, Mohammad Pourjafar-Chelikdani², and Kayvan Sadeghy^{1*}

1. School of Mechanical Engineering, College of Engineering, University of Tehran, Tehran, Iran

2. Caspian Faculty of Engineering, College of Engineering, University of Tehran, Rezvanshahr, Iran

*sadeghy@ur.ac.ir

Abstract

Spontaneous imbibition refers to infiltration of a wetting fluid into a porous material solely by the capillary pressure. In the present work, a generalized version of the Richards equation is introduced which enables investigating the effect of a fluid's elasticity on the quasi-steady regime needed to be established on the test line of rapid diagnostic kits. The idea is to revise the effective viscosity such that it incorporates the extra resistance caused by the large extensional viscosity of viscoelastic fluids. It is numerically shown that elasticity lowers the average velocity at the test line of the kit. On the other hand, it extends the time duration over which the velocity is nearly constant. The conclusion is that elasticity can be used as a passive means to control the average velocity in diagnostic kits. The new Richards equation can be used to determine the best location for drawing the test line.

Keywords: spontaneous imbibition, porous media, rapid diagnostic kits, viscoelastic fluid, Richards equation

Introduction

Spontaneous imbibition (SI) refers to the flow driven by capillary action when a wetting fluid such as water displaces a non-wetting fluid such as air from the pores of a material such as sandstone or cellulosic paper. This type of flow plays a key role in the operation of rapid diagnostic kits, which is why it has been the subject of extensive studies in the past. Studies carried out in the past were mostly devoted to Newtonian fluids. In the present work, we numerically investigate the effect of a fluid's elasticity on the imbibition phenomenon.

Theoretical Method

Fig. 1 shows the geometry of the membrane used in this study. It comprises a rectangular segment made of nitrocellulose membrane (NC) connected to a circular sector segment made of the same material. The rectangular part is of crucial importance as it is equipped with the "test line" on which chemical reactions take place to detect the

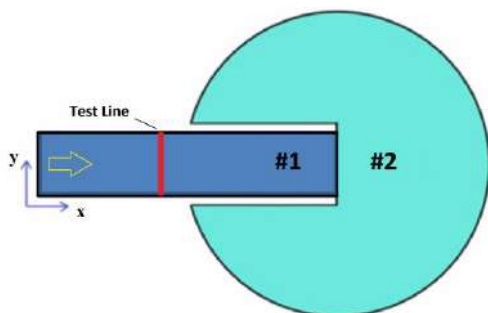


Fig. 1. The homogeneous nitrocellulose membrane used in this study to represent a typical diagnostic kit.

presence of a virus such as Covid-19. Mendez *et al.* [1] showed that for Newtonian fluids the circular pad makes the average velocity nearly constant on the test line for several minutes thereby increasing the device sensitivity. In a recent work, Asadi *et al.* [2] numerically demonstrated that for shear-thinning fluids obeying the power-law model ($\tau = m \dot{\gamma}^n$) the duration of the quasi-steady regime is shortened. In this work, we show, for first time that for viscoelastic fluids this useful regime is extended. To that end, we have modified the Richards equation so that it can be used for viscoelastic fluids.

For inelastic shear-thinning fluids, Asadi *et al.* [2] successfully modified Richards Equation as:

$$\varepsilon \left(\frac{\partial S}{\partial t} \right) = \bar{\nabla} \cdot \left(\frac{k(S)}{\mu_{\text{eff}}} \frac{\partial p_c(S)}{\partial S} \bar{\nabla} S \right), \quad (1)$$

where S is the saturation (i.e., moisture content in the pores), ε is the porosity, k is the permeability and p_c is the capillary pressure, where (k, p_c) are known functions of S . In this equation, μ_{eff} is the effective viscosity which for power-law fluids is a function of (m, n) . For elastic shear-thinning fluids, it is speculated that μ_{eff} should include a term related to the fluid's elasticity. In an inspiring experimental work, Barboza *et al.* [3] showed that for PAA polymer solutions, the viscosity in the Dracy's law (which is the basis of the Richards equation) should include the fluid's extensional viscosity. Based on this idea, the Richards equation can be re-written as:

$$\varepsilon \left(\frac{\partial S}{\partial t} \right) = \bar{\nabla} \cdot \left(\frac{k(S)}{(1+\alpha)\mu_{\text{eff}}} \frac{\partial p_c(S)}{\partial S} \bar{\nabla} S \right), \quad (2)$$

where α is a measure of a fluid's elasticity level, and it is positive for strain-hardening materials (i.e., $\alpha > 0$). In the present work, we numerically solve this equation using the PDE solver of COMSOL in order to obtain the saturation field, $S(x,y,t)$.

Having found $S(x,y,t)$ we can compute the liquid uptake from which we can determine the average velocity as a function of time for different values of the elasticity parameter (α) on the test line which is placed at $x=4$ cm from the inlet edge; see Fig. 1. For the simulations, the system is assumed to be initially dry ($S=0$). At inlet section, we impose $S=1$ with no-gradient imposed on all other edges of the membrane as the physical boundary conditions.

Results and Discussion

Fig. 2 shows that without the circular pad, the average

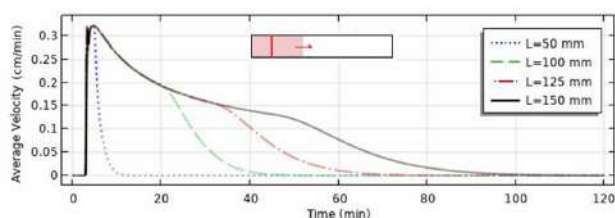


Fig. 2. Velocity at the test line with no circular pad ($n=1$).

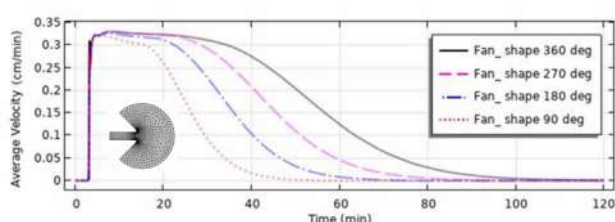


Fig. 3. Effect of the pad angle on the average velocity ($n=1$).

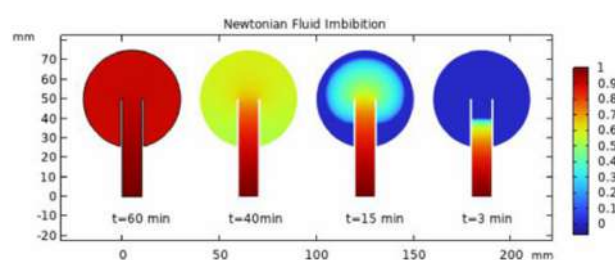


Fig. 4. Time evolution of the saturation field ($n=1$).

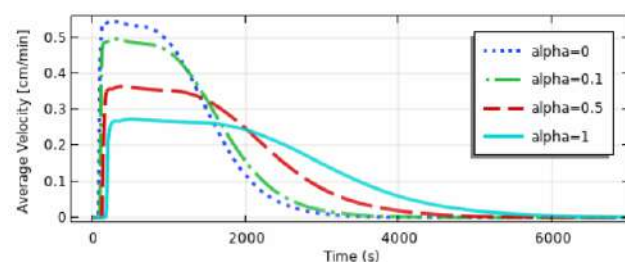


Fig. 5. Effect of the elasticity number (α) on the average velocity at the test line ($t=330$ s, $n=0.9$, $x=4$ cm).

velocity at the test line is not constant. On the other hand, as is seen in Fig. 3, with circular segment the average velocity becomes nearly constant for roughly 15 min for $\theta=360^\circ$; i.e., the circular pad, which becomes fully-saturated after roughly 60 min. For the circular pad, Fig. 4 shows that elasticity causes the average velocity to drop, but it increases the time span over which the quasi-steady regime can be established for a kit.

Conclusion

A general mathematical framework based on the Darcy's law has been developed for predicting the spontaneous imbibition of viscoelastic liquids in paper-based microfluidic kits. The main aim of the study is to obtain a quasi-steady flow by choosing appropriate geometry and absorbent pad microstructure for viscoelastic fluids. The results represent viscoelasticity helps to broaden this flow regime. The conclusion is that polymer additives can be used to passively control the quasi-steady regime in rapid diagnostic kits.

References

- [1] S. Mendez et al., "Imbibition in porous membranes of complex shape: Quasi-stationary flow in thin rectangular segments", *Langmuir*, **26**, 1380-1385, 2020.
- [2] H. Asadi, M. Pourjafar-Chelikdani, N.P. Khabazi, and K. Sadeghy, "Quasi-steady imbibition of physiological liquids in paper-based microfluidic kits: Effect of shear-thinning", *Phys. Fluid.*, **34**, 2022.
- [3] M. Barboza, C. Rangel, and B. Mena, "Viscoelastic effects in flow through porous media", *J. Rheol.*, **23**, 1979.

Rheological and Morphological Analysis as Approaches to Investigate Barrier Properties of PLA/EVOH Blend Films

Maedeh Asadi, Hossein Nazokdast*, and Hamid Garmabi*

Department of Polymer Engineering, Amirkabir University of Technology, Tehran, Iran

*Nazdast@aut.ac.ir, Garmabi@aut.ac.ir

Abstract

PLA as a biodegradable polymer was blended with EVOH having excellent barrier properties. The research was aimed at achieving a laminar blend morphology to minimize the solvent permeability. EVA was used as the compatibilizer. The rheological behaviors and morphology of the compatibilized blends were thoroughly investigated. A viscosity upturn was observed at low frequency region for samples containing more than 10% EVOH, indicating a structural change. The optimized blend showed a 66% reduction in solvent permeability, compared to the neat PLA.

Keywords: barrier properties, food packaging, laminar morphology, PLA, EVOH, rheological analysis

Introduction

The use of plastic materials in food and beverage packaging has increased, replacing traditional options like metal and glass. However, the main drawback is their reliance on non-renewable petroleum sources and slow decomposition in the environment [1,2]. To address this, researchers are exploring poly(lactic acid) (PLA) as a biodegradable alternative for food packaging to reduce dependence on petroleum-based plastics. However, its barrier properties need improvement to meet strict requirements for food packaging [3,4]. In most cases, one polymeric material cannot offer all the properties required; therefore, a combination of polymers is employed. In cases involving immiscible polymer blends, the recommended phase morphologies that exhibit superior barrier properties are the co-continuous and laminar structures. Particularly, the laminar structure assumes an orientation perpendicular to the diffusion path. Within this configuration, the platelet-like formations function as obstacles for permeating molecules by providing a long tortuous path. EVOH is a suitable candidate for enhancing the barrier properties of PLA due to its remarkable low permeability to oxygen, carbon dioxide, hydrocarbons, and organic solvents [5,6].

Experimental

The PLA (grade 4032D) with 98% L-lactic isomer content was provided by NatureWorks Co. (USA). EVOH under the trade name F101A, a random copolymer containing 32 mol% ethylene segments was obtained from Kuraray Co. (Japan) and ethylene vinyl acetate (EVA grade VS430) with 19% VA content was derived from Lotte Chemical Co. (Korea). Methyl ethyl ketone (MEK) with 0.98 mass fraction purity was supplied by Merck Chemical Co. (Germany) for the solvent permeability test.

PLA/EVOH blends with EVOH contents of (S1) 10, (S2) 20, and (S3) 30 wt% were prepared using a single-

screw Brabender extruder (Germany) equipped with a planar die. The screw speed was fixed at 10 rpm and the temperature zones of the barrel from the hopper to the die were set at 170, 180, 200, 210, and 210 °C. The films were further molded using a hot-press (Mini Test Press, ToyoSeiki) at 205 °C with a pressure of 35 MPa. The ratio of the compatibilizer to the dispersed phase has been considered almost constant (0.3) in all samples.

Results and Discussion

Rheological Analysis

To determine the range of strain amplitude below which the linear viscoelastic behavior prevails, the strain amplitude sweep experiment was performed on blend samples at an angular frequency of 1 rads^{-1} in the overall range of 0.001–10 (figure not shown). Therefore, all measurements were performed in an amplitude of 1%. The complex viscosity of PLA, EVOH, and PLA/EVOH blends has

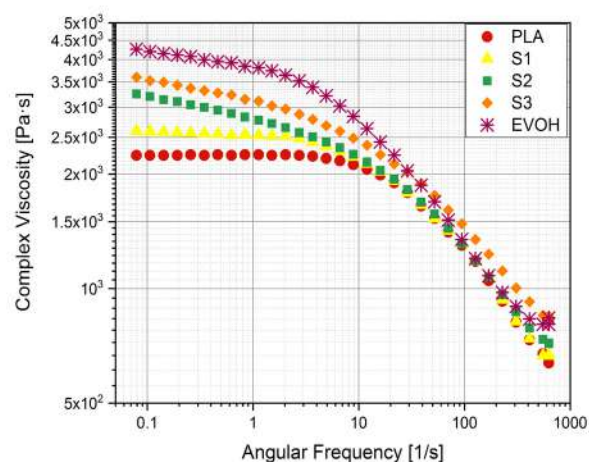


Fig. 1. Complex viscosity vs. frequency for the neat PLA and EVOH and their blends at 210 °C and 1% strain.

been shown versus frequency in Fig. 1. It can be seen the melt viscosity of the dispersed phase is higher than the viscosity of the matrix. This could be attributed to the higher physical entanglement of EVOH and the presence of hydrogen bonding. Also, the neat PLA displayed a Newtonian liquid behavior at low frequency. The blends exhibited a higher complex viscosity at low frequency and distinct shear-thinning behavior during the frequency range. For compositions more than 10% ($\geq 20\%$), an upturn in viscosity is seen at low frequencies which indicates a change in the blend structure and also reflects the shape-relaxation behavior of the dispersed droplets. It can be suggested that the dispersed phase droplets have been elongated, forming a semi-co-continues structure. This significant enhancement in the melt viscosity of PLA/EVOH blends led to an increase in melt strength, which was favorable for the processing of producing films.

Morphological Analysis

SEM micrographs of the cryo-fractured cross-sectional surface of PLA/EVOH blends with various compositions are presented in Fig. 2. The visual evidence from these images indicates that upon blending these two polymers, three distinct morphological types generated: the first exhibits an ellipsoidal shape of the EVOH phase dispersion (sample 1), the second displays a lamellar or ribbon-like structure (sample 2), and the third showcases a laminar morphology (sample 3). An increase in EVOH content resulted in a gradual enlargement of droplet size and an increase in the occurrence of the coalescence process. Since the melt viscosity of the matrix is lower than that of the dispersed phase, this phenomenon occurs rapidly.

Barrier Properties

When two polymers are blended, the barrier properties of the resulting system strongly depend on the blend morphologies. The laminar system corresponds to an immiscible system with an ideal morphology similar to the structure of an alternating multilayer film. The permeability

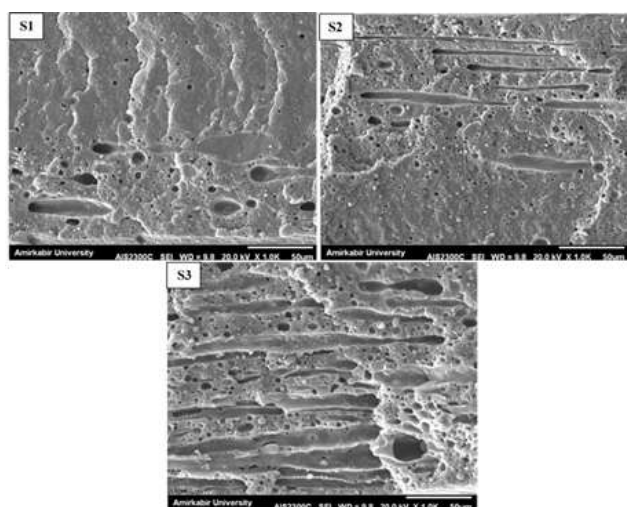


Fig. 2. The SEM images of prepared blends.

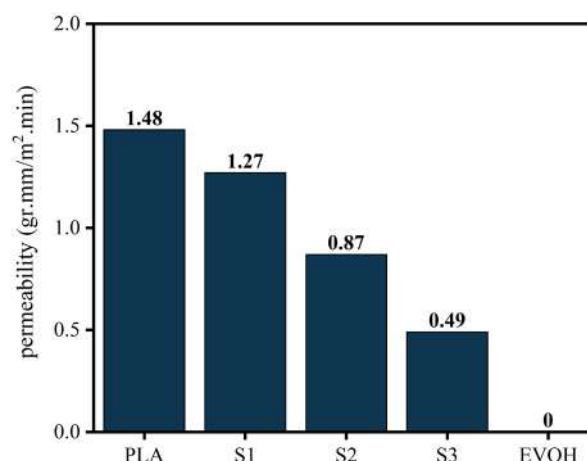


Fig. 3. Permeability of PLA, EVOH, and blend samples.

of these systems to the solvent MEK was examined. Based on the results, as the EVOH content increased to 30%, the solvent permeability 66% decreased. Remarkably, all samples even at a low EVOH content (around 10 wt%), have a negative deviation from the mixing law. It seems the unexpectedly high solvent barrier properties of samples can be ascribed to the combination of two dominant effects: the tortuous diffusion path through the laminar morphology and adding barrier polymer to a matrix. These discrete semi-planar EVOH domains effectively prolong the diffusion pathway of the solvent molecules, leading to a low permeability coefficient, referred to as the “tortuosity effect”.

Conclusion

In this research, films with high solvent barrier properties were prepared using compatibilized PLA/EVOH blends. The amount of EVOH affected the viscosities and had a significant influence on both the enhancement of melt viscosity and the development of a laminar morphology. The tortuosity effect and adding barrier polymer are the main factors leading to the high barrier properties of PLA/EVOH blends.

References

- [1] C.M.N. Romagnolli, G.P. Leite, T.A.R. Rodrigues, and C.L. Morelli, **11**, 2020.
- [2] M. Nofar, A. Maani, H. Sojoudi, M.C. Heuzey, and P.J. Carreau, *J. Rheol.*, **59**, 2015.
- [3] X. Li et al., *Polym. Adv. Technol.*, **29**, 2018.
- [4] Z. Gui, W. Zhang, C. Lu, and S. Cheng, *J. Macromol. Sci. Part B Phys.*, **52**, 2013.
- [5] M.R. Kamal, H. Garmabi, S. Hozhabr, and L. Arghyris, *Polym. Eng. Sci.*, **35**, 1995.
- [6] J. Kim, S. Oh, S.M. Cho, J. Jun, and S. Kwak, *J. Appl. Polym. Sci.*, **137**, 2020.

Polygonal Model to Investigate Polymer Droplet Deformation

Saleh Heydarpour and Mohammad Hossein Navid Famili*

Tarbiat Modares University, Tehran, Iran

*nfamili@modares.ac.ir

Abstract

One of the important challenges in investigating the rheology of polymer solutions is the deformation of a droplet under stress in the matrix until the moment of breakup. In the presented model, the shape of the droplet is considered as a polygon. Each side of this polygon can be changed independently from other sides. The side change is a function of the velocity gradient. Knowing the sides the geometric shape of the droplet can be drawn at any moment. In the experimental part, polyethylene glycol water-soluble form with concentration of 37% is used as the dispersed phase and PDMS is used as the matrix. By comparing the results of the geometric dimensions of the droplet shape in the experiment and the model (the ratio of length to width and the ratio of lateral surface area), a deviation of less than 10% is observed. Also the breakup is accurately predicted.

Keywords: drop deformation, velocity gradient, interface, normal vector, viscous drop

Introduction

In order to study the change of the drop shape, first, the shape of the drop is assumed to be a disc with a polygonal cross-section and a constant thickness. The cross section of the droplet is considered to be a regular 2000 square with radius r_0 and thickness r_0 . Each side is cut and can be changed direction and size independently of other sides. After changing each side, the shape of the droplet is drawn again by combining the sides. This process is repeated every time until breakup.

Theoretical

The normal vectors at all points over the droplet and the length of all sides (lateral area of each side) are precisely defined (S). Eq. (1) displays the deformation rate of normal vector (\bar{n}) by velocity gradient tensor (L). Eq. (2) also verifies the rate of the change of the length of any side (lateral area of each side) by the velocity gradient [1,2]:

$$\frac{d(\bar{n}_i)}{dt} = (\bar{n}_i \cdot \bar{L}_i \cdot \bar{n}_i) \bar{n}_i - \bar{L}_i^T \cdot \bar{n}_i \rightarrow \dot{n}_i^t = \dot{n}_i^{t-1} + \Delta t ((\bar{n}_i \cdot \bar{L}_i \cdot \bar{n}_i) \bar{n}_i - \bar{L}_i^T \cdot \bar{n}_i) \quad (1)$$

$$\frac{d(S_i)}{dt} = (tr \bar{L}_i \cdot \bar{n}_i \cdot \bar{L}_i \cdot \bar{n}_i) S_i \rightarrow \dot{S}_i^t = \dot{S}_i^{t-1} + \Delta t ((tr \bar{L}_i \cdot \bar{n}_i \cdot \bar{L}_i \cdot \bar{n}_i) S_i) \quad (2)$$

Δt indicates the time step of solving differential Eqs. (1) and (2), while i and t represent the points on droplet and time respectively. To calculate the velocity gradient components at the interface, Eqs. (3) to (7) must be solved simultaneously for each point. Eqs. (8) to (11) show the components of the L tensor:

$$(\bar{\sigma}_{over})_i = \lambda^{-1} |\mu_m - \mu_d| \begin{bmatrix} \dot{\gamma}_{max} & \dot{\gamma}_{mxy} \\ \dot{\gamma}_{mxy} & \dot{\gamma}_{mxy} \end{bmatrix} - \mu_d \begin{bmatrix} 2(\frac{\partial u}{\partial x})_i & (\frac{\partial u}{\partial y})_i + (\frac{\partial v}{\partial x})_i \\ (\frac{\partial u}{\partial y})_i + (\frac{\partial v}{\partial x})_i & 2(\frac{\partial v}{\partial y})_i \end{bmatrix} \quad (3)$$

$$(\bar{\sigma}_d)_i = \mu_d \left[2\left(\frac{\partial u}{\partial x}\right)_i - \frac{\Gamma S_i'}{V \mu_d} ((n_{xi}^t)^2 - 0.5) \left(\left(\frac{\partial u}{\partial y}\right)_i + \left(\frac{\partial v}{\partial x}\right)_i - \frac{\Gamma S_i'}{V \mu_d} n_{xi}^t n_{yi}^t \right) \right. \\ \left. \left(\left(\frac{\partial u}{\partial y}\right)_i + \left(\frac{\partial v}{\partial x}\right)_i - \frac{\Gamma S_i'}{V \mu_d} n_{xi}^t n_{yi}^t \right) - 2\left(\frac{\partial v}{\partial y}\right)_i - \frac{\Gamma S_i'}{V \mu_d} ((n_{yi}^t)^2 - 0.5) \right] \quad (4)$$

$$(\sigma_{TANGENTIAL})_i^t = ((\sigma_{over})_i^t \cdot \bar{n}_i - (\sigma_d)_i^t \cdot \bar{n}_i) \cdot \bar{n}_i = 0 \quad (5)$$

$$(\sigma_{NORMAL})_i^t = ((\sigma_{over})_i^t \cdot \bar{n}_i - (\sigma_d)_i^t \cdot \bar{n}_i) \cdot \bar{n}_i = -\Gamma \frac{V_i^t}{V} \kappa_i^t \left(\bar{n}_i \cdot \bar{n}_i \right) \quad (6)$$

$$(\nabla \cdot \bar{U})_i^t = 0 \rightarrow \left(\frac{\partial u}{\partial x}\right)_i^t + \left(\frac{\partial v}{\partial y}\right)_i^t = 0 \rightarrow \left(\frac{\partial v}{\partial y}\right)_i^t = -\left(\frac{\partial u}{\partial x}\right)_i^t \quad (7)$$

$$L_{xyi}^t = \left(\frac{\partial u}{\partial y}\right)_i^t = \frac{(n_{xi}^t - n_{yi}^t)}{8\mu_d (2n_{xi}^t - n_{yi}^t)} \left[\frac{Q_i^t + \Gamma \frac{S_i^t}{V} ((n_{xi}^t)^4 - (n_{yi}^t)^4 + 4n_{xi}^t n_{yi}^t)}{+4\Gamma \frac{V_i^t}{V} \kappa_i^t ((n_{yi}^t)^2 - (n_{xi}^t)^2 + 2n_{xi}^t n_{yi}^t)} \right] \quad (8)$$

$$Q_i^t = 2\lambda^{-1} |\mu_m - \mu_d| \left[\dot{\gamma}_{max} n_{xi}^t (2n_{yi}^t - n_{xi}^t) + \dot{\gamma}_{mxy} n_{yi}^t (2n_{yi}^t - n_{xi}^t) \right. \\ \left. + \dot{\gamma}_{mxy} n_{xi}^t (2n_{xi}^t + n_{yi}^t) + \dot{\gamma}_{mxy} n_{yi}^t (2n_{xi}^t + n_{yi}^t) \right] \quad (9)$$

$$L_{xyi}^t = \left(\frac{\partial v}{\partial x}\right)_i^t = \frac{\lambda^{-1} |\mu_m - \mu_d| \left[\dot{\gamma}_{max} n_{xi}^t n_{yi}^t + \dot{\gamma}_{mxy} n_{yi}^t - \dot{\gamma}_{mxy} n_{xi}^t - \dot{\gamma}_{mxy} n_{xi}^t n_{yi}^t \right]}{2\mu_d \left(-(n_{xi}^t)^2 + 4n_{xi}^t n_{yi}^t + (n_{yi}^t)^2 \right) (n_{xi}^t - n_{yi}^t)} \\ + \frac{\mu_d L_{xyi}^t (2(n_{xi}^t - n_{yi}^t)^2 + 8(n_{xi}^t)^2 n_{yi}^t)}{2\mu_d \left(-(n_{xi}^t)^2 + 4n_{xi}^t n_{yi}^t + (n_{yi}^t)^2 \right) (n_{xi}^t - n_{yi}^t)} \quad (10)$$

$$L_{xxi}^t = \frac{L_{xyi}^t}{n_{yi}^t - n_{xi}^t} + L_{yxi}^t \quad (11)$$

Symbols $\dot{\gamma}$, Γ , V_i , V , κ , μ_d , μ_m , λ , u and v indicate the shear rate, interfacial tension coefficient, the volume of each sector, total volume of droplet, curvature, viscosity of droplet, viscosity of matrix, droplet to matrix viscosity ratio, velocity in x direction and velocity in the y direction respectively.

Experimental

The deformation of the droplet in the matrix was investigated

by concentric rheometer. The rheological parameters used are as follows. $\mu_d=0.2$ Pa.s, $\mu_m=0.5$ Pa.s, $\gamma_{mxy} = \dot{\gamma}_{myx} = 4.08$ s⁻¹, $r_0=0.0012$ m, $\Gamma=0.009$ N.m⁻¹, $\lambda=0.4$.

Results and Discussion

The shape of the droplet is illustrated in Figs. 1 and 2 from the initial time until it breaks up in order to compare the experimental and simulation outcomes. As can be seen in Fig. 2, the moment of breakup of droplet coincides with the experimental results. To ensure reproducibility, the experimental part was performed 4 times. The results of this repetition are shown as bars in Figs. 3 and 4. In Fig. 3, for a better comparison of the model and experimental results, the ratio of the lateral area of the droplet at any time to the initial droplet is plotted. Also, in Fig. 4, the ratio of the length of the stretched droplet to its width is plotted

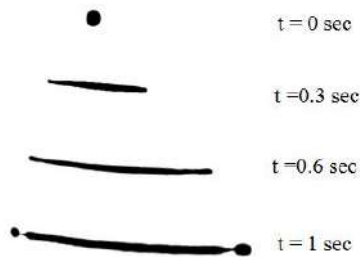


Fig. 1. Experimental result of PEG 37 droplet deformation.

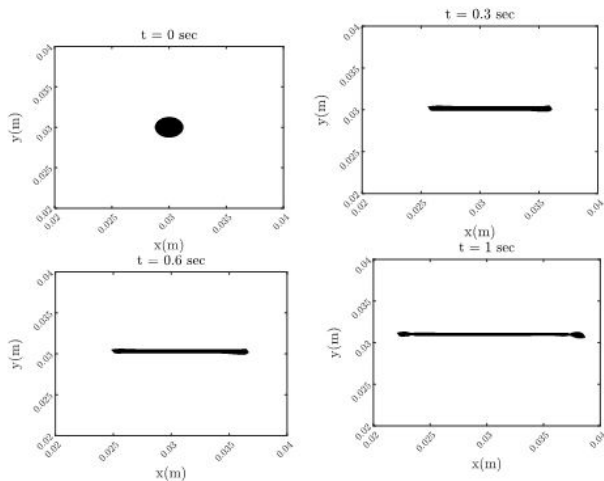


Fig. 2. Model result of PEG 37 droplet deformation.

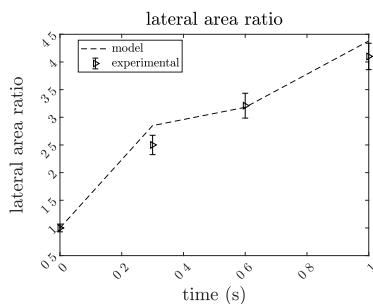


Fig. 3. Lateral area to initial lateral area ratio of droplet.

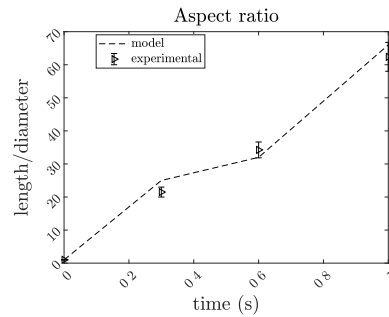


Fig. 4. Length to diameter ratio of droplet vs time.

versus time. Figs. 3 and 4 confirm that the deviation of model and experimental results is less than 10%.

Conclusion

In the presented model, viscous behavior is assumed for matrix and droplet (PDMS as matrix and PEG in aqueous solution with 37% concentration as droplet).

By assuming the shape of the droplet as a 2000-sided polygon and changing the normal vector of each side and drawing it again after the change, the new shape of the droplet is obtained. Using this model, the shape of the drop can be drawn at any time. This model can be used for any initial drop shape (regular or irregular polygon). The obtained results show that the moment of the droplet breakup is predicted with high accuracy and the dimensions of the droplet are in significant agreement with the experimental results. This model opens a new way to investigate emulsions and polymer blends.

References

- [1] R. Abeyaratne, *Lecture Notes on The Mechanics of Elastic Solids Volume II: Continuum Mechanics*, Cambridge MA and Singapore, Electronic Publication, 2012, pp. 71-73.
- [2] L.G. Leal, *Advanced Transport Phenomena: Fluid Mechanics and Convective Transport Processes*, Cambridge University Press, vol. 7, 2007.

Rheological Analysis as a Determining Factor in the Manufacturing Process of Expanded Polypropylene

Sina Bazrpash, Zahra Mohammadi, and Seyed Reza Ghaffarian Anbaran*

Department of Polymer Engineering and Color Technology, Amirkabir University of Technology, Tehran, Iran

*sr_ghaffarian@aut.ac.ir

Abstract

Polypropylene bead foams have been popular in various industries due to their suitable properties and ability to produce multiple geometries. However, the lack of practical criteria in determining the required strength of the base polymer has always made this process difficult. In this research, the effect of the presence of kaolin nanoparticles in the production process of expanded polypropylene was investigated concerning the possibility of creating a physical network of connections using rheological tests, and the sample containing the ideal amount of nanoparticles was identified as the optimal sample.

Keywords: expanded polypropylene, rheological analysis, kaolin, bead foaming, physical crosslink

Introduction

Using foams with a specific structure and unique properties, such as high non-reactivity, heat insulation, and sound insulation, has become popular in various industrial fields. However, producing this class of materials with complex geometries is challenging and has been the focus of many studies and research. Among the approaches applied in response to this challenge is using the production process of bead foams. In this process, the basic masterbatch is first prepared according to the required properties, and then the beads with specific dimensions are made. Then these beads are transformed into granular foams under a certain pressure and temperature stage. These foamed beads will be turned into the final product in specific moulds with various geometries [1].

In this regard, the use of polymers such as polyethylene, polystyrene, or polypropylene as the raw material of this category of foams has been suggested, of which polypropylene has been favoured with higher thermal resistance, as well as mechanical properties and full recycling capability [2]. However, the use of different grades of polypropylene to achieve the ideal melt strength in the foaming process without considering a suitable standard has caused various and sometimes weak types of bead foams of this polymer to be produced, or sometimes due to the low strength of the base polymer melt, the process could not lead to the production of foamed beads [3].

In this research, to increase the melt strength of the polymer, first, nanocomposite modifications based on polypropylene/kaolin nanoparticles were prepared, and then rheological behaviour was used to check the number of changes obtained. Afterwards, bead foams will be produced according to the accepted rheological behaviour, and their feasibility will be studied.

Experimental

In this study, polypropylene terpolymer containing up to 5% by weight of ethylene and butene was used. For the synthesis of nanocomposite samples, firstly, the terpolymer sample was converted into maleic polypropylene during the modification process, and then a double-screw extruder was used to uniformly spread kaolin nanoparticles modified using silane in the polymer bed. Ensuring the uniform dispersion of nanoparticles has been looked at using an X-ray diffraction test. Using the thermal behaviour of the resulting samples, the temperature, pressure and time of the foaming process were determined, and then rheological tests such as the frequency sweep test were performed at the temperature of the foaming process. The naming of the samples is based on the amount of nanoparticles (phr) in each instance as PP, PP/Nano (99.90/0.10), PP/Nano (99.75/0.25), PP/Nano (99.50/0.50).

Results and Discussion

Carrying out the specified modifications on the base polymer and the nanoparticles used caused the creation of hydroxyl and maleic anhydride groups on the nanoparticle and polymer chain. For this reason, according to Fig. 1, with the increase in the amount of nanoparticles, although the shear thinning behaviour is still observed, the complex viscosity of the samples with Attention has been paid to the increase in the density of physical crosslinks due to hydrogen bonding.

Fig. 2 shows Cole-Cole plots of η^* (η'' against η'). According to this figure, for the sample without nanoparticles, the graph is in the form of a semicircle and without a tail, which indicates its linear structure, while the samples containing nanoparticles deviate from this behaviour, and this issue is evident in higher η' . Violation

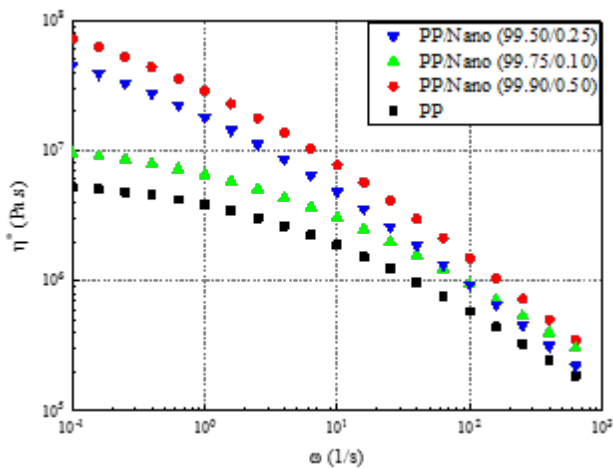


Fig. 1. Complex viscosity (η^*) as a function of frequency (ω) for blends with different nanoparticle content.

of the semicircle shape and creation of a tail in the diagram of samples containing nanoparticles is caused by the increase in the relaxation time of the chains due to the result of physical crosslinks.

Fig. 3 shows the van Gorp-Palmen (vGP) plots for the investigated samples. The selection without nanoparticles has a linear behaviour and a reduction from its linear structure. For the samples containing nanoparticles, it is clear that at constant G' , the value of δ is lower than the sample without nanoparticles, which indicates the increase of elasticity of the pieces. Also, samples with nanoparticles have a transmission angle marked in the figure, and the value, the relative maximum of each graph, decreases with increasing amount of nanoparticles. Such an observed trend also indicates the presence of physical transverse connections in the masterbatch structure.

Suppose the obtained results are related to the melt resistance of the samples. In that case, it is clear that the base polymer's melt resistance has increased with the amount of nanoparticles for the received samples. But in the final production stage, a model with the amount of nanoparticles

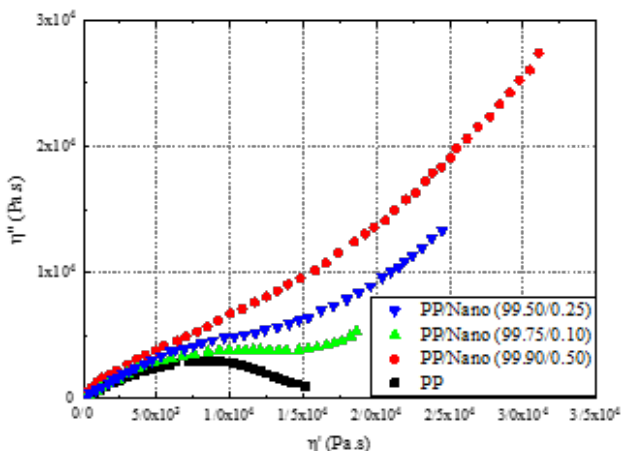


Fig. 2. Cole-Cole plots of viscosity (η^*) for blends with different nanoparticle content.

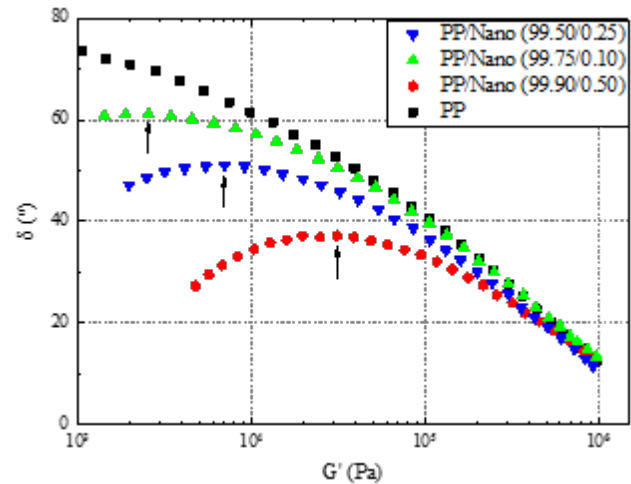


Fig. 3. van Gorp-Palmen (vGP) plots of blends with different nanoparticle content.

equal to 0.5 phr was determined, which did not allow the growth of air cells and the formation of foam due to the increase in melt resistance, and the sample containing 0.25 was used as the optimal ones.

Conclusion

At first, nanocomposite was prepared with based on polypropylene (terpolymer) and modified kaolin nanoparticles. Using a detailed examination of the results of rheology tests for samples synthesized with different amounts of nanoparticles, it was determined that the presence of nanoparticles would increase the density of physical crosslinks and, eventually, the elastic behaviour of the base polymer will lead to an increase in melt strength. Further, the sample containing 0.25 phr was selected as the optimal sample by performing the foaming process.

References

- [1] D. Tammaro, A. Ballesteros, C. Walker, N. Reichelt, and U. Trommsdorff, "Expanded beads of high melt strength polypropylene moldable at low steam pressure by foam extrusion", *Polymers (Basel)*, **14**, 205, 2022.
- [2] J. Kuhnigk, T. Standau, D. Dörr, C. Brütting, V. Altstädt, and H. Ruckdäschel, "Progress in the development of bead foams--a review", *J. Cell. Plast.*, **58**, 707-735, 2022.
- [3] P. Guo, Y. Xu, M. Lyu, and S. Zhang, "Fabrication of expanded ethylene--propylene--butene-1 copolymer bead", *Ind. Eng. Chem. Res.*, **61**, 2392-2402, 2022.

Rheological Behavior of PVC Plastisol: The Effect of Filler, Thickener, Plasticizer Contents

Sogol Ghasemi^{1*}, Mohsen Mohseni¹, Fatemeh Goharpey¹, and Masoumeh Izadi²

1. Department of Polymer and Color Engineering, Amirkabir University of Technology, Tehran, Iran

2. Maral Rang Co., Tehran, Iran

*sevgilghasemi@gmail.com

Abstract

In this study, the researchers investigated the rheological properties of plastisol coatings, which are used in applications such as sealing, insulation under body cars, and more. The researchers found that the three parameters of K-Value, plasticizer percentage, and concentrate thickener particle size significantly influence the rheological properties of plastisol coatings. Manipulation of these parameters allowed the researchers to control the gel and melting processes. The use of a thickener in plastisol coatings resulted in a more thixotropic fluid, with increasing thickener particle size leading to a faster process. The researchers also found that the high concentration of resin, thicknesses, and mechanical properties of plastisol coatings make them a good choice for applications requiring such features. The study highlights the importance of rheology in plastisol coatings, and its potential to optimize the manufacturing process and improve the quality of the final product.

Keywords: plastisol, rheology, thixotropic fluid, coating, sealing

Introduction

Polyvinyl chloride (PVC) plastisol, which is commonly used in the coating industry, undergoes a transformation from a suspension state to a polymer melt state during the gel and melting process. This transition affects its rheological behavior and is of great importance in understanding and controlling the properties of the plastisol [1].

One factor that influences the rheology of plastisol is the particle size and distribution of the PVC resin. A uniform particle size distribution with smaller particles increases the contact surface area and particle interactions, which leads to an increase in viscosity [2].

The molecular weight of the PVC resin also plays a role in its rheological behavior. Higher molecular weight samples have a higher modulus, meaning they exhibit greater resistance to flow. Lower molecular weight samples, on the other hand, have a lower modulus and lower viscosity [3].

The presence of fillers in the plastisol can also affect its rheology. Fillers increase interactions between particles and can lead to an increase in viscosity. Similarly, the use of a surface active agent can directly impact interactions between particles and alter the rheological behavior of the plastisol. The type and amount of softener used in the plastisol formulation also significantly affect its rheology. Increasing the amount of softener can reduce the modulus before and after the gel and melting process, making the plastisol less resistant to flow. Additionally, the type of softener can affect the solubility of the PVC resin and influence the rate of aging during storage [4].

Experimental

In order to investigate the effect of the mentioned factors on the rheological properties of plastisol, the experiment was designed to investigate the effect of the amount of plasticizer, the amount of thickener, and K-value of PVC on the rheological properties of the material. In this experiment, Minitab software and Box-Behnken method were used, changing three variables. 15 samples were designed and made using the dispersion method of solid particles in plasticizer binder and then vacuuming the sample with a pressure of 5 bar. After that, the 3ITT test was performed on all samples to check the amount of material recovery percentage in 60 s. Also, the usual rheometry test used in the quality control of these materials was also performed to determine the yield point and viscosity of the materials. These rheometric tests were performed using ANTON PAAR-RHEOLAB QC rheometer device and CC17 cup. Table I shows general formulation of plastisol that used in this research.

Results and Discussion

According to the Figs. 1, 2, and 3 it can be concluded that by

Table I. General formulation of plastisol.

Components	Percentage %
Resin(PVC)	30
Plasticizer(DOP)	20
Filler(CaCO ₃)	40
Additives	7
Thickener	3

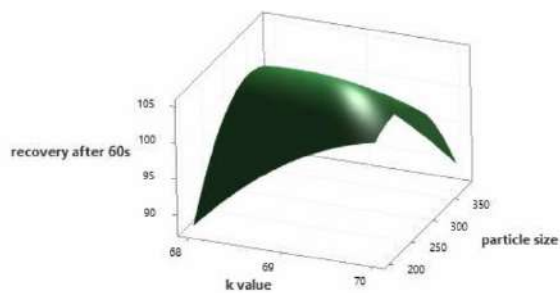


Fig. 1. Surface plot of recovery after 60 s vs particle size, K-value-hold values DOP content 24%.

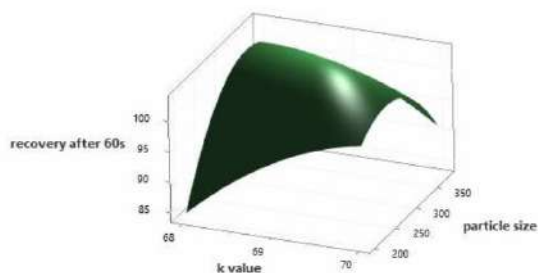


Fig. 2. Surface plot of recovery after 60 s vs particle size, K-value-hold values DOP content 28%.

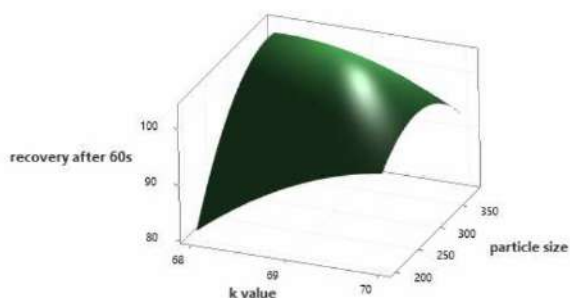


Fig. 3. Surface plot of recovery after 60 s vs particle size, K-value-hold values DOP content 32%.

increasing the K-value, the amount of return time increases because by increasing the length of the resin chain more time is needed to return the transferred tension to the chain. Increasing the particle size up to an optimum point has an effect. First, by increasing the particle size, the incremental process returns to and after passing the size of about three hundred microns, this trend becomes downward. Increasing the amount of plasticizer also has the effect of reducing the

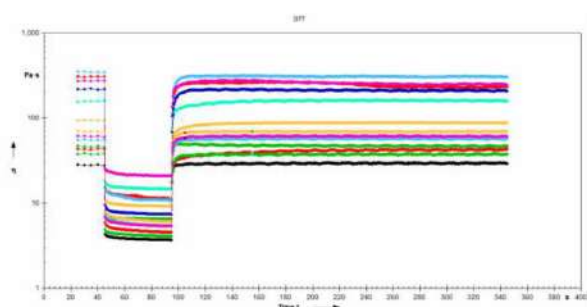


Fig. 4. 3ITT test results for recovery after 60 s.

recovery time. Increasing the amount of plasticizer causes it is possible for the viscosity to decrease significantly, this decrease in viscosity facilitates the transfer of stress because it actually leads to a decrease in the total size of the plastisol particles and this decrease in the process accelerates stress transfer.

The usual rheometric test determines the yield stress, viscosity at infinite stress, and the type of fluid. However, there were three samples in which the viscosity was too low to measure. Fig. 4 shows 3ITT result of these samples.

Conclusion

1. Increasing the amount of plasticizer decreases the yield point and viscosity infinitely.
2. Increasing the K-Value and particle size increases both the yield point and viscosity.
3. Increasing the concentration of thickener particles leads to a more thixotropic fluid.
4. The use of a thickener generally results in a more thixotropic fluid, but increasing the particle size of the thickener speeds up the process.

References

- [1] L.I. Trademark Office Hill, (1982). U.S. Patent No. 4,358,499. Washington, DC: U.S. Patent and Trademark Office.
- [2] N. Nakajima and E.R. Harrell, "Rheology of PVC plastisol: Particle size distribution and viscoelastic properties", *J. Colloid Interf. Sci.*, **238**, 105-115, 2001.
- [3] S.J. Willey and C.W. Macosko, "Steady Shear Rheological Behavior of PVC Plastisol", *J. Rheol. (N. Y. N. Y)*, 1978.
- [4] Y. Abdesselam et al., "Rheology of plastisol formulations for coating applications", *Polym. Eng. Sci.*, 2017.

Molecular Perspective of Elongational Rheology of a Viscoelastic Fluid

Abbas Sheikh

Polymer Engineering Department, Faculty of Chemical Engineering, Tarbiat Modares University, Tehran, Iran

a.sheikh@modares.ac.ir

Abstract

The study investigated the uniaxial elongational flow behavior of the FENE-P chains through the application of a micro-macro approach. This was compared and contrasted with the Rouse chains to reveal the effect of finite extensibility on the rheological behavior. The method yielded results consistent with analytical predictions for the Hookean dumbbells and successfully replicated the prior simulation outcomes for the FENE-P chains. Since this methodology relies on a molecular model, it also facilitated the acquisition of additional structural data of the ensemble of chains, such as end-to-end distance and radius of gyration, and their changes over time were explored. The findings unveiled distinct rheological responses of the FENE-P chains during elongation as opposed to shear, offering valuable insights into the relationship between chain structure and its rheological behavior.

Keywords: FENE-P chains, inception uniaxial elongational flow, smoluchowski approach

Introduction

Elongational flows are dominant in polymer processes such as fiber spinning, film blowing, the tenter method for biaxial orientation, and blow molding. Also, a class of standard flows for studying non-Newtonian fluids is elongational. However, despite the kinematical simplicity of standard elongational flows, including uniaxial, biaxial, and planar ones, they are not as widely used as shear flows due to difficulties in practice. There is no such limitation in simulating the rheological behavior of non-Newtonian fluids. In addition, the experimental equipment for elongational flows undergoes a lot of improvements during these years. Viscoelastic fluids behave differently in shear compared to elongation. This is affected by parameters like molecular weight and its distribution, chain architecture, interactions, and entanglement. Employing molecular-based constitutive equations enables us to follow the origin of the rheological performance of polymeric fluids [1,2].

In this paper, the transient elongational rheology of the FENE-P chain model in uniaxial elongational flow is studied. To this end, a recent micro-macro approach has been utilized [3]. After double verification of the methodology for the elongational flow with analytical results [4] and simulation data [5] in the same conditions, some structural information, such as end-to-end distance, and the gyration tensor, have been obtained as a function of time. This continued until the steady state. Thus, steady-state rheological and structural data are available.

Theoretical

The methodology employed here has been explained elsewhere for the elastic dumbbells in shear flows. In this work, an extension of this methodology is made to elastic

chains and elongational flows. Based on the Smoluchowski approach, for an ensemble of elastic chains with N beads and $N-1$ springs in which the connector vector \mathbf{Q}_i joins the i^{th} bead to its next one, the evolution equation for the second moment, $\hat{\mathbf{o}}_{jk} = \langle \mathbf{Q}_j \mathbf{Q}_k \rangle$ reads [4,5]:

$$\frac{d\hat{\mathbf{o}}_{jk}}{dt} = \hat{\mathbf{e}} \cdot \hat{\mathbf{o}}_{jk} + \hat{\mathbf{o}}_{jk} \cdot \hat{\mathbf{e}}^T + \frac{2k_B T}{\zeta} A_{jk} \ddot{\mathbf{a}} - \frac{H}{\zeta} \sum_{m=1}^{N-1} h_m (\hat{\mathbf{o}}_{jm} A_{mk} + A_{jm} \hat{\mathbf{o}}_{mk}) \quad (1)$$

where t is the time, κ represents transpose of the velocity gradient, $\nabla \mathbf{v}$, and κ^T is its transpose, k_B , T , ζ and δ are one-by-one Boltzmann's constant, the absolute temperature, the friction coefficient, and the unit tensor. A_{jk} is jk^{th} component of the Rouse matrix. For the FENE-P model:

$$h_m = \left[1 - \left\langle \left(\frac{Q_m}{Q_0} \right)^2 \right\rangle \right]^{-1} \quad (2)$$

where Q_0 is the maximum extensibility, beyond which the force becomes infinite. If $h_m=1$, e.g., $Q_0 \rightarrow \infty$, the Rouse chain model is recovered.

The solvent contribution was calculated using the Newton law of viscosity, $\hat{\mathbf{o}}_s = -\mu_s (\hat{\mathbf{e}} + \hat{\mathbf{e}}^T)$.

In which μ_s is the solvent viscosity. To calculate the polymer contribution to the extra stress tensor in a dilute solution, the Kramers form has been used:

$$\hat{\mathbf{o}}_p = (N-1)nk_B T \ddot{\mathbf{a}} - nH \sum_{j=1}^{N-1} h_j \langle \mathbf{Q}_j \mathbf{Q}_j \rangle \quad (3)$$

where n is the number of polymer molecules per unit volume. The extra stress is equal to the sum of the solvent and polymer contributions $\hat{\mathbf{\sigma}} = \hat{\mathbf{o}}_p + \hat{\mathbf{o}}_s$.

Results and Discussion

As the first step, the micro-macro approach was verified. This was done using analytical relations for the simplest elastic chains, that is, Hookean dumbbells [4] and simulation results [5] in the same flow. Exactly the same results were obtained.

As the configuration tensor, $\hat{\sigma}_{jk} = \langle \mathbf{Q}_j \mathbf{Q}_k \rangle$, is the main structural parameter in obtaining material parameters, other structural data could also be arrived at. The mean square end-to-end distance could be obtained according to Eq. (6):

$$\langle r^2 \rangle = \langle (r_N - r_1)^2 \rangle = tr \sum_j \sum_k \langle \mathbf{Q}_j \mathbf{Q}_k \rangle = tr \sum_j \sum_k \hat{\sigma}_{jk} \quad (4)$$

where $\langle r^2 \rangle$ is mean square end-to-end distance and tr means trace of the matrix. Another structural data is the gyration tensor, G , from which the radius of gyration, R_g , would be obtainable:

$$G = \frac{1}{N} \sum_{j=1}^N \langle (r_j - r_c)(r_j - r_c) \rangle = \frac{1}{N} \sum_{j,k=1}^N C_{jk} \langle \mathbf{Q}_j \mathbf{Q}_k \rangle \quad (5)$$

$$R_g^2 = tr(G)$$

in which r_j is the location of the bead j with respect to an arbitrary origin, r_c is location of the center of mass, and C_{jk} is the jk^{th} element of the Kramers matrix. For the Rouse

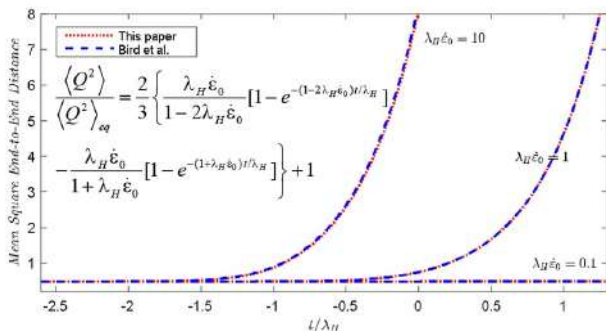


Fig. 1. Molecular stretching for Hookean dumbbells upon inception of uniaxial elongation over time in log scale.

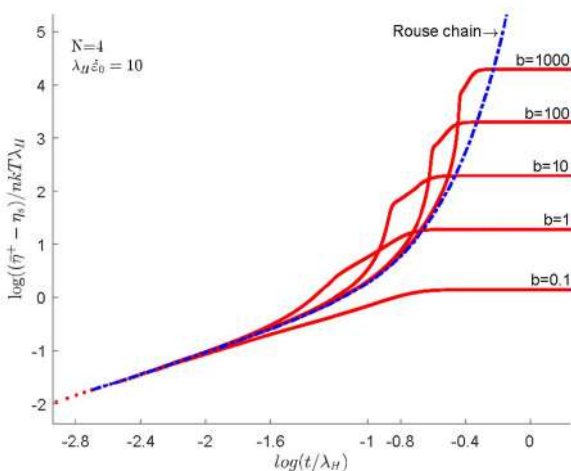


Fig. 2. The elongational viscosity for four-bead FENE-P chains at different b s as well as four-bead Rouse chain upon inception of uniaxial elongation over time.

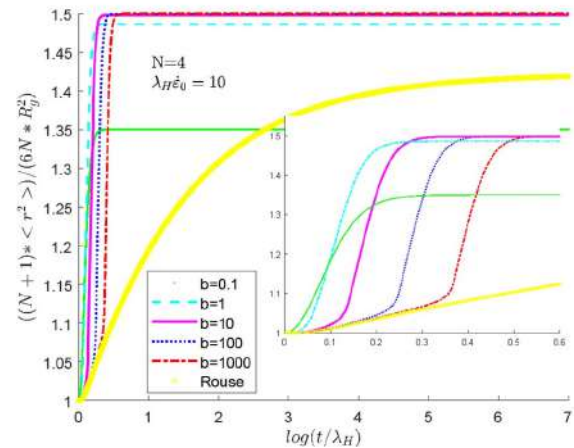


Fig. 3. Ratio of square end-to-end distance to square radius of gyration in exactly the same conditions as Fig. 2.

chain there is no limitation on the increase of $\langle r^2 \rangle$ and R_g^2 due to flow. However, as shown in Fig. 3, their ratio would approach a horizontal asymptote. Although this is implied from their definitions, the trend of the FENE-P chain is very different from the Rouse even at high b s. The different behavior of the models could be assigned to the strength of the elongational flow in separating the chain ends and changing its dimension.

Conclusion

The micro-macro approach utilized in this research represents an innovative technique that has the potential for application in more complex flows. The influence of finite extensibility is particularly pronounced in elongational flows compared to shear flows. The combination of molecular models and elongational flows enables us to seek for the structural origins of the rheological behavior.

References

- [1] V. Tirtaatmadja and T. Sridhar, *J. Rheol.*, **39**, 1133-1160, 1995.
- [2] H. Watanabe, O. Hassager, Y. Matsumiya, Q. Huang, *Extensional Rheology of Unentangled Linear Polymer Melts*. In *Recent Advances in Rheology: Theory, Biorheology, Suspension and Interfacial Rheology*, 2022 Melville, New York: AIP 2022.
- [3] A. Sheikh, *Rheologica Acta*, **56**, 135-148, 2017.
- [4] R.B. Bird, C.F. Curtiss, R.C. Armstrong, O. Hassager, *Dynamics of Polymeric Liquids, Volume 2: Kinetic Theory*. 2nd ed, Wiley, 1987.
- [5] J.M. Wiest and R.I. Tanner, *J. Rheol.*, **33**, 281-316 1989.

Comparison of CA and 2S2P1D Models in Predicting the Rheological Properties of Cationic Bitumen Emulsion

Ali Agahi kesheh¹, Hossein Abedini^{2*}, and Mohammad Abedini³

1. Department of Chemical Engineering, North Tehran Branch, Azad University, Tehran, Iran

2. Iran Polymer and Petrochemical Institute (IPPI), Tehran, Iran

3. Department of Civil Engineering, Birjand Branch, Islamic Azad University, Birjand, Iran

* h.abedini@ippi.ac.ir

Abstract

Predicting the rheological properties of materials in the linear viscoelastic region (LVE) is of particular importance. In this study, a comparison has been made between mathematical and mechanical methods to predict the rheological properties of cationic bitumen emulsion residue. In this study, the CA mathematical method and the 2S2P1D mechanical method have been used to predict the rheological properties of bitumen residue.

Keywords: 2s2p1d model, CA model, cationic bitumen emulsion, rheological models, frequency sweep test

Introduction

In this study, which was carried out on the residue of cationic bitumen emulsion, using the frequency sweep test, which is performed by the DSR device, the graphs of $|G^*|$ and we produce δ . CA mathematical method and 2S2P1D mechanical method were used. The necessary correlation between complex modulus data $|G^*|$ and the measured and modeled phase angle (δ) is evaluated using graphical methods:

Model CA [1]:

$$|G^*| = G_g \times \left[1 + \left(\frac{W_c}{\omega} \right)^{\frac{\log 2}{R}} \right]^{\frac{-R}{\log 2}} \quad (1)$$

$$\delta = \frac{90}{\left[1 + \left(\frac{\omega}{W_c} \right)^{\frac{\log 2}{R}} \right]} \quad (2)$$

$$R = \frac{\log 2 \times \log \left(\frac{|G^*|}{G_g} \right)}{\log \left(1 - \frac{\delta}{90} \right)} \quad (3)$$

Model [2]: 2S2P1D

$$G^* = \frac{G_g - G_0}{1 + A + iB} \quad (4)$$

$$A(\omega) = \alpha(\omega\tau)^{-K} \times \cos\left(\frac{k\pi}{2}\right) + (\omega\tau)^{-h} \times \cos\left(\frac{h\pi}{2}\right) \quad (5)$$

$$B(\omega) = -(\omega\beta\tau) - \alpha(\omega\tau)^{-K} \times \sin\left(\frac{k\pi}{2}\right) + (\omega\tau)^{-h} \quad (6)$$

$$\times \sin\left(\frac{h\pi}{2}\right)$$

Experimental

In this study, cationic emulsion bitumen with 60% base bitumen produced by Asphalt & Bitumen West Company was used. There are different methods to produce bitumen residue. In this study, the Force Draft Oven method was used to make the sample. In this test, we used four different temperatures: 30, 45, 60, and 75 °C, and the frequency range was considered from 0.01 Hz to 15 Hz with a strain range of 1% for each temperature. After performing this test, the master curve was produced by the software of the DSR device. We selected $T_{ref} = 45$ °C. Like other previous studies, instead of calculating the initial parameters of the formulas of the chosen methods, it can be used from previous studies. Because our goal in this study is the fit or rheological parameters of the introduced models. So, we only need a series of initial data to fit the data. In this study, MATLAB software was used to fit the data.

Results and Discussion

In the CA method, we have three parameters to fit the data

Table I. The CA parameters.

G_g	W_c	R
1.00+E05	1.36	1.6

Table II. 2S2P1D parameters.

α	β	G_0	G_g
0.3156	8.56	0	5.8E+06

Table III. 2S2PID parameters.

h	k	τ
0.624	0.614	4.36E-05

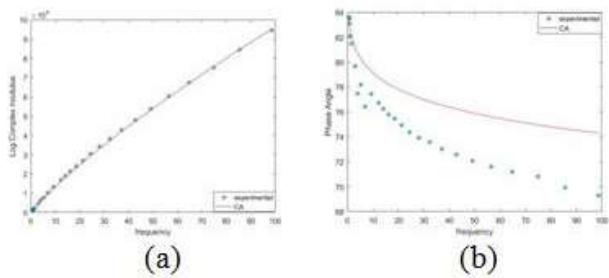


Fig. 1. CA model: (a) $\log |G^*|$ and (b) phase angle.

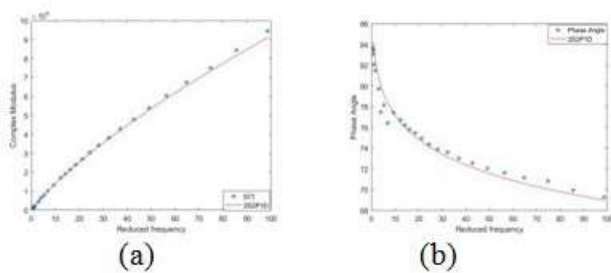


Fig. 2. 2S2P1D model, (a) $|G^*|$ and (b) phase angle.

still, in the 2S2P1D method, we have seven parameters to fit, of course, the value of G_0 is very small and close to zero and can be ignored, but in this study, it is fitted along with other parameters. All the parameters in both methods are fitted manually and using the trial and error method until a good curve is obtained. In this study, the Serror function was defined in such a way that it simultaneously fits the parameters in such a way that the number of values obtained for the two formulas $|G^*|$ and δ are the same in each direction.

- The 2S2P1D model is more reliable in predicting rheological properties due to having more rheological parameters than the CA model. Figs. 1 and 2.
- The CA model in predicting $|G^*|$ graph It is more accurate than the 2S2P1D model and it is the opposite in the δ diagram. Figs. 1 and 2.

References

- [1] M.J. Farrar, T.F. Turner, J.P. Planche, J.F. Schabron, and P.M. Harnsberger, "Evolution of the crossover modulus with oxidative aging: Method to estimate change in viscoelastic properties of asphalt binder with time and depth on the road", *Transp. Res. Rec.*, **2370**, 76-83, 2013.
- [2] N.I.M. Yusoff, D. Mounier, G. Marc-Stéphane, M.R. Hainin, G.D. Airey, and H. Di Benedetto, "Modelling the rheological properties of bituminous binders using the 2S2P1D Model", *Constr. Build. Mater.*, **38**, 395-406, 2013.

Chemorheological Characterization of Polyurethane Systems Containing Different Isocyanates Using Taguchi Method

Hamid Reza Shams-Zarandi and Abbas Kebritchi*

Department of Chemical Engineering, Imam Hossein University of Technology, Tehran, Iran

*a.kebritchi@ippi.ac.ir

Abstract

Urethane group, the main repeating unit in polyurethanes, consists of two main components: alcohol (OH) and isocyanate (NCO). Having long enough time (long pot life) to cast the polyurethane, is a value in aerospace industries. Due to isocyanate responsibility for reactivity of polyurethane, in this paper, a comparison of reactivity of four different isocyanates (i.e., isophorone diisocyanate, toluene diisocyanate, hexamethylene diisocyanate and dimeryl diisocyanate) has been done. The polyurethane synthesized based on hydroxyl-terminated polybutadiene (HTPB) with low molecular weight chain extenders in different temperature and R ratio conditions. Viscometry was used to determine the pot life of system as a chemorheological property. Also, to save time and cost, Taguchi method was used to manage the number of experiments. The presence of an organometallic compound as a curing catalyst (i.e. DBTDL) changed the expected result related to isocyanates (order of reactivity) as follows: IPDI<TDI<HDI<DDI.

Keywords: polyurethane, chemorheology, taguchi method, isocyanate, pot life

Introduction

Polyurethanes (PUs) are a class of versatile materials with great potential for use in different applications, especially based on their structure-property relationships [1]. Polyols and isocyanates are the core components in the production of polyurethanes, but they may have chain extenders (CEs) in the structure too. CEs are low molecular weight diols/diamines cause chain extension [2]. The success in the processing of a reacting system necessitates a thorough understanding about the change in its rheological properties during reaction process. The study of rheological changes occurring during the course of a chemical reaction is defined as chemorheology [3]. Available time for processing (pot life), determined by rheological properties (such as viscosity), must be long enough to allow the proper performance of operations such as casting. Consequently, special attention must be given to the selection of the isocyanate, which affects the reactivity and determines the pot life of the reactive mixture [4]. Using four different isocyanates in polyurethane formulations, determining related pot lives and predicting the order of isocyanates reactivity in a lot of PU systems using Taguchi method, are the main works done in this paper.

Experimental

PU systems prepared using HTPB as the prepolymer and four different isocyanates including isophorone diisocyanate (IPDI), toluene diisocyanate (TDI), hexamethylene diisocyanate (HDI) and dimeryl diisocyanate (DDI) as curing agents. Also four linear aliphatic low molecular weight diols including 1,2-ethanediol (EDO), 1,4-butanediol

(BDO), 1,6-hexanediol (HDO) and 1,8-octanediol (ODO) in four different weight percent (i.e. 0, 0.5, 1, and 1.5%) were used as chain extenders. The choice to accelerate the reaction rate, was dibutyltin dilaurate (DBTDL) as a catalyst. Experiments done in four temperature conditions (i.e. 50, 60, 70, and 80 °C) and the NCO/OH ratio (R) was set in four numbers (i.e. 0.7, 0.8, 0.9, and 1). Viscometry (using Brookfield viscometer model DV2T) was used to determine the pot life of PU systems according to h-t diagrams. The code of spindle used in all experiments was 06. Pot life determination due to above components and conditions need to doing 1024 experiments that practically is impossible. Therefore, we preferred using Taguchi method which decreased the number of experiments to 16 dramatically (based on statistics) and predicted the means of other 1008 experiments (i.e. determining the order of isocyanates reactivity in other PU systems).

Results and Discussion

According to the chemorheological results acquired based on Taguchi method, the reactivity of four different isocyanates used, obtained as follows:

IPDI<TDI<HDI<DDI. This trend of reactivity is shown in Fig. 1 acquired from Taguchi method by means of Minitab software. Also, to show the powerful capability of Taguchi method in prediction of results, the trend of reactivity of isocyanates has shown in Table I for 4 PU systems (note that these four experiments have not been done in laboratory). As seen, the order of reactivity of isocyanates for these 4 PU systems is the same. The importance of isocyanates is in their high reactivity toward hydroxyl groups, which

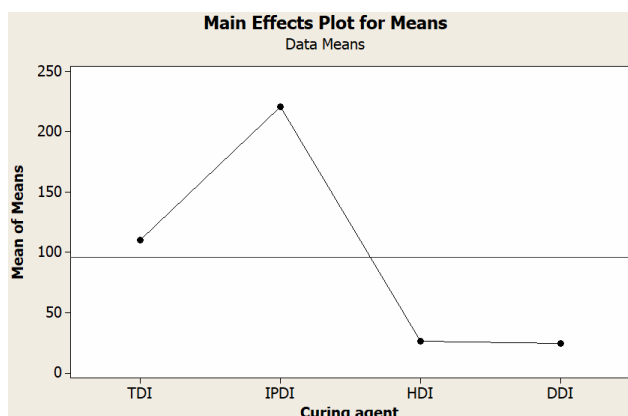


Fig. 1. Main effects plot for means. According to this plot, the higher the position of curing agent (isocyanate), the more pot life is acquired.

Table I. Prediction of order of reactivity of isocyanates based on Taguchi method (T is temperature (°C)) (CE weight percent is set on 1%).

PU system	T	R	Order of reactivity of isocyanates
HTPB-EDO	50	0.7	IPDI<TDI<HDI<DDI
HTPB-BDO	60	0.8	IPDI<TDI<HDI<DDI
HTPB-HDO	70	0.9	IPDI<TDI<HDI<DDI
HTPB-ODO	80	1	IPDI<TDI<HDI<DDI

makes the polyurethane production more efficient. Indeed, isocyanates are responsible for the PU reactivity and curing Properties. Two different types of isocyanates (aliphatic and aromatic) are generally used in the fabrication of polyurethanes. Regarding the resonance structure of isocyanate and due to electronegativity difference, while negative partial charges are generated at both nitrogen and oxygen, the carbon center becomes positively charged. It

is susceptible to nucleophile attacks with active hydrogen (i.e. R-OH). The reactivity of isocyanates can be increased if R is an electron withdrawing group such as an aromatic group. This explains the high reactivity of aromatic isocyanates such as TDI compared to aliphatic ones such as HDI and IPDI. Also it must be noted that catalysts display differential reactivities toward different isocyanates. For example, organometallic compounds (especially organotin ones) are most effective toward the aliphatic isocyanates [5]. Fig. 2 shows two PU systems containing HTPB and Butacene (a polymeric binder with ferrocenyl groups (an organometallic compound) chemically bonded to HTPB) as macroglycols. According to results, the order of reactivity of isocyanates in Butacene based system is as follows: IPDI<TDI<HDI. This shows the catalytic effect of Butacene due to its ferrocenyl groups.

Conclusion

As mentioned above, the reactivity of isocyanates in PU systems related to the aromaticity and kind of catalyst used. Due to use of DBTDL, an organotin material as a catalyst in experiments, the order of reactivity of different isocyanates used came as follows: IPDI<TDI<HDI<DDI.

References

- [1] J.O. Akindoyo, M.D.H. Beg, S. Ghazali, M.R. Islam, N. Jeyaratnam, and A.R. Yuvaraj, "Polyurethane types, synthesis and applications—a review", *RSC Advances*, **6**, 114453, 2016.
- [2] F.M. De Souza, P.K. Kahol, and R.K. Gupta, "Introduction to polyurethane chemistry", *J. Am. Chem. Soc. Washington, DC*, 2021.
- [3] H. Haddadi, E. Nazockdast, and B. Ghalei, "Chemorheological characterization of thermosetting polyurethane formulations containing different chain extender contents", *Polym. Eng. Sci.*, 2008.
- [4] B. Lucio and J.L. De la Fuente, "Catalytic effects over formation of functional thermoplastic elastomers for rocket propellants", *Polym. Adv. Technol.*, **33**, 807-817, 2022.
- [5] M. Szycher, "Szycher's handbook of polyurethanes", 2nd ed, CRC, U.S., 2013.

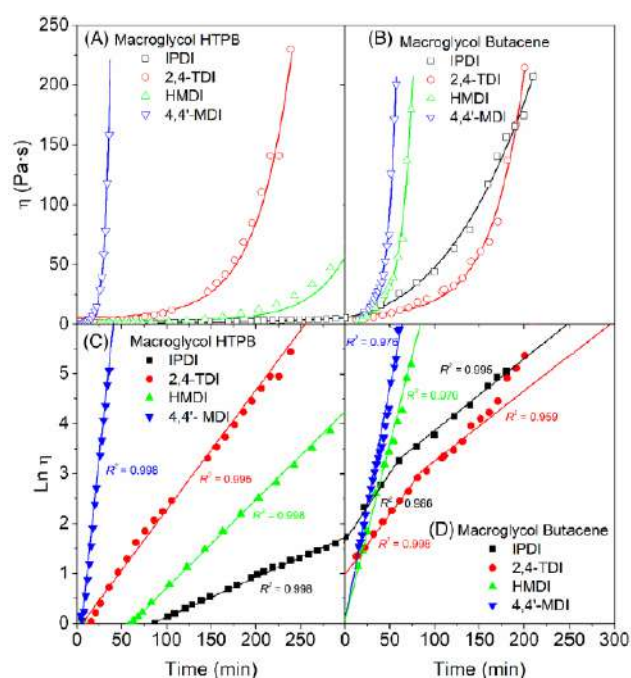


Fig. 2. Viscosity versus time and Ln (viscosity) versus time diagrams for PU systems based on HTPB and Butacene macroglycols [4].

Chemorheological Characterization of Polyurethane Systems Containing Different Chain Extender Contents Using Taguchi Method

Hamid Reza Shams-Zarandi and Abbas Kebritchi*

Department of Chemical Engineering, Imam Hossein University of Technology, Tehran, Iran

*a.kebritchi@ippi.ac.ir

Abstract

Polyurethane may consist of alcohol, isocyanate and chain extenders (CEs). Having long enough time (long pot life) to cast the polyurethane, is a value in aerospace industries. Due to incorporation of diol CEs in forming urethane group, in this paper, the effect of weight percent of four different diol CEs (i.e. EDO, BDO, HDO, and ODO) on pot life is studied. The polyurethane synthesized based on hydroxyl-terminated polybutadiene (HTPB) with four different isocyanates (i.e. IPDI, TDI, HDI, and DDI) in different temperature and R ratio conditions. Viscometry was used to determine the pot life of system as a chemorheological property. To save time and cost, Taguchi method was used to manage the number of experiments. Increasing the CE content up to 1% may increase the reaction rate but from 1% to 1.5% cause a pot life increasement which may refer to the plasticization effect of these low molecular weight diols.

Keywords: polyurethane, chemorheology, taguchi method, CE content, pot life

Introduction

Polyurethanes (PUs) are an immensely versatile class of polymers which understanding the structure-property relationship of them is a key element in designing new materials with improved properties [1]. The urethane group is the major repeating unit in PUs and is produced from the reaction between alcohol (-OH) and isocyanate (-NCO). Different additives may be used in PU synthesis. One group of compounds that often play important roles in the polymeric morphology of PU are the chain extenders ($f=2$). These compounds are usually amine and hydroxyl terminated, with low molecular weights [2]. The success in the processing of a reacting system necessitates a thorough understanding about the change in its rheological properties during reaction process. The study of rheological changes occurring during the course of a chemical reaction is defined as chemorheology [3]. Available time for processing (pot life), determined by rheological properties (such as viscosity), must be long enough to allow the proper performance of operations such as casting [4]. Using different contents of CEs in polyurethane formulations, determining related pot lives and predicting the order of pot life in a lot of PU systems using Taguchi method, are the main works done in this paper.

Experimental

PU systems prepared using hydroxyl terminated polybutadiene (HTPB) as the prepolymer and four different weight percent (i.e. 0, 0.5, 1, and 1.5%) of four linear aliphatic low molecular weight diols including 1,2-ethanediol (EDO), 1,4-butanediol (BDO), 1,6-hexanediol (HDO) and 1,8-octanediol (ODO) as chain extenders. Also,

isocyanates including isophorone diisocyanate (IPDI), toluene diisocyanate (TDI), hexamethylene diisocyanate (HDI) and dimeryl diisocyanate (DDI) were used as curing agents. The choice to accelerate the reaction rate, was dibutyltin dilaurate (DBTDL) as a catalyst. Experiments done in four temperature conditions (i.e. 50, 60, 70, and 80 °C) and the NCO/OH ratio (R) was set in four numbers (i.e. 0.7, 0.8, 0.9, and 1). Viscometry (using Brookfield viscometer model DV2T) was used to determine the pot life of PU systems according to h-t diagrams. The code of spindle used in all experiments was 06. Pot life determination due to above components and conditions need to doing 1024 experiments that practically is impossible. Therefore, we preferred using Taguchi method which decreased the number of experiments to 16 dramatically (based on statistics) and predicted the means of other 1008 experiments (i.e. determining the order of pot life of systems including different CE contents).

Results and Discussion

According to the chemorheological results acquired based on Taguchi method, the pot life of PU system decreased by increasing the weight percent of CE from 0% to 1%. But the increasing of CE weight percent from 1% to 1.5% may increase the pot life. The related trend of pot life is shown in Fig. 1 acquired from Taguchi method by means of Minitab software. Also, to show the powerful capability of Taguchi method in prediction of results, the trend of pot life change has shown in Table I for 4 PU systems (note that these four experiments have not been done in laboratory). As seen on, the trend of pot life for these PU systems is the same. According to one of paper, increasing the CE content

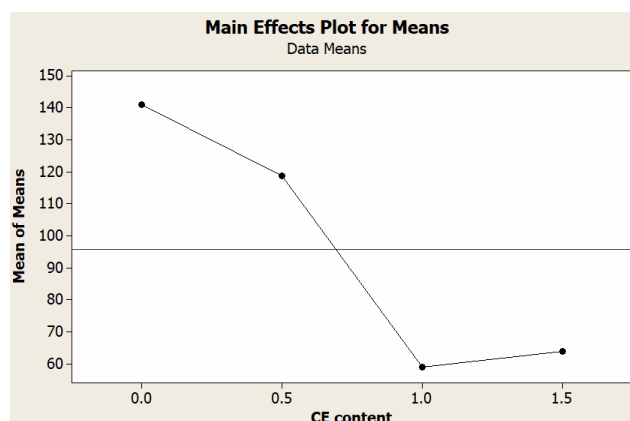


Fig. 1. Main effects plot for means. The effect of CE weight percent on pot life of PU system.

Table I. Prediction of the trend of pot life based on Taguchi method (T is temperature (°C)).

PU system	T	R	Curing agent	Trend of pot life
HTPB-EDO	50	07	IPDI	Decreasing (0-1%), increasing (1-1.5%)
HTPB-BDO	60	08	TDI	Decreasing (0-1%), increasing (1-1.5%)
HTPB-HDO	70	09	HDI	Decreasing (0-1%), increasing (1-1.5%)
HTPB-ODO	80	1	DDI	Decreasing (0-1%), increasing (1-1.5%)

in PU formulation may decrease the pot life [3]. The PU system in mentioned paper includes PTMEG (poly tetra methylene ether glycol) as a polyol, P-MDI (polymeric

Sample code	Frequency (s ⁻¹)	G' ² -G'' Crossover time (S)
CEL1	1	1400
	5	1400
	10	1410
	20	1470
	50	1510
CEL2	1	780
	5	770
	10	790
	20	810
CEL 3	1	≈ 360
	5	≈ 360
	10	≈ 360
	20	≈ 360

Fig. 2. Effect of increasing CE weight percent on gel time (G'²-G'' crossover) of PU system in different frequencies [3].

diphenyl methane diisocyanate) as the curing agent and BDO is used in three weight percent (1.3, 2.5, and 4.5%) as a chain extender. Fig. 2 shows the results of gel time by increasing the CE weight percent. Increasing the BDO weight percent results in an increase of P-MDI (crosslinking agent) concentration in PU formulation. Consequently, higher reaction rates would be expected due to the high density of functional groups [3]. It must be noted that increasing CE% more than a special weight may increase the pot life due to its plasticization effect in that special weight percent [5].

Conclusion

As mentioned above, increasing the weight percent of CE may decrease the pot life of PU system. But more than a special amount of CE%, increasing the weight percent of CE would increase the pot life due to its plasticization effect.

References

- [1] F.M. De Souza, P.K. Kahol, and R.K. Gupta, "Introduction to polyurethane chemistry", *J. Am. Chem. Soc. Washington, DC*, 2021.
- [2] J.O. Akindoyo, M.D.H. Beg, S. Ghazali, M.R. Islam, N. Jeyaratnam, and A.R. Yuvaraj, "Polyurethane types, synthesis and applications—a review", *RSC Advances*, **6**, 114453, 2016.
- [3] H. Haddadi, E. Nazockdast, and B. Ghalei, "Chemorheological characterization of thermosetting polyurethane formulations containing different chain extender contents", *Polym. Eng. Sci.*, 2008.
- [4] B. Lucio and J.L. De la Fuente, "Catalytic effects over formation of functional thermoplastic elastomers for rocket propellants", *Polym. Adv. Technol.*, **33**, 807-817, 2022.
- [5] M. Thirumal, D. Khastgir, N.K. Singha, B.S. Manjunath, and Y.P. Naik, "Mechanical, morphological and thermal properties of rigid polyurethane foam: effect of chain extender, polyol and blowing agent", *Cell. Polym.*, **28**, 145-158, 2009.

Rheology and Morphology of Poly(lactic acid)/Poly(butylene adipate-co-terephthalate) (PLA/PBAT) Blend in Presence of POSS Nanoparticles

Masoumeh Beig Mohammadi and Jafar Khademzadeh Yeganeh*

Department of Polymer Engineering, Qom University of Technology, Qom, Iran

*khademzadeh@qut.ac.ir

Abstract

In this study, we investigated the effect of POSS nanoparticles on the rheological and morphological properties of PLA/PBAT blend. The incorporation of NPs induced compatibilization, subsequently the size of PBAT droplets was greatly decreased and the interfacial adhesion improved. Frequency sweep behavior of the storage modulus for the samples was studied. The results show that the increase in storage modulus, by increasing NPs content.

Keywords: poly(lactic acid), poly(butylene adipate-co-terephthalate), nanoparticles, rheology, morphology

Introduction

In recent years, the extensive use of conventional petroleum-based polymers has raised considerable concerns due to their environmental pollution and sustainability issues. Therefore, the development of new biodegradable polymers to substitute the petroleum-based plastics and rubbers is of crucial significance. Polylactic acid (PLA), is a linear aliphatic polyester and a bio-based polymer achieved from renewable resources such as corn and starch. High strength and modulus of PLA, has made it a suitable alternative to conventional polymers. But the high brittleness and low crystallinity of this polymer, has limited its widespread commercial applications. This problem can be solved using different methods. Poly (butylene adipate-co-terephthalate) (PBAT) is an aliphatic-aromatic copolymer. It has a great toughness, flexibility, low glass transition temperature, and it is fully biodegradable. PBAT has been considered as a good nominee for the toughening the PLA owing to its high flexibility. In this work, by blending PLA with PBAT, with this technique is the most economic, effective, and practical method, the strength of PLA has increased and the effect of polyhedral oligomeric silsesquioxane (POSS) nanoparticles on the morphology and rheological properties of mixtures, has been investigated.

Experimental

The PLA used in this study, with the brand name 2003D, specific density of 1.24 g/cm³ and melt flow index (40 g/10 min at 190 °C and 2.16 Kg) was supplied from Nature Works (USA). The POSS with the brand name FL0578-TriFluoropropyl and the appearance of powder, a molecular weight of 1193.16 g/mol (where R=CH₂CH₂CF₃) and its molecular formula is (SiO_{1.5})_n(C₃H₄F₃)_n (n=8,10,12) was supplied from Hybrid Plastics (USA). The used PBAT,

with the brand name F Blend C1200 ecoflex®, is from BASF, Germany, which is supplied as white spherical pellets with a molecular weight of 126 kg/mol and a density of 1.26 g/cm³. The melt blending approach was adopted to obtain the specimens using a lab internal mixer (Brabender Plasticator, Germany) at 190 °C and a rotor speed of 60 rpm for 10 min.

Results and Discussion

Scanning Electron Microscopy (SEM)

SEM was performed to investigate the morphology of the samples (Fig. 1). As anticipated, PLA/PBAT (75/25) sample showed a droplet-matrix morphology in which, PLA was the matrix (Fig. 1a). the interfacial adhesion between the phases was poor and some voids can be observed which formed due to interfacial debonding between the PLA matrix and the PBAT droplets implying a fully incompatible polymer blend. Upon incorporating 1 wt% NPs, the interfacial strength improved. The NPs dispersed in the PLA phase acted as physical barriers and prevented droplet coalescence and the average droplet size was decreased. Decreasing particle size leads to an increase in the contact area between PLA and PBAT, which allows stress to be better transmitted from PLA matrix to PBAT droplets (Fig. 1b). also, upon incorporating 3 wt% NPs, the average droplet size was so decreased (Fig. 1c).

Transmission Electron Microscopes (TEM)

To explore the exact location of nanoparticles, TEM analysis was employed (Fig. 2). In these images, the black domains represent the POSS nanoparticles. The nanoparticles have more affinity toward PLA, thus, they predominantly localized in the PLA matrix and some of them also resided at the interface around PBAT particles.

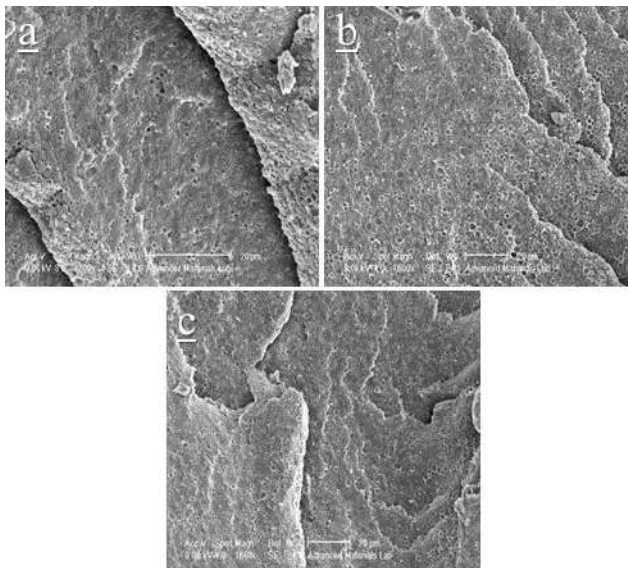


Fig. 1. SEM images of: (a) PLA/PBAT blend with (b) 1 wt%, and (c) 3 wt% of POSS.

Rheological Behavior

Fig. 3 shows storage modulus G' as a function of frequency for neat PLA/PBAT blend and with different percentages of POSS nanoparticles. The neat PLA/PBAT blend exhibited terminal behavior with a shoulder at the storage modulus which can be attributed to the contribution of the interface to the blend elasticity and the shape relaxation of the PBAT droplets in the PLA matrix. According to SEM images, the decrease of droplet size and improved interface upon NPs introduction should increase the modulus. But it can be seen that the addition of 1 wt% POSS to the blend, has reduced elasticity, viscosity values and modulus due to lubrication effect of POSS. At POSS loadings of 3 wt% and higher, the low-frequency storage modulus was enhanced. This is indicative of solid-like viscoelastic behavior implying that the NPs has formed a percolated network in the PLA matrix which spanned the sample and restrained the long-range motion of polymer chains. Besides, the compatibilization effect of nanoparticles induced high interfacial area

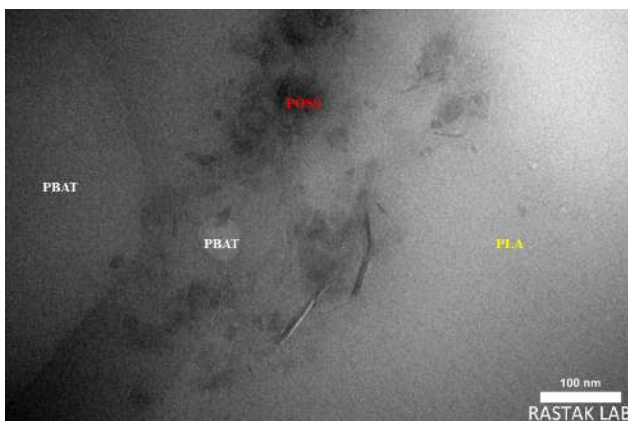


Fig. 2. TEM image of PLA/PBAT/POSS (75/25/3) blend.

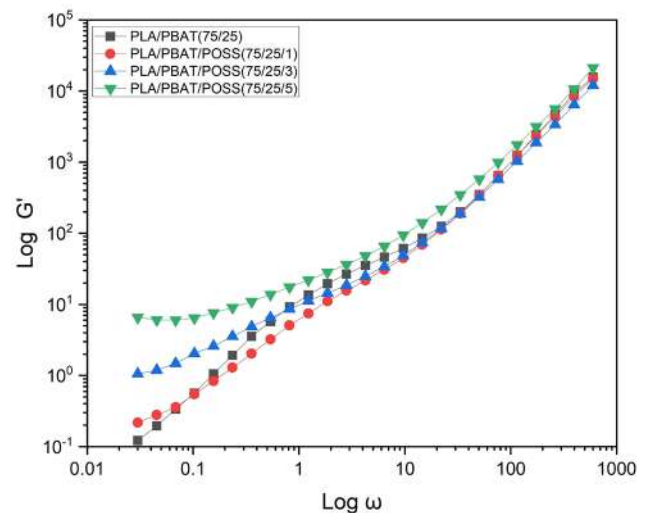


Fig. 3. Storage modulus of neat blend with nanoparticles.

which increased dynamic moduli at low frequencies. At high frequencies, storage modulus was also enhanced suggesting short-range dynamics of polymer chains is restricted especially in the entanglement length scales.

Conclusion

In this study, the poly(lactic acid)/poly(butylene adipate-co-terephthalate) blend prepared and the effect of the POSS NPs on the rheological and Morphological properties was investigated. The incorporation of 1 and 3 wt% of NPs induced compatibilization, the size of PBAT droplets was greatly decreased and the interfacial adhesion improved which allows stress to be better transmitted from PLA matrix to PBAT droplets. In the presence of 1 wt% POSS, the storage modulus Decreased due to lubrication effect of POSS. At POSS loadings of 3 wt% and higher, the storage modulus was enhanced in all frequency range indicating both long-range dynamics and short-range dynamics in the blend have been influenced.

References

- [1] S. Moradi and J.K. Yeganeh, "Highly toughened poly (lactic acid) (PLA) prepared through melt blending with ethylene-co-vinyl acetate (EVA) copolymer and simultaneous addition of hydrophilic silica nanoparticles and block copolymer compatibilizer", *Polym. Test.*, **91**, 106735, 2020.
- [2] D. Bajelan and A. Javidi, "Biodegradable poly (lactic acid)/poly (butylene adipate-co-terephthalate) nanocomposite", *Iran. J. Polym. Sci. Technol. (Persian)*, **36**, 87-101, 2023.
- [3] N.T. Kilic, B.N. Can, and M. Kodal, "Compatibilization of PLA/PBAT blends by using Epoxy-POSS", *Appl. Polym.*, **136**, 47217, 2018.

The Effect of Wood Flour Content on Mechanical Properties and Rheological Behavior of PLA/WF Composites Filaments for 3D Printing

Parisa Vahedi¹, S. Reza Ghaffarian Anbaran^{1*}, and S. Amirmasoud Rezadoust²

1. Department of Polymer Engineering, Amirkabir University of Technology, Tehran, Iran

2. Iran Polymer and Petrochemical Institute, Pazhoohesh Blvd., 149771311, Tehran, Iran

*sr_ghaffarian@aut.ac.ir

Abstract

In this study, biodegradable poly lactic acid (PLA) composite filaments reinforced with cellulose fibers of beech wood flour were prepared as feedstock for 3D printing using the fused deposition modeling (FDM) technique. The effect of wood flour content (5, 15, and 25 wt%) on the rheological behavior and mechanical properties of these materials was investigated. The results showed that with the addition of wood flour (WF) to pure PLA, the storage modulus (G') gradually increased, indicating a solid-like behavior and the formation of a network-like structure in the blend, leading to an increase in storage modulus and a decrease in mechanical strength. These structures become more pronounced with an increase in the WF content in the composite, which also affects the printability of PLA/WF composites.

Keywords: polymer composites, 3D printing, rheological behavior, storage modulus, PLA/WF composites

Introduction

The 3D printing technology, also known as additive manufacturing (AM) or rapid prototyping (RP) has greatly developed over the last decade. It involves the production of an object by printing each layer separately based on digital models and adding layers of material on top of each other [1]. This technology enables users to create real objects based on a computer-generated three-dimensional model, allowing them to efficiently produce objects with specific shapes and complex geometries, particularly for prototyping and small-scale production. Among various 3D printing methods, FDM is one of the most widely used technologies for rapid prototyping, primarily due to its reliability, simplicity, low cost, minimal waste, and availability of materials [2].

In this method, a thermoplastic filament, which serves as the feedstock for the 3D printer, is fed to the liquefier head and heated to the melting temperature. The semi-molten material is then extruded and deposited layer by layer onto a platform to build the 3D model [3]. Thermoplastic filaments used in 3D printers, such as ABS, PE, and PP, are mainly derived from fossil fuels and petroleum products, despite being cheaper and more accessible. Consequently, their consumption has been replaced by bio-based plastics such as PLA, PHB, and starch in many developed countries, which offer advantages such as renewability, biodegradability, and easy composting after use [4]. PLA, as an important type of aliphatic polyesters, is a biodegradable and environmentally friendly polymer that is considered one of the most popular matrices for FDM printers due to its excellent printability [5]. Additionally, to improve the

performance of PLA, some biodegradable additives with cellulose sources, such as wood flour, are used. WF, which is significantly cheaper than thermoplastics and possesses advantages such as high modulus, low cost, renewability, abundance, and easy accessibility, is widely used in the thermoplastic composite industry [6].

The aim of this project is to prepare PLA/WF composites with different percentages of wood flour (by using a melt mixing process) and utilize them as feedstock for FDM 3D printers. The rheological and mechanical properties of these composites will be investigated. The addition of WF will not only improve the modulus but also reduce production costs and decrease the reliance on thermoplastics, providing a wood-like appearance to the printed parts.

Experimental

The PLA/WF composites with three different WF content (5, 15, and 25 wt%) were prepared using a twin-screw extruder to obtain a uniform compound. After drying the granules 'compound they were fed into a single-screw extruder at 175-185 °C to produce the filaments. Tensile test were done according to ISO 527-5A.

To investigate the rheological behavior of samples, the oscillatory mode of a RMS rheometer was utilized. The dynamic properties of the molten samples, such as storage modulus, were examined through various tests at a temperature of 205 °C. To determine the linear viscoelastic region, a strain sweep test was performed at a frequency of 1 Hz and a strain amplitude ranging from 0.01% to 100%. The strain value of 4% was considered as the safe strain within the linear viscoelastic region for all samples. Furthermore,

Table I. Tensile test results of PLA/WF composite filaments.

Sample	Elastic modulus	Tensile strength
PLA	1043 ±11.7	49.8 ±1.42
PLA/WF5%	1120 ±16	52.8 ±0.8
PLA/WF15%	1290 ±21	48.1 ±0.85
PLA/WF25%	1345 ±32	44.75 ±1.32

the time sweep test showed that the storage modulus of the samples remained unchanged after approximately 2 h at a temperature of 205 °C. This indicates the sample's stability under strain sweep test conditions.

Results and Discussion

According to the values obtained from the tensile test, as shown in Table I, it is evident that the addition of wood particles to pure PLA increases the storage modulus. This is because wood itself is a solid material and acts as a filler, enhancing the stiffness. Additionally, the WF used has a modulus of approximately 1.8 GPa, which is higher than that of pure PLA, thereby leading to an increase in the final modulus of the composite.

Assessing the rheological response in the molten state, especially at low frequencies, is a valuable method for investigating the properties of polymer composites. Referring to Fig. 1, which represents the results of the strain sweep test for various PLA/WF composites at a strain of 0.4% and a temperature of 205 °C, it can be observed that the storage modulus (G') gradually increases with the addition of WF to pure PLA. This is because the large and rigid wood particles create spatial hindrance, limiting the movement of the polymer chains and resulting in an increase in the dynamic storage modulus. Furthermore, as the percentage of WF increases, the slope of the curves at low frequencies decreases, deviating from the rosin behavior and tending towards Maxwell (or non-terminal) behavior. In general, the reduced slope of the storage modulus curve (becoming frequency-independent)

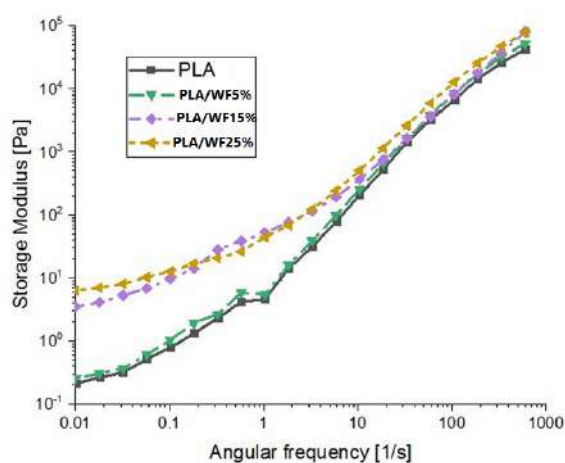


Fig. 1. Plot of storage modulus as a function of frequency for pure PLA and PLA/WF composites with varying WF content.

at low frequencies in micro-composites indicate particle agglomeration and clustering. Here, it is also observed that as the WF content increases, the compound becomes more solid-like and forms a network-like structure within the composite, leading to an increase in modulus and a decrease in mechanical strength. Additionally, with an increase in the wood percentage, the plateau length extends at low frequencies, indicating a more pronounced structure formation. These observations support the results of tensile test too.

Conclusion

In this study, wood powder particles with different contents were added to PLA matrix and the effect of WF% on the tensile properties and rheological behavior of the composite filament for 3D printer feedstock was examined. It was observed that with the addition of wood particles, the elastic modulus increases. The investigation of the elastic and structural properties of PLA/WF composites also showed that in the linear strain region, the storage modulus (G') increases with the increase of WF content, and the slope of the curve at low frequencies decreases. This indicates that the particles have clustered within the polymer matrix, leading to a decrease in strength and an increase in modulus.

References

- [1] J.-Y. Lee, W.S. Tan, C.K. Chua, C.Y. Tang, *J. Membr. Sci.*, **499**, 480-490, 2016.
- [2] K. Garousi, The Study of Processing Parameters in Producing Conductive Nanocomposites Using FDM Printer, Polymer Eng. faculty of Amirkabir University of Technology, Tehran, 2019.
- [3] F. Ning, W. Cong, J. Qiu, J. Wei, and S. Wang, *Compos. Part B: Eng.*, **80**, 369-378, 2015.
- [4] D. Hammiche, A. Boukerrou, B. Azzeddine, N. Guermazi, and T. Budtova, *Int. J. Polym. Anal. Charact.*, **24**, 236-244, 2019.
- [5] Y. Dong, A. Ghataura, H. Takagi, H.J. Haroosh, A.N. Nakagaito, and K.-T. Lau, *Compos. Part A: Appl. Sci. Manuf.*, **63**, 76-84, 2014.
- [6] N. Ayrimis, *Polym. Test.*, **71**, 163-166, 2018.

Viscoelastic Flows of PTT Fluids in Concentric Cylinder Rheometer

Abdellah Baglari, Mohammad Hassan Hassan Khani, and Mohammad Hossein Navid Famili*

Polymer Engineering Department, Faculty of Chemical Engineering, Tarbiat Modares University, Tehran, Iran

*nfamili@modares.ac.ir

Abstract

This study conducted an analysis of unsteady, non-linear viscoelastic fluid behavior using the Phan-Thien-Tanner (PTT) model within a concentric Rheometer. The governing equations, encompassing continuity and momentum flow in the steady state, along with the PTT constitutive equation in the transient state, were discretized utilizing the concentric finite volume method. Subsequently, the governing equations were solved iteratively using the Incomplete Cholesky Conjugate Gradient Square Method (ICCGS). To investigate the viscoelastic effect, a stress relaxation test was conducted at varying stress relaxation times. The results demonstrated that as the relaxation time increased, the time required to reach the steady state also increased. Additionally, the rate of drop in stored elastic stress decreased. Thus, highlighting the substantial influence of the viscoelastic effect on stress and first normal stress.

Keywords: polymer mixtures, numerical simulation, adaptive mapping method, viscoelasticity, finite volume

Introduction

In many flow processes the behavior of the fluid is non-Newtonian. Especially in biological flow and environmental or chemical processes, such as blood flow, sedimentation processes or polymer melts, we can observe viscoelastic flow phenomena like the characteristic fading memory effect. The simulation of fluids with viscoelastic behavior is particularly challenging due to two major issues: First, the proper modelling of the physical characteristics and the right choice of a viscoelastic model is crucial in order to not develop unphysical models or even ill-posed problems with non-unique or even without solutions [1].

The need for high flexibility in simulating irregular geometries has led to the development of methods based on non-orthogonal grids. Almost all efforts made to develop approaches based on this grid are carried out through the use of coordinate transformation. As a result, by selecting co-aligned and non-co-aligned velocity components as the cell-face velocities, the tensor algebra becomes more complex, which is employed to obtain the momentum equations in the transformed region [2].

The solution of flow using two types of grid arrangement, namely cell-centered or vertex-centered, can be performed. In the vertex-centered grid arrangement, vector variables such as velocity are stored on the cell surfaces, while scalar variables such as pressure, temperature, etc. are stored at the cell centers. The velocities on the surfaces can be co-aligned or non-co-aligned, making their conversion to Cartesian velocity components challenging. However, the cell-centered grid arrangement, which stores all variables at the cell centers and utilizes Cartesian velocity components, reduces the algebraic and geometric complexity of the problem [2]. Sarkar and Showalter [1] solved the upper-convected Maxwell viscoelastic constitutive equation by

presenting a semi-analytical method. The advantage of this method is its stability for multiphase systems and the separation of viscous and elastic terms in a natural way.

In this research, this approach is used in combination with Roychowdhury [3] discretization technique.

Theoretical

The conservation equations for mass and momentum were discretized utilizing the finite volume method within the framework of a non-orthogonal grid. The PTT equation was resolved utilizing a semi-analytical approach in conjunction with the momentum equation. The continuity equation for an immiscible fluid is as follows [3]:

$$\overline{\nabla} \cdot \overline{v} = 0 \quad (1)$$

And momentum equation [3]:

$$\rho \overline{v} \cdot \overline{\nabla} \overline{v} = -\overline{\nabla} \cdot p + \overline{\nabla} \cdot \overline{\tau} \quad (2)$$

where \overline{v} the velocity vector, p is the dynamic pressure, and $\overline{\tau}$ is the deviatoric stress tensor. The viscoelastic constitutive equation of PTT can be written as follow [4]:

$$H(\text{tr} \tau) \tau + \lambda \overline{\dot{\tau}} + \frac{\lambda \zeta}{2} (\dot{\gamma} \cdot \tau + \tau \cdot \dot{\gamma}) = \eta \dot{\gamma} \quad (3)$$

where $\text{tr} \tau$ is the effect of the stress tensor, λ is the relaxation time, and η is the shear viscosity and Oldroyd's upper convected derivative:

$$\overline{\dot{\tau}} = \frac{\partial \tau}{\partial t} + v \cdot \nabla \tau - \nabla v \cdot \tau - \tau \cdot \nabla v \quad (4)$$

The function is presented in two linear and exponential forms [5]:

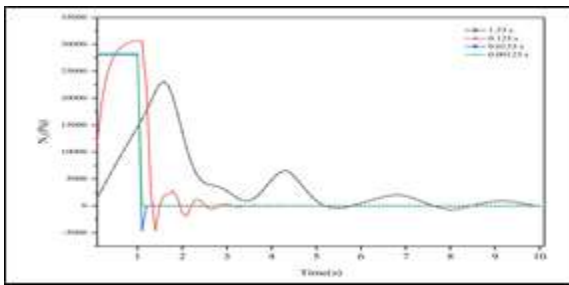


Fig. 1. The graph of the normal stress difference with time in the stress relaxation test.

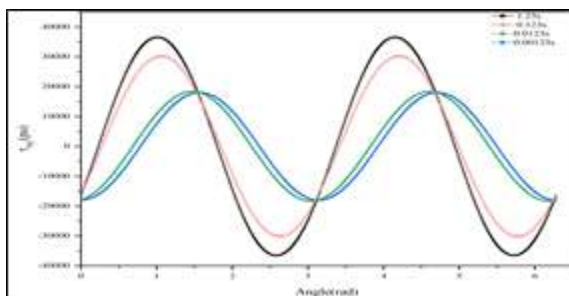


Fig. 2. The graph of the effect of stress relaxation time on shear stress.

$$H(t\tau) = \begin{cases} 1 + \frac{\varepsilon \lambda t \tau}{\eta_0} \\ \exp\left(\frac{\varepsilon \lambda t \tau}{\eta_0}\right) \end{cases} \quad (5)$$

Results and Discussion

Fig. 1 illustrates the variation of the first normal stress difference over time for different stress relaxation times. The stress relaxation test duration is one second, and the total test duration spans 10 s. It is evident from the figure that the time required to attain a steady state increases with longer stress relaxation times. When the stress relaxation time is set to 0.123 s, the normal stress difference reaches a steady state within one second. As time progresses, the stress relaxation occurs at a faster rate. On the other hand, when the stress relaxation time is set to 1.23 s, the graph displays an initial increase after stress removal, followed by a more gradual decline. Consequently, the time required to reach the stored stress value noticeably extends.

Fig. 2 presents the impact of stress relaxation time on shear stress. The observed trend indicates a substantial increase in the influence on shear stress as the stress relaxation duration grows. Hence, based on the numerical findings, it can be deduced that viscoelasticity plays a crucial role in modulating the rheological properties of the system.

Conclusion

This study employed the finite volume numerical method to simulate nonlinear viscoelastic flow within the

rheometer geometry of co-axial cylinders. The obtained numerical results highlight several key findings. Firstly, it was observed that an increase in stress release time leads to a lengthened duration for the system to reach a stable state, while the recovery of stress after the stress relaxation test exhibits a reduced slope. These findings suggest the existence of significant viscoelastic effects in fluids, underscoring the importance of considering such effects in the design of devices involved in the production of polymeric materials, medical materials, biomaterials, and related fields. Moreover, the research emphasizes that neglecting the viscoelastic contribution can undermine the accurate characterization and understanding of shear stress behavior in these systems.

References

- [1] K. Sarkar and W.R. Schowalter, "Deformation of a two-dimensional drop at non-zero Reynolds number in time-periodic extensional flows: Numerical simulation", *J. Fluid Mech.*, **436**, 177-206, 2001.
- [2] D.G. Roychowdhury, S.K. Das, and T. Sundararajan, "An efficient solution method for incompressible N-S Equations using non-orthogonal collocated grid", *Int. J. Numer. Methods Eng.*, **45**, 741-763, 1999.
- [3] D.G. Roychowdhury, *Computational Fluid Dynamics for Incompressible Flow*, Taylor and Francis, 2020.
- [4] E.S.P.B.V, S.A. White, D.G. Baird, and P. Materials, "numerical simulation studies of the planar entry flow of polymer melts", *J. Non-Newton. Fluid. Mech.*, 47-71, 1988.
- [5] S. Thohura, M.M. Molla, and M.M.A. Sarker, "Numerical simulation of non-Newtonian power-law fluid flow in a lid-driven skewed cavity", *Int. J. Appl. Comput. Math.*, **5**, 2019.

Numerical Investigation and Experimental Observation of Viscoelastic Multiphase Flows

Abdellah Baglari, Mohammad Hassan Hassan Khani, and Mohammad Hossein Navid Famili*
Polymer Engineering Department, Faculty of Chemical Engineering, Tarbiat Modares University, Tehran, Iran

*nfamili@modares.ac.ir

Abstract

Mixing plays a crucial role in the polymer processing operations within diverse industrial settings. To effectively analyze mixing processes, it is imperative to comprehend the pertinent mixing parameters, which encompass strain and stress distribution among others. These parameters exert direct influence on the morphology of the mixing components, thereby underscoring the significance of understanding the morphological aspects in order to enhance the desired product's quality. Consequently, the simulation of flow commences by discretizing continuity and motion equations via the implementation of the finite volume method, employing surface approximation techniques. Accordingly, the subsequent undertaking involved the tracking of two homogeneous fluids utilizing Adaptive Mapping Method (AMM). In order to assess the quantitative attributes, a series of investigations were devised within the confines of a co-axial cylinder rheometer. The outcome depicts an exceptional concurrence between the results obtained from numerical simulations and the corresponding experimental visual representations, thereby substantiating the viability of this approach for simulating viscoelastic assumptions.

Keywords: polymer mixtures, numerical simulation, adaptive mapping method, viscoelasticity, finite volume

Introduction

Polymer mixtures are remarkable materials that exhibit distinct characteristics including exceptional elasticity, toughness, low density, and enhanced processability in comparison to metals. Consequently, these materials are ubiquitously encountered in diverse sectors encompassing the textile, food, transportation, and healthcare industries, thereby prompting researchers to devote significant interest to this domain [1]. Despite the significant advancements achieved in simulating the behavior of single-phase viscoelastic fluids, the research and development of computational models for multiphase fluids, specifically those exhibiting high Weissenberg numbers, continue to be an active area of investigation [2]. The characterization of the viscoelastic phenomena in drop-matrix two-phase systems has been examined by MuradOglu and Izbasaro in the context of a capillary tube containing an obstacle. In their study, the researchers employed surface tracking techniques, namely front tracking, to monitor the interfacial behavior between the two phases. Additionally, the finite difference method was utilized to discretize the governing flow equations [2]. In the current study, the governing equations are formulated in Cartesian coordinates employing Cartesian velocity components. The discretization is performed directly in the physical domain without employing any coordinate transformation techniques. To enhance the convergence rate of the

numerical solution, the preconditioned conjugate gradient squared method is employed to solve the resulting system of algebraic equations. The Phan-Thien-Tanner (PTT) model [3], which incorporates both elastic and viscous effects, is utilized to represent the behavior of viscoelastic fluids, considering their nonlinear characteristics.

Theoretical

The conservation equations for mass and momentum [4] were discretized utilizing the finite volume method within the framework of a non-orthogonal grid. The PTT equation was resolved utilizing a semi-analytical approach in conjunction with the momentum equation. The parameters of the model utilized in the computer program have been enumerated in Table I.

Based on ATM logic, having the initial position of the particles, their final position is calculated as follows:

$$X_{new} = X_{old} + U \cdot dt \quad (1)$$

$$Y_{new} = Y_{old} + V \cdot dt \quad (2)$$

Table I. Parameters entered in the computer program.

ω (rad/s)	Wi	dt
0.04	1.85	0.001

Table II. PTT rheological model parameter.

PTT model Parameter					Polymer
η_1	η_2	ζ	λ	ε	
1850	11100	0.0063	1.23	0.01	LDPE

In these equations, X_{old} and X_{new} are old and new Positions of Markers Respectively and for Y is the same as X.

Results and Discussion

The findings of the stress relaxation test pertaining to the homogenous blending of linear low-density polyethylene are presented in Figs. 1, 2, and 3. The red and black particles depicted in the figure symbolize the presence of polyethylene material, which is positioned within the confines of the rheometer, occupying the interstitial region between the two enclosing walls. The inner wall of the rheometer is visualized as the inner circle (referred to as the “bob”), while the outer wall is represented by the outer circle (referred to as the “cup”). Based on simulation and experimental findings, it has been observed that during the mixing process, polymer fluid layers initiate interpenetration, which subsequently intensifies over time. This interpenetration is accompanied by the uniform movement of particles along the flow field. It is worth noting that within a homogeneous system, particles exhibit identical molecular properties, thereby leading to



Fig. 1. Experimental results of mixing in stress relaxation test in coaxial cylinders rheometer for polyethylene system. (a) Initial 15 s under tension and (b) next 10 s under no tension.

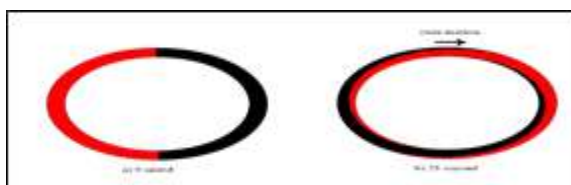


Fig. 2. Mixing simulation results in stress relaxation test in co-axial cylinders rheometer for polyethylene system. (a) The first 15 s of the simulation under stress and (b) the next 10 s of the simulation under stress.

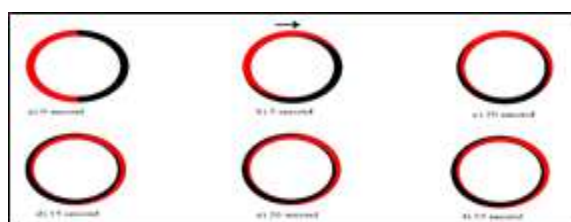


Fig. 3. Simulation results of homogeneous mixing of polyethylene in coaxial cylinder rheometer with time.

the application of consistent forces, including tension and pressure. To validate the obtained outcomes, a laboratory dynamic test was designed, employing the rheometer’s coaxial cylinder geometry along with the application of the rheometer clutch and brake. The numerical and experimental findings exhibited satisfactory agreement.

Conclusion

The present study focuses on simulating the homogenous mixing of polymers in an asymmetric geometry, taking into account the assumption of viscoelasticity. A comprehensive analysis was conducted by comparing visual observations, numerical simulations, and experimental data in order to assess the advancement of flow layers. Through this comparative analysis, insights can be gained into the uniform and layered mixing behavior of polymers, particularly in relation to the influence of their high molecular weight in contrast to smaller molecules.

References

- [1] R.K. Mishra, S. Thomas, and N. Kalarikkal, “Micro and nano fibrillar composites (MFCs and NFCs) from polymer blends, Woodhead, 2017.
- [2] D. Izbassarov and M. Muradoglu, “A front-tracking method for computational modeling of viscoelastic two-phase flow systems”, *J. Non-Newton. Fluid Mech.*, **223**, 122, 2015.
- [3] E.S.P.B.V, S.A. White, D.G. Baird, and P. Materials, “Numerical simulation studies of the planar entry flow of polymer melts”, **30**, 47-71, 1988.
- [4] D.G. Roychowdhury, *Computational Fluid Dynamics for Incompressible Flow*, Taylor and Francis, 2020.

Computational Modeling of Heterogeneity in Polymer Mixtures

Abdellah Baglari, Mohammad Hassan Hassan Khani, and Mohammad Hossein Navid Famili*
Polymer Engineering Department, Faculty of Chemical Engineering, Tarbiat Modares University, Tehran, Iran

*nfamili@modares.ac.ir

Abstract

The simulation of multiphase flow was conducted with the assumption of viscoelasticity employing the Adaptive Mapping Method (AMM). In this study, the governing equations including continuity, momentum, and constitutive equations were discretized using the finite volume Eulerian approach. Subsequently, the resulting velocities were utilized to calculate the particle velocity values based on the Lagrangian approach. Additionally, the diffusion coefficients for heterogeneous viscoelastic fluids were adjusted in this investigation. The numerical findings indicate a notable distinction in particle velocities between the material's bulk region and its surface, primarily driven by the influence of surface tension and viscoelastic stresses. Furthermore, it is observed that surface expansion intensifies over time, attributable to the inherent resistance of the phases to undergo through mixing.

Keywords: heterogeneity, computational modeling, adaptive mapping method, viscoelasticity, polymer melts

Introduction

The preparation methodologies for polymer blends can be broadly categorized into two main types: melt blending and solution blending. The melt mixing technique is widely employed in conventional and industrial applications due to its practicality. This approach obviates the need for sourcing a compatible solvent for polymer dissolution, thereby mitigating potential challenges associated with subsequent separation processes and environmental concerns. In polymer blends, the resulting morphology is crucially influenced by the level of miscibility, thereby exerting a substantial influence on the ultimate properties of the blend. Blending multiple fluids exhibiting disparate viscosities within diverse geometric configurations represents a critical and intricate endeavor within the realm of polymer industry. Simulation-based approaches applied in the context of such processes facilitate a more comprehensive comprehension of the underlying phenomena that transpire during the blending operation [1].

Köpplmayr and Mayrhofer conducted a simulation of the polymer melt mixing process within an extruder using the Volume of Fluid (VOF) method and employing the OpenFoam software toolbox. To achieve this, they implemented a feeding channel at the end of the extruder's two exits and directed the materials through a rectangular die. By introducing color into the system, they were able to visually distinguish and apply the steady-state assumption. Their investigation revealed that the viscosity ratio and viscoelastic characteristics of the phases influence the formation of the interface between the two phases as well as the occurrence of secondary flow [2].

In this study, a research investigation was conducted on the process of heterogeneous polymer melt mixing,

specifically focusing on low-density polyethylene (LDPE) and polystyrene (PS). The finite volume method was employed in conjunction with modifications made to the coefficients of the equations governing the behavior of viscoelastic fluids, as well as utilizing AMM tracking technique. Additionally, the parameters of the Phan-Thien-Tanner (PTT) viscoelastic equation [3] were determined by analyzing rheological data [4] obtained at a temperature of 180 °C.

Theoretical

Upon discretizing the governing flow equations, the resulting set of equations can be expressed as follows:

$$a_p \phi_p = a_w \phi_w + a_e \phi_e + a_n \phi_n + a_s \phi_s + \bar{b}_p + \delta P_i \quad (1)$$

$$\bar{b}_p = b_{no} + b_p \quad (2)$$

$$a_e = d_e^1 + \max(-F_e, 0), a_w = d_w + \max(F_w, 0) \quad (3)$$

$$a_n = d_n^1 + \max(-F_n, 0), a_s = d_s + \max(F_s, 0)$$

$$a_p = a_e + a_w + a_n + a_s - S_p + [(F_e - F_w) + (F_n - F_s)] \quad (4)$$

$$b_{no} = [(d_e^2 + d_n^2)\phi_{ne} - (d_w^2 + d_n^2)\phi_{wn} - (d_e^2 + d_s^2)\phi_{se} + (d_w^2 + d_s^2)\phi_{sw}] \quad (5)$$

The variables d , F , and δP represent the modified coefficients associated with immiscible fluids, flux, and pressure gradient, respectively.

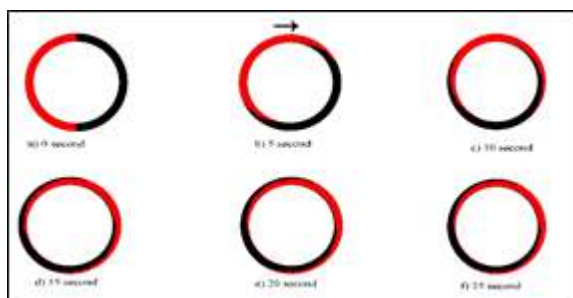


Fig. 1. Simulation results of heterogeneous mixing of low-density polyethylene with polystyrene in coaxial cylinder rheometer with time.

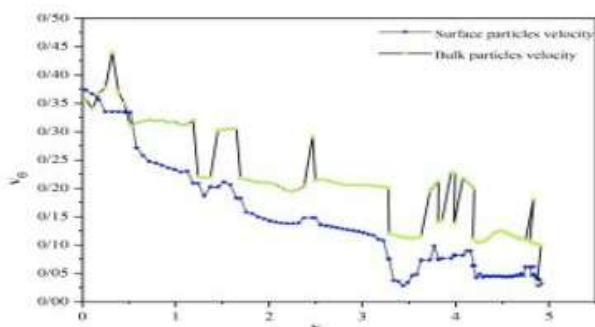


Fig. 2. Comparison of the dimensionless velocity of surface particles with the bulk in heterogeneous mixing of low-density polyethylene and polystyrene.

Ultimately, upon successfully solving the equations and deriving the respective velocities, the ultimate position of the particle arises.

Results and Discussion

The numerical findings are illustrated in Fig. 1, where the color red signifies low-density polyethylene while black corresponds to polystyrene. Notably, Fig. 1 evidently showcases the elimination of the slow and layered mixing flow pattern resulting from the distinct surface tension characteristics of low-density polyethylene and polystyrene. The observed behavior signifies the inherent resistance of the phases to intermix, which manifests in a reduced front tension. As a consequence, a more significant drop is associated with the applied tension.

Fig. 2 illustrates the outcomes pertaining to the autonomous movement of surface and bulk particles in a heterogeneous mixing system. The graph portrays that the mobility of the designated particle at the surface, situated between the two phases, diverges from that of the bulk particles. Additionally, particles located at the surface encounter a degree of surface tension induced by the presence of the second phase, as effectively demonstrated

Table I. PTT rheological model parameter.

PTT model Parameter					Polymer
η_1	η_2	ζ	λ	ϵ	
1850	11100	0.0063	1.23	0.01	LDPE
1360	9500	0.0058	1.04	0.1	PS

Table II. Parameters entered in the computer program.

Ω (rad/s)	Wi	dt	Surface tension (mN/m)
0.04	1.56-1.85	0.001	33.2

by the simulation findings.

Conclusion

This study investigates the heterogeneous polymer mixing of a system comprising low-density polyethylene and polystyrene, considering the presence of viscoelasticity. By employing tracking techniques, the obtained results reveal the absence of distinct layered motion within the flow and the occurrence of flow layer branching. Given the distinctive rheological and physical characteristics of each phase, a comparative analysis of surface and bulk particle velocities was conducted. The findings indicate that surface particles exhibit higher velocities when compared to those in the bulk region, which can be attributed to the influence of surface tension and viscoelastic stresses at the surface.

References

- [1] E. Khalaj, "Numerical simulation of the mapping method and experimental investigation of blending in twin screw extruder based on the miscibility of blend components", Tarbiat Modares, 2019.
- [2] T. Köpplmayr and E. Mayrhofer, "Numerical simulation of viscoelastic layer rearrangement in polymer melts using OpenFOAM®", *AIP Conf. Proc.*, **1664**, 2015.
- [3] E.S.P.B.V, S.A. White, D.G. Baird, and P. Materials, "Numerical simulation studies of the planar entry flow of polymer melts", **30**, 47-71, 1988.
- [4] Z. Tadmor and C.G. Gogos, Principles of Polymer Processing, 1937.

The Effect of Surface Chemically Modification of Montmorillonite on Rheological and Morphological Behavior of Thermoplastic Polyurethane

Mohammad Soroush Abzan¹, Melika Mirmomen², and Shervin Ahmadi^{3*}

1. Department of polymer engineering and color technology, Amir Kabir University of Technology, Tehran, Iran

2. Department of applied chemistry, Kharazmi University, Tehran, Iran

3. Iran Polymer and Petrochemical, Tehran, Iran

*sh.ahmadi@ippi.ac.ir

Abstract

Rheological properties and morphology are directly related to each other. In this research, the effect of surface chemically modification of montmorillonite nanoparticles (MMT) by grafting of nitrogen and phosphorus functional groups through silane coupling agent on rheological behavior was investigated. The result of the rheological analysis showed that the dispersion state of nanoparticles was increased by surface chemically modification. Also, by increasing the degree of dispersion of MMT nanolayers, the storage and loss modulus, and complex viscosity increased and the damping factor decreased. The FE-SEM images showed the MMT agglomerates broken due to the chemical surface modification process.

Keywords: rheology, morphology, surface modification, nanoparticle, dispersion state

Introduction

Due to their high surface energy, nanoparticles form agglomerates when dispersed in the polymer matrix. Improper distribution of nanoparticles in the polymer matrix occurs when stress is applied to the nanocomposite, concentrated at the interface of the agglomerates, and the nanocomposite sample fractures from this area [1]. To improve the dispersion state of nanoparticles in the polymer matrix, the surface chemical modification of nanoparticles is done by placing different functional groups with high steric hindrance. Surface chemical modification of nanoparticles is one of the effective methods to improve nanoparticle dispersion state in the polymer matrix. Increasing the dispersion state of nanoparticles through surface modification leads to the formation of a three-dimensional network and greater effectiveness in lower loading amounts of nanoparticles [2,3].

Experimental/Theoretical

Materials

Montmorillonite with grade 20A of the company American Saturn was produced under the brand name Cloisite 20A. TPU Desmopan® 385S by Covestro is a hydrolysis stabilized ester-based thermoplastic polyurethane block copolymer grade (Leverkusen, Germany). N-(2-Aminoethyl)-3-aminopropyltrimethoxysilane Merck KGaA (Darmstadt, Germany), CAS-No: 1760-24-3. Exolit® AP 422 is a Fine-grained white ammonium polyphosphate (APP) powder with low water solubility produced by a German Clariant company. Acetic acid and ethanol 96% were purchased from Merck (Darmstadt, Germany).

Chemical Modification of Montmorillonite

Three types of MMT nanoparticles were prepared in the

pure state (M), functionalized with amino silane (SM), as well as silanized MMT reacted with ammonium polyphosphate (SMP), which was added to polyurethane in different amounts. First, 2 g of MMT nanoparticles were dispersed in 300 mL of 96% pure ethanol solvent. Then, mass ratio of 5:1 (MMT: APTES), amino silane was added to the stirring solution at 60 °C. Then acetic acid was added dropwise to the solution until pH=3.5. To prepare the SMP, after silanization of MMT, ammonium polyphosphate was added to the solution. TPU granules were placed in a vacuum oven at a temperature of 80° for 8 h to remove moisture. Then the granule and nanoparticle in the combination of 2 wt% were manually mixed and poured into the microcomponder @ 180 °C, and 150 rpm.

Characterization

Rheological Behavior

An Anton Paar MCR-501 rheometer is employed to study the rheological behavior of samples with a cone angle of 1°, a diameter of 25 mm, and a gap distance of 59 μm at the rim.

Field Emission Scanning Electron Microscopy (FE-SEM)

FESEM was used to characterize the morphology of the nanocomposite samples.

Results and Discussion

RMS

Rheology is one of the powerful methods for investigating the dispersion behavior of nanoparticles in polymer matrix. In Figs. 1a and 1b, the behavior of the storage and loss modulus is shown. According to Fig. 1, with the surface chemically modification of the MMT nanoparticles and the

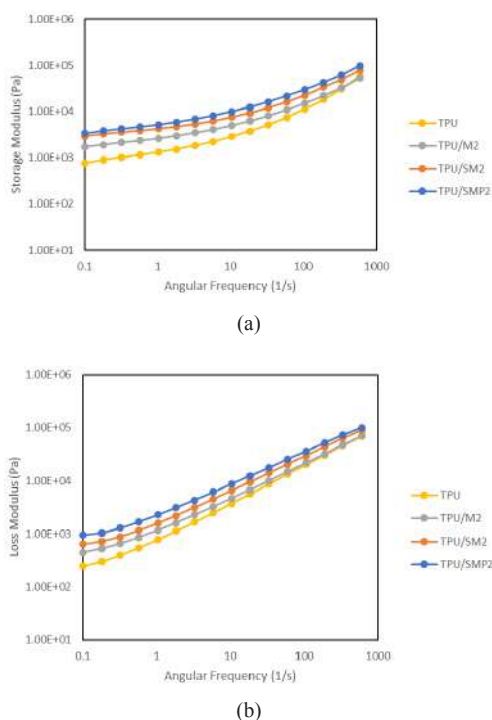


Fig. 1. (a) Storage modulus and (b) loss modulus of TPU and its nanocomposites.

increase of the interlayer space, the storage and loss modulus increases continuously. The increase in the storage modulus at low frequencies indicates the non-terminal or solid-like behavior, which is a reason for the improvement in the dispersion state of MMT nanoparticles in the polymer matrix.

Figs. 2a and 2b shows the effect of nanoparticle surface

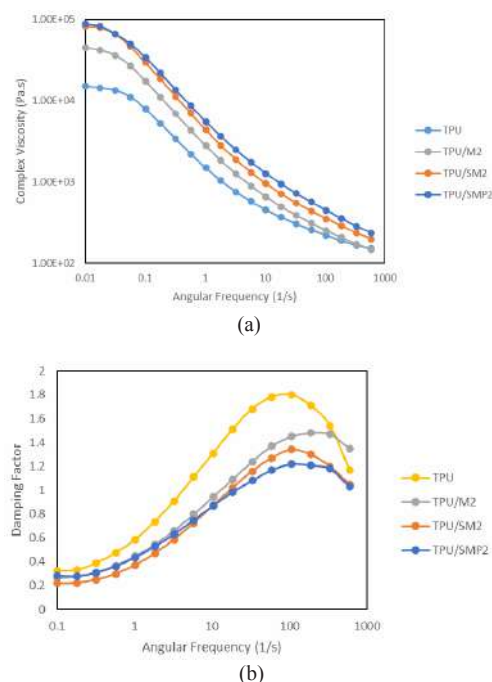


Fig. 2. (a) Complex viscosity and (b) damping factor of TPU and its nanocomposites.

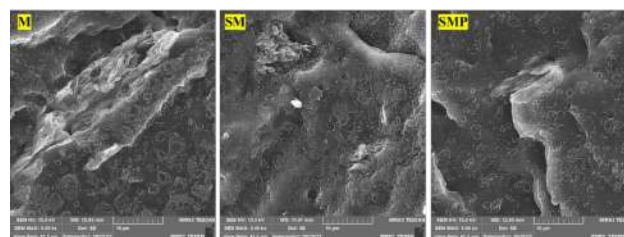


Fig. 3. FE-SEM images of surface fracture of TPU/M2, TPU/SM2, and TPU/SMP2 nanocomposites.

chemically modification on complex viscosity behavior and damping factor. According to Fig. 2a, by modifying the nanoparticle surface and increasing the interlayer space of MMT nanoparticles, the complex viscosity increases, and the Newtonian plateau region decreases. Also, the shear thinning behavior gradually increased and with the nanoparticle surface chemically modification, the shear thinning behavior is observed in a lower frequency range. Also, according to Fig. 2b, improving the dispersion state of nanoparticles from M to SM to SMP reduces the damping factor.

FE-SEM

In Fig. 3, from left to right, the image of the fracture surface of samples TPU/M2, TPU/SM2, and TPU/SMP2 is shown respectively. According to Fig. 3, with surface chemically modification, the agglomerates of montmorillonite are broken, and the interlayer space increases.

Conclusion

Rheology has a strong relationship with the morphology and topology of polymer and polymer nanocomposite. Any changes that occur in the chemical structure of the nanocomposite in the nanophase or polymer phase, can be traced by the rheological behavior. By modifying the surface of montmorillonite nanoparticles and increasing the interlayer space, in combination with constant percentages, the storage modulus and viscosity increase, and the damping factor decrease.

References

- [1] M.S. Abzan, R. Mirzaee, S. Ahmadi, N. Karimpour-Motlagh, and H.A. Khonakdar, "Affected polymer layer and thermo-mechanical behavior correlation in nylon-6/polycarbonate/graphene-oxide nanocomposites: A quantitative study of polymorphism", *Thermochim Acta*, **703**, 178995, 2021.
- [2] W. Wu, W. Zhao, Q. Sun, B. Yu, X. Yin, X. Cao et al., "Surface treatment of two dimensional MXene for poly(vinylidene fluoride) nanocomposites with tunable dielectric permittivity", *Compos. Commun.*, **23**, 100562, 2021.
- [3] S. Azizi, C.M. Ouellet-Plamondon, P. Nguyen-Tri, M. Fréchette, and E. David, "Electrical, thermal and rheological properties of low-density polyethylene/ethylene vinyl acetate/graphene-like composite", *Compos. Part B Eng.*, **177**, 107288, 2019.

Structural Transition from Liquid to Gel of Phase Change Material Nanoemulsions

S. Pantea Hosseini Largani, Hamed Salimi-Kenari*, S. Reza Nabavi, and Ahmad Ali Rabienataj Darzi

1. Department of Chemical Engineering, University of Mazandaran, Mazandaran, Iran

2. Department of Applied Chemistry, Faculty of Chemistry, University of Mazandaran, Babolsar, Iran

3. Department of Mechanical Engineering, University of Mazandaran, Babolsar, Iran

*h.salimi@umz.ac.ir

Abstract

Thermal energy storage has the potential for energy-saving and environmental pollution reduction. Technologies based on phase change materials (PCMs) absorb latent heat during melting and release it during solidification. In this sense, phase change material nanoemulsions have emerged as a promising option that creates a higher heat transfer rate due to the large surface-to-volume ratio of the dispersed phase on very small scales offering better energy storage density. In the present study, novel PCM nanoemulsions were designed and characterized as possible storage and heat transfer media for thermal applications. This study focuses on producing nanoemulsions with fine droplets of commercial paraffin RT42, stabilized with SDS using the sonication method. The primary objective of this research is to investigate the impact of PCM volume fraction and droplet size, on the rheological characterization of the final nanoemulsions. Rheological investigations revealed that nanoemulsions with volume fractions $\geq 30\%$ transformed from liquid-like states to viscoelastic gels due to the depletion attractions caused by SDS micelles in the continuous phase, resulting in strong gel formation. Furthermore, the gelation mechanism was evaluated at various PCM volume fractions.

Keywords: nanoemulsion, viscoelastic gel, thermal energy storage, phase change material, stability

Introduction

Thermal energy storage (TES) has great energy-saving potential and can reduce environmental pollution. Among various TES systems, latent heat storage using phase change materials (PCMs) is most favorable because of its compact size and nearly constant operating temperature. Nano-emulsions of PCMs with small droplets of 20–200 nm dispersed in water with the aid of emulsifiers can retain high stability and long shelf life. Recent studies have demonstrated the remarkable versatility of nanoemulsions, existing in a wide range of structures spanning from liquid-like dispersions to viscoelastic gels. Nanoemulsions exhibit gel-like behavior due to high effective volume fraction, droplet interaction, and dispersed phase aggregation-induced gelation. This occurs due to polymers, nanoparticles, or micelles affecting osmotic pressure balance [1]. Concerning the viscoelastic behavior of nanoemulsions at higher volume fractions, this study aims to acquire a deeper comprehension of the mechanisms of gelation by characterizing the interactions between droplets.

Experimental

The paraffin RT42 (Rubitherm Technologies GmbH, Germany) was selected as the PCM. Sodium dodecyl sulfate (SDS) purchased from Sigma-Aldrich was provided as a surfactant. The surfactant solution was prepared by adding

SDS into deionized water and stirring in a magnetic stirrer at 60 °C for 5 min. In another beaker, paraffin was heated to 60 °C and then added to surfactant solution (with the surfactant: paraffin volume ratio of 1:10) drop-wise along with continuous stirring. The magnetic stirrer was operated at 700 rpm for 10 min at 60 °C. Finally, the mixed solution was sonicated for 20 min. The total PCM volume fraction varied between 10 and 45%, while the other parameters were kept constant.

Results and Discussion

Due to the effect on PCM particle size, the PCM volume fraction has a substantial impact on the thermophysical properties of nanoemulsions. The particle size within the nanoemulsion can be controlled by modifying the PCM volume fraction, resulting in significant effects on the performance of the final nanoemulsions. Fig. 1 depicts the droplet size distribution of nanoemulsions with various volume fractions ranging from 10 vol% to 45 vol%. The samples have a growth ranging from 110 nm to 164 nm with the increase in PCM volume fraction. Measuring apparent viscosity is essential for understanding flow behavior and improving formulations across a variety of applications. The pseudoplastic behavior ($m < 1$) of the nanoemulsions, typical for this type of material, leads to viscosity reduction as shear rates increase. This can be attributed to disrupted interdroplet interactions or droplet

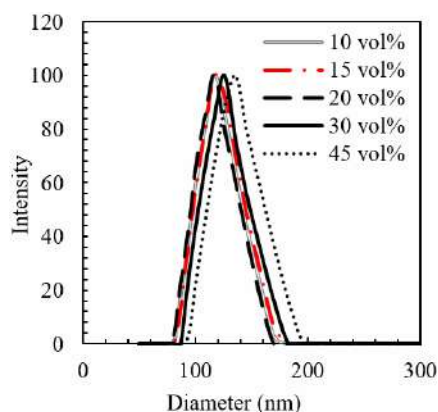


Fig. 1. Droplet size distribution of the nanoemulsions at different PCM volume fractions.

Table I. m and k values of the nanoemulsions at different volume fractions.

Volume fraction (%)	m	k
10	0.46	0.24
15	0.19	0.19
20	0.05	0.71
30	0.08	205.1
45	0.25	179.6

alignment within the shear field [2]. The resulting pseudoplastic rheology was quantified using the power law fluid model, yielding fluidity index (m), and consistency coefficient (K) values for varying volume fractions, as detailed in Table I. The K values rise as the PCM volume fraction increases. This increase in droplet concentration causes PCM droplets within the nanoemulsion to be packed more densely, resulting in the generation of a more structured network, and increased resistance to flow. The viscoelastic behavior of the samples at 30 and 45 vol% was determined by the strain sweep measurements at 0.01 to 1000% strain and a constant frequency of 10 rad/s. Based on these experiments, a linear viscoelastic region (LVR) was identified, where the storage (G') and loss moduli (G'') were not influenced by the applied strain. As shown

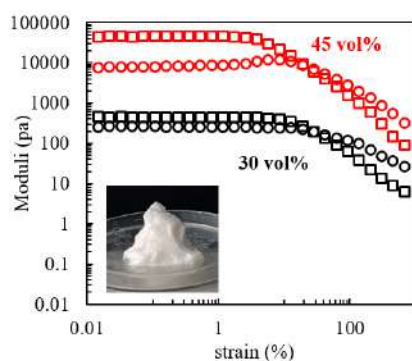


Fig. 2. Strain dependence of the storage G' (square) and loss moduli G'' (circle) of nanoemulsions containing 30 and 45 vol%.

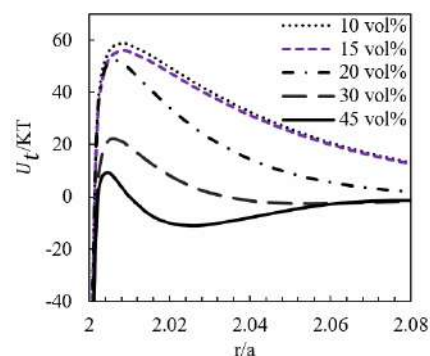


Fig. 3. The comparison of the overall interaction potentials of nanoemulsions at different volume fractions.

in Fig. 2, G' is significantly greater than G'' within the LVR reflecting their dominant elastic nature. At a larger strain, known as yield strain, the G' values of the sample showed deviation from linearity and dropped gradually due to the structural relaxation process leading to gel network breakdown and flow of materials. At higher strains, G'' dominates over G' , indicating the liquid-like behavior of the samples [3]. Nanoemulsions transform gelled systems by stabilizing them with an anionic surfactant, increasing effective radius due to a thick electrical double layer around the droplet surface. Fig. 3 illustrates the comparison of the overall interaction potential of nanoemulsions at different volume fractions, indicating that higher SDS concentration and volume fraction boost depletion attraction between droplets. This suggests that nanoemulsions form gel networks by increasing the volume fraction as a result of an increased concentration of depletants (SDS micelles) and higher depletion attraction energy [4].

Conclusion

Research indicates that fluid-like nanoemulsions become viscoelastic gels at volume fractions over 30% because of excess SDS micelles causing depletion attraction forces, resulting in an aggregated nanodroplet network.

References

- [1] P. O'Neill, L. Fischer, R. Revellin, and J. Bonjour, *Appl. Therm. Eng.*, **192**, 1-17, 2021.
- [2] Y. Wang, S. Li, T. Zhang, D. Zhang, and H. Ji, *Sol. Energy Mater. Sol. Cells.*, **171**, 60-71, 2017.
- [3] S.S. Datta, D.D. Gerrard, T.S. Rhodes, T.G. Mason, and D.A. Weitz, *Phys. Rev. E*, **84**, 1-6, 2011.
- [4] Z. Abbasian Chaleshtari, H. Salimi-Kenari, and R. Foudazi, *Langmuir*, **37**, 76-89, 2021.

Relationship between Microstructure and Rheological Properties of PLA/EVA in the Presence of POSS Nanoparticles

Vida Varjavand and Jafar Khademzadeh Yeganeh*

Department of Polymer Engineering, Qom University of Technology, Qom, Iran

*khademzadeh@qut.ac.ir

Abstract

In this paper, we investigated the effect of hydrophobic POSS nanoparticles on the properties of Polylactic acid/Ethylene vinyl acetate copolymer blend, PLA/EVA. For this purpose, PLA/EVA blend, with a fixed composition of 75/25 was prepared in the presence of various quantities of the POSS nanoparticles. In presence of the nanoparticles, the diameter of scattered EVA particles decreased, the compatibility increased and the interface of the two phases became indistinguishable. Blending gives pure and brittle PLA a ductile behavior and increases the elongation at break of compound. Addition of nanoparticles significantly enhanced the toughness of the blends. Frequency sweep behavior of the storage modulus for the samples was studied.

Keywords: PLA, EVA, poss nanoparticles, morpholog, rheology

Introduction

The use of biodegradable polymers on the lack of environmental contamination has been the focus of attention in recent decades, due to increased environmental pollution by the excessive use of synthetic plastics. These polymers decompose over a time of up to several years and return to environmental cycle, and using them has minimal negative effects on environment compared to petroleum-based polymers. Therefore, biodegradable polymers are a good alternative to conventional plastics. Polylactic Acid (PLA) is one of the biodegradable polymers that made from 100% renewable sources, it is also biocompatible which in contact with body does not cause toxicity. It has been used in a variety of applications including medical applications. Other advantages of PLA is easy molding to most molding methods including injection molding and thermoforming. Despite the advantages mentioned for PLA, due to the glass transition temperature above ambient temperature (approximately 60 °C), this polymer is brittle with low toughness and this is one of the major limitations of its use in industry which inevitably necessitates the modification and improvement of the properties of this polymer. The purpose of this work is increasing the elongation at break and impact strength of PLA by compounding with EVA in the presence of hydrophobic nanoparticles.

Experimental

Poly lactic acid by trade name 2003D, with a specific density of 1.24 g/cm³ and a melt flow index of 5.92 g/cm³ (at 190 °C and 2.16 kg) was provided by NatureWorks. Random copolymer ethylene vinyl acetate with 18% vinyl acetate with a density of 0.932 g/cm³ and a melt flow index

of 2.5 g/cm³ were prepared by CEETECH. The POSS Nanoparticles derivative used in this research was FL0578-TriFluoropropyl POSS® Cage Mixture, with a molecular formula of (C₃H₄F₃)_n (SiO_{1.5})_n (n=8, 10, and 12) in powder form and a molecular weight of 1193.16 g/mol, which was supplied from Hybrid Plastics, Inc. (USA). All samples were melt-mixed in an internal mixer made by Brabender at 200 °C at 60 rpm for 10 min. Percentage composition of all samples was fixed to 75/25 of PLA/EVA, and values of nanoparticles 1, 3, and 5 wt%. Tensile test was performed at a speed of 5 mm/min, using the SANTAM STM-20 at ambient temperature, and rheology test was performed with RMS 302 dynamic rheometer with 1% strain (in linear area).

Results and Discussion

Scanning electron microscopy (SEM) was performed to investigate the morphology of the samples as shown in Fig. 1. As anticipated, PLA/EVA (75/25) sample showed a droplet-matrix morphology in which, PLA was the matrix. The blend exhibited a well-distinguished interface and large EVA droplets and the cavities caused by interfacial debonding were visible. This indicates an incompatible polymer blend leading to a weak interfacial adhesion between the phases. After incorporating POSS Nanoparticles the size of EVA droplets was greatly decreased and the interfacial adhesion improved. Fig. 2. shows the storage modulus, G', as a function of angular frequency, ω , for PLA/EVA blend with different percentages of nanoparticles. As the particle loading increases, the dependence of low frequency G' on ω weakens and G' increases.

At low volume fractions of Nanoparticles, the low

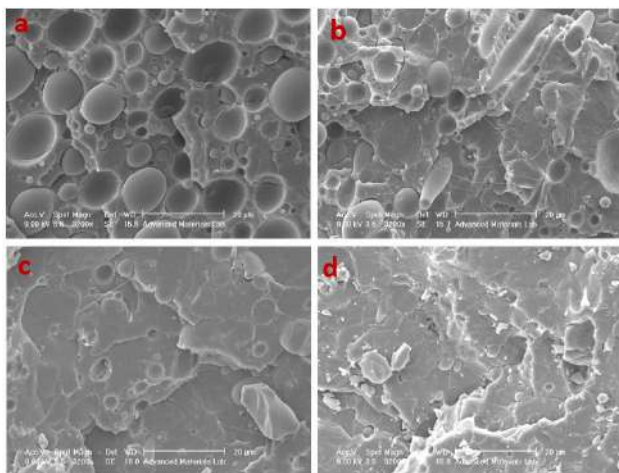


Fig. 1. SEM images of samples: (a) PLA/EVA, (b) PLA/EVA/1% POSS, (c) PLA/EVA/3%POSS, and (d) PLA/EVA/5% POSS.

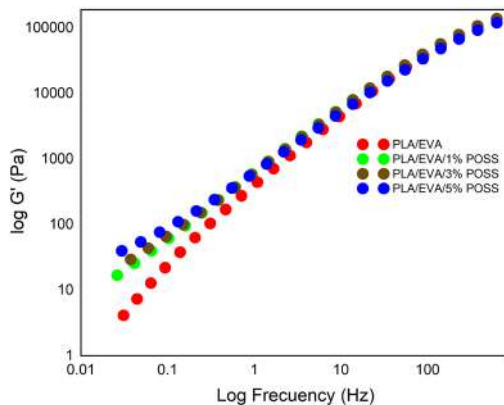


Fig. 2. Storage modulus of PLA/EVA blend containing different amounts of nanoparticles.

frequency response is dominated by the particle-induced changes in polymer chain dynamics, while at high loadings the agglomeration of nanoparticles and particle–particle interactions mainly contribute to the overall viscoelastic behavior. Therefore, long-range polymer relaxation in the EVA phase is restrained. Also, according to SEM results, the compatibility effect of nanoparticles creates a high surface that increases the dynamic moduli at low frequencies. At high frequencies, the effect of nanoparticles on the rheological behavior is relatively weak suggesting that the nanoparticles do not significantly influence the short-range dynamics of polymer chains, particularly in the entanglement length scales.

Conclusion

In this research, PLA with very high toughness and impact strength was prepared by mixing it with EVA in presence of POSS polyhydroooligomeric silsquioxane nanoparticle. The SEM photos showed that the with the addition of different percentages of POSS nanoparticles, the size of the EVA

droplets is significantly reduced and the adhesion of the two phases is improved and a strong interface between the two phases is created. The reason for the formation of this structure can be attributed to the significant reduction of interfacial tension. Finally, the microstructure of the blends was assessed through the rheological measurements which indicated the NPs-PLA favorable interaction and compatibilizing effect of nanosilica in decreasing the EVA droplet size.

References

- [1] Z. Hoseini, J. Khademzadeh Yeganeh, and S. Moradi, “A highly toughened poly(lactic acid)/ethylene-co-vinyl acetate blend with the simultaneous addition of hydrophobic nanoparticles and compatibilizer”, *Iran. J. Polym. Sci. Technol. (Persian)*, **33**, 509-524, 2020.

Investigation of Effect of Rheology Modifier's on Rheological Behavior of Water-Based Paint

Mersad Javaheri and Hossein Yahyaei*
Amirkabir University of Technology, Tehran, Iran

*yahyaei@aut.ac.ir

Abstract

In the last few decades, the use of water-based paint systems has received much attention due to their environmental properties. Despite all the efforts made, water-based systems face a series of problems. One of the fundamental issues in the production of water-based coatings is their rheological properties. Thickeners are used for correction. There are three common types of thickeners used in water-based systems: cellulose, acrylic, and urethane thickeners. In this research, paint samples containing cellulose, acrylic, and urethane thickeners were prepared, each in three different concentrations. The rheological behavior, sag resistance, stability and resistance to sedimentation over time and washing properties of each sample have been investigated. The results confirm that all thickeners induce thixotropic behavior. Overall, the urethane thickener exhibits superior properties compared to other additives. However, when used in small quantities, its stability, resistance to leaching, and resistance to sedimentation are much lower than those of other additives.

Keywords: rheology, water-based paint, sag resistance, thickening agent, sedimentation

Introduction

One of the most important issues in the world is environmental pollution. Organic solvents are among the most effective factors to environmental pollution. Various methods have been proposed to reduce volatile organic compounds (VOCs). One of these methods is utilization of water-based paints. Water-based paints, when compared to solvent-based paints, exhibit inferior properties, encompassing physical and mechanical properties, chemical resistance, and rheological properties. Paints need to display non-Newtonian rheological behavior, specifically shear-thinning, to prevent sagging on inclined or vertical surfaces. A coating material lacking a yield stress will sag due to the force of gravity. It is preferable for the paints to exhibit thixotropic behavior. Paints typically have a yield stress, and the sagging behavior can be divided into two zones: an outer slumping zone and an inner sagging zone. The storage modulus of paint is crucial in its resistance to sagging. Thickener additives are used to prevent sagging and maintain the stability of paint particles [1]. In general, two categories can be distinguished for water-based paint thickeners: associative and non-associative. Associative thickeners are typically polymers with both hydrophilic and hydrophobic groups in their structure [2]. These additives contain hydrophobic groups within their molecules, which do not interact with polar water molecules but instead interact with resin particles. Additionally, they can combine and create micelles within the aqueous phase. On the other hand, their hydrophilic components interact with the polar molecules of the aqueous matrix. Consequently, by establishing a network, they enhance the paint's viscosity. A commonly used thickener for water-based paint is ethyl-hydroxy-cellulose (HEC), which is a water-soluble polymer with a high molecular weight. These additives swell

as they absorb water, leading to an increase in viscosity owing to their high molecular weight [3]. Aqueous-based acrylic thickeners are typically high molecular weight copolymers of (meth)acrylic acid and their esters. Linear acrylic copolymers exhibit high viscosity upon dissolution, while loosely crosslinked acrylic polymer thickeners experience the swelling of polymer particles rather than true dissolution [4]. Hydrophobic modified polyurethanes, abbreviated as PUR, are non-ionic additives and represent the most recent thickeners additive in water-based paints. They possess a urethane structure formed by connecting di-isocyanates with poly-ethers and capping their ends with non-polar components [5]. In recent years, the effects of various factors on the rheological behavior of paints have been investigated. In this study, we investigated the impact of a rheology modifier on the properties of acrylic water-based paint.

Experimental

Selecting the appropriate resin is a pivotal step in the design of coatings. A water-based ambient-cure resin was used in this project. Three different types of thickening agents, namely urethane, acrylic, and cellulose, were employed in combination with various percentage ratios. The paint contained additives at percentages of 0.5, 0.75, and 1% for samples with cellulose additives, 0.5, 2, and 4% for samples with acrylic additives and 1, 2, and 3% for samples with urethane additives. One important aspect to consider in the sample preparation process pertains to the resin and coalescing agent additive. The primary role of the coalescing agent additive is to soften the surface of the resin droplets, facilitating improved film formation in the resin. To achieve this, the resin coating samples and coalescing agent additive were combined two days prior

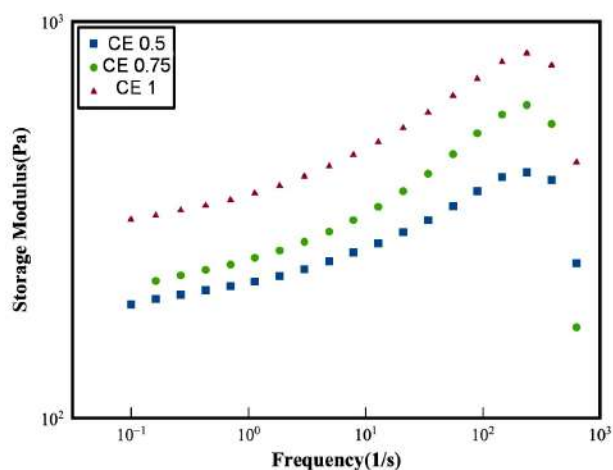


Fig. 1. The changes in storage modulus with respect to frequency for cellulose samples.

to preparation and stored in a sealed container, isolated from oxygen. After preparing the samples, they were allowed to rest for 2 days before undergoing testing and examination. To conduct the stability test, the samples were poured into sealed containers, and subsequently, they were assessed based on the extent of two-phase formation. After conducting this test, two phases were observed in the sample that contained 1% urethane thickener. The rheological properties of the samples were examined using the RMS device. The investigation of rheological properties was conducted using the frequency sweep mode of the RMS device, and the results for each sample are displayed in Figs. 1-3. All the samples underwent pre-shearing for 1 min before the test. As observed in the graphs, the storage modulus in urethane samples increased by up to $2 \times 10^4\%$ with increasing frequency, while in acrylic samples, it saw a 10% increase, and in cellulose samples, it increased by 250%. The urethane additive provides better sag resistance compared to acrylic and cellulose additives. Paint containing a urethane additive is highly suitable for spray application. The urethane sample exhibited weaker shear-thinning behavior compared to the cellulose and acrylic

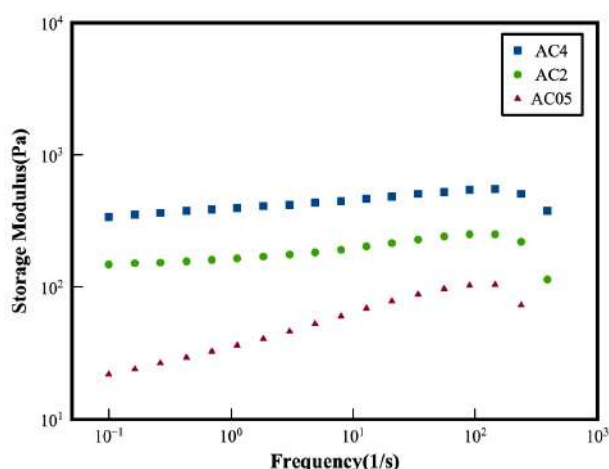


Fig. 2. The changes in storage modulus with respect to frequency for acrylic samples.

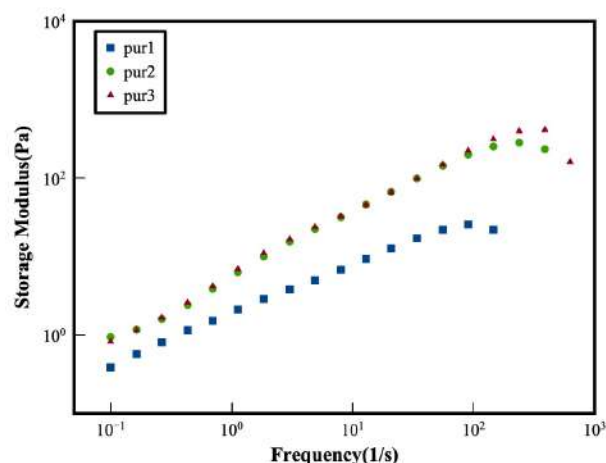


Fig. 3. The changes in storage modulus with respect to frequency for urethane samples.

samples. By increasing the frequency from 10-1 to 103, the viscosity of cellulose and acrylic samples decreases by 1.7×10^4 and $2.9 \times 10^4\%$, respectively, and for the urethane sample, it decreases by only $1.9 \times 10^3\%$. It is evident that the elastic modulus does not change significantly with an increase in the concentration of urethane additive from 2% to 3%. This observation suggests that an increase in additive concentration does not lead to the formation of significantly more networks.

Conclusion

This study examined how cellulose, acrylic, and urethane thickener additives affect the rheological behavior of water-based acrylic paint. The urethane thickening additive provides greater sag-resistance because of its higher storage modulus.

References

- [1] C.S. Wang, G. Chapelle, P. Carreau, and M.C. Heuzey, "Prediction of sag resistance in paints using rheological measurements", *Prog. Org. Coatings*, **153**, 2021. doi: 10.1016/j.porgcoat.2021.106139
- [2] G. Fonnum, J. Bakke, and F.K. Hansen, "Associative thickeners. Part I: Synthesis, rheology and aggregation behavior", *Colloid Polym. Sci.*, **271**, 380-389, 1993. doi: 10.1007/BF00657419
- [3] L.M. Zhang, "Cellulosic associative thickeners", *Carbohydr. Polym.*, **45**, 1-10, 2001. doi: 10.1016/S0144-8617(00)00276-9
- [4] M. Jassal, B.N. Acharya, P. Bajaj, and R.B. Chavan, "Acrylic-based thickeners for pigment printing-a review", *J. Macromol. Sci. Polym. Rev.*, **42**, 1-34, 2002, doi: 10.1081/MC-120003093
- [5] E. Orgilés-Calpena, F. Arán-Aís, A.M. Torró-Palau, C. Orgilés-Barceló, and J.M. Martín-Martínez, "Addition of different amounts of a urethane-based thickener to waterborne polyurethane adhesive", *Int. J. Adhes. Adhes.*, **29**, 309-318, 2009. doi: 10.1016/j.ijadhadh.2008.06.004

Synthesis and Rheological Characterization of Persian Gum-g-Polyvinyl Acetate Copolymer Dispersions in Water Prepared by Redox System

Shaghayegh Rostampour, Ali Ahmadi-Dehnoei, and Somayeh Ghasemirad*

Polymer Engineering Department, Faculty of Chemical Engineering, Tarbiat Modares University, Tehran, Iran

*ghasemirad@modares.ac.ir

Abstract

Persian gum is an available useful biopolymer, the properties of which in dispersion form in water including rheological behaviour require modification to enable its wider use in various industries. In this study, vinyl acetate (VAc) was grafted onto the PG chains at various amounts using a redox system to reduce the gel-like behaviour of PG dispersion. The results of FTIR spectroscopy on PG and PG-g-PVAc after removing PVAc homopolymers using Soxhlet extraction method confirmed the successful grafting of monomers onto PG. The shear stress of the polymer dispersions in water versus shear rate followed the Herschel-Bulkley model with shear-thinning behavior. Furthermore, the increase in the VAc content from 0 wt% to 80 wt% decreased the yield stress of the polymer dispersions from 10.7 Pa to 0.9 Pa. Moreover, flow behavior index and fluid consistency of the dispersions increased from 0.27 to 0.47 and decreased from 166.6 Pa.sⁿ to 4.7 Pa.sⁿ, respectively.

Keywords: Persian gum, vinyl acetate, grafting, Herschel-Bulkley model, shear-thinning behavior

Introduction

In recent years, polysaccharides were used in wide applications such as drug delivery, film, coating and other industries due to their biodegradability, safety, low price, biocompatibility, and availability from agricultural resources [1]. However, they need to be modified to replace synthetic polymers and to achieve desirable and specific properties such as rheological characteristics and solubility [2]. The grafting techniques have been of interest to many researchers to modify polysaccharides [1]. Grafting reaction, in particular, improves the rheology of substances [2]. Persian gum (PG) is a natural polysaccharide that is mainly native to Iran and is obtained from wild almond trees [3]. This biopolymer is used in various applications such as food industry, soil stabilization, thickening, film formation, rheology modification, and texturing [3]. In most of these applications, the viscosity and rheological properties of the product are crucial, which must be modified due to the gelling properties of PG [2,3]. In the present study, vinyl acetate (VAc) was grafted onto PG using a K₂S₂O₈/NaHSO₃ redox system and the effect of the grafted polymer content on the rheological behavior of PG-g-PVAc was investigated.

Experimental

PG-g-PVAc was prepared at PG:VAc compositions of 100:0, 80:20, 50:50, and 20:80, respectively. First, PG powder was dissolved in water in a five-necked round-bottom flask at 80 °C using a mechanical stirrer at 280 rpm

for 85 min. Then, the reaction temperature was cooled to 60 °C. PG dispersion was deoxygenated under nitrogen gas for 30 min at 60 °C. Then, initiators system comprising potassium persulfate as oxidant and sodium hydrogen bisulfite as reductant were dissolved in distilled water at equal molar ratios. Finally, initiators system and monomer were dropped into the reaction flask at an appropriate rate. The graft polymerization continued for 4 h at 60 °C. To determine the grafting parameter, the dispersions were dried, powdered, and purified using Soxhlet extraction with acetone at 70 °C for 48 h to remove PVAc homopolymers. Grafting percentage was calculated using Eq. (1) [4]:

$$G (\%) = \frac{\text{weight of grafted polymer}}{\text{weight of copolymer}} \times 100 \quad (1)$$

Fourier transform infrared spectroscopy (FTIR) of the Soxhlet extracted powders was performed on a Perkin-Elmer Frontier Spectrometer (USA) to confirm the grafting of VAc on PG. The rheological properties of the dispersions were measured using a MCR 300 rheometer (Anton Paar, Austria) with a parallel plate geometry (25 mm diameter and 1 mm gap). The shear rate varied from 0.01 1/s to 1000 1/s and the temperature was 25 °C. According to the results, the data were fitted to the Herschel-bulkley model, using Eq. (2) [2]:

$$\tau = \tau_0 + K \dot{\gamma}^n \quad (2)$$

where τ , τ_0 , K , $\dot{\gamma}$ and n are the shear stress, yield stress,

Table I. Grafting and rheological parameters of PG-g-PVAc.

Sample code	G(%)	τ_0 (Pa)	n	K (Pa.s ⁿ)	R^2
PG dispersion	-	10.7	0.27	166.6	0.98
PGPVAc-20	16.3 ± 1	8.0	0.28	147.2	0.99
PGPVAc-50	35.4 ± 2	3.7	0.36	49.5	0.99
PGPVAc-80	70.9 ± 1	0.9	0.47	4.7	0.99

fluid consistency, shear rate, and flow behavior index, respectively.

Results and Discussion

Table I shows the grafting percentage of the samples dried after Soxhlet extraction. Grafting percentage increased with the increase in the amount of monomer. This can be attributed to the presence of more monomers around PG chains and the weak mobility of PG macroradicals, and as a result, an increase in the probability of collision of PG

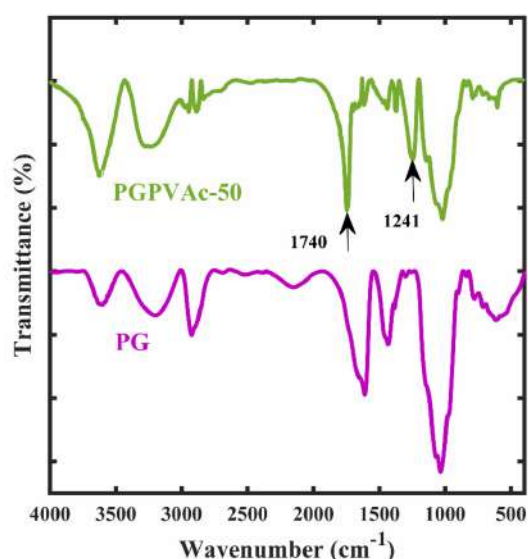


Fig. 1. FTIR spectrum of PG and purified PGPVAc-50.

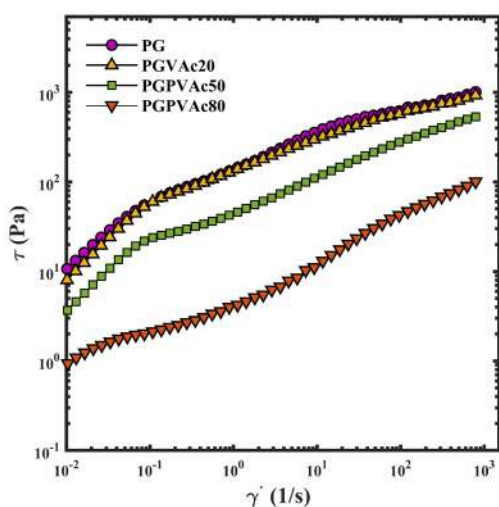


Fig. 2. Shear stress of PG and PG-g-PVAc dispersions in water versus shear rate.

macroradicals and VAc molecules and more VAc grafting on PG chains [4]. FTIR spectroscopy was also used to confirm the graft modification of PG after Soxhlet extraction, Fig. 1. Compared with PG, PG-g-PVAc showed new characteristic peaks of ester group at 1241 and 1740 cm^{-1} [4], which verified the successful grafting of PVAc onto the PG chains. Fig. 2 shows the shear stress of the polymer dispersions in water versus shear rate. All samples had shear-thinning behavior [4]. With the addition of 0, 20, 50, and 80 wt% monomer, the yield stress (τ_0) decreased from 10.7 Pa to 8.03, 3.7, and 0.9 Pa, respectively. This result indicated that a lower force is required to start movement of the PG-containing dispersion with the existence of higher amount of PVAc in the dispersion [4]. The obtained n values of less than 1 also confirmed their shear-thinning behavior, Table I. By using higher amount of monomer in the formulation, n became closer to 1, which meant weakening the shear-thinning behavior with the increase in the monomer content. Furthermore, the value of K , which indicates the resistance of the fluid to flow, decreased sharply with the increase in the monomer content from 0 to 80 wt%, and reached from 166.6 Pa.s^n to 4.7 Pa.s^n . The results were attributed to the reduction in the number of entanglements and also hydrogen bonds in the system and the reduction of gelation in the dispersions with higher VAc content.

Conclusion

A PG-based copolymer was synthesized via graft copolymerization of vinyl acetate monomer using a redox system. The results indicated that with increase in the PVAc content in PG-g-PVAc copolymer, the grafting percentage increased. The grafting of VAc on the backbone of PG led to the weakening of the shear-thinning behavior toward Newtonian behaviour, reducing the force required for movement and reducing the resistance of the dispersions to flow. Hence, it can be concluded that by modifying PG through grafting with PVAc using a redox system at a desirable PVAc content, its rheological behavior will be improved.

References

- [1] A. Singh, B. Mangla, S. Sethi, S. Kamboj, R. Sharma, and V. Rana, *Carbohydr. Polym.*, **156**, 45-55, 2017.
- [2] K.P. Tulegenovna, E. Negim, K.M. Al Azzam and M.A. Bustam, *Int. J. Technol.*, **13**, 389-397, 2022.
- [3] S. Abbasi, Persian gum, in: Razavi SMA (Ed.), *Emerging natural hydrocolloids: Rheology and functions*, John Wiley & Sons Ltd, Oxford, 273-298, 2019.
- [4] L. Chen, Z. Xiong, H. Xiong, Z. Wang, Z. Din, A. Nawaz, P. Wang, and C. Hu, *Carbohydr. Polym.*, **200**, 477-486, 2018.

Effect of Solid Content and Comonomers Addition Rate on the Rheological Behaviour of Polymer Brush Systems

Amir Parvaz and Somayeh Ghasemirad*

Polymer Engineering Department, Faculty of Chemical Engineering, Tarbiat Modares University,
P.O. Box 14115-114, Tehran, Iran

*ghasemirad@modarse.ac.ir

Abstract

Polymer brush systems have gained considerable attention in various areas such as adhesives and coatings. In these applications, the rheological properties of these systems, which are primarily fluid, are of great importance. Herein, the effect of synthesis variables on the rheological properties of the solution of an acrylic copolymer brush grafted to magnetite (Fe_3O_4) nanoparticles was investigated. The Herschel-Bulkley model fitted the flow curves of the polymer brush systems and revealed the yield-pseudoplasticity of the studied systems. An increase in the solid content led to an increase in the viscosity and a decrease in the yield stress of the solutions. Moreover, an increase in the comonomers addition rate resulted in obtaining solutions with a lower viscosity and a reduced yield stress. Thus, the rheological properties of the solutions of polymer brushes can be efficiently controlled with their synthesis variables, especially by adjusting their solid content.

Keywords: polymer brush, acrylic, Fe_3O_4 , yield-pseudoplasticity, herschel-bulkley model

Introduction

Polymer brushes consist of polymer chains grafted to a surface [1]. The crowded environment within polymer brushes and the stretched conformation of polymer chains provide unique physicochemical properties, leading to developments in inorganic-organic nanostructures, adhesives, anti-fouling coatings, biomedical carriers, and materials for use in lubrication, photonics and energy storage [2,3]. In most of these applications, the polymer brush system is primarily fluid [4], and its flow behaviour and rheological properties determine its performance.

To elucidate the importance of synthesis variables in the flowability of polymer brush systems, the present study has focused on the effect of solid content and comonomers addition rate on the rheological behaviour of acrylic polymer brush grafted to magnetite (Fe_3O_4) nanoparticles in a mixture of organic solvents.

Experimental

The polymer brush systems were prepared by synthesizing Fe_3O_4 nanoparticles by coprecipitation method, modifying it with methacryloxypropyltrimethoxysilane, and grafting poly(butyl acrylate-co-acrylic acid) on it in toluene/ethyl acetate mixture. The x and y in the sample codes of Cx-Ry designate their solid content (i.e., solution concentration, %) and comonomers addition rate (mL/min). The rheological properties of the systems were measured at 25 °C using a mechanical mixer equipped with a torque meter (Heidolph, Germany).

Results and Discussion

According to the torque versus rotation speed curves, the polymer brush systems showed a yield-pseudoplastic behaviour, Fig. 1. The applied torque increased with the increase in the concentration of the solutions and also the decrease in the monomer addition rate. The torque (M)-speed (N) data was converted into shear stress (τ)-shear rate ($\dot{\gamma}$) data using the following equations:

$$\omega = \frac{2\pi}{60} N \quad (1)$$

$$\tau = \frac{M}{2\pi(L R_b^2)} \quad (2)$$

$$\dot{\gamma} = \frac{2\omega R_c^2 R_b^2}{x(R_c^2 - R_b^2)} \quad (3)$$

where ω , L, R_b , R_c , and n are angular velocity of spindle, effective length of spindle (assumed to be 5.5 cm), radius of container, radius of spindle, and radius at which shear rate is being calculated, respectively [5]. The Hershel-Bulkley model was applied to make a comparison on the flow behaviours of the polymer brush systems, expressed as follows:

$$\tau = \tau_0 + k\dot{\gamma}^n \quad (4)$$

where τ_0 , k, and n are yield stress, viscosity

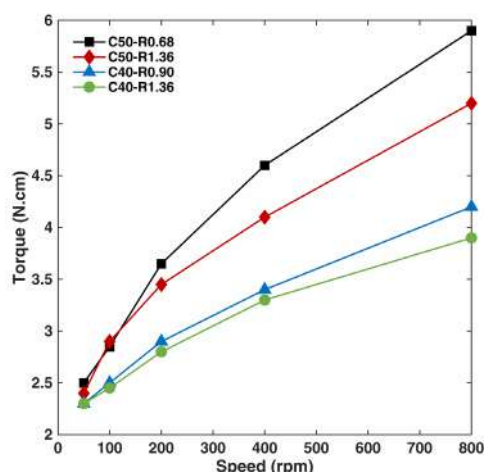


Fig. 1. Torque of the polymer brush systems versus speed.

Table I. Rheological parameters of the Herschel-Bulkley model.

Sample code	τ_0 (Pa)	k (Pa.s ⁿ)	n	R^2
C50-R0.68	89.84	21.1	0.487	0.998
C50-R1.36	87.04	25.94	0.422	0.998
C40-R0.90	131.4	6.22	0.583	0.999
C40-R1.36	127.1	8.192	0.517	0.997

coefficient, and shear rate exponent, respectively [6]. The correlation coefficients, R^2 , for the Herschel-Bulkley model were more than 0.99, implying that this model well fitted the rheological behaviour of the studied systems, Table I. The obtained n values of less than 1 also confirmed their yield-pseudoplasticity. Surprisingly, the less concentrated systems had higher yield stress, which was attributed to the existence of more compact clusters of the brush particles in the less viscous medium with a higher value, closer to 1, and a lower k value. The faster monomer addition rate, expected to lead to the formation of more free chains in the solvent, reduced the n value and increased the k value,

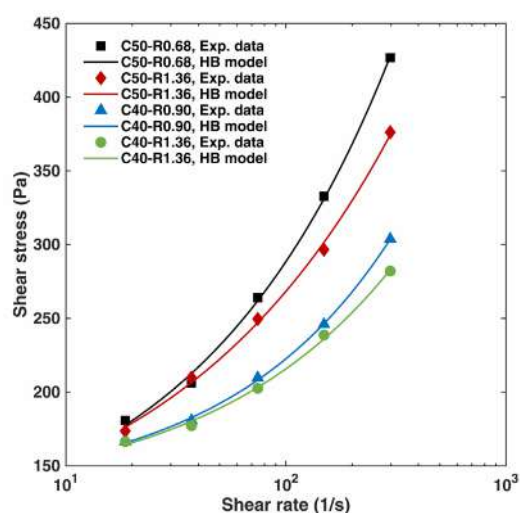


Fig. 2. Shear stress of the polymer brush systems versus shear rate.

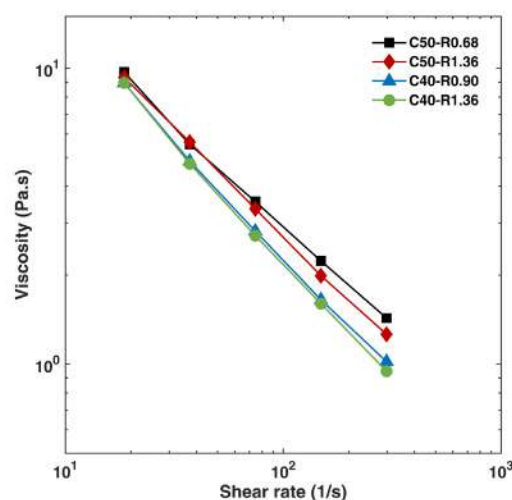


Fig. 3. Viscosity of the polymer brush systems versus shear rate.

though minorly decreased the yield stress. The viscosity was also calculated by dividing shear stress to shear rate, Fig. 3. The results revealed that the more concentrated systems had higher viscosity. Moreover, the lower monomer addition rate led to an increase in the viscosity due to reducing the number of free chains in the solvent. Such an effect was more apparent at higher shear rates.

Conclusion

The results of this study showed that the solution of an acrylic copolymer brush grafted to magnetite nanoparticles in the toluene/ethyl acetate mixture is yield-pseudoplastic. Furthermore, its flow characteristics can be controlled by its synthesis variables, such as its solid content and the comonomers addition rate. An increase in the former and a decrease in the latter increase its viscosity.

Acknowledgement

The authors would like to acknowledge financial support from Tehran Chamber of Commerce Industries, Mines and Agriculture.

References

- [1] P. Polanowski, J.K. Jeszka, and K. Matyjaszewski, *Macromolecules*, **56**, 2608-2618, 2023.
- [2] L. Yin, L. Liu, and N. Zhang, *Chem. Commun.*, **57**, 10484-10499, 2021.
- [3] A. Ahmadi-Dehnoei and S. Ghasemirad, *Int. J. Adhes. Adhes.*, **111**, 102973, 2021.
- [4] S.X. Zheng and H.S. Chen, *Prog. Org. Coat.*, **177**, 107403, 2023.
- [5] S. Devrani, R. Sharma, M.P. Rajesh, and A. Kapoor, *Asian J. Chem.*, **29**, 1953-1958, 2017.
- [6] C. Liang, B. Wang, J. Chen, Y. Huang, T. Fang, Y. Wang, and B. Liao, *Colloids Surf. A: Physicochem. Eng.*, **513**, 136-145, 2017.

The Effect of Different *Escherichia coli* (*E. coli*) Bacteria Concentration in Polymer Solution Behavior

Arezoo Zarei and Nadereh Golshan Ebrahimi*

Polymer Engineering Department, Faculty of Chemical Engineering, Tarbiat Modares University,
P.O. Box 14115-114, Tehran, Iran

*ebrahimn@modares.ac.ir

Abstract

Nowadays, with the studies done by scientists in various fields, it can be said that one of the most important branches is the study of active fluids. Due to the presence of self-propelled particles, these fluids show a unique behavior compared to fluids that contain colloidal particles. The purpose of this research is to investigate the effect of the presence of *E. coli* bacteria and its concentration on the rheological behavior of a relatively concentrated polyvinylpyrrolidone (PVP) solution. Experiments by shear rheometer showed that the presence of this bacterium at low shear rate leads to a decrease in relative viscosity, and this decrease in viscosity occurs more as the concentration of bacteria increases. At a higher shear rate, an increase in viscosity and then its stability will be observed.

Keywords: active fluid, bacteria, *E. coli*, viscosity, rheological behavior

Introduction

Active suspension solutions have mobile particles that move in the fluid without the intervention of external forces and with their own self-propelled force. For example, suspension solutions of microorganisms such as bacteria have a different rheological response than suspension solutions of colloids or nanoparticles. Bacteria swim in fluids with low Reynolds numbers and with the help of their flagella, which provides the driving force for their movement. The viscosity of suspension solutions containing bacteria is different compared to solutions without bacteria [1]. According to the type of fluid flow they induce in the field, the microorganisms are divided into two categories: pushers and pullers. The flagella of the pushers are located back of them, which move forward by pushing the fluid and reduce the viscosity of the polymer solution. The flagellum of the pullers is located in front of the cell body, which moves forward with fluid stretching and increases the viscosity of the polymer solution. Active fluid is a viscous suspension solution of particles, cells, or macromolecules that can convert chemical energy into mechanical work by generating stress in the micro scale. In this case, these systems show unusual rheological characteristics [2,3]. The elasticity of polymer solution has been shown to enhance the speed of bacteria motion. In addition to viscoelastic effects, the effect of shear-thinning behavior has also been proposed to explain the speed increase of flagellated bacteria swimming in polymer solutions [4]. In this study, we investigated the effect of the concentration of bacteria in the polymer solution.

Experimental

In the active fluid used here, bacteria are still motile but do not divide. The cell we used in the experiments was *E. coli*, which was cultured overnight at 25 °C in LB medium shaken at 240 rpm. After washing the bacteria suspension two times by centrifuging at 6000 rpm for 10 min, the suspending fluid (or solvent) is prepared by dissolving the polyvinylpyrrolidone 360 k polymer (PVP-K90). The cell was resuspended into a motility medium containing 10 mM potassium phosphate, 0.1 mM K-EDTA, 34 mM K-acetate, 20 mM sodium lactate, and 2 g (PVP-K90) [5]. The viscosity measurements were performed using a rheometer (MCR 502, Anton Paar), in a bob and cup Couette geometry at 25 °C (for best motility of *E. coli*). The inner bob (radius $R_i=13.332$ mm, length 40.002 mm, and underside cone angle 120°) is suspended by a torsion wire into a cup (inner radius $R_c=14.455$ mm). The cup rotates at an angular rate Ω , controlled by a computer. We probe the effect of different bacteria concentrations on the rheological properties of the polymer solution.

Results and Discussion

Our rheometer experiments demonstrate the striking influence of bacteria swimming on the effective viscosity of the suspension. In Fig. 1, we plot the relative viscosity as a function of the shear rate for different bacterial concentrations. Fig. 2 shows relative viscosity as a function of bacteria concentration at different low shear rates. For higher bacterial concentrations, and at the lowest applied shear rate, a net effective viscosity reduction is observed.

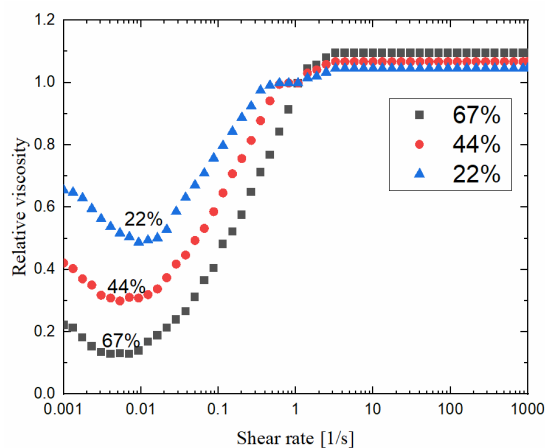


Fig. 1. Relative viscosity as a function of shear rate (square $\phi=67\%$, circle $\phi=44\%$, and triangle $\phi=22\%$).

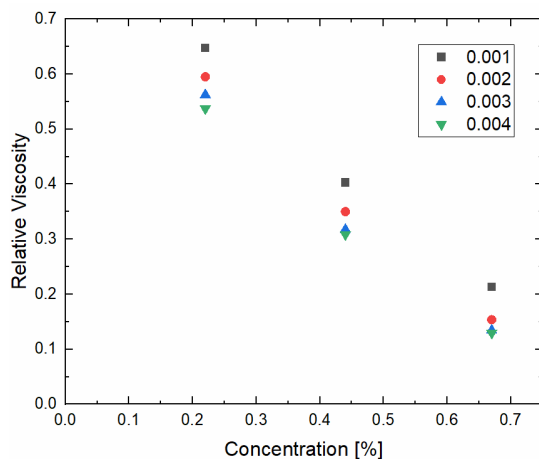


Fig. 2. Viscosity as a function of the bacteria concentration for different low shear rates.

This drop in effective viscosity increases with an increase in bacterial concentration in the fluid. At high shear rates, bacterial activity of the *E. coli* in the suspension are still active, as pushers, they are making the superfluidic regime possible. Microorganisms such as bacteria induced mechanical swimmers becomes negligible, and the bacteria behave as passive rods in suspension. As long as the energy into suspending fluids during their motion. A suspension of such active particles shows complex dynamic behavior according to applied shear. The reduced viscosity is due to the force exerted by the swimming mechanisms of the active agents such as bacteria. As a result, the presence of bacteria has changed the behavior of the solution. At higher shear rate, the suspension reaches a maximum viscosity, because it reduces the activity of bacteria and shows the effect of increasing viscosity on the suspension instead of reducing it.

Conclusion

In conclusion, our experiments show that the bacterial

activity has a measurable influence on shear viscosity. In the current research, PVP solutions were used to investigate the rheological behavior of different concentrations of bacteria. We brought direct experimental evidence, at low shear rates, for an active viscous plateau whose value decreases with concentration and at higher shear rates increases. Other applications of this kind of research represent the importance of the role of rheology in analyzing the behavior of other bioactive particles.

Acknowledgement

This work was financially supported by grants from Tarbiat Modares University. We also thank Dr. Khoshbakhti as the operator of the rheometer.

References

- [1] D. Kim, Y. Kim, and S. Lim, *Phys. Fluid.*, **34**, 2022.
- [2] M.J. Bowick, N. Fakhri, M.C. Marchetti, and S. Ramaswamy, *Phys. Rev. X*, **12**, 10501, 2022.
- [3] J.Y.Y Chui, C. Douarche, H. Auradou, and R. Juanes, *Soft Matter*, **17**, 7004-7013, 2021.
- [4] A. Zöttl and J.M. Yeomans, *Nat. Phys.*, **15**.
- [5] H.M. López, J. Gachelin, C. Douarche, H. Auradou, and E. Clément., *Phys. Rev. Lett.*, **115**, 1-5, 2015

Investigating the Impact of Carbon Nanoparticles Hybrid Incorporation on the Structure of Acrylamide-Based Double Network Hydrogels

Asal Mirmohamadali, Hossein Nazokdast*, and Fatemeh Goharpey

Polymer Engineering Department, Amirkabir University of Technology, P.O. Box, 15875-4413, Tehran, Iran

*nazdast@aut.ac.ir

Abstract

Nowadays, strain sensors are considered as vital devices in different sizes and sensitivities due to their many applications in industry, medicine, robotics, electronics, automotive and other fields. These sensors, with the help of polymeric materials reinforced with nanoparticles, including carbon nanotube-graphene oxide hybrid, have brought a significant improvement in the properties and measurement accuracy. This study investigated mechanical and rheological enhancement of double network hydrogels via graphene oxide and carbon nanotube hybrid nanoparticles. The nanocomposites showed increased tensile moduli and elasticity over 1500%. The 2:1 hybrid (GO: CNT) exhibited optimal performance, with tensile modulus rising to 95 kPa and elasticity reaching 3000% strain. Improvements stemmed from synergistic interactions between well-dispersed nanoparticles and the polymer matrix. This reinforcement strategy holds potential for augmenting mechanical properties of double network hydrogels for diverse applications.

Keywords: electronic skin, hydrogel, self-healing, nanocomposite

Introduction

Adding nanoparticles to the structure of sensor polymers improves their mechanical, electrical and sensitivity properties and can create sensors with specific and more accurate applications. Also, new polymer combinations of additives and different nanoparticles allow researchers to design and manufacture sensors with unique characteristics and optimal performance and use them in many fields of application [1,2].

Due to the importance of strain sensors and the increasing interest in using hydrogels reinforced with nanoparticles, the current research was carried out with the aim of improving the performance of strain sensors and improving their measurement accuracy. In this research, firstly, the synthesis and preparation of polyacrylamide/agar hydrogel with double network structure has been discussed. Then, the effect of carbon nanotube-graphene oxide hybrid as a reinforcing nanoparticle in increasing the mechanical strength and sensitivity of strain sensors has been investigated.

Experimental

Chemicals and Materials

Acrylamide (AAm, $\geq 99\%$), N,N'-methylenebisacrylamide (MBAA, 99%, cross-linker) and sodium dodecyl sulfate (SDS, surfactant) were purchased from Sigma-Aldrich and used as received. Carbon nanotube (CNT, 90%, diameter 9.5 nm and length 1.5 μm) and graphene oxide (GO, particle size 1-5 μm) were purchased from Nanocyl (Belgium) and Borhan Nano Scale Innovators Knowledge-Based Co. respectively. Potassium persulfate (KPS, $\geq 99\%$,

thermal initiator) and Agar (Am, $\geq 99\%$) were purchased from Sigma-Aldrich (Germany).

Synthesis of Nanocomposite Double Network Hydrogels

Synthesis of polyacrylamide/agar/carbon nanotube and graphene oxide hybrid nanocomposite hydrogel was done in two steps. First, a solution of water and surfactant was prepared for dispersion of nanoparticles, then CNT particles and graphene oxide were added to the solution and placed in an ultrasonic bath for dispersion. After complete dispersion, acrylamide, agar and chemical binding agent were added and the suspension was degassed under nitrogen gas for 30 min. In the next step, the temperature of the reactor was gradually increased to 90 °C by an oil bath and was stirred for one hour at medium speed by a magnetic stirrer. Then the reactor temperature was reduced to 60° and a certain amount of KPS initiator was added. After mixing, the contents of the reactor were quickly transferred into the molds. In order to form a physical network of agar, molds were placed at 4 °C for 30 min. Finally, the molds were kept in the oven at a temperature of 60 °C for 7 h to form a chemical network. In order to prepare acrylamide/agar, acrylamide/agar/carbon nanotube and acrylamide/agar/graphene oxide hydrogels, soluble components were added to water, CNT suspension, and graphene oxide suspension, respectively.

Mechanical Measurements

In order to measure the strength and elasticity of the synthesized hydrogels, they were subjected to mechanical tensile tests. In this way, rectangular samples with relative

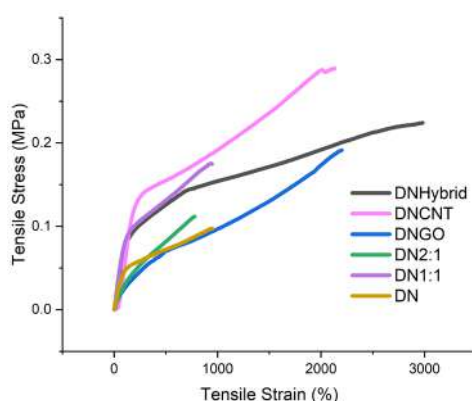


Fig. 1. Stress-strain curve under uniaxial tension for polyacrylamide-agar hydrogels and the resulting nanocomposites.

lengths of $30 \times 5 \times 2.5 \text{ mm}^3$ were prepared. In this test, the tensile speed of the upper clamp 100 mm/min was kept constant.

Rheological Tests

The rheological behavior and viscoelastic properties of the investigated samples were studied using a dynamic rheometer (RMS) manufactured by the Paar Physica USD 200, Austria company. The amplitude sweep test was performed in the strain range of 0.001-1000%, with a constant frequency of 1 rad/s at four temperatures of 35, 50, 70, and 90°.

Results and Discussion

Mechanical Behavior

As shown in Fig. 1 The double network hydrogel with medium modulus and 1000% elasticity demonstrated remarkable performance. Adding 1% graphene oxide and carbon nanotubes by weight significantly increased the modulus and elasticity of both hydrogels. In the nanocomposites, strong hydrogen and van der Waals bonds between the nanoparticles and polyacrylamide/agar chains increased elasticity and durability. Investigating hybrids with nanoparticle ratios of 1:2, 1:1, and 2:1 showed the 2:1 ratio hybrid had lower modulus and elasticity than the

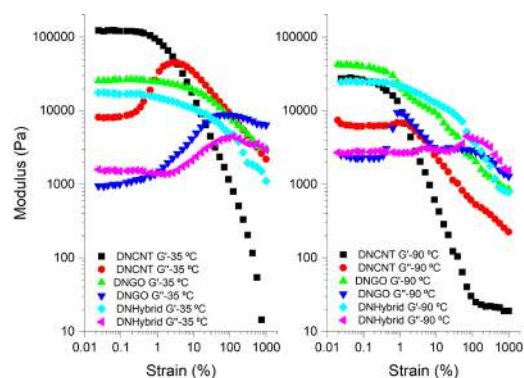


Fig. 2. G' (solid symbols) and G'' (open symbols) during strain sweep at (a) 30 °C and (b) 90 °C.

equal ratio hybrid. This may be due to carbon nanotube accumulation reducing uniform contact with graphene oxide, stressing accumulation centers and causing sample failure [3]. The hybrid with more graphene oxide showed excellent results, nearly doubling the modulus versus pure graphene oxide sample. The appropriate nanoparticle ratio and compatible interactions increased elasticity up to 3052% strain through hydrogen bonds between the nanoparticle network and consistent, uniform connections to the agar physical network. This sample was selected for further characterization.

Rheological Properties

Concerning the strain sweep tests (Fig. 2), the linear viscoelastic regime, in which the moduli are not dependent on the strain, is clearly observed for all the hydrogels. For carbon nanotube (DNCNT) and graphene oxide nanocomposite (DNGO) samples at low strains at both temperatures of 35 and 90 °C, the loss modulus (G'') is always lower than the storage modulus (G'), indicating quasi-solid behavior, this difference is also seen in the hybrid sample. In all three samples, increasing the temperature results in a decrease in the G'' peak, which is due to the increased contribution of the agar network in withstanding stress. Also, the G'' overshoot arises from energy dissipation during chain and bond rearrangements and network disruption from bond opening [4]. After the peak, network degradation and crosslink fracture begin, and the G' value shows a sharp drop, becoming smaller than G'' at a specific strain, indicating destruction and liquid-like behavior of the hydrogel. The critical strain is defined as the crossover point of G' and G'' . It measures the maximum shear strain a hydrogel can withstand, an important parameter to consider for different engineering and biomedical applications.

Conclusion

In summary, the hybrid with a higher proportion of graphene oxide showed excellent results. The optimized nanoparticle ratio and compatible interactions yielded outstanding elasticity exceeding 3000% strain, attributed to hydrogen bonding between the nanoparticle network and uniform connections to the physical agar network. Overall, this work demonstrates the potential of hybrid nanoparticle reinforcement to substantially augment the mechanical performance of double network hydrogels for diverse applications.

References

- [1] C. Cui, Q. Fu, L. Meng, S. Hao, R. Dai, and J. Yang, *ACS Appl. Bio Mater.*, **85**, 121.
- [2] M. Liu, Z. Fan, T. Zuo, and Z. Zhu, *Adv. Fiber Mater.*, **4**, 361-389, 2022.
- [3] K. Pan, S. Peng, Y. Chu et al., *J. Polym Sci.*, 1–13. 2020.
- [4] S. Tarashi, H. Nazockdast, and G. Sodeifian, *Polymer*, **188**, 122138, 2019.

Polyacrylamide/Agar Double Network Hydrogels Reinforced with Nanoparticles

Asal Mirmohamadali, Hossein Nazokdast*, and Fatemeh Goharpey

Polymer Engineering Department, Amirkabir University of Technology, P.O. Box 15875-4413, Tehran, Iran

*nazdast@aut.ac.ir

Abstract

This work investigated the mechanical enhancement of double network hydrogels using graphene oxide and carbon nanotube nanoparticles. Incorporating graphene oxide or carbon nanotubes individually increased the modulus and elasticity by generating additional hydrogen bonding and network interactions. The carbon nanotube nanocomposite displayed the highest modulus of 83 kPa owing to strong restricted network dissociation. Rheological characterization revealed all hydrogels demonstrated a quasi-solid behavior at low strains with storage modulus exceeding loss modulus. At higher strains, sharp declines in storage modulus marked the onset of gel decomposition. A decrease in loss modulus with increasing temperature highlighted the role of the agar physical network. Overall, strategic integration of nanoparticles significantly augmented the mechanical performance of double network hydrogels, enabling tunable properties for diverse applications in biomedicine, soft robotics, and flexible electronics.

Keywords: electronic skin, hydrogel, rheology, nanocomposite

Introduction

Multifunctional smart materials capable of self-healing and shape memory have recently attracted significant interest. Self-healing hydrogels are particularly promising soft materials that can maintain and restore integrated network structure and mechanical performance after damage. This has created great potential for applications in electronic skin, wearable devices, and biomedicine. A variety of reversible covalent bonds non-covalent interactions have been widely utilized to prepare self-healing hydrogels. These chemistries allow hydrogels to reversibly reconnect crosslinks and regenerate after mechanical disruption. Overall, the development of self-healing hydrogels holds promise for realizing resilient, damage-tolerant soft materials across diverse fields [1]. The goal of this study was to mechanically characterize Agar- Acrylamide nanocomposite hydrogels and to provide a reliable rheological protocol for sol-gel transition. The contribution of each biopolymer to the gel's mechanical properties was investigated.

Experimental

Chemicals and Materials

Acrylamide (AAm, $\geq 99\%$), N,N'-methylenebisacrylamide (MBAA, 99%, cross-linker) and sodium dodecyl sulfate (SDS, surfactant) were purchased from Sigma-Aldrich and used as received. Carbon nanotube (CNT, 90%, diameter 9.5 nm and length 1.5 μm) and graphene oxide (GO, particle size 1-5 μm) were purchased from NANOCYL (Belgium) and Borhan Nano Scale Innovators Knowledge-Based Co. respectively. Potassium persulfate (KPS, $\geq 99\%$, thermal initiator) and Agar (Am, $\geq 99\%$) were purchased from Sigma-Aldrich (Germany).

Synthesis of Nanocomposite Double Network Hydrogels

Synthesis of polyacrylamide/agar/carbon nanotube and graphene oxide nanocomposite hydrogel was done in two steps. First, In order to prepare acrylamide/agar, acrylamide/agar/carbon nanotube and acrylamide/agar/graphene oxide hydrogels, soluble components were added to water, CNT suspension, and graphene oxide suspension, respectively and placed in an ultrasonic bath for dispersion. After complete dispersion, acrylamide, agar and chemical binding agent were added and the suspension was degassed under nitrogen gas for 30 min. In the next step, the temperature of the reactor was gradually increased to 90 °C by an oil bath and was stirred for one hour at medium speed. Then the reactor temperature was reduced to 60° and a certain amount of KPS initiator was added. After mixing, the contents of the reactor were quickly transferred into the molds. In order to form a physical network of agar, molds were placed at 4 °C for 30 min. Finally, the molds were kept in the oven at a temperature of 60 °C for 7 h to form a chemical network.

Mechanical Measurements

In order to measure the strength and elasticity of the synthesized hydrogels, they were subjected to mechanical tensile tests. In this way, rectangular samples with relative lengths of 30*5*2.5 mm³ were prepared. In this test, the tensile speed of the upper clamp 100 mm/min was kept constant.

Rheological Tests

The rheological behavior and viscoelastic properties of the investigated samples were studied using a dynamic

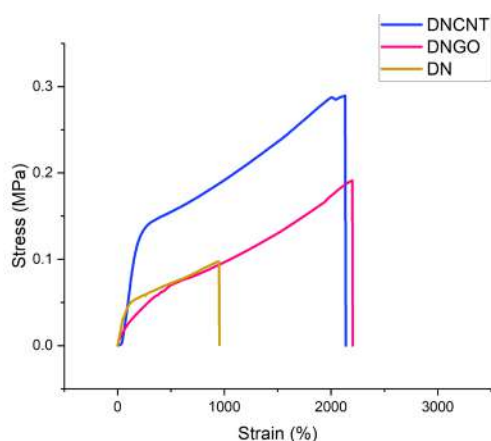


Fig. 1. Stress-strain curve under uniaxial tension for polyacrylamide-agar hydrogels and the resulting nanocomposites.

rhometer (RMS) manufactured by the Paar Physica USD 200, Austria company. The amplitude sweep test was performed in the strain range of 0.001%-1000%, with a constant frequency of 1 rad/s at four temperatures of 35, 50, 70, and 90°.

Results and Discussion

Mechanical Behavior

Consistent with previous studies [2,3], the present results demonstrate that nanoparticle incorporation enhances the mechanical performance of the material, as evidenced by the data in Fig. 1. All the hydrogels exhibited elastomeric behavior with a yield zone and strain hardening at high stretches. The high modulus and yielding behavior stem from strong nanoparticle-network bonding and agar double helices, respectively. The acrylamide/agar double network hydrogel (DN) had a modulus of 69 kPa, indicating acceptable strength comparable to literature. Beyond the yield point, the acrylamide dissipative network ruptured and load transferred to the physical agar network. With further loading, the agar double helices unraveled into aligned chains until sample failure at 97 kPa and 950% strain. The elongated yield region for graphene oxide nanocomposite (DNGO) suggests an additional GO physical network interacting with agar chains. At 191 kPa and 2200% strain, the physical network failed. The carbon nanotube hydrogel (DNCNT) exhibited the highest modulus (83 kPa) and strength, owing to restricted chemical network dissociation from nanotube-acrylamide hydrogen and ionic bonding. Its behavior mirrored the DNGO sample, except for a higher modulus attributed to stronger hydrogen bonding between nanotubes and acrylamide. At 289 kPa and 2134% strain, this sample failed.

Rheological Properties

Fig. 2 illustrates the strain sweep test results for nanocomposite hydrogels at two different temperatures. For the DNCNT and DNGO samples, at low strain values and temperatures of 35 and 90 °C, the loss modulus (G'') remained lower than the storage modulus (G'), indicating

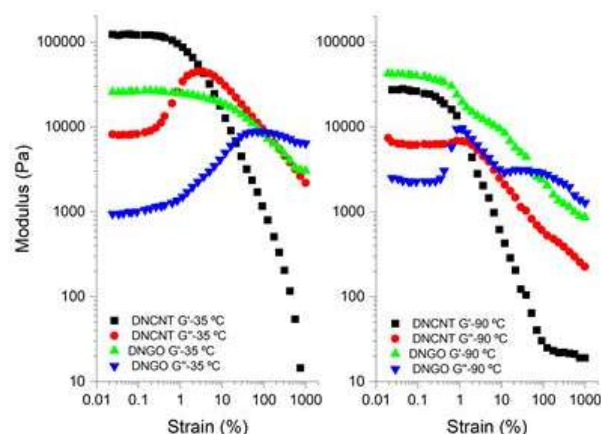


Fig. 2. G' and G'' during strain at: (a) 35 °C and (b) 90 °C NCDN hydrogels.

quasi-solid behavior and confirming the gel-like nature of the hydrogels. As strain increased, a sharp rise in G'' and decrease in G' occurred, signaling the onset of gel decomposition. The intersection of the G' and G'' curves at the critical strain, followed by a precipitous decline in G' relative to G'' , marks the sol-gel transition point. This modulus reduction likely stems from compromised physical structure and molecular unraveling, with loss of intermolecular interactions, in the acrylamide network [4]. The data also reveals that at higher temperatures, a decrease in G'' overshoot can be seen, probably due to enhanced contribution of the agar physical network.

Conclusion

In summary, the results confirm that incorporating nanoparticles significantly enhances the mechanical performance of double network hydrogels. The hydrogels exhibited elastomeric behavior with a defined yield point. The double network hydrogel showed decent strength while graphene oxide and carbon nanotubes generated additional interactions, increasing elasticity and modulus respectively. Rheological tests verified quasi-solid behavior at low strains and gel decomposition at higher strains. Overall, strategic nanoparticle selection and incorporation enables substantial mechanical improvements in double network hydrogels.

References

- [1] B. Fu, B. Cheng, X. Jin, X. Bao, Z. Wang, J. Hu, *O Appl. Polym. Sci.*, 2019.
- [2] K. Pan, S. Peng, Y. Chu et al., *J. Polym. Sci.*, 1-13, 2020.
- [3] P. Zhu, M. Hu, Y. Deng, and C. Wang, *Adv. Eng. Mater.*, **18**, 2016.
- [4] S. Tarashi, H. Nazockdast, and G. Sodeifian, *Polymer*, **188**, 122138, 2020.

Effect of Diol and Diamine Chain Extenders on Chemorheological Behavior of HTPB Based Polyurethane

Mohammad Mohammadi Serajeloo* and Abbas Kebritchi

Chemical Engineering Department, Imam Hossein Comprehensive University, Tehran, Iran

*m.serajelo@ihu.ac.ir

Abstract

In this study polyurethanes samples were made based on hydroxyl-terminated polybutadiene. Ethylene diamine and Ethylene glycol were used as chain extenders in the desired percentage composition. The results of the investigation with viscometer showed that the addition of chain extenders causes significant changes in the chemo-rheological properties and the process of increasing the viscosity of the polymer binder system and increasing the amount of chain extender to the percentage different composition causes the rapid growth of the reaction. By increase in the concentration of chain extender there was a rapid increase in the viscosity of the formed polyurethane. This was more noticeable and faster for diamine chain extender than diol.

Keywords: HTPB, TDI, chemorheology, chain extender

Introduction

Polyurethanes are a group of Engineering Polymers that attract significant attention from both industry and universities. Their range of application ranges from coatings, adhesives, injection molds and elastomeric parts that are used in common daily life to complex biomedical engineering applications [1]. Due to its Biomedical Applications, Building and Construction Applications, automotive, textile and in several other industries due to its superior properties in terms of Hardness, elongation, strength and commutative modulus, PUs have become one of the most common and researched materials in the world [2].

The urethane group is the major repeating unit in PUs, and is produced from the reaction between alcohol ($-OH$) and isocyanate (NCO); albeit PUs also contain other groups, such as ethers, esters, urea and some aromatic compounds [2]. Choosing a suitable diisocyanate and chain extender results in various influences on the final properties of PUs. Mechanical properties of PU elastomers depend strongly on the ratio of hard and soft segments and the structure or length of Chain extenders [3]. Chain extenders are low molecular weight hydroxyl or amine terminated compounds that play an important role in polymer morphology. The choice of chain extender and diisocyanate determines the characteristics of the hard segment and to a large extent the physical properties of polyurethane. The most important chain extenders are linear diols such as ethylene glycol, 1,4-butanediol, 1,6-hexanediol, and hydroquinone bis(2-hydroxyethyl)ether. These diols form well crystallized hard segments with Isocyanates. Diamines react faster with isocyanates and results in the formation of the hard segment with a higher density of secondary bonding, high hard segment T_g , and high thermal stability of the polymer.

Experimental

Polyurethane elastomers were prepared using hydroxyl-terminated Polybutadiene (HTPB) and toluene diisocyanate (TDI). Ethylene glycol and Ethylene DiAmine were used as Chain Extender in percentages (0.5, 1.0, and 1.5 wt%). DBTDL catalyst was used to improve the process of one-shot polyurethane synthesis. The samples were subjected to a viscometric test with a Brookfield viscometer at a constant temperature of 50 °C.

Results and Discussion

Polyurethane samples were tested by Brookfield viscometer and the results of viscosity increase over time were recorded and measured. Viscosity-time graphs provide graphs for the samples, and the blue graphs correspond to the samples containing ethylene diamine chain extender and the red

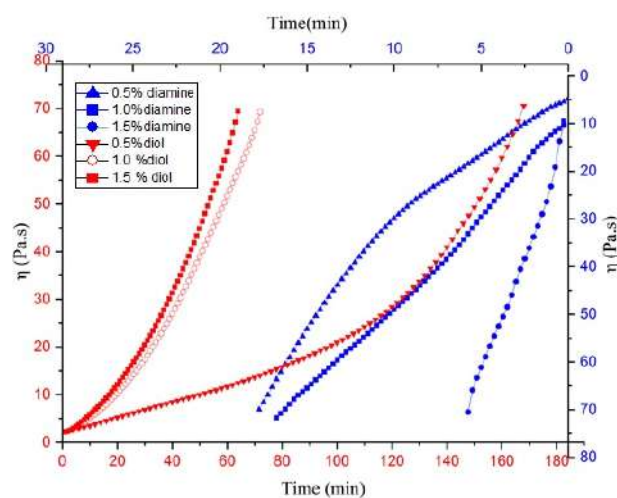


Fig. 1. Viscosity-time plot of polyurethane made with diamine chain extender in three concentration in 50 °C.

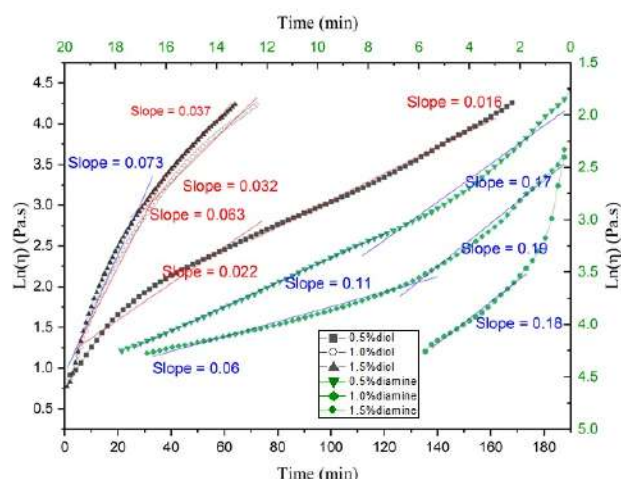


Fig. 2. Ln (Viscosity)- time plot of polyurethane made with diol chain extender in three concentration in 50 °C.

Table I. Equations of the regression lines obtained from the viscosity Ln diagram based on increasing chain in differenPU Based on HTPB/TDI values.

Sample	Regression line	Ethylene glycol (w%)	Ethylene diamine (wt%)
1	$\eta = 1.42 + 0.016t$ $\eta = 1.14 + 0.022t$	0.5	-
2	$\eta = 1.97 + 0.032t$ $\eta = 0.96 + 0.063t$	1.0	-
3	$\eta = 1.92 + 0.037t$ $\eta = 0.92 + 0.073t$	1.5	-
4	$\eta = 1.92 + 0.17t$ $\eta = 0.92 + 0.11t$	-	0.5
5	$\eta = 2.41 + 0.19t$ $\eta = 3.62 + 0.06t$	-	1.0
6	$\eta = 3.62 + 0.06t$	-	1.5

graphs in Fig. 1 indicate the sample containing ethylene glycol extender chain. Due to the same length of the carbon chain, the difference in the reactivity of the increasing chain can be seen in the diagram. Diamine chain extender has a high viscosity increase rate. And it caused the growth of the polymer chain and the formation of urea bonds, which caused the growth of the polymer chain and the increase of the molecular weight and finally the increase of the viscosity of the polymer. Fig. 1 shows the viscosity-time plot of polyurethane that used ethylene diAmine Chain extender in three different amount of chain extenders.

Fig. 2 shows the obtained results of Ln viscosity-time according to our samples. By drawing regression lines for these graphs and finding the mean of the lines, we can find the rate constants of the viscosity-time graphs. According to the chemistry of isocyanate, the reaction occurs in 2 general stages. Table I shows the lines obtained from the graphs of Ln viscosity over time. The viscosity of the curing mixture increases with time as the urethane formation advances. The viscosity build up during the cure process can be attributed chiefly to three factors: (i) increase in molecular weight as a result of polymer chain

growth; (ii) chain branching due to the presence of tri- or higher functional moieties present in the prepolymer or in the additives. (iii) The chain extender in the composition helps to connect the polyurethane chains and increase.

Conclusion

The results of this experimental study show that the presence of larger amounts of increasing chains in the polyurethane composition leads to faster growth and connections between chains. The diamine chain extender leads to further increase more to the process of increasing the viscosity.

References

- [1] J.O. Akindoyo, M. Beg, S. Ghazali, M.R. Islam, N. Jeyaratnam, and A.R. Yuvaraj, "Polyurethane types, synthesis and applications—a review", *Rsc Adv.*, **6**, 114453-114482, 2016.
- [2] V. Sekkar et al., "Pot life extension of hydroxyl terminated polybutadiene based solid propellant binder system by tailoring the binder polymer microstructure", *J. Macromol. Sci. Part A*, **54**, 171-175, 2017.
- [3] S. Oprea, "the effect of chain extenders structure on properties of new polyurethane elastomers", *Polym. Bull.*, **65**, 753-766.

Effect of Diol and Diamine Chain Extenders on Chemorheological behavior of HTPB/TDI based Polyurethane

Mohammad Mohammadi Serajehloo* and Abbas Kebritchi

Chemical Engineering Department, Imam Hossein Comprehensive University, Tehran, Iran

*m.serajelo@ihu.ac.ir

Abstract

In this study polyurethanes samples were made based on hydroxyl-terminated polybutadiene. Ethylene diamine and Ethylene glycol were used as chain extenders in the desired percentage composition. The results of the investigation with viscometer showed that the addition of chain extenders causes significant changes in the chemo-rheological properties and the process of increasing the viscosity of the polymer binder system and increasing the amount of chain extender to the percentage different composition causes the rapid growth of the reaction. By increase in the concentration of chain extender there was a rapid increase in the viscosity of the formed polyurethane. This was more noticeable and faster for diamine chain extender than diol.

Keywords: HTPB, TDI, chemorheology, chain extender

Introduction

Polyurethanes are a group of engineering polymers that attract significant attention from both industry and universities. Their range of application ranges from coatings, adhesives, injection molds and elastomeric parts that are used in common daily life to complex biomedical engineering applications [1]. Due to its biomedical applications, building and construction applications, automotive, textile and in several other industries due to its superior properties in terms of hardness, elongation, strength and commutative modulus, PUs have become one of the most common and researched materials in the world [2]. The urethane group is the major repeating unit in PUs, and is produced from the reaction between alcohol ($-OH$) and isocyanate (NCO); albeit PUs also contain other groups, such as ethers, esters, urea and some aromatic compounds [2]. Choosing a suitable diisocyanate and chain Extender results in various influences on the final properties of PUs. Mechanical properties of PU elastomers depend strongly on the ratio of hard and soft segments and the structure or length of chain extenders [3]. Chain extenders are low molecular weight hydroxyl or amine terminated compounds that play an important role in polymer morphology. The choice of chain extender and diisocyanate determines the characteristics of the hard segment and to a large extent the physical properties of polyurethane. The most important chain extenders are linear diols such as ethylene glycol, 1,4-butanediol, 1,6-hexanediol, and hydroquinone bis(2-hydroxyethyl)ether. These diols form well crystallized hard segments with isocyanates. Diamines react faster with isocyanates and results in the formation of the hard segment with a higher density of secondary bonding, high

hard segment T_g , and high thermal stability of the polymer.

Experimental

Polyurethane Elastomers were prepared using hydroxyl-terminated polybutadiene (HTPB) and toluene diisocyanate (TDI). Ethylene glycol and Ethylene diamine were used as Chain Extender in percentages (0.5, 1.0, and 1.5 wt%) DBTDL catalyst was used to improve the process of one-shut polyurethane synthesis. The samples were subjected to a viscometric test with a Brookfield viscometer at a constant temperature of 50 °C.

Results and Discussion

Polyurethane samples were tested by brookfield viscometer and the results of viscosity increase over time were

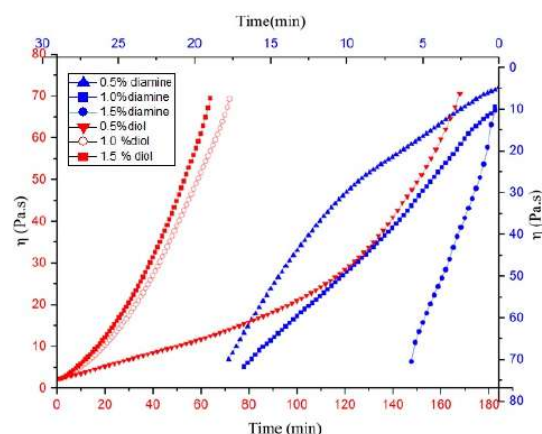


Fig. 1. Viscosity-time plot of polyurethane made with diol and diamine chain extender in three Concentration in 50 °C.

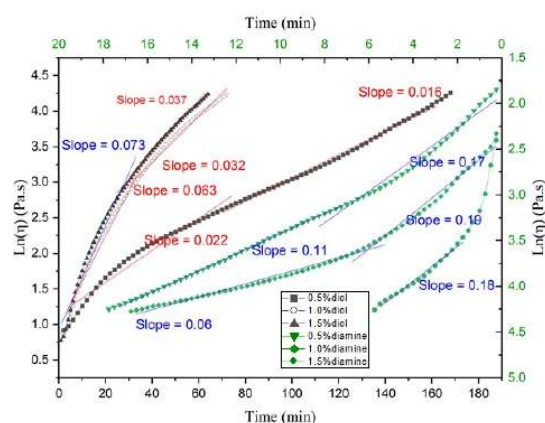


Fig. 2. Ln(Viscosity)-time plot of polyurethane made with diol and diamine chain extender in three concentration in 50 °C.

recorded and measured. Viscosity-time graphs provide graphs for the samples, and the blue graphs correspond to the samples containing ethylene diamine chain extender and the red graphs in Fig. 1 indicate the sample containing ethylene glycol chain extender. Due to the same length of the carbon chain, the difference in the reactivity of the increasing chain can be seen in the diagram. Diamine chain extender has a high viscosity increase rate. And it caused the growth of the polymer chain and the formation of urea bonds, which caused the growth of the polymer chain and the increase of the molecular weight and finally the increase of the viscosity of the polymer. Fig. 1 shows the viscosity-time plot of polyurethane that used ethylene diamine chain extender in three different amount of chain extenders.

Fig. 2 shows the obtained results of Ln(viscosity)-time according to our samples. The green graphs correspond to the samples containing Ethylene diamine chain extender and the black graphs shows Ln(viscosity)-time plots for containing Ethylene Glycol polyurethanes. By drawing regression lines for these graphs and finding the mean of the lines, we can find the rate constants of the viscosity-time graphs. According to the chemistry of isocyanate, the reaction occurs in 2 general stages. Table I shows the lines

Table I. Equations of the regression lines obtained from the Ln(viscosity) diagram based on increasing chain in different PU HTPB/TDI based polyurethane values.

Sample	Regression line	Ethylene glycol	Ethylene diamine
1	$\text{Ln}(\eta) = 1.42 + 0.016t$	0.5	-
	$\text{Ln}(\eta) = 1.14 + 0.022t$		
2	$\text{Ln}(\eta) = 1.97 + 0.032t$	1.0	-
	$\text{Ln}(\eta) = 0.96 + 0.063t$		
3	$\text{Ln}(\eta) = 1.92 + 0.037t$	1.5	-
	$\text{Ln}(\eta) = 0.92 + 0.073t$		
4	$\text{Ln}(\eta) = 1.92 + 0.17t$	-	0.5
	$\text{Ln}(\eta) = 0.92 + 0.11t$		
5	$\text{Ln}(\eta) = 2.41 + 0.19t$	-	1.0
	$\text{Ln}(\eta) = 3.62 + 0.06t$		
6	$\text{Ln}(\eta) = 3.6 + 0.06t$	-	1.5

obtained from the graphs of Ln viscosity over time. The viscosity of the curing mixture increases with time as the urethane formation advances. The viscosity build up during the cure process can be attributed chiefly to three factors: (i) increase in molecular weight as a result of polymer chain growth; (ii) chain branching due to the presence of tri- or higher functional moieties present in the prepolymer or in the additives. (iii) The Chain Extender in the composition helps to connect the polyurethane chains and increase.

Conclusion

The results of this experimental study show that the presence of larger amounts of increasing chains in the polyurethane composition leads very faster growth and connections between chains. The diamine chain extender leads to further increase more to the process of increasing the viscosity.

References

- [1] J.O. Akindoyo, M. Beg, S. Ghazali, M.R. Islam, N. Jeyaratnam, and A.R. Yuvaraj, "Polyurethane types, synthesis and applications—a review", *Rsc Adv.*, **6**, 114453-114482, 2016.
- [2] V. Sekkar, A.S. Alex, V. Kumar, and G.G. Bandyopadhyay, "Pot life extension of hydroxyl terminated polybutadiene based solid propellant binder system by tailoring the binder polymer microstructure", *J. Macromol. Sci. Part A*, **54**, 171-175, 2017.
- [3] S. Oprea, "The effect of chain extenders structure on properties of new polyurethane elastomers", *Polym. Bull.*, **65**, 753-766, 2010.

Increasing Electrorheological Effect of Chitosan by Adding Zinc Oxide and Cellulose Fibers

Parisa Nouralizadeh and Nadereh Golshan Ebrahimi*

Chemical Engineering Faculty, Polymer Engineering Department, Tarbiat Modares University, Tehran, Iran

*ebrahimn@modares.ac.ir

Abstract

Smart fluids exhibit sudden changes in rheological properties, including viscosity and yield stress, in response to external stimuli. Electric field-sensitive fluids (electrorheological fluids) consist of insulating fluid with suspended particles that exchange from liquid to semi-solid states under an electric field. They are nominated for quick reactions, reversibility, and environmental control. Chitosan, with advantages like good dispersion and polarizable functional groups, has been studied for electrorheological use. Electrically conductive additives, e.g., zinc oxide, are examined for enhancing conductivity of mixture while minimizing environmental impact. This study combines cellulose fibers and zinc oxide in chitosan polymer, analyzing raw materials through FTIR and investigating the resulting of electrorheological behavior in edible oil.

Keywords: electrorheological fluids, chitosan, zinc oxide, rheological properties

Introduction

In recent decades, stimuli-responsive materials, have received much attention in the field of science and technology due to their extraordinary properties. These materials are named smart materials because they have the ability to reversibly change their properties under the influence of external stimuli such as temperature, electric field, mechanical and magnetic fields [1]. One of the most important smart materials are electrorheological fluids (ERFs), which are suspensions of micron-size, electrically polarizable particles in a nonconductive fluid and they form fibrillar structures under applied electric fields [1]. The rheological properties of ERFs such as viscosity and yield stress, are reversibly adjustable by an applied electric field [2]. In general, ERFs consist of three main components: continuous phase, dispersed phase and additives. The most effective part is filler or the dispersed phase. Polysaccharides are biodegradable and biocompatible polymer fillers. These materials play an important role in the polarization of particles due to their polar groups and lead to electrorheology effect under an electric field. Chitosan has both OH and NH₂ polar groups, therefore electrorheological fluids with chitosan show higher yield stress compared to other polysaccharides [3]. According to research on electrorheological materials, presence of cellulose as an additive can increase the mechanical strength of ERFs in industrial applications. Zinc oxide is also used in order to create a large band gap (which leads to higher breakdown voltage). In order to be able to use the electrorheological fluid in the industry, its conductivity, yield stress and modulus should be optimized and can be used in the long term [3]. In this research, the continuous

phase of edible oil and the dispersed phase of chitosan were used. Also, to improve the electrorheological properties, a metal oxide with conductive properties and cellulose fibers with high strength and good dispersion properties were added to the mixture.

Theoretical

The general process of the ER effect is as follows: ER particles are polarized under the action of an external electric field, forming a dipole phenomenon. Particles with a dipole moment produce a directional arrangement, which changes the particles from a disordered state to an ordered state, forming a chain or column structure and thereby presenting an external ER effect. At present, most scientific researchers believe that the polarization of particles is the main cause of ER effects. Polarization is caused by mechanisms such as surface polarization, which is considered the main factor of ER behavior under DC or AC fields. The static yield stress, τ_y , as a function of the electric field strength, E is as follows:

$$\tau_y \propto E^a \quad (1)$$

The power value a , for chitosan is 1.47 [3]. According to the experimental observations and the approximate calculation of the dielectric coefficient of the mixture, the value of a is expected to increase approximately between 0.4 to 0.6. This means that by applying a smaller amount of external stimulus, a higher yield stress will be achieved.

Experimental

In order to prepare ERFs, chitosan, zinc oxide, and

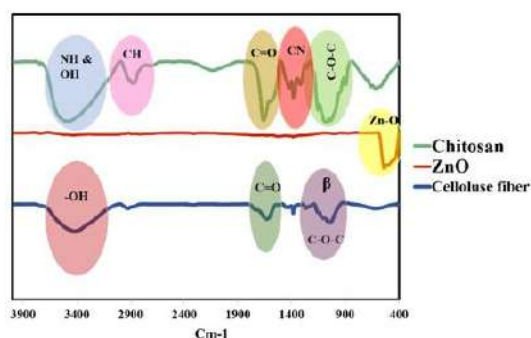


Fig. 1. FT-IR spectra of samples.

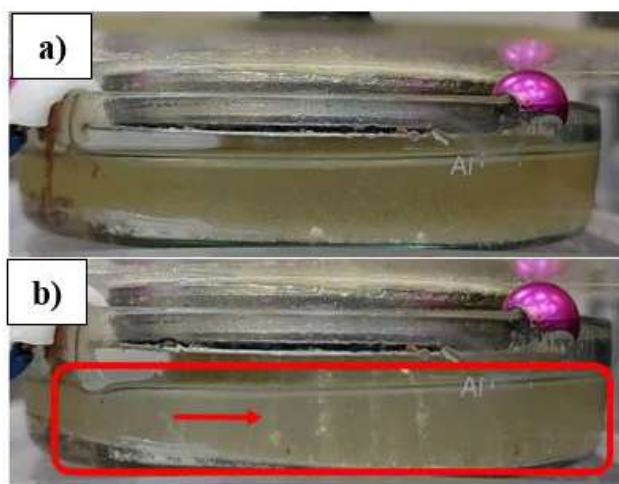


Fig. 2. Chitosan: (a) under 2 kV and (b) under 8 kV DC electric field.

cellulose fibers were mixed together and edible oil was added to them as a continuous phase and mixed by an ultrasonic bath machine. At first, FTIR analysis was done to ensure the accuracy of the raw materials, and then ERF was prepared to check the electrorheological properties.

Results and Discussion

According to Fig. 1, FTIR analysis of chitosan, zinc oxide, and cellulose fiber samples as seen, the important peaks in the samples have been fully analyzed in the figure. In order to investigate and justify the ER phenomenon, a rotational rheometer with an external electric field is needed, and the existing device is in the preparation process. Next, in order to experimentally investigate the effect of adding zinc oxide and cellulose fibers to the electrorheological mixture of chitosan in oil, a simulation experiment was carried out. According to Figs. 2 and 3, a stronger electrorheology effect was observed by adding two materials in a lower electric field. According to Fig. 2, increasing the electric field from 2 kV to 8 kV, resulted in thin fibers of chitosan particles by applied external electric field. Also as Fig. 3 illustrates, in spite of the imposing external field, spanning from 2 kV to 5 kV, which has a lower range, the fibers demonstrated stronger and thicker in shape.

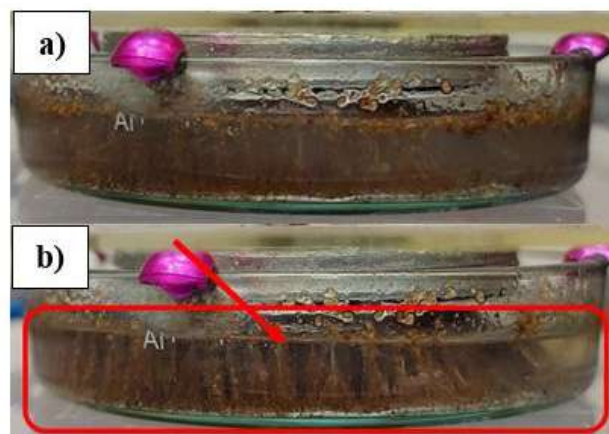


Fig. 3. Chitosan, zinc oxide and cellulose fibers: (a) under 2 kV and (b) under 5 kV DC electric field.

Conclusion

ERFs are a class of smart fluids that are prepared from three components: continuous phase, dispersed phase, and additive. Additives used in ERFs will affect the final electrorheological properties of ERFs. In this work, chitosan polymer material and additives of cellulose fibers and zinc oxide have been used in order to increase the yield stress and stability in ERFs.

References

- [1] N. Kuznetsov, V. Kovaleva, S. Belousov, and S. Chvalun, "Electrorheological fluids: from historical retrospective to recent trends", *Mater. Today Chem.*, **26**, 101066, 2022.
- [2] Y. Liang et al., "Efficient electrorheological technology for materials, energy, and mechanical engineering: From mechanisms to applications", *Engineering*, 2022.
- [3] J.H. Sung and H.J. Choi, "Biocompatible Polysaccharide-Based electrorheological Suspensions", *J. Macromol. Sci. Part B: Phys.*, **44**, 573-581, 2005.

A Theoretical Novel Procedure to Predict the Microstructure of a Polymeric Nanocomposite by Mutual Rheological and Dielectric Measurements

Sara Radmehr*, Faezeh Tajmahi, and Mohammad Hossein Navid Famili

Polymer Engineering Department, Chemical Engineering Faculty, Tarbiat Modares University, Tehran, Iran

*sara.rdmehr@gmail.com

Abstract

Composite materials property is highly dependent to the property of matrix and filler as well as the morphology of the mixture. Therefore, it is essential to have a quantitative description of the morphology of a composite. Moreover, highly-filled nanocomposites are more susceptible to forming aggregates because of the high surface to volume ratio of nanoparticles, making it more of a necessity to know the particle distribution. Herein, a new technique is introduced to enable us to have a more reliable understanding of a nanocomposite microstructure. For this purpose, simultaneous rheological and dielectric experiments are conducted and by combining experimental data with theoretical models we are able to predict aggregate size distribution and compactness of aggregates.

Keywords: structure/property relationship, parallel plate rotational rheometer, fourier transform rheology (FTR), dielectric spectroscopy, aggregate size distribution

Introduction

Polymeric composites are vastly used in special applications in industry due to their versatile functionality. The final property of polymeric composites significantly depends on the property of its components (polymer matrix and filler) as well as the morphology of the mixture (matrix-filler and filler-filler interactions). This makes it crucial to have a precise quantitative characterization of the morphology in order to attain a desirable function from a composite material [1]. In addition, determining and hopefully controlling the morphology of nanocomposites with high particle content has become more challenging due to high surface to volume ratio of nanoparticles. This results in more aggregation in the mixture and makes it more difficult to have a definite understanding of particle dispersion and aggregate size distribution (ASD) [2].

The morphology of composites has been studied by various methods so far, which are divided into two microscopic methods (such as optical and electron microscopy, laser backscattering, focused-beam reflectance measurement, etc.) and through macroscopic properties (rheological and dielectric properties) investigation. However, the main problem with microscopic methods is the generalization of the microstructure of a very small part of the sample to the whole sample. The macroscopic properties such as rheological, electrical and dielectric properties are a reflection of the internal structure and studying them has also brought a lot of information about the microstructure of a blend. A model for effective permittivity of a nanocomposite has been suggested first by

Maxwell-Garnett equation and then modified by Golbang to take particle interactions into account [3]. In another rheological study, an estimation of droplet size distribution is proposed by taking the Fourier transform of the total oscillatory shear stress values, calculating the statistical parameters and assuming the Gaussian distribution of the droplets [4]. Here, a new model is introduced in order to obtain a more reliable estimation of ASD and its compactness in a nanocomposite with the help of combining long amplitude oscillatory shear tests (LAOS) with dielectric spectroscopy.

Experimental/Theoretical

First, according to the size of the filler particles we assume a radius range for spherical aggregates:

$$\sigma(R \nabla \omega) = \mu_m (\nabla V + \nabla V^T) -$$

$$\Gamma \sum_{i=1}^{\text{types of aggregates}} \frac{\phi_{fi}}{L_{ci}} \left(\frac{K}{trK} - \frac{1}{3} \delta \right) \quad (1)$$

Then, from Eq. (1) we calculate the total stress tensor of the system resulting from all spherical aggregates, which is a modification of total stress of the system obtained by Batchelor [5]. Here μ_m is the viscosity of the matrix, ∇V is velocity gradient tensor of the flow, Γ is interfacial tension, ϕ_{fi} is aggregate volume fraction, L_{ci} is the characteristic length of each aggregate and K is the area tensor for spherical inclusions [6]. Next, we take Fourier Transform from each component of the stress tensor to get the third, fifth and seventh harmonic values for each aggregate which are related to the contribution of the drop [4]:

$$\sigma(R \square t) = \sum_{\substack{j=-\infty \\ \text{odd}}}^{\infty} I(j\omega_1) \exp(ij\omega_1 t) \quad (2)$$

$$= \sum_{\substack{j=1 \\ \text{odd}}}^{\infty} I_R(j\omega_1) \cos(j\omega_1 t) + I_I(j\omega_1) \sin(j\omega_1 t)$$

$$I_{k \square exp} = \sum b_i I(k\omega \square R_i) \quad (3)$$

In Eq. (2), i is the imaginary unit, $I_R(j\omega_1)$ and $I_I(j\omega_1)$ are, respectively, the real and imaginary part of $I(j\omega_1)$, the (complex) coefficient of the j th harmonic in the Fourier domain. The ASD can be calculated then with the help of rheometry test data in various shear rates by using Eq. (3):

$$\epsilon_{eff} = \epsilon_m + \frac{\sum_{i=1}^{\text{types of inclusions}} 3\epsilon_m \phi_f \frac{\epsilon_f - \epsilon_m}{\epsilon_f + 2\epsilon_m}}{1 - \sum_{i=1}^{\text{types of inclusions}} (A + \phi_f) \frac{\epsilon_f - \epsilon_m}{\epsilon_f + 2\epsilon_m}} \quad (4)$$

A new model for predicting effective permittivity is also developed from Golbang's equation for spherical aggregate with different radii (Eq. (4)). Here, ϵ_m is the permittivity of matrix, ϵ_f is the permittivity of filler, and A is geometrical factor showing particle-particle interaction [3] which is obtained by $A = \sum_{i=1}^n v \frac{3\cos^2\theta_i - 1}{4\pi r_i^3}$. Aggregate volume fraction is $\phi_f = n_i 4\pi R_i^3$, n_i being the aggregate size distribution. The permittivity of each aggregate can be calculated with Eq. (4). Then, the volume fraction of particles in aggregate (aggregate compactness) can be estimated by sufficient rheo-dielectric experiment data.

Results and Discussion

Simulation results of our new theory to predict the effective permittivity beside Golbang's and Maxwell-Garnett equations are depicted in Fig. 1. Maxwell-Garnett model has a good prediction only for low volume fraction of particles because the interaction between the particles is not included. In the Golbang model, it is assumed that all the aggregates have the same size and different aggregate sizes effect is not seen in it. Overall, all three models have a good match in the low volume fraction of particles, but with increasing the volume fraction the difference between increases and the new model has higher values for the

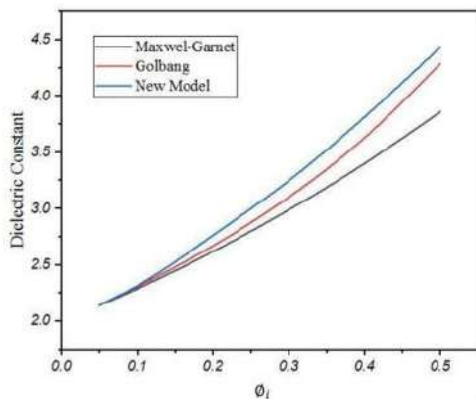


Fig. 1. Dielectric coefficient predicted by different models.

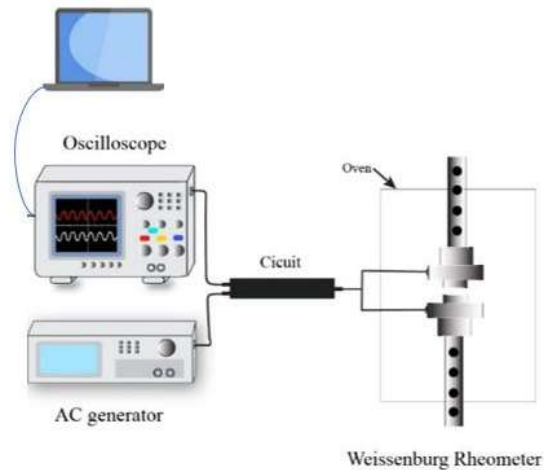


Fig. 2. Setup of the combination of a rheometer and a dielectric analyzer.

dielectric constant. The schematic depiction of rheo-dielectric setup is shown in Fig. 2. As it can be seen, in this experiment a LAOS test is conducted on the polymeric nanocomposite by rotational rheometer with parallel plate geometry (Weissenburg rheometer). Simultaneously, an AC current is applied to upper and lower plates of the rheometer (playing the role of capacitor plates) by wires, and the data goes back to oscilloscope and is transferred to MATLAB software to calculate dielectric constant.

Conclusion

Here, the rheo-dielectric technique is presented to attain a quantitative description of a nanocomposite morphology, which is aggregate size distribution and its compactness. By use of this technique we can hopefully predict the microstructure, resulting in a controlled functionality of composite materials.

References

- [1] M. Slouf, *Morphological Analysis of polymer Systems with Broad Particle Size Distribution*, Elsevier, 2015.
- [2] L. Brivadis, "New inversion methods for the single/multi-shape CLD-to-PSD problem with spheroidal particles", 2022.
- [3] A. Golbang, "Relationship between electromagnetic and rheological properties for the evaluation of nanostructure formation in a polymeric system", *Tarbiat Modares University, Doctoral Thesis*, 2017.
- [4] P.L.M. Massimiliano Grosso, "A new methodology for the estimation of drop size distributions of dilute polymer blends based on LAOS flows", 2007.
- [5] Batchelor, "The stress system in a suspension of force-free particles", *Fluid Mech*, 1970.
- [6] Wetzel and Tucker, "Area tensors for modeling microstructure during laminar liquid-liquid mixing", 1998.

Effect of CNTs Nanoparticles on Rheology and Morphology of PLA/POE Blend

Shima Abbasi and Jafar Khademzadeh Yeganeh*

Department of Polymer Engineering, Qom University of Technology, Qom, Iran

*khademzadeh@qut.ac.ir

Abstract

In this article, the effect of ethylene-octene copolymer as a polyolefin elastomer (POE) on the rheological and morphological properties of polylactic acid (PLA) in the presence of carbon nanotubes (CNTs) has been investigated. For this purpose, PLA/POE blend was prepared with the composition of 75/25 in the presence of different amounts of nanoparticles (0/25%- 0/5%- 1%). The addition of carbon nanoparticles causes better compatibility, reduction of droplet size and improvement of surface adhesion between phases. It was also observed in the TEM images that the nanoparticles were mainly placed in the PLA matrix. The effect of nanoparticles on the microstructural properties of the sample was investigated through rheological evaluations.

Keywords: polylactic acid, ethylene octane copolymer, nanotube, compatibility, storage modulus

Introduction

Today, due to the lack of oil resources and environmental problems (environmental pollutants), in recent years, the industry has been using biodegradable (degradable) and environmentally friendly polymers such as PLA (polylactic acid) to replace plastic. Oil-based products have been investigated. Aliphatic polyester is bio-based, derived from renewable sources such as sugar beet and corn, and has many applications including food containers, foils and small packaging such as pill coatings, bioabsorbable implants and medical devices. It has suture thread, sanitary packaging and automotive industries. Among the advantages of polylactic acid, we can mention clarity, ease of processing, high strength and rigidity, high mechanical properties and resistance. Among the disadvantages and weaknesses is the inherent fragility of PLA, which prevents its applications in various industries, combining PLA with other rubber polymers such as: POE, EVA, etc. also improves. These compounds usually have weak surface adhesion between the phases, which causes surface separation between the matrix and the droplets, which indicates an incompatible polymer. We can improve its physical, mechanical, and rheological properties by using nanoparticles and various compatibilizers in the PLA compound.

Experimental

Polylactic acid (PLA) with a specific density of 1.241 g/cm³ and a melt flow index (6 g/10min at 210 °C and a weight of 16.2 kg) that was prepared from NatureWorks under the brand name 2003D. Also, polyolefin elastomer (polyethylene octane) (POE) with a melt flow index of

5 g/10min and a specific density of 0.87 g/cm³ has been used. In this study, carbon nanotubes (CNTs) were used. Before mixing, the used materials were dried in a vacuum chamber at 50 °C for 12 h. The samples were prepared by melt mixing in an internal mixer, with a screw speed of 60 rpm at a temperature of 200 °C for 10 min. Then, the samples for different tests were prepared by pressure molding at 200 °C for 5 min.

Results and Discussion

SEM

According to the SEM images provided in Fig. 1, in the neat sample, the particle size is large and the adhesion between the phases is weak, by adding 0.25% of CNT nanoparticles,

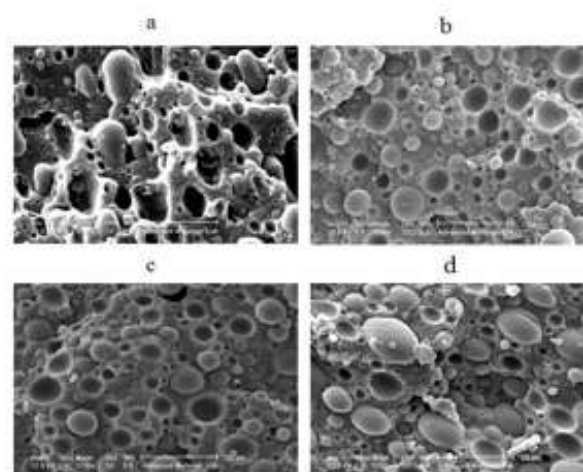


Fig. 1. SEM image of PLA/POE/CNTs blends for: (a) neat, (b) CNT 0/25%, (c) CNT 0/5%, and (d) CNT 1%.

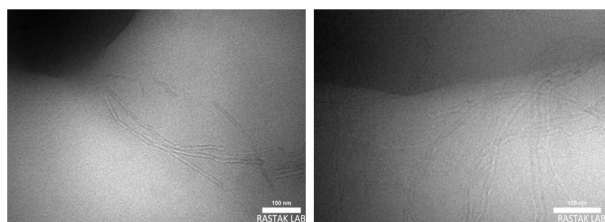


Fig. 2. TEM image of PLA/POE/ 0/5% CNTs blend.

the droplet size is significantly reduced and the adhesion is improved, which indicates that the nanoparticles have created compatibility. At 0.5% of nanoparticles, the size of the droplets does not change much compared to 25%, but with the addition of 1% of nanoparticles, the size of the droplets becomes larger and the interface becomes weak, and the accumulation of nanoparticles can be seen in the image.

TEM

To investigate localization of nanoparticles, TEM images have been obtained for PLA/POE blends containing 0.5% CNTs. According to the Fig. 2, the black parts correspond to the POE dispersed phase, and the white and brighter parts in the image show the PLA phase and the (thread) string-like parts, which appear in the image, are nanotubes, which show that they are well spread and separated. As can be seen in the pictures, the nanoparticles (nanotubes) are mainly located in the PLA phase, which indicates a good compatibility between PLA and nanoparticles.

Rheological Behavior

Fig. 3 shows the storage modulus G' as a function of angular frequency for PLA/POE blends with different percentages of nanoparticles. It can be seen that with the increase in the content of nanoparticles, the dependence of low frequency G' on frequency weakens and G' increases. This can be attributed to the nanoparticles that are dispersed in the polylactic matrix and limit the movement of the lactic chain part and prevent the relaxation of the PLA molecular

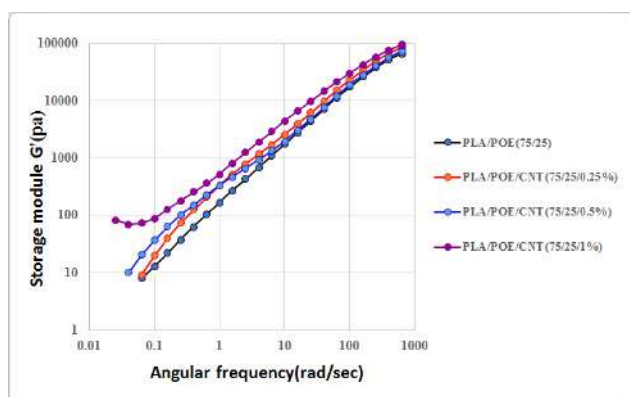


Fig. 3. Storage modulus as a function of frequency for PLA/POE blends with and without nanoparticles.

chains. This indicates favorable interaction between nanoparticles and PLA matrix as was observed in TEM images. At high frequencies, the effect of nanoparticles on the rheological behavior is relatively weak suggesting that the nanoparticles do not significantly influence the short-range dynamics of polymer chains. CNTs contents above 1 wt% led to a drastic enhancement in the low-frequency storage modulus making it almost independent of frequency indicating that CNTs established a percolated network in the PLA matrix.

Conclusion

Using the results, it was observed that nanoparticles improved the compatibility and interfacial adhesion, and in the amount of 0.25%, according to the SEM images, the highest amount of compatibility was created. The analysis of transmission electron microscopy, TEM and rheological behaviour showed that the nanoparticles have a good affinity for the PLA matrix phase. According to the rheological results, the compatibility effect of nanoparticles creates a high surface that increases the dynamic moduli at low frequencies. CNTs contents above 1 wt% makes storage modulus almost independent of frequency indicating that CNTs established a percolated network in the PLA matrix.

References

- [1] J. Khademzade Yeganeh and S. Moradi, "Highly toughened poly(lactic acid) (PLA) prepared through melt blending with ethylene-co-vinyl acetate (EVA) copolymer and simultaneous addition of hydrophilic silica nanoparticles and block copolymer compatibilizer", *Polym. Test.*, 1-14, 2020.

Investigating the Rheological Behavior of Plasticized Polylactic Acid/Carbon Nanotube (PLA/CNT) Nanocomposites

Mohammad Mahdi Farhoush* and Hamid Garmabi
Amirkabir University of Technology, Tehran, Iran

*mmfarhoush@aut.ac.ir

Abstract

The present study investigates the rheological behavior of conductive plasticized PLA/CNT nanocomposites with attention to higher processability goals. Due to the low toughness and poor processability of PLA/CNT nanocomposites, the plasticizing method was used to improve these properties. Using short-range oscillating rheology, the rheology of the samples was examined, and according to the obtained results, with increasing the percentage of CNT in the samples, the storage modulus increased, and the sample showed quasi-solid network behavior at low frequencies.

Keywords: polylactic acid, carbon nanotubes nanocomposites, plasticizer, rheology

Introduction

In the last two decades, the development and production of biodegradable and recyclable polymers have been significant due to the environmental problems caused by commercial polymers. Polylactic acid (PLA) is a leader among biopolymers due to its biodegradability, recyclability, desirable mechanical properties, and low cost [1]. PLA has a brittle behavior with low crystallinity kinetics and poor melt strength, which makes its use even more common in applications such as packaging [2]. There are various ways to overcome the problem of toughness and poor processability, including plasticizing and blending with flexible polymers. Plasticizers make them flexible by weakening the interaction between the main segments of the rigid polymer. Oligomeric plasticizer suffers from phase separation and a decrease in mechanical properties. These plasticizers, like monomers, increase the strain and decrease the T_g in the polymer structure. In this study, the effect of poly(tetramethylene ether) glycol (PTMEG) has been investigated the rheological behavior of PLA/CNT nanocomposites.

Experimental

Materials

Polylactic acid (PLA), grade 8052D, produced by Natureworks LLC, USA, was used. Poly(tetramethylene ether) glycol (PTMEG) ($M_n=2900$ g/mol) was purchased from Sigma-Aldrich. Multiwalled carbon nanotubes (Nanocyl®-7000 with average diameter, length, and specific surface area of 9.5 nm, 1.5 μ m, and 250–300 m^2g^{-1} , respectively) were supplied. Nitric acid (65%) and chloroform ($CHCl_3$) were purchased from (Dr. Mojallali, Iran).

Sample Preparation

Nitric acid and MWCNTs (150 mL of nitric acid, 1 g MWCNTs) were stirred and treated for 30 min in the ultrasonic bath after that refluxed at 85 °C for 24 h. Then, oxidized MWCNTs were dried in a vacuum oven at 55 °C for 24 h. Functionalized MWCNTs and pure MWCNTs as masterbatch prepared a PLA nanocomposite. The PLA (40 g/l) was initially solubilized, and functionalized MWCNTs (2 g/l) were dispersed in chloroform [3]. First, the PLA was dried in an oven at 70 °C for 24 h. Carbon nanotubes were modified and master batched in 0.25, 0.5, 0.75, and 1%. An internal mixer was used to mix the materials, and the process was performed for 10 min at 180 °C temperature and a rotor speed of 60 rpm. Pristine PLA/CNT (0.75%) nanocomposite was prepared using the same procedure.

Results and Discussion

The rheological behavior of PLA/CNT nanocomposites was investigated based on the results of the oscillatory rheology test, and the curves of storage modulus, loss modulus, and complex viscosity were compared in terms of frequency for nanocomposites. According to the results obtained from the short-range oscillatory. Rheology test, the following samples were examined and compared.. PLA, PLAPTM85/15, PLAPTM/fCNT0.25, PLAPTM/fCNT0.5 PLAPTM/pCNT0.75, PLAPTM/fCNT0.75, PLAPTM/fCNT1

Rheological Measurement Results

Comparing the storage modulus in terms of frequency is shown in Fig. 1. Generally, the storage modulus is sensitive to elasticity. The pure PLA sample indicated general polymer behavior and chain tension

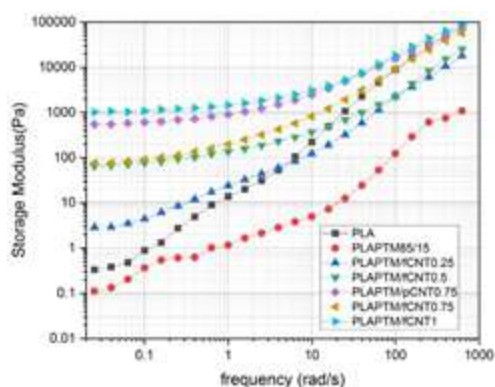


Fig. 1. Storage modulus according to the frequency of poly(lactide) acid nanocomposites, PTMEG oligomer, and carbon nanotube.

relaxation. On the other hand, the PLAPTM85/15 blend caused a sharp drop in the storage modulus at low frequency. This decrease in the storage modulus is caused by the reduction in the density of entanglements and the increase in the free volume of the chain. However, with the addition of CNT to the PLAPTM85/15 blend, the storage modulus was increased from the beginning, and a plateau was observed at low frequency. Also, relaxing the chains at low frequency is more complicated, and the melt has a solid-like response. The changes of complex viscosity in terms of frequency are shown in Fig. 2. The results indicate that adding PTMEG caused plasticization and increased free volume in the chain. As it is known, with the increase in the number of nanotubes in the system at low frequency, the viscosity also increased, and at low frequency, an upward jump was observed. This phenomenon is due to the formation of a network and the interaction of nano with nano and nano with polymer, which has limited the chain. Moreover, the length of the Newtonian region decreased with the increase in the percentage of nanotubes, and the systems at higher frequencies showed a shear-thinning behavior. Also, at high frequencies, the difference between the viscosity of the samples decreases. Complex viscosity regarding frequency PLA/CNT nanocomposites, PTMEG Fig. 3 shows the amount of storage modulus and viscosity on

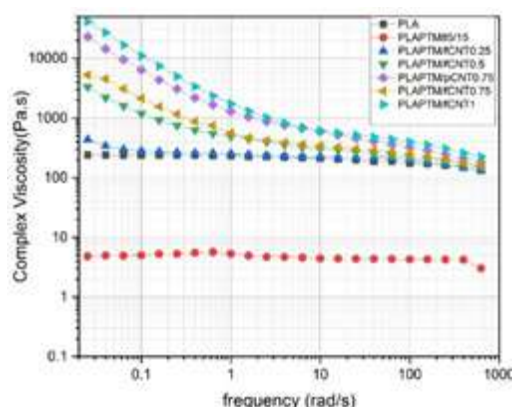


Fig. 2. Complex viscosity in terms of frequency of poly(lactide) acid nanocomposites PTMEG oligomer, and carbon nanotube.

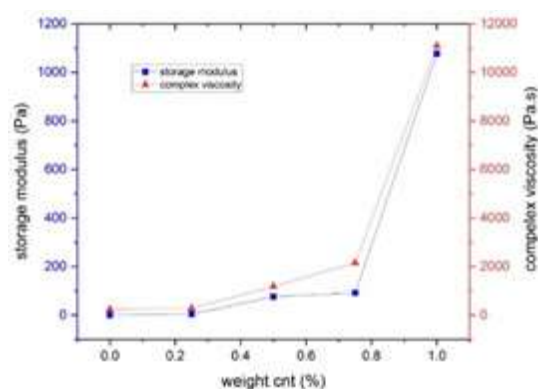


Fig. 3. Storage modulus and viscosity in terms of different percentages of modified CNT at a constant frequency.

different percentages of CNT. This figure determines the rheological percolation threshold and the optimal ratio of CNT to achieve the desired flowability properties. Also, the optimal rate of CNT for this system was obtained around 0.7% to 0.8%.

Conclusion

Blending PLA and PTMEG has increased chain mobility and free volume of poly(lactide) acid. According to the oscillatory rheology test, PLA has shown the general behavior of polymers, and the chains have relaxed at low frequencies. Also, adding plasticizer dramatically reduces the storage and loss modulus and the viscosity obtained due to the large free volume. By mixing with PTMEG. On the other hand, by adding carbon nanotubes to all percentages, an increase in the modulus and the non-terminal behavior of the samples were observed, indicating the creation of a network structure in the system.

References

- [1] F.H. Isikgor and C.R. Becer, "Lignocellulosic biomass: a sustainable platform for the production of bio-based chemicals and polymers", *Polym. Chem.*, **6**, 4497-4559, 2015
- [2] V. Nagarajan, A.K. Mohanty, and M. Misra, "Perspective on poly(lactide) acid (PLA) based sustainable materials for durable applications: Focus on toughness and heat resistance", *ACS Sustain. Chem. Eng.*, **4**, 2899-2916, 2016.
- [3] O. Yousefzade, H. Garmabi, and J. Puiggali, "Cooperative rearranging region and dynamical heterogeneity of nanocomposites in poly (l-lactide) and functionalized carbon nanotubes systems", *Thermochim. Acta*, **667**, 35-41, 2018.



Rheological Characterization of Electrophotographic Printing Ink

M. Mohammad Raei Nayini and Maryam Ataefard*

Department of Printing Science and Technology, Institute for Color Science and Technology,
P.O. Box 32465-654, Tehran, Iran

*ataefard-m@icrc.ac.ir

Abstract

Digital printing is affected by several parameters therefore, Process changes aimed at improving printer engine performance must take into consideration not only the process variables, but also the melt rheological variables. The thermo-mechanical properties of Konica Minolta BizHub C350 toners (in four colors) have been investigated with DSC and rheometer, It was found that by increasing the temperature, the toner particles undergo initial surface fusing at around 70 °C which is followed by reduction in viscosity. However, the melting of the particles takes place at 155-172 °C which is resulted in completely merged particles. The melting temperature of the fur colors are occurred at a specific order that matches the standard printing sequence of four-color printing.

Keywords: rheology, toner, electrophotographic printing

Introduction

The flow properties of fine powders at very low consolidation levels are relevant to small scale industrial application of powder flow, such as in small process hoppers or in everyday applications such as toner flow in cartridges. Toners are fine powders (particles typically lie in the size interval from a few μm to 12 μm) that are used in modern laser printers and photocopiers. They are in fact complicated mixtures that consist of a thermoplastic base material within which the colorant (organic or inorganic pigment nanoparticles and/or dyes) and different ingredients such as a charge control agent (CCA), flowing agents, pigments, UV-stabilizers and other additives have been mixed [1]. Fusing is the final process in electrophotographic printing. If the toner has not melted enough, the adhesion on paper is very poor. The optimal fusing temperature of the toner can be estimated from the viscosity and the viscoelastic transition of the toners. Digital printing quality is affected by several parameters including printer, paper and toner which determine the final printing quality. The toner must strike a balance between softness for effective fuser binding and sufficient hardness to prevent fusion in the photoreceptor during development. Therefore, the rheological properties of the toner play a crucial role in facilitating coalescence, spreading, and successful penetration into the paper, ultimately leading to the best printing results [2]. To meet these stringent requirements, it is essential to carefully tune the physical and mechanical properties of the toner, as well as ensure the appropriate particle size and shape. In continuation of our works, the aim of this study is to investigate the rheological behavior of four most common used color toner as well as their physical characteristics. In this work authors

combined the thermomechanical measurement with other analysis to better understand the toner properties.

Experimental

Material

Konica Minolta BizHub C350 toner in four colors (cyan 350, magenta 350, yellow 350 and black 350) are used. A4 size paper with 80g/m² base weight was printed in a controlled environment (23 °C, 50% relative humidity) using a colour laser printer.

Characterization

Viscosities of bulk molten toner of the four process colors have been measured at different temperatures using an Anton paar MCR300 rheometer with cone-plate set-up in controlled shear stress mode. In each case the shear rate was increased from 0.01 Hz to 10 Hz and reversed back down to 0.01 Hz, with 7 measurements distributed on a logarithmic scale for both increasing and decreasing shear rates. Thermal behavior of the toner was conducted on a differential scanning calorimeter (DSC, PerkinElmer USA). Approximately 5 mg of each sample was loaded onto a pan and sealed with a covering lid. The measurements were taken over a temperature range of 0-150 °C at a heating rate of 10 °C/min in an atmosphere of nitrogen.

Results and Discussion

The thermal characteristics of the toners, namely T_g (glass transition temperature), are important. This importance is due to having a direct effect on the fixing properties of toners onto the paper substrate. A moderate T_g value is generally required for the toner to have appropriate fixing properties. A too high T_g results in large-scale energy

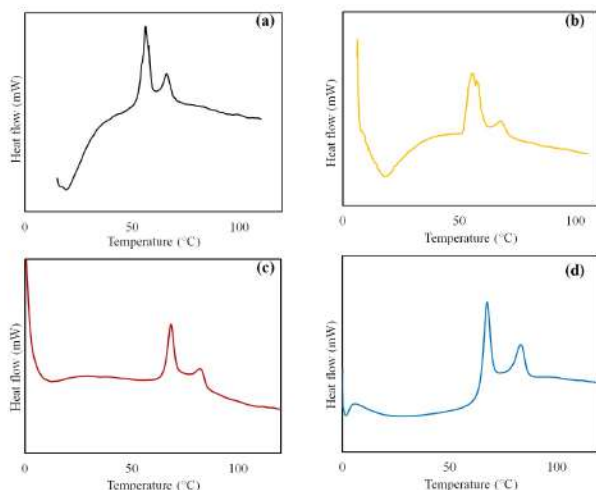


Fig. 1. DSC diagrams of the sample: (a) black 350, (b) yellow 350, (c) magenta 350, and (d) cyan 350. In all the curves, endo peak is up.

consumption during the printing process, and a too low T_g causes the toner to stick to the printer cartridge. For an industrial toner, to have suitable fixing properties for energy-efficient laser printing, T_g should normally be in the range of 50 °C to 70 °C. Fig. 2 shows the results of DSC analysis of commercial industrial toner. The slight shift of the base line is recognizable that can be attributed to the T_g . It is noteworthy that, in all the curves, the T_g is coincided with enthalpy relaxation peak and initial melting stages, which has been reported in other researches [3].

Thermal changes in the toner during the fusing process can be divided into three stages (Fig. 2):

1. Warming: Increase in temperature of toner particles and paper
2. Softening: Melting of the toner starts from the surface of particles and toner particles start to cohere and adhere to each other.
3. Melting: Partly melted toner Adheres to the paper [6]. At stage 1, the temperature rises from room temperature to about 70 °C, but no melting occurs in this range. In stage 2, the toner starts to melt on the surface (from about 70 °C to 85 °C). When the toner is heated for the first time, the softening (glass transition) temperature is higher than when it is heated for the second time, when the toner is already Glass-like [4]. Toner particles first cohere, and in stage 3, the toner starts to melt and adhere to the paper, too. In this stage, which is also accompanied with complete emergence of the separate particles with each other, the adhesion on paper is almost



Fig. 2. Schematic illustration of the fusing stages of toner in electrophotographic printing.

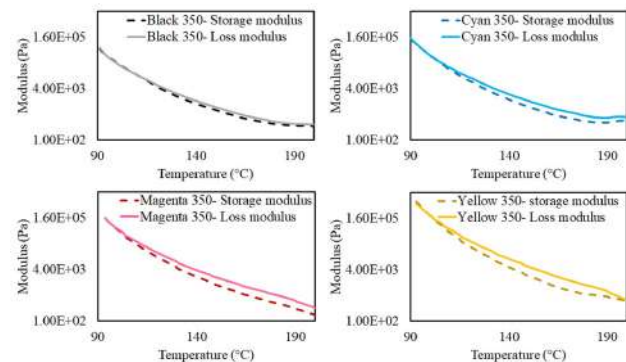


Fig. 3. Viscosity components of the toners, as a function of temperature.

complete. The toner continues to penetrate and spread as the temperature increases [5].

The melting stages of the toner can be followed by scrutinizing the rheological properties of the samples. As it can be seen in Fig. 3, in all the samples, complex viscosity as well as storage modulus and loss modulus are reduced expectedly by elevating the temperature. It is attributed to the higher mobility of the polymer chains at increased temperatures.

Conclusion

There are several parameters that influence characteristics of the final printing quality in electrophotographic printing. This study discussed the melt rheological behavior. Rheometer along with DSC analysis are used to investigate the thermo-rheological behavior of Konica Minolta BizHub C350 toner in four colors (cyan, magenta, yellow and black). Fusing as a critical step in development process in electrophotographic printers is monitored through Rheological investigation. The order of ultimate fusing temperature of the toners is found to be in good correlation with standard printing sequence of four-color printing, where the black color prints first and cyan prints afterward which is finally followed by yellow and magenta.

References

- [1] Marshall, *Recent Progress in Toner Technology, IS & T, Society for Imaging Science and Technology*, Springfield, IL, 1997, pp. 299-345.
- [2] G. Bruni, I. Tomasetta, D. Barletta, M. Poletto, and P. Lettieri, "Sensitivity analysis on a rheological model for the flowability of aerated fine powders", *Chem. Eng. Trans.*, **17**, 735-40, 2009.
- [3] F. Einarsson, Thermal analysis of toners, *Annu Trans. Nord Rheol. Soc.*, **10**, 155-60, 2002.
- [4] T. Hartus, "Adhesion of electrophotographic toner on paper", *Graph Arts Finl*, **30**, 13-15, 2001.
- [5] T. Hartus, Thermal studies of ink solvent and toner behaviour on coated paper: Modelled in various printing methods using ink-coating component mixtures and laboratory scale print tests, PhD Thesis, Aalto University, Espoo, Finland, 2020.

Investigating the Rheology Behavior of Reactive and Non-Reactive HEUR with the Same Hydrophilic and Hydrophobic Segments

Seyed Farzan Tajbakhsh and Saeed Pourmahdian*

Department of Polymer Engineering and Color Technology, Amirkabir University of Technology, 158754413, Tehran, Iran

*pourmahd@aut.ac.ir

Abstract

To become more eco-friendly, water-based coatings were employed. Additionally, thickeners were added to adjust the rheological behavior of water-dispersed coats. However, to modify the rheological behavior of water-borne ultraviolet (UV) curable resins, a polymerizable thickener was demanded. Hydrophobic Ethoxylate Urethanes (HEUR) containing hydrophilic segments and hydrophobic tails as an excellent associative thickener were chosen. To be compatible with the UV-curable resin, a HEUR with reactive groups placed in hydrophobic tails was synthesized. In this research, a reactive and a nonreactive HEUR were synthesized and their rheological behavior in water solution was compared. The results illustrate that in high concentrations of thickener, a Newtonian plateau followed by a shear thinning behavior was observed. In the same concentrations, viscosity in different shear rates was approximately equal for both thickeners. It is concluded that the rheological behavior in HEURs is mainly dominated by the length of hydrophilic chain and the hydrophobic tail.

Keywords: HEUR, polymerizable thickener, colloidal systems, water dispersed coats, associative thickener

Introduction

Nowadays, awareness about how harmful is volatile organic components (VOC) and the importance of reducing their emissions has increased. In addition, one way to reduce the emission is to employ water-borne coats instead of solvent-based ones [1]. While water-dispersed coatings have non-Newtonian rheological behavior, thickeners and rheological additives were added to solve the problems [1]. Hydrophobic Ethoxylate Urethanes (HEUR) are one of the best associative thickeners applied in the coating industry [2]. However, traditional HEURs could not be used in UV curable water-dispersed urethane acrylates as a suitable thickener [3]. In this research, a polymerizable HEUR (R-HC) was synthesized. Their rheological behavior in water was investigated and compared with a nonreactive HEUR (N-HC) with the same hydrophilic chain and hydrophobic tail.

Experimental

Material

Poly(ethylene glycol) 10000 (PEG), Isophorone diisocyanate (IPDI), Stearyl alcohol, Glycidyl methacrylate, and Stearic acid were obtained from E. Merck, Germany. Toluene was purchased from Mojalali Chemicals.

Synthesizing

R-HC and N-HC were synthesized starting from dissolving PEG in toluene, subsequently IPDI was added and the

reaction was kept at 80 °C for 3 h. Secondly, two different hydrophobic alcohols, an alcohol with a saturated structure and an alcohol with methacrylate attached to it, were added. Temperature rose to 85 °C and the reaction was continued for 12 h. The synthesized HEURs were precipitated and kept in a vacuum oven for 24 h to obtain a white powder [3,4].

Characterization and Rheology Measurements

The Fourier-transform infrared spectroscopy (FTIR) and Steady shear Rheology tests were performed using a Nicolet Model 360 Avatar apparatus with the KBr pellet method and Brookfield DV-II+ Pro Extra, respectively.

Results and Discussion

FTIR spectra of the R-HC and N-HC are compared in Fig. 1. The strong peaks at 1720 (C=O) and 3300 (N-H) cm^{-1}

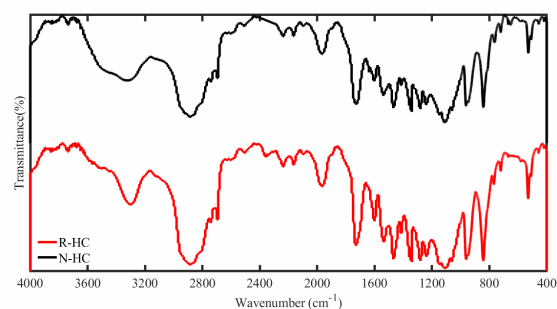


Fig. 1. FTIR spectrum of R-HC and N-HC.

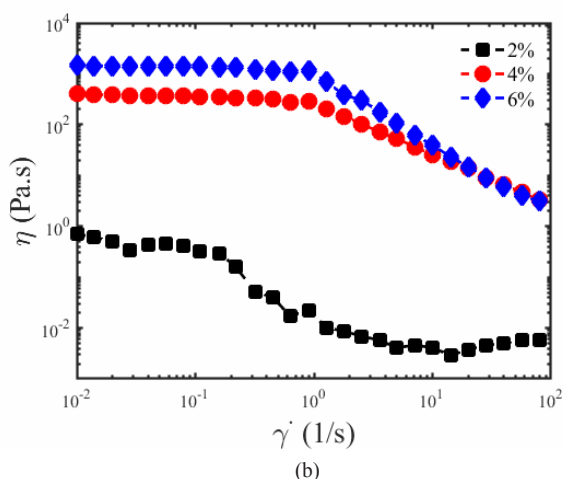
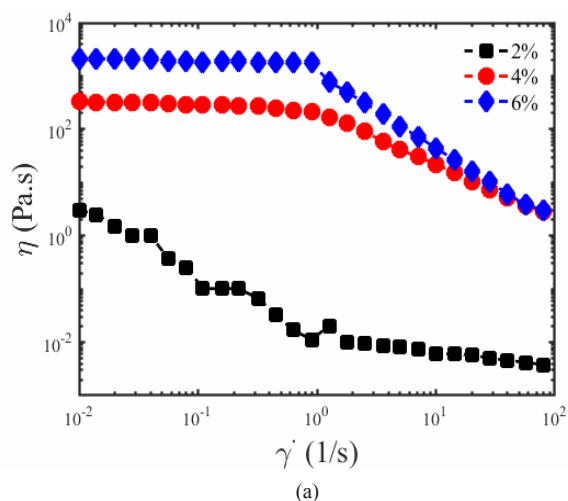


Fig. 2. Steady shear measurements of: (a) R-HC and (b) N-HC.

presented in both spectrums are related to urethane structure and confirm that HEURs are synthesized successfully [4]. The small peak at 2400 cm^{-1} is attributed to the unsaturated bonds in the R-HC structure, which is absent in the N-HC [3]. The steady shear rheological properties of R-HC and N-HC in aqueous solution in different concentrations (2, 4, and 6% HEUR wt. Water wt.) were investigated (Figs. 2a and 2b). It is obvious that in both figures for concentrations higher than 2%, the solution viscosity almost remains stable in the low shear rate region ($<1\text{ s}^{-1}$) and shows that the solution has Newtonian behavior. By increasing the shear rate, a shear thinning behavior was observed, indicating the breaking up of the solution associative network under high shear. In solutions with high concentrations of HEUR, viscosity at Newtonian plateaus gradually equals in R-HC and N-HC.

Figs. 3a and 3b demonstrate the recovery of the thickener under multiple shears alternating (0.03 and 100 s^{-1}) loops. Both thickeners have approximately recovered to the same amount of viscosity after several cycles.

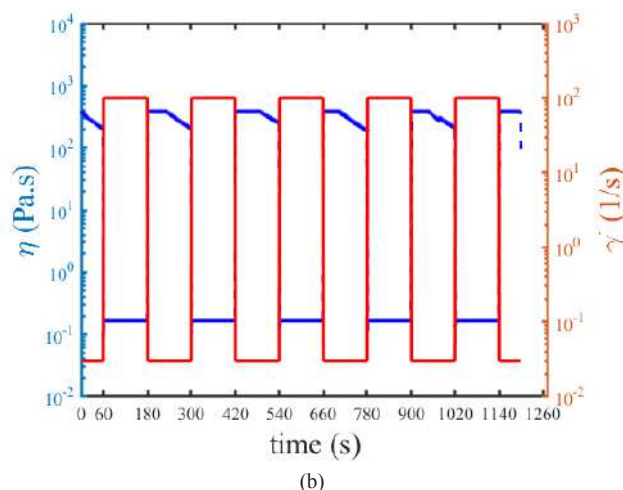
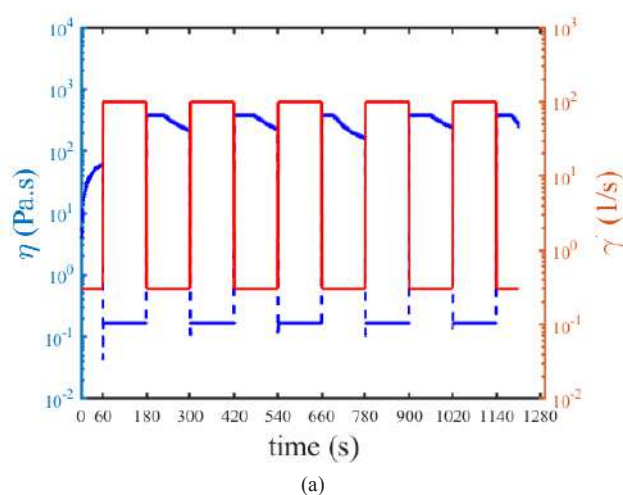


Fig. 3. Multiple alternating shear rate test at 6% thickener: (a) R-HC and (b) N-HC

Conclusion

To sum up, although using the methacrylate groups as the polymerizable functions in HEURs would change the structure of thickener, the results show that its presence has not affected the rheological behavior. The rheological behavior is mainly dominated by the length of the hydrophilic chain and the hydrophobic tail.

References

- [1] U. Kästner, *Colloid. Surf. A Physicochem.*, **183-185**, 805-821, 2001.
- [2] E. Orgilés-Calpena, F. Arán-Aís, A.M. Torró-Palau, C. Orgilés-Barceló, and J.M. Martín-Martínez, *Int. J. Adhes.*, **29**, 309-318, 2009.
- [3] T. Guan, Z. Du, J. Peng, D. Zhao, N. Sun, and B. Ren, *Macromol*, **53**, 7420-7429, 2020.
- [4] M. Barmar, *J. Appl. Polym. Sci.*, **111**, 1751-1754, 2009.

Comparison between the Mechanical Properties of LDPE/HDPE Cast Films Containing Various Injection-Grade HDPE

Romina Esmaeilzade*

Department of Polymer Engineering and Color Technology, Amirkabir University of Technology

*rodinesm@gmail.com

Abstract

With the aim of improving the mechanical properties of cast films made from LDPE, two injection-grade HDPEs are chosen to be blended with the LDPE. Rheological testing is utilized to understand the differences between the molecular weight of these two HDPE grades, and the higher complex viscosity, storage, and loss modulus of the HD-52505 grade proves its higher molecular weight. The mechanical testing of the cast film samples made with LDPE and 4 wt% of these HDPE grades shows that the stress and strain at break in both MD and TD directions is higher for the cast films made with HD-52505 due to its higher molecular weight and consequent higher crystallinity.

Keywords: low-density polyethylene, high-density polyethylene, cast film, rheological properties, mechanical properties

Introduction

Manufacturers of plastic products meet the performance requirements of their customers through polymer and process selections. Low-density polyethylene is among the most commonly used polyolefins in the packaging industry [1]. The generally lower properties of LDPE may cause some issues in its usage for some applications. There are many methods for modifying the properties of LDPE. Blending LDPE with other polyolefin materials is one of these methods. HDPE and LLDPE are among the most commonly blended polyolefins with LDPE due to their higher performance [2]. LDPE and HDPE represent the same class of polyolefins although their incompatibility is well known. This leads to reduced mechanical properties in comparison to single polymers, especially at high concentrations. But with the aim of enhancing the mechanical properties of LDPE, and keeping in mind the immiscibility of LDPE and HDPE, small amounts of HDPE could be incorporated into LDPE without sacrificing its mechanical properties, and even enhancing them, even if the HDPE was not specifically tailored for film production. This opens up LDPE to being used in even more applications that it was previously unsuitable for due to its low mechanical strength. The lower side branches of HDPE and consequently its higher crystallinity improves the mechanical properties of the products made with LDPE/HDPE blends. However, the level of impact that the HDPE has on the mechanical properties varies in accordance with the chain structure of the HDPE and, consequently, its own mechanical properties [3]. This study aims to investigate the effect of various HDPE grades on the mechanical properties of a widely used LDPE grade.

Experimental

LDPE was acquired from Bandar Imam Petrochemical Company and has a density of 0.921 g/cm³ and a melt index of 0.76 g/10min. The HDPE injection grades were HD-52505 and Luban8007 and were purchased from Jam Petrochemical Company and Orpic Polymer and had a density of 0.952 and 0.965 g/cm³ and melt index of 5 and 8 g/10 min, respectively. The cast films were prepared using an industrial multilayer cast film unit at Lafaf Zarrin Company. The films contained 4 wt% of HDPE and the extrusion was carried out at 220 °C with the distance between the die exit to the nip roll of 15 cm and a draw ratio of 75. The films were produced under chill roll temperatures of 80 and air-cooling rates of 12 L/s.

The MCR 502 parallel plate rheometer between the frequency range of 0.04 rad/s to 100 rad/s was utilized to evaluate the rheological properties of the blends within the linear viscoelastic region at 160, 180, and 200 °C under a Nitrogen atmosphere. Zwick/Roell Z005 tensile tester was utilized for the assessment of the mechanical properties of the blown films at room temperature adhering to the ASTM D882 standard. Analysis of stress-strain curves presented the data for stress at yield and break and strain at yield and break.

Results and Discussion

The rheological testing of the HDPE grades offers a chance to evaluate the molecular weight of the grades. The higher complex viscosity, storage, and loss modulus of the HD-52505 grade, which are displayed in Figs. 1 and 2, indicate that its molecular weight is higher than that of the Luban8007. The mechanical testing of the cast

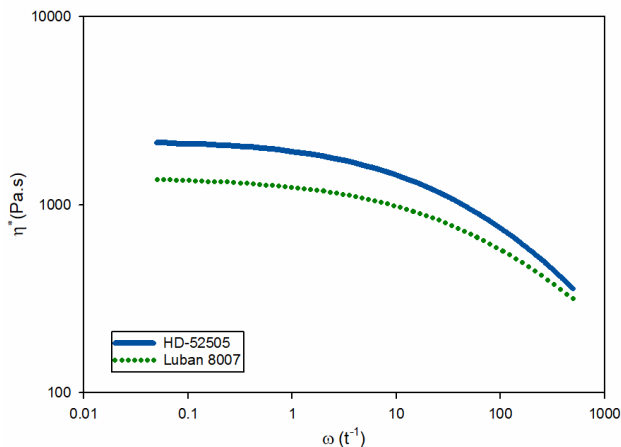


Fig. 1. Complex viscosity of the two HDPE grades.

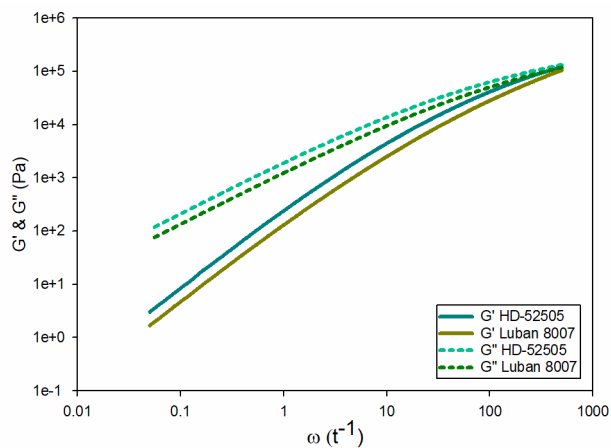


Fig. 2. Storage and loss modulus of the two HDPE grades.

film samples presents the data for the stress and strain at break of the samples. For better visualization, the stress at break data has been multiplied by 10. The results which are presented in Fig. 3 indicate that the stress and strain at break of the cast film containing the HD-52505 grade at both MD and TD directions is higher than the film

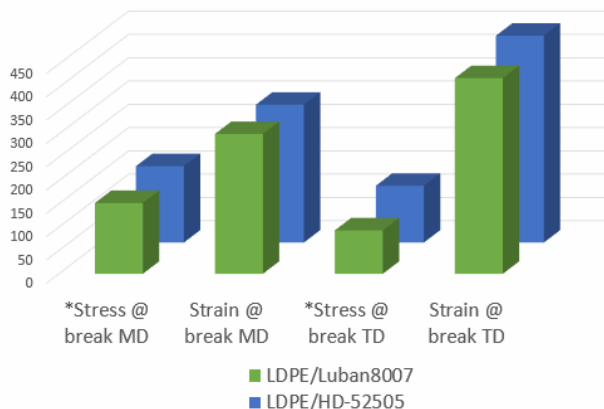


Fig. 3. Stress and strain at break in MD and TD direction of the cast film samples.

made with the Luban8007 grade. The higher molecular weight of the HD-52505 grade, which results in the higher crystallinity of this grade is the reason for these elevated mechanical properties. The low concentration of the HDPE in both samples causes the film components to be miscible and for the film to have one single phase. Increasing the HDPE loading in the film could cause phase separation and result in reduced mechanical properties.

Conclusion

Two injection-grade HDPEs were selected to be added to LDPE to form cast films with the aim of increasing the mechanical properties of LDPE films. The rheological testing of the HDPE grades, which displayed a higher complex viscosity, storage, and loss modulus for the HD-52505 grade indicated that this grade has a higher molecular weight compared to the Luban8007. Cast films of the HDPE and LDPE were produced containing only 4 wt% of HDPE to maintain the single-phase composition of the films. The mechanical testing results of the cast films displayed that the higher molecular weight and the consequent higher crystallinity of the HD-52505 grade cause higher stress and strain at break in both MD and TD directions.

References

- [1] X. Jin, D.A. Zumbrunnen, A. Balasubramanian, and K. Yam, "Tailored additive release rates in extruded plastic films produced with smart blending machines", *J. Plast. Film Sheet.*, **25**, 115-140, 2009.
- [2] M. Munaro and L. Akcelrud, "Correlations between composition and crystallinity of LDPE/HDPE blends", *J. Polym. Res.*, **15**, 83-88, 2007.
- [3] A. Van Belle, R. Demets, N. Mys, K. Van Kets, J. Dewulf, K. Van Geem, S. De Meester, and K. Ragaert, "Microstructural contributions of different polyolefins to the deformation mechanisms of their binary blends", *Polymers*, **12**, 2020.

Investigation on the Transient Solution of Electric Field Driven Orientation and Deformation of the Angled Droplet

Tahereh Asadollahi and Nadereh Golshan Ebrahimi*

Department of Polymer Engineering, Faculty of Engineering, Tarbiat Modares University, Tehran, Iran

*ebrahimn@modares.ac.ir

Abstract

Solving a problem theoretically provides us with a broader context for understanding the situation. In this case, we discuss an example that can be investigated by theoretically solving the transient deformation and orientation of an angled spheroidal droplet in a finite conducting host medium under an electric field. We employed two different experimental systems to explore this problem and concluded that it is possible to study the system's relaxation using the adopted method.

Keywords: electrohydrodynamic, leaky dielectric, droplet deformation, orientation, relaxation

Introduction

The behavior of a liquid droplet when subjected to an external electric field is gaining greater significance, primarily because of its diverse applications across various scientific domains. When an electric field is applied to an immiscible leaky dielectric droplet suspended in a leaky dielectric host medium, leading to hydrodynamic flow both inside and outside the droplet. This flow balances the tangential viscous stresses with electric stresses even in a steady state. This phenomenon is referred to as electrohydrodynamics (EHD). Depending on the electrical properties of the two fluids, the droplet can deform into a prolate or an oblate shape [1]. The problem of transient deformation and orientation of angled spheroidal leaky dielectric droplet in a finite conducting host medium under electric field solved, theoretically [2]. Fig. 1 illustrates the schematic representation of this EHD problem. The solution involves two distinct calculations: one for the electric field and another for the fluid flow within each of the two fluids. These calculations are then combined by applying the interfacial charge conservation equation at the droplet's

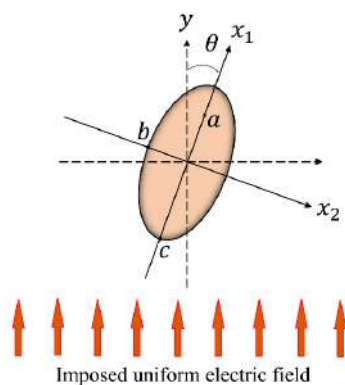


Fig. 1. A schematic of the droplet configuration [2].

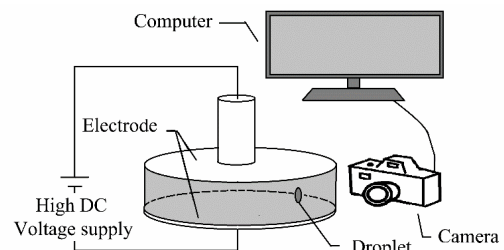


Fig. 2. Schematic diagram of the experimental setup [2].

surface. This allows us to compute the deformation rate of the droplet at each time step and for each θ angle. By knowing the droplet's orientation at any given moment and employing the angular rate equation, we can determine the droplet's new orientation. Dynamics of the orientation of the spheroid droplet in an electric field can be expressed as [2]:

$$d\theta/dt = M(\theta)/\mu \quad (1)$$

where M is torque value and the coefficient μ depends upon the viscosity of the medium. By knowing the initial value of θ and elongation, the value of θ and elongation will be

Table I. EHD properties of liquids.

Fluid	Conductivity σ ($S m^{-2}$)	Permittivity ϵ/ϵ_0	Viscosity μ (Pa s)	Interfacial tension in motor oil γ ($N m^{-1}$)
water	5.5×10^{-6}	78.4	0.001	0.011
PEG	1.7×10^{-6}	14.1	0.1017	0.0033
Motor oil	1.41×10^{-9}	2.2	0.36	



Fig. 3. Transient behavior of the water droplet [2].



Fig. 4. Transient behavior of the PEG droplet [2].

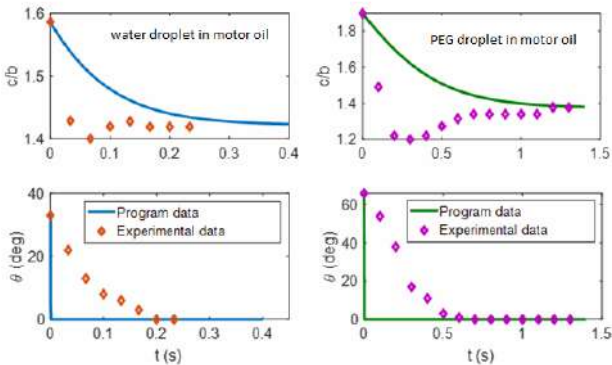


Fig. 5. Comparison between program results and experimental data.

obtained at any moment, step by step.

Theoretical analysis provides us with a deeper understanding of the underlying processes. In this context, we are discussing a specific case that can be examined further.

Experimental

Fig. 2 shows a schematic diagram of the experimental setup. Motor oil was used as the continuous phase, and distilled water and Polyethylene glycol (PEG) were used as the dispersed phase. Table I represents the properties of fluids.

By rotating and then suddenly stopping the bottom plate, an initial angle (θ_0) will create. Over time, this angle tends to zero and finally, the main axis of the droplet becomes aligned with the direction of the electric field.

Results and Discussion

Figs. 3 and 4 show the transient behavior of a water and

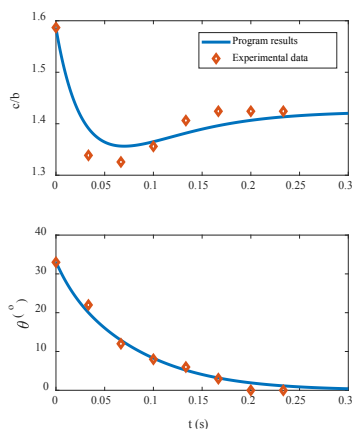


Fig. 6. Comparison between current model's prediction and experimental data of the water droplet in the motor oil.

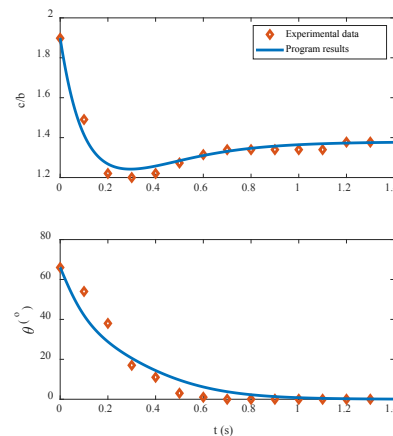


Fig. 7. Comparison between current model's prediction and experimental data of the PEG droplet in the motor oil.

PEG droplet in motor oil, respectively. It's noticeable that while approaching equilibrium, the elongation of the droplets initially decreases and then undergoes a slight increase.

By substituting the matrix viscosity with μ , the order of $d\theta/dt$ in the program results does not align with the order observed in the experiment (Fig. 5).

By adding a factor to μ , for fitting them, program results and experiment became coincident (Figs. 6 and 7).

The factor for the water droplet was about 80, while for PEG, it was about 60. These factors can be related to the relaxation properties of the materials.

Conclusion

This method of investigation provides new knowledge about electrodeformation and relaxation of droplet.

Acknowledgement

The kind assistance of Tarbiat Modares University is greatly acknowledged.

References

- [1] S. Mandal and S. Chakraborty, *Phys. Fluid.*, **29**, 072109, 2017.
- [2] T. Asadollahi and N.G. Ebrahimi, *Comput. Phys. Commun.*, 108866, 2023.

Calculating the Pressure Term for a Spheroidal Droplet

Tahereh Asadollahi and Nadereh Golshan Ebrahimi*

Department of Polymer Engineering, Faculty of Engineering, Tarbiat Modares University, Tehran, Iran

*ebrahimn@modares.ac.ir

Abstract

At times, it's possible to discover that the results described in an article cannot be attained using commonly available mathematical equations. We encountered one such instance when attempting to implement the equations from an article. In that article, a droplet underwent deformation under the influence of an electric field. Our objective was to calculate the pressure both inside and outside the droplet using the stream functions outlined in that article, enabling us to incorporate them into the stress balance equations on the droplet's surface. In the process of calculating the pressure, we faced challenges when using conventional formulas, leading to differing results through two distinct approaches. The article in question did not explicitly specify the methodology for pressure calculation; nevertheless, it presented the final computational results. We presented the method for calculating pressure in that paper, which cannot be obtained through conventional methods. This method is also applicable to other scenarios presenting similar challenges.

Keywords: pressure formulation, stream function, droplet deformation, spheroid, induced flow

Introduction

Sometimes, it happens that we do not arrive at the results presented in an article using the available general formulas. This situation occurred while calculating the pressure inside and outside a droplet using the stream functions provided in Zhang *et al.*'s paper [1]. They presented a transient analysis of droplet deformation under direct-current (DC) electric fields. In this paper, we aim to explain how they calculated the pressure term so that other researchers can utilize these equations in their work.

Theory

Consider a neutrally buoyant droplet of radius r_0 , suspended in an immiscible host medium. An external field may cause a droplet to deform into a prolate spheroid. Since we assumed that the droplet shape, remains spheroidal during the process, the prolate spheroidal coordinate system was used to analyze this problem. As shown in Fig. 1, these coordinates (ξ , η , φ) are related to the rectangular coordinates (x_1 , x_2 , x_3), $x_1 = a\xi\eta$, $x_2 = a\sqrt{(\xi^2 - 1)(1 - \eta^2)} \cos \varphi$, $x_3 = a\sqrt{(\xi^2 - 1)(1 - \eta^2)} \sin \varphi$ where $a = \sqrt{c^2 - b^2}$ is half of the focal length and $1 \leq \xi < \infty$, $-1 \leq \eta \leq 1$, $0 \leq \varphi \leq 2\pi$ [28]. Metric coefficients of the prolate spheroidal coordinate system are $h_\xi = \frac{a\sqrt{\xi^2 - \eta^2}}{\sqrt{\xi^2 - 1}}$, $h_\eta = \frac{a\sqrt{\xi^2 - \eta^2}}{\sqrt{1 - \eta^2}}$ and $h_\varphi = a\sqrt{\xi^2 - 1}\sqrt{1 - \eta^2}$ [2].

$\xi_0 \equiv c/a$ denotes the surface of the prolate spheroid, c and b are the major and minor semi-axis, respectively and a is the semi-focal length of the spheroidal droplet. \vec{E}_0 is the external uniform electric field, in the x_2 -direction the interface has a constant interfacial tension coefficient γ and the subscripts

d and m denote droplet and matrix, respectively.

Induced hydrodynamic flow inside and outside of the droplet, can be expressed in terms of the Stokes stream-function (Ψ), $\Gamma^4\Psi = \Gamma^2(\Gamma^2\Psi) = 0$, where the operator Γ^2 in prolate spheroidal coordinates given as $\Gamma^2 = \frac{1}{a^2(\xi^2 - \eta^2)} \left((\xi^2 - 1) \frac{\partial^2}{\partial \xi^2} + (1 - \eta^2) \frac{\partial^2}{\partial \eta^2} \right)$. The stream function is related to the velocity components. $v_\eta = -\frac{1}{h_\varphi h_\xi} \frac{\partial \Psi}{\partial \xi}$, $v_\xi = \frac{1}{h_\varphi h_\eta} \frac{\partial \Psi}{\partial \eta}$

At the interface, v_ξ and v_η represent the normal and tangential velocities, respectively. There is no flow across the interface and the tangential velocities of the host fluid and the droplet, coincide at the interface.

$$u_\eta^d = u_\eta^m, \quad u_\xi^d = u_\xi^m, \quad \text{at } \xi = \xi_0 \quad (1)$$

By taking into account that, Ψ is bounded anywhere and symmetric around ($\xi=1$ and $\eta=0$), an approximated solution for it inside and outside the droplet is [1]:

$$\Psi^d = (B_1 G_3(\xi) + B_2 G_5(\xi)) G_3(\eta) \quad (2)$$

$$\Psi^m = (A_1 H_1(\xi) + A_2 H_3(\xi)) G_3(\eta) \quad (3)$$

where G_n and H_n are the first and second kind of Gegenbauer polynomials and defined as

$$G_3(\xi) = \frac{\xi(1-\xi^2)}{2}, G_5(\xi) = \frac{\xi(1-\xi^2)(3-7\xi^2)}{8}, H_1(\xi) = -1, H_3(\xi) = \frac{\xi(1-\xi^2)}{4} \ln\left(\frac{\xi+1}{\xi-1}\right) + \frac{\xi^2}{2} - \frac{1}{2}$$

Then we can write:

$$\Psi = \frac{\eta(1-\eta^2)\psi(\xi)}{2} \quad (4)$$

By using Eq. (2), A_1 and A_2 can be obtained in terms of B_1

and B_2 .

The general balance of tangential and vertical stresses due to hydrodynamic (T), electric (S) and surface tensions, must be satisfied at any point on the interface, which are written in the spheroidal coordinates, respectively, as follows [2]:

$$\int u_\eta \cdot (T_{\xi\eta}^m - T_{\xi\eta}^d + S_{\xi\eta}^m - S_{\xi\eta}^d) ds = 0 \quad (5)$$

$$\int u_\xi \cdot \left(T_{\xi\xi}^m - T_{\xi\xi}^d + S_{\xi\xi}^m - S_{\xi\xi}^d - \gamma \left(\frac{1}{R_1} + \frac{1}{R_2} \right) \right) ds = 0 \quad (6)$$

where $ds = a^2 \sqrt{\xi^2 - 1} \sqrt{\eta^2 - 1} d\varphi d\eta$ and R_1 and R_2 are the principal radii of the curvature, and the integration is carried over the interface [1]. The tangential and normal components of the hydrodynamic stress vector are given by [2],

$$T_{\xi\eta} = \mu \left[\frac{h_\eta}{h_\xi} \frac{\partial}{\partial \xi} \left(\frac{u_\eta}{h_\eta} \right) + \frac{h_\xi}{h_\eta} \frac{\partial}{\partial \eta} \left(\frac{u_\xi}{h_\xi} \right) \right] \quad (7)$$

$$T_{\xi\xi} = -P + \mu \left(2 \frac{1}{h_\xi} \frac{\partial u_\xi}{\partial \xi} + 2 \frac{u_\eta}{h_\xi h_\eta} \frac{\partial h_\xi}{\partial \eta} \right) \quad (8)$$

where

$$\frac{\partial P}{\partial \eta} = \mu \frac{\partial(r^2 \Psi)}{\partial \xi} \frac{h_\eta}{h_\xi h_\varphi} = \mu \frac{\partial(r^2 \Psi)}{\partial \xi} \frac{1}{(1-\eta^2)} \quad \text{and}$$

$$\frac{\partial P}{\partial \xi} = -\mu \frac{\partial(r^2 \Psi)}{\partial \eta} \frac{h_\xi}{h_\eta h_\varphi} = -\mu \frac{\partial(r^2 \Psi)}{\partial \xi} \frac{1}{(\xi^2-1)}$$

here $P = \int \partial P / \partial \eta d\eta$ or $P = \int \partial P / \partial \xi d\xi$.

In some cases, the results of these two integrations may not be consistent with each other. For instance, this happened when dealing with the expression $B_2 G_5(\xi) G_3(\eta)$ within the stream function. In such cases, we proceed in accordance with the explanation that will follow. If we represent this expression as $\Psi_1 = B_2 G_5(\xi) G_3(\eta)$,

$$P_1 = \int \partial P_1 / \partial \eta d\eta = \int \mu \frac{\partial(r^2 \Psi_1)}{\partial \xi} \frac{1}{(1-\eta^2)} d\eta \quad (9)$$

By swapping ξ and η in the stream function as

$$\Psi_2 = B_2 G_5(\eta) G_3(\xi),$$

$$P_2 = \int \partial P_2 / \partial \eta d\eta = \int \mu \frac{\partial(r^2 \Psi_2)}{\partial \xi} \frac{1}{(1-\eta^2)} d\eta \quad (10)$$

The corresponding pressure for this expression will be as $P = P_1 + P_2$.

Results and Discussion

By using the method outlined for pressure calculation, the obtained results, align with those presented by Zhang *et al.*.

Conclusion

In this work, we presented the method for calculating pressure in Zhang *et al.*'s paper, which cannot be obtained using conventional methods.

Acknowledgement

The kind assistance of Tarbiat Modares University is

greatly acknowledged.

References

- [1] J. Zhang, J.D. Zahn, and H. Lin, "Transient solution for droplet deformation under electric fields", *Phys. Rev. E*, **87**, 043008, 2013.
- [2] N. Benteinis, and S. Krause, "Droplet deformation in dc electric fields: the extended leaky dielectric model", *Langmuir*, **21**, 6194-6209, 108866, 2023.

Effects of Various Fillers on the Properties of Silicone Rubber-Based Blends for Electrical Industry: A Rheometric Study

Matin Moazami Goudarzi and Mohsen Najafi*

Department of Polymer Engineering, Faculty of Engineering, Qom University of Technology, Qom, Iran

*najafi.m@qut.ac.ir

Abstract

This article investigates the effect of incorporating fillers into silicone rubber to enhance its properties for outdoor insulator applications. The study focuses on the impact of TiO_2 , SiO_2 , and ATH fillers on the polymer blend's rheological behavior, specifically examining the T90 value in MDR testing. The experimental design utilizes a Box-Behnken approach with three variables: TiO_2 , SiO_2 , and ATH at different levels. The blends are prepared through melt mixing and vulcanized using a hot press. The results reveal that increasing the phr of ATH and TiO_2 generally leads to higher stiffness, as indicated by higher torque values. Moreover, the addition of more fillers in the polymer blend increases its viscosity and stiffness, resulting in an increased T90 value during the curing process. These findings highlight the importance of filler content optimization for achieving desired mechanical properties in silicone rubber blends for insulation applications.

Keywords: silicone rubber, outdoor insulator, fillers, rheometer, box-behnken

Introduction

Composite materials have been widely employed as insulating materials in power transmission systems for more than five decades due to their exceptional mechanical and electrical properties. These properties make composites an ideal choice for producing high voltage insulators. However, the long-term application of composites has revealed certain drawbacks, including susceptibility to erosion and tracking, low resistance to surface pollution and acid, degradation under heat radiation, and premature failure [1]. To address these limitations, silicone rubber has emerged as a superior alternative to ordinary organic rubbers. Silicone rubber offers enhanced heat resistance, chemical stability, electrical insulation, abrasion resistance, weatherability, and ozone resistance [2]. While silicone rubber has demonstrated better performance than most organic polymers for outdoor insulator applications, pure silicone rubber exhibits limited resistance to tracking and erosion. Therefore, improvements are necessary to enhance its service life and effectiveness. One approach to achieving this is by incorporating fillers into the polymer, which can enhance specific properties and reduce costs [3]. In terms of experimental and theoretical considerations, increasing the filler content in a given material tends to improve its tracking performance. However, it may have adverse effects

on other properties. The extent of property improvement in nanocomposites depends on several factors, including filler concentration, filler morphology (such as particle size and structure), the degree of dispersion and orientation within the matrix, and the level of adhesion to the polymer chains (Table I). Provides an overview of the property modifications of the typical fillers used in silicone rubber compounds [3]. In this study, to investigate the response pattern and determine the optimal combination of variables, a Box-Behnken experimental design with three variables was employed. The goal was to examine the effects of the aforementioned fillers listed in Table I on the rheometric properties of silicone rubber compounds.

Experimental

In this experiment, TiO_2 , SiO_2 , and ATH were variables, while silicone (50 phr) and DCP (2 phr) were constant parameters (Table II). illustrates three levels of variables according to the experimental design plan. According to the Box-Behnken method, 15 formulations were prepared for the experiment. Blends were formulated through melt mixing in an internal mixer operating at a rotational speed of 60 r/min and 70 °C and a mixing duration of 5 min. The process involved initially introducing silicone rubber into the mixing chamber, followed by the addition of

Table I. Property Modification of each filler.

Filler	Property modification
TiO_2	Relative permittivity, thermal stability, photocatalytic
SiO_2	Thermal conductivity, anti-tracking & erosion
ATH	Anti-tracking agent and flame retardant

Table II. Variables phr.

Variables	Leves (PHR)		
	-1	0	+1
TiO_2	10	20	30
SiO_2	10	20	30
ATH	10	15	20

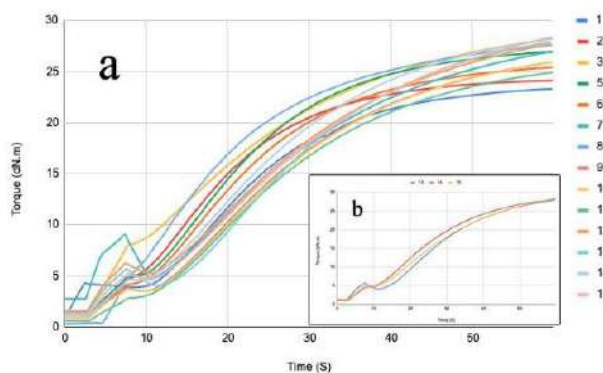


Fig. 1. Rheometer curve at the first minute: (a) all samples, (b) repetition of samples at the middle point, according to Box-Benken method.

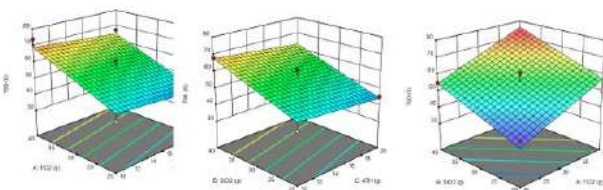


Fig. 2. T90 in different phr of materials.

fillers to the blend. Finally, a vulcanizing agent, DCP, was incorporated into the blend. The resulting blend was used for MDR tests and the rest of the blend was subjected to vulcanization using a hot press (Carver) at a temperature of 180 °C for a duration of 5 min.

Results and Discussion

The MDR (Moving Die Rheometer) tests were conducted using a die temperature of 175 °C, an oscillation frequency of 1.66 Hz, and an oscillation amplitude of 0.5. The torque range was set at 100 dN.m, and the time range for the tests was 10 min. Increasing the phr of ATH and TiO₂ generally results in higher torque values, indicating increased stiffness. The phr of SiO₂ does not follow a clear trend in relation to torque values. It varies across samples but does not consistently correlate with higher or lower stiffness (Fig. 1). The addition of more fillers can lead to increased viscosity and stiffness in the polymer blend. This increased stiffness may result in a longer time for the material to reach 90% of its maximum torque during the curing process, leading to an increased T90 value (Fig. 2).

Conclusion

The incorporation of fillers, such as TiO₂, SiO₂, and ATH, in silicone rubber blends significantly influences their mechanical behavior and curing process. Increasing the phr of ATH and TiO₂ generally increases stiffness, while the effect of SiO₂ on stiffness varies. The addition of more fillers leads to increased viscosity and stiffness, resulting in a longer time (higher T90 value) for the material to reach 90% of its maximum torque during

curing. These observations emphasize the importance of carefully optimizing the filler content in polymer blends to achieve desired mechanical properties. Further research and experimentation are required to identify the optimal combination of fillers and their concentrations to enhance the performance and longevity of silicone rubber blends for outdoor insulator applications.

Acknowledgement

We also thank Bespar-Sazeh-Alvand Company for their generous contributions and cooperation in providing raw materials for this research.

References

- [1] M. Liang and K. Loon Wong, "Improving the long-term performance of composite insulators use nanocomposite: A review", *Energy Proc.*, **110**, 168-173, 2017.
- [2] J.P. Reynders, I.R. Jandrell, and S.M. Reynders, "Review of aging and recovery of silicone rubber insulation for outdoor use", *IEEE Trans. Dielect. Electr. Insul.*, **6.5**, 620-631, 1999.
- [3] G. Momen and M. Farzaneh, "Survey of micro/nano filler use to improve silicone rubber for outdoor insulators", *Rev. Adv. Mater. Sci.*, **27**, 1-13, 2011.

Curing characteristics and rheological properties of (styrene butadiene rubber /ethylene propylene diene monomer) blend in the presence of a hybrid of carbon black and nanoclay

Fatemeh Layaee Vahed and Azam Jalali-Arani*

Amirkabir University of Technology (Polytechnic of Tehran), Polymers and Paints Department, Tehran, Iran

*ajalali@aut.ac.ir

Abstract

This research investigates the curing rheometric characteristics and rheological properties of the blends based on styrene butadiene rubber (SBR) and ethylene propylene diene monomer (EPDM) rubber in the presence of a hybrid of carbon black and nanoclay (Closite 15A). For this purpose, these characteristics and properties were evaluated on blends containing a certain percentage of both rubbers (50/50) and carbon black (20 phr) and different amounts of nanoclay. The results obtained from curing test showed a decrease in scorch and cure times with increasing the amount of nanoclay, while the minimum torque of rheometry increased. The rheological test showed increase in the storage modulus and complex viscosity of the blends as the amount of nanoclay increased.

Keywords: SBR, EPDM, curing, rheological properties

Introduction

Polymer blends are of interest in many cases because they make it possible to achieve desirable properties or reduce the price. One of these is the blend of ethylene propylene diene monomer (EPDM) and styrene butadiene (SBR) rubber. EPDM is an elastomer with high ozone resistance, but it is not economically viable, it also has poor tensile strength and poor adhesion. In contrast, SBR, which is a rubber produced by the domestic petrochemical industries, has a lower price. Despite its good mechanical properties and abrasion resistance, SBR does not have high ozone resistance. Therefore, the study of blending these two elastomers can be considered both in terms of accessing the desired properties of both polymers and in terms of reducing the price and cost. This blend can be used in many cases. [1,2] On the other hand, the use of reinforcing materials in the rubber compounds has been of interest since the past. In this regard, carbon black has been used as a reinforcement in the most cases. In recent years, with the introduction of nanoparticles to the polymer industries, many researches have been conducted on the use of these nanoparticles in rubber compounds. It has been observed that the use of nanoparticles can help to improve the functional properties of elastomers. [3,4] Recent research on rubber compounds containing a hybrid of two particles or nanoparticles shows that the presence of a nanoparticle along with carbon black leads to a better dispersion of nanoparticle, which improves the rheological properties of the final product compared to the compound containing each of them [5]. In this work, the simultaneous use of carbon black and nanoclay in the SBR/EPDM blend is investigated and the effect of their presence on the curing characteristics as well as the

rheological properties of the compound is evaluated.

Experimental

To prepare samples, SBR-1502 with a density of 0.93 g/cm³ produced by Bandar Imam Petrochemical Co. EPDM (KEP270) with a density of 0.86 g/cm³, closite15A with a density of 0.17 g/mL and carbon black N330 were used.

The necessary materials for vulcanization including zinc oxide, stearic acid, sulfur, and accelerators, were obtained from domestic rubber factories. In this research, blends of SBR/EPDM (50/50) containing a constant amount of carbon black and different amounts of nano caly were prepared. The amount of zinc oxide (5 phr), stearic acid (1 phr), sulfur (2 phr) and accelerators (1.5 phr) were considered the same in all compounds.

The prepared samples were named based on the nanoclay content. For example, (S50/C1) shows a blend with 1 phr of nanoclay. The mixing of materials (except curing agents) was done on a laboratory two-roll mill at a temperature of 80 °C. Then, curing agents were added to the mixture at a lower temperature. Rheometric curing test was performed on the samples, and based on the results obtained, the sheet sample was molded for the next tests. The rheometric test on the samples was performed according to the ASTM D2084 standard by an oscillating disk rheometer at a temperature of 160 °C. Rheomechanical spectrometer (RMS; MCR 301) at 160 °C was used to perform the rheological tests.

Results and discussion

Table I shows the results obtained in the curing rheometry test. These results show that by the use of nanoclay and increasing its amount, the scorch and cure times are reduced.

Table I. Results obtained from the rheometric test.

	Cure time (min)	Scorch time (min)	Min torque (lb.ft)	Max torque (lb.ft)
S50/C0	8.64	2.19	34.05	115.51
S50/C1	4.64	2.09	36.56	112.35
S50/C3	3.83	1.36	37.06	109.48
S50/C5	3.75	1.04	37.35	107.54

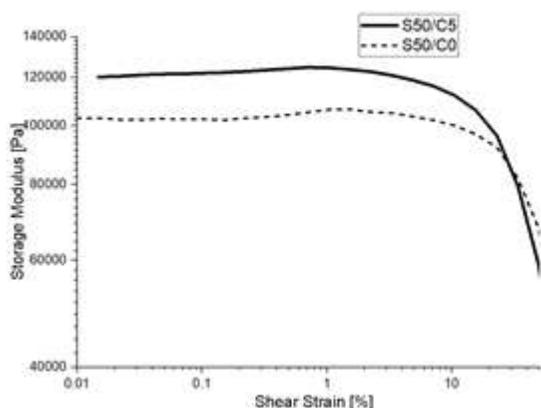


Fig. 1. Storage modulus of pure sample and sample with 5 phr nanoclay.

Also, an increase in the minimum torque is observed, but the maximum torque decreases.

To determine the region of linear viscoelastic behaviour, a strain scan test (Fig. 1) was performed, followed by a frequency sweep test (Figs. 2 and 3) in the linear range of strain (the strain range of 1%). Fig. 1 shows the storage modulus versus strain for a sample with carbon black compared to another compound containing a combination of carbon black and nanoclay. As can be seen, the blend containing both particles shows a non-linear behavior at a lower strain, and this indicates the effect of the presence of nanoclay on the rheology of the blend.

Figs. 2 and 3 show the storage modulus and complex viscosity of the samples containing different amounts of nanoclay, respectively. These figures show that with the

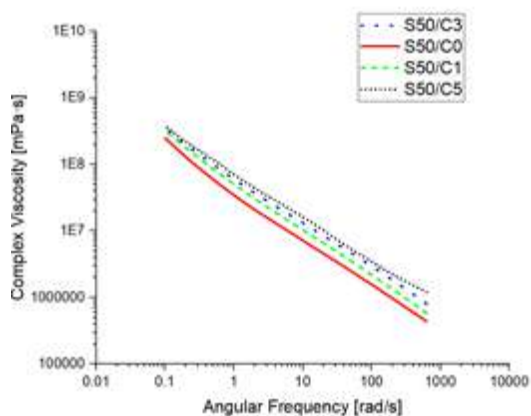


Fig. 2. Complex viscosity of SBR/EPDM SBR/EPDM with different amounts of nanoclay.

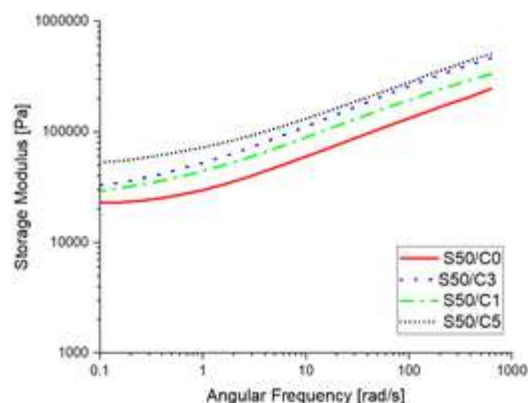


Fig. 3. Storage Modulus of SBR/EPDM with 0, 1, and 3 different amounts of nanoclay.

increase in the amount of nanoclay, the storage modulus as well as the complex viscosity increase. The increase in modulus in the blend containing 5 phr of nanoclay is significant at low frequencies.

Conclusion

In this work EPDM/SBR/Carbon black/Cloisite 15A nanocomposites were prepared and characterized. The obtained results showed that the scorch and optimum cure time values decreased with increasing nanoclay content and the minimum torque of rheometry was increased. This was attributed to the effect of nanoclay on the curing reaction the storage modulus and complex viscosity of the blends increased with the increase in the amount of nanoclay used, and the blend with 5 phr nanoclay showed a noticeable increase in the storage modulus at low frequencies.

References

- [1] A.J.-A. Aida Shoushtari Zadeh Naseri, "Study on the morphology, static and dynamic mechanical properties of (styrene butadiene rubber/ethylene propylene diene monomer/organoclay) nanocomposites vulcanized by the gamma radiation", *Appl. Polym.*, 2016.
- [2] M.G.K.T. Muraleedharan Nair, "Mechanical and aging properties of cross-linked ethylene propylene diene rubber/styrene butadiene rubber blends", *Appl. Polym. Sci.*, **93**, 2606-2621, 2004.
- [3] S.V.G. Anand, *Effect of Nanosilica and Crosslinking System on the Mechanical Properties and Swelling Resistance of EPDM/SBR Nanocomposites with and without TESPT*, Springer, 2020.
- [4] S.V.G. Anand, *Effect of Nanoclay/Nanosilica on the Mechanical Properties, Abrasion and Swelling Resistance of EPDM/SBR Composites*, Springer Nature, 2019.
- [5] A.J.-A. Hedayatollah Sadeghi Ghari, "Nanocomposites based on natural rubber, organoclay and nano-calcium carbonate: Study on the structure, cure behavior, static and dynamic-mechanical properties", *Appl. Clay Sci.*, 2015.

Utilizing Rheometry for Characterizing Cure Shrinkage in Photocurable Resins for Digital Light Processing (DLP) 3D Printing

Atefeh Nejadbrahim^{1*}, Morteza Ebrahimi², and Xavier Allonas³

1. Polymer Engineering Department, Qom University of Technology, Qom, Iran

2. Polymer and Color Engineering Department, Amirkabir University of Technology, Tehran, Iran

3. Laboratory of Molecular Photochemistry and Engineering, University of Haute Alsace, 3b Rue Alfred Werner, 68093 Mulhouse, France

*atefeh.nejadbrahim@gmail.com

Abstract

Shrinkage is a critical phenomenon observed in photo-curable resins utilized in vat photo-polymerization. This study aims to investigate and characterize the shrinkage behavior of two photo-curable systems during the curing process. The research involves employing rheometry measurement technique to quantify the magnitude of shrinkage in these resins. The effects of resin formulation and curing parameters on shrinkage are evaluated to gain deeper insights into this complex phenomenon. The obtained data aids in optimizing resin compositions and printing conditions to minimize shrinkage-related issues, such as dimensional inaccuracies and structural distortions. The findings contribute to advancing the understanding and control of shrinkage in photocurable resins for improved DLP 3D printing capabilities.

Keywords: shrinkage, photo-rheometry, dimensional accuracy, 3D printing, vat photo-polymerization

Introduction

Vat photopolymerization is one of the most popular 3D printing techniques utilizing a light source for solidifying a photopolymer. Digital light processing (DLP), based on vat photopolymerization method, is very similar to lithography and is also known as dynamic mask photolithography. Build time, oxygen sensitivity and adhesion between different layers are improved in this technique. However, vertical resolution, dimensional accuracy, and shrinkage are still the main challenges of 3D DLP-manufactured articles. Shrinkage, was studied by several researchers. For example, Stampfl *et al.* [1] and Schoerpf *et al.* [2] used monofunctional monomers and chain transfer agents and Chiappone *et al.* [3] proposed using acrylate/epoxy hybrid systems to overcome this problem to some extent. However, these strategies caused other problems such as the deterioration of long-term mechanical properties of photo-cured systems and also the requirement of using dual photoinitiator systems (i.e. radical and cationic photoinitiators), respectively. Therefore, in this study, a three-component PIS based on safranin O was employed in digital light processing 3D printing to investigate the dual function of the dye as photosensitizer and photoabsorber. In addition, the effect of curing protocol of this PIS on shrinkage was investigated. The performances of this new three-component PIS regarding resolution and shrinkage were compared to those obtained using trimethylbenzoyl diphenylphosphine oxide (TPO) as photoinitiator.

Experimental

Safranin O (SFH+) (dye content $\geq 85\%$) was purchased from Sigma-Aldrich. Pentaerythritol tetrakis(3-mercaptopropionate) (RSH, 95%) was supplied by Aldrich. Diphenyliodonium hexafluorophosphate (IOD+, 98%) was obtained from TCI. Trimethylbenzoyl diphenylphosphine oxide (TPO) was purchased from Aldrich. Acetonitrile (99.97%) and isopropyl alcohol were received from Biosolve. Ethoxylated (3) bisphenol A diacrylate (SR349) was provided by Sartomer. Dimethyl sulfoxide (DMSO) was purchased from Aldrich to adjust the viscosity of formulations.

DLP Printing System

3D printing tests were conducted using a commercial DLP 3D printer from B9 Creator company (V1.2, B9Creations, USA). The radiation intensity measured at the surface of the vat was 170 mW/cm².

The 3D printer had an XY resolution of 30 μm , the layer thickness was adjusted on 20 μm and each layer was

Table I. Composition of the 3D printing sample formulation.

Sample code	Composition
3KSRD	SR349 /DMSO (10 phr)/ SFH ⁺ (0.2 phr)/ RSH (3 phr)/ IOD ⁺ (3 phr)
1KTPO	SR349/DMSO (10 phr) TPO(1 phr)

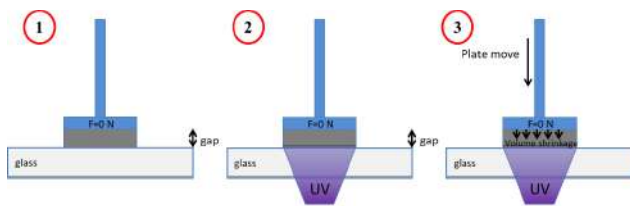


Fig. 2. Schematic representation of the shrinkage measurement apparatus.

exposed to radiation for 6 s, while the exposure time for the first two layers was set to be 30 s. Two formulations for 3D printing were prepared, as shown in Table I.

Shrinkage Measurements

Shrinkage measurements of samples were conducted using an MCR 302 photorheometer from Anton Paar, which was combined with a light source accessory for the curing of samples. The experimental setup is presented in Fig. 2. The test was performed in the oscillation mode of the rheometer. The smooth aluminum plate was fixed at an initial 0.5 mm gap and a zero Newton normal force was applied to samples. The samples were irradiated in the same condition as RT-FTIR analysis. The light was directed under a glass plate by using an optical fiber, which would allow the photopolymerization of samples. The shrinkage of sample led to the gap reduction. So the variation of the gap during the photopolymerization would represent the shrinkage according to Eq. (2), where the d_{final} and $d_{initial}$ are the distance between the glass and aluminum plate at the beginning and end of photopolymerization, respectively.

$$shrinkage(\%) = \left(1 - \frac{d_{final}}{d_{initial}}\right) \times 100 \quad (1)$$

Results and Discussion

As noted earlier, shrinkage in printed parts is an important issue intrinsically due to the free radical photopolymerization. For this reason, the effect of new proposed PIS on the shrinkage was studied by photorheometry technique. As

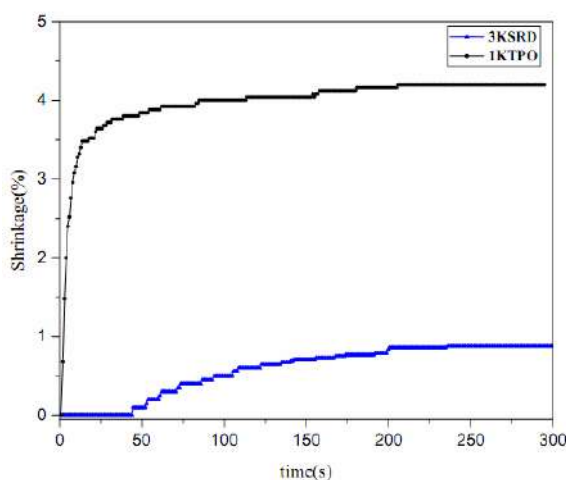


Fig. 3. Effect of PIS on shrinkage.

can be seen in Fig. 3, the linear shrinkage of 3KSRD and 1KTPO were measured to be 0.9 and 4.2%, respectively. It means that the shrinkage of printed part improved significantly when the three-component PIS was used. As the monomer and photopolymerization conditions are almost the same for both samples, different behavior of the two systems could be related to the different photoinitiating systems. In fact, the polymerization rate of 1KTPO system was remarkably higher than that for 3KSRD system which led to a higher inhomogeneity and internal stress formation in the cured sample. It seems that this higher inhomogeneity and internal stress caused a more considerable shrinkage in 1KTPO system. It is worth mentioning that our proposed new three-component PIS (i.e. SFH+/RSH/IOD+) could provide a soft-start curing protocol which caused achieving relatively high conversion and low shrinkage in an appropriate time [4,5].

References

- [1] B. Steyrer, P. Neubauer, R. Liska, and J. Stampfl, *Materials*, **10**, 1445-11456, 2017.
- [2] S. Schoerpf, Y. Catel, N. Moszner, C. Gorsche, and R. Liska, *Polym. Chem.*, **10**, 1357-1366, 2019.
- [3] A. Chiappone, S. Lantean, I. Roppolo, M. Sangermano, and C.F. Piri, *Inventions*, **3**, 29-41, 2018.
- [4] H. Lu, J.W. Stansbury, and C.N. Bowman, *J. Dent. Res.*, **84**, 822-826, 2005.
- [5] N. Emami and K.J. Soderholm, *J. Mater. Sci. Mater. Med.*, **16**, 47-52, 2005.

Investigation on Processability of Polybutylene Adipate Terephthalate (PBAT) for Fused Filament Fabrication (FFF)

Amin Makaremy and Mehdi Rafizadeh*

Department of Polymer Engineering, Amirkabir University of Technology, Tehran, Iran

*mehdi@aut.ac.ir

Abstract

In 3D printing, fused filament fabrication has been widely studied as one of the most common methods. It is essential to determine the suitable polymer and its appropriate grade. The two schools of thought of interlayer penetration and polymer processability are the indicators used in the study, and in both cases, rheology plays a crucial role in determining and distinguishing. In this research, processability has been investigated with two components: entropic and enthalpic. This study evaluated fluidity, the discrepancy of storage and loss modules, and the VGP diagram (phase angle versus complex modulus). Finally, among the two PBAT grades examined, one sample has shown more processability than PBATS.

Keywords: 3D printing, FFF, FDM, PBAT, processability

Introduction

3D printing by fused filament fabrication (FFF) method is considered low cost and similar to conventional processes in the polymer industry [1-3]. In the meantime, according to many studies, printability is still one of the topics of interest, and many researchers have investigated this issue. In addition to this case, considering the importance of biodegradable polymers for environmental pollution, the use of polyesters as an alternative to conventional plastics has been investigated [1,4]. Among polyesters, polybutylene adipate terephthalate (PBAT) can be biodegradable and provides many desired properties due to its copolymer structure and the presence of ester bonds. There are various approaches to check printability, each focusing on a specific part of the process. Two main approaches are the diffusion of printed layers into each other and processability [2,3]. Processability is rooted in the two components of elastic or dissipative fluid behavior. It is essential to check the processability before the diffusion of the layers, and according to it, if there is a problem in this case, it would be possible that the feedstock used cannot be used. In this regard, the preparations for printing these polymers will be examined by studying the processability of two grades of PBAT in this research.

Experimental

Two different grades of PBAT were purchased from BASF and Zhuhai Kingfa Biomaterial: Ecoflex S BX 7025 (PBATH) and ECOPOND A400 (PBATS), respectively.

Results and Discussion

Fig. 1 illustrates the fluidity diagram of materials. In this graph, fluidity is increased with increasing frequency,

which implies shear-thinning behavior. According to this diagram, at 180 °C, the PBATS sample and at 200 °C, PBATH have more fluidity, but it should be known that the viscosity shows both entropic and enthalpic sources. Considering this issue, two materials with the same fluidity can have different melt behavior. Therefore, examining these cases regarding the origin of fluid behavior is essential. Fig. 2 indicates the graphs of G' and G'' at two temperatures of 180 and 200 °C for the two investigated grades. According to this diagram, it can be seen that the PBATS samples intersect at lower frequencies at both temperatures and exhibit solid elastic behavior [5]. This behavior reveals that PBATS has more entanglement or elastic origin than PBATH. The presence of the elastic component resulting from the entropy of the chains mainly leads to viscoelastic failures, which can be considered as an indicator of processability.

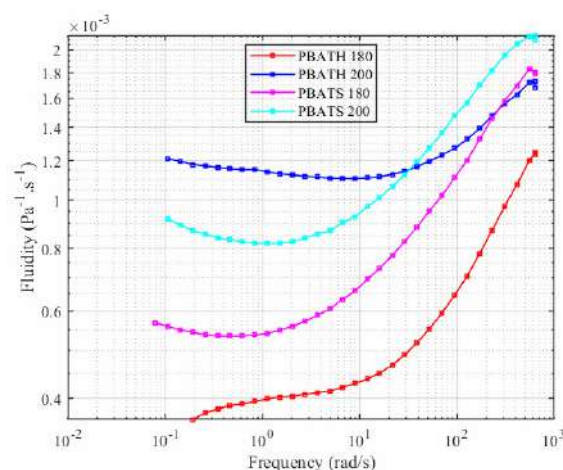


Fig. 1. Fluidity of two samples in 180 and 200 °C.

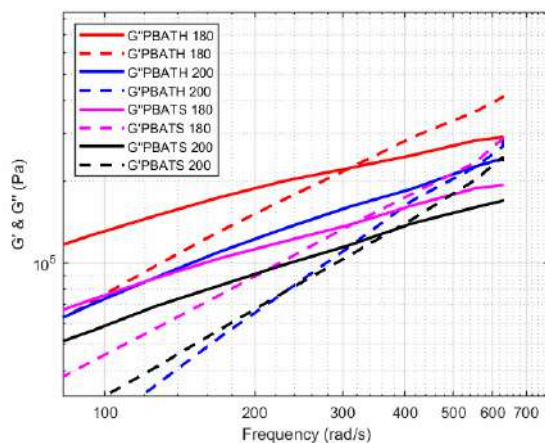


Fig. 2. Intersection of G' and G'' vs frequency.

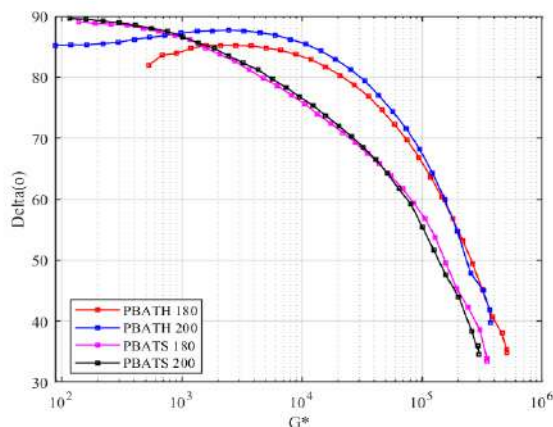


Fig. 3. VGP plot for two samples in 180 and 200 °C.

Fig. 3 shows the VGP diagram or Black diagram. In this graph, where the phase angle is plotted against the complex modulus, angles close to 90 and 0° indicate viscous and elastic behavior, respectively. In the two investigated temperatures, it can be seen in a wide range that the PBATS sample is located at lower angles than the PBATH. Hence, due to the use of pure polymers and the lack of materials with elastic solid behavior, this issue can indicate the elasticity of chains with entropic origin, as explained earlier. According to this criterion, this material is probably less processable than PBATH.

Conclusion

This research used rheology as a powerful tool to understand the origin of fluid behavior. The studies showed that viscosity cannot be a suitable criterion for determining processability alone for FFF despite its high use. With the aid of the intersection of the storage and loss modules, the amount of entanglement and the elastic behavior of two samples were compared at two temperatures of 180 and 200 °C, and the VGP diagram revealed that PBATS has a more elastic behavior in a wide range. Finally, it can be concluded that the PBATH sample is more processable

than the PBATS sample, and consequently, it will be a more suitable candidate for use in the FFF process.

References

- [1] A. Costanzo, D. Cavallo, and C. McIlroy, "High-performance co-polyesters for material-extrusion 3D printing: A molecular perspective of weld properties", *Addit. Manuf.*, **49**, 102474, 2022.
- [2] A. Das, E.L. Gilmer, S. Biria, and M.J. Bortner, "Importance of polymer rheology on material extrusion additive manufacturing: Correlating process physics to print properties", *ACS Appl. Polym. Mater.*, **3**, 1218-1249, 2021.
- [3] D. Vaes and P. Van Puyvelde, "Semi-crystalline feedstock for filament-based 3D printing of polymers", *Prog. Polym. Sci.*, **118**, 101411, 2021.
- [4] M.V. Candal et al., "Thermo-rheological effects on successful 3D printing of biodegradable polyesters", *Addit. Manuf.*, **36**, 101408, 2020.
- [5] Y. Lyu, Y. Chen, Z. Lin, J. Zhang, and X. Shi, "Manipulating phase structure of biodegradable PLA/PBAT system: Effects on dynamic rheological responses and 3D printing", *Compos. Sci. Technol.*, **200**, 108399, 2020.

Evaluating Interlayer Penetration of Polybutylene Adipate Terephthalate (PBAT) for Fused Filament Fabrication (FFF)

Amin Makaremy, Sina Bazrpash, and Mehdi Rafizadeh*

Department of Polymer Engineering, Amirkabir University of Technology, Tehran, Iran

*mehdi@aut.ac.ir

Abstract

3D printing, especially FFF, has received much attention among the various polymer processing methods. In this method, it is necessary for the layers of the components to penetrate each other and thereby increase the final properties of the printing part. Various methods have been devised to evaluate this issue, but the importance of knowing this issue before doing the process is much greater. For this reason, rheology was used to evaluate the materials due to the molten nature of the materials in this process. According to Reptation theory, with the help of storage modulus, zero-shear viscosity, and the Cole-Cole diagram, the relaxation time was investigated in two PBAT samples. Finally, it was determined that at 180 °C, the PBATS sample, and at 200 °C, PBATH would have the lowest relaxation time and the highest penetration.

Keywords: 3D printing, FFF, PBAT, interlayer penetration, relaxation time

Introduction

There are several methods to process polymers; extrusion, injection, compression molding, and 3D printing are among these methods. 3D printing has attracted attention for reducing costs, material waste, and high speed. Among the 3D printing methods, the fused filament fabrication (FFF) method is the most widely used due to its more straightforward construction and lower price. On the other hand, polyesters have been studied extensively due to the importance of plastics' biodegradability and suitable properties. In the family of polyesters, polybutylene adipate terephthalate (PBAT) as an aliphatic-aromatic co-polyester has been researched in recent years [1-3]. Along with those mentioned above, finding a way to evaluate the material before the process is critical. Different criteria have been proposed to check the printability of the sample; viscosity, entanglement number, and relaxation time are among these criteria. Despite these cases, a comprehensive procedure for investigating pure polymers has not been introduced. However, we can investigate this issue with diffusion depth and processability. Viscosity, Cole-Cole diagram, and relaxation time spectrum can be used to discuss diffusion. In this research, the diffusion criteria will be investigated with the help of rheological tests in two PBAT grades [3-5].

Experimental

Two different grades of polybutylene adipate terephthalate (PBAT) were purchased from BASF and Zhuhai Kingfa Biomaterial: Ecoflex S BX 7025 (PBATH) and ECOPOND A400 (PBATS), respectively.

Results and Discussion

Fig. 1 shows the storage modulus behavior of two samples

at high frequencies. According to this diagram, it can be understood that all samples converge to a relatively specific value at high frequencies, which is located at the beginning of the rubbery zone. In addition to this issue, considering the dynamics of chains above the entanglement threshold, which is Reptation type, could be used to evaluate the relaxation time, which is a criterion of diffusion ($\tau_n = \eta_0/G_0$); it is only enough to check the value of zero shear viscosity. Fig. 2 shows the graph of viscosity in terms of frequency. In this graph, two different grades have shown shear-thinning behavior at 180 and 200 °C temperatures. Also, in all samples, the viscosity decreased with increasing temperature. The PBATH sample has shown more changes with temperature, and the slope of viscosity reduction with frequency has also been higher. According to the graph, the zero-shear viscosity at 180 °C is higher in the PBATH sample, and at 200 °C, the PBATS sample has a higher

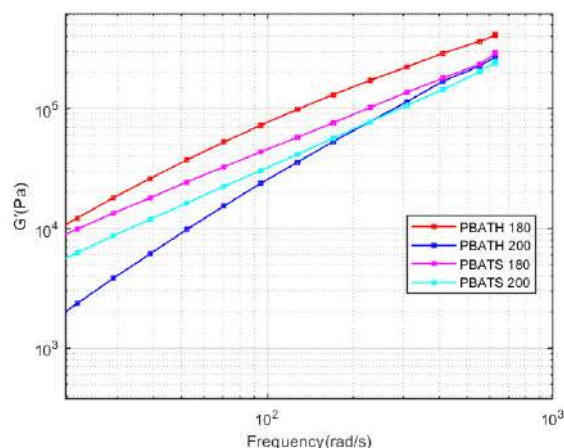


Fig. 1. Storage modulus of two samples in 180 and 200 °C.

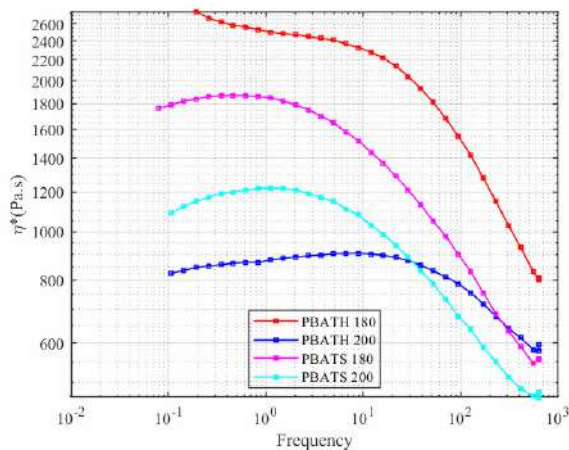


Fig. 2. Complex viscosity of two samples in 180 and 200 °C.

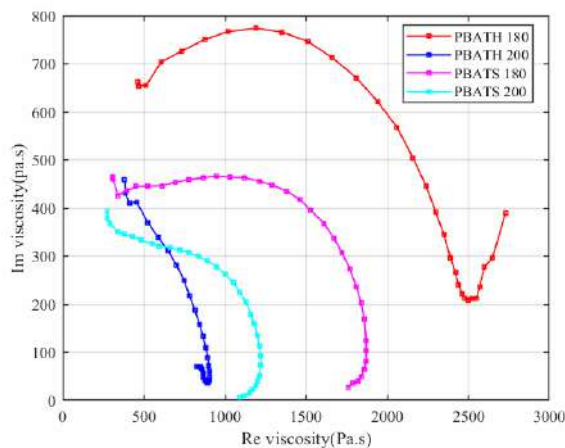


Fig. 3. Cole-Cole plot for two samples in 180 and 200 °C.

value. Generally speaking, the diffusion will be higher for PBATS and PBATH at 180 and 200 °C, respectively. In addition to this issue, it is still necessary to use the Cole-Cole diagram to better investigate a broader range of frequencies. Cole-Cole diagram shows imaginary viscosity in terms of real viscosity. In this diagram, the relaxation time of the chain is reduced by reducing the radius of semicircles seen in viscoelastic materials. According to Fig. 3, it can be seen that the samples of both materials show a decrease in relaxation time as the temperature increases and also confirms the Points mentioned in the previous section. Considering all the noted cases, it can be concluded that at 180 and 200 °C, respectively, PBATS and PBATH grades show better interlayer penetration.

Conclusion

This research investigated interlayer penetration as a measure of printability in the FFF process. Specifically, due to the presence of materials in the molten phase and the movement of polymer chains based on Reptation, rheology was used as a powerful method for evaluation. With the help of loss modulus, viscosity, and Cole-Cole graph, relaxation

or Reptation time was investigated. According to the viscosity plot, storage modulus, and zero shear viscosity, it was determined that PBATS and PBATH samples would have the lowest relaxation time and the highest penetration at temperatures of 180 and 200 °C, respectively. Besides that, relaxation time in the frequency range was checked in the Cole-Cole diagram, and generally, the same results were obtained on a broader frequency range. Finally, it was concluded that at 180 °C, PBATS samples and at 200 °C, PBATH samples show the lowest relaxation time and the highest penetration.

References

- [1] D. Vaes and P. Van Puyvelde, "Semi-crystalline feedstock for filament-based 3D printing of polymers", *Prog. Polym. Sci.*, **118**, 101411, 2021.
- [2] A. Costanzo, D. Cavallo, and C. McIlroy, "High-performance co-polyesters for material-extrusion 3D printing: A molecular perspective of weld properties", *Addit. Manuf.*, **49**, 102474, 2022.
- [3] A. Das, E.L. Gilmer, S. Biria, and M.J. Bortner, "Importance of polymer rheology on material extrusion additive manufacturing: Correlating process physics to print properties", *ACS Appl. Polym. Mater.*, **3**, 1218-1249, 2021.
- [4] M.V. Candal et al., "Thermo-rheological effects on successful 3D printing of biodegradable polyesters", *Addit. Manuf.*, **36**, 101408, 2020.
- [5] Y. Lyu, Y. Chen, Z. Lin, J. Zhang, and X. Shi, "Manipulating phase structure of biodegradable PLA/PBAT system: Effects on dynamic rheological responses and 3D printing", *Compos. Sci. Technol.*, **200**, 108399, 2020.

Effect of Rheology Properties on the Printability of Temperature Sensitive and Polyelectrolyte Hydrogels

Naeim Janatsharifi¹, Somaye Akbari¹, Sarah Rajabi², and Shadab Bagheri-khoulenjani^{1*}

1. Department of Polymer Engineering, Amirkabir University of Technology, Tehran, Iran

2. Stem Cell Research Institute, Royan Research Institute, Tehran, Iran

*s.bagheri@aut.ac.ir

Abstract

Design and fabrication of bioinks is crucial in a successful 3D-bioprinting process. In this paper, temperature-sensitive polyelectrolyte hydrogels suitable for extrusion-based 3D-bioprinters were prepared based on (carrageenan), polyelectrolyte (Carboxymethyl chitosan) and dendrimer nanostructures (dendrimer), and its rheological properties and printability were investigated. In the temperature sweep test, the UCST behavior of the carrageenan polymer was observed at the optimum point of 38 °C, in the frequency sweep test, the formation of hydrogel was ensured, and in the flow curve test, the ability of shear thinning was observed. Then the printability of the printed filaments was checked with an optical microscope and the ImageJ program, and the speed of the nozzle movement (200 mm/s) and its flow rate (0.75×10^{-4} mL/s) were selected.

Keywords: 3D printing, rheology properties, polyelectrolyte, temperature sensitive

Introduction

Polymeric scaffolds are porous structures used in tissue engineering for cell growth and tissue construction. Nowadays, 3D bioprinting is one of the most common methods for fabricating scaffolds due to the ability to print cells and a wide range of biological materials with varying viscosities. Extrusion-based 3D bioprinting is one of the bioprinting methods. In bioprinting based on extrusion, materials with various rheological properties can be used, such as shear thinning and temperature sensitive materials [1]. Bioinks are solutions of biomaterials containing living cells. Carboxymethyl chitosan, carrageenan and dendrimer nanostructures [2] are frequently utilized in various biomedical applications due to their unique properties such as biocompatibility, sensitivity to temperature, and the ability to form gels at specific temperatures and conditions. Hydrogels are materials widely used in bioink preparation, but their rheological properties should be optimized for improving the printability of the bioinks. Hydrogels that made from polyelectrolytes and temperature-sensitive materials are a type of reversible physical hydrogel. In this research, the aim is to prepare and investigate the rheological properties of temperature sensitive bioink, which can be used in an extrusion-based 3D printing [3].

Experimental

Carboxymethyl chitosan (CMCh) was synthesized by previous studies [4]. 2.5 w/v% of CMCh (C), 1% dendrimer nanostructures (D) and 1% carrageenan (K) were dissolved separately in distilled water at a temperature of 50 °C and then mixed together. Following are the tests conducted with RMS model MCR 302 Anton Paar. In order to test the thermodynamic behavior of Bioink, a temperature sweep test was conducted at an angular frequency of 10 rad/s and a strain of 0.5%, then to examine the gel formation, a frequency sweep test was taken in the range of 0.1 rad/s to 100 rad/s at a strain of 0.5% and a temperature of 37 °C.

To check the shear-thinning, a flow curve test was performed at 37 °C. A Nikon Eclipse E200 optical microscope was used to perform the printability tests. The diameters were measured using the ImageJ program to measure the filament diameter.

Results and Discussion

3.1 Temperature Sweep

UCST behavior of carrageenan polymer is illustrated in Fig. 1. The optimal temperature for this compound is 38 °C. According to this graph, even after reaching the plateau area, the storage modulus remains higher than the loss modulus. It is assumed that this is due to the formation of electrostatic interaction between dendrimer nanostructures and other polymers present in the hydrogel.

3.2 Frequency Sweep

Fig. 2 shows the results of the frequency sweep test.

Fig. 1 indicates that between 0.1 and 100 rad/s, the storage

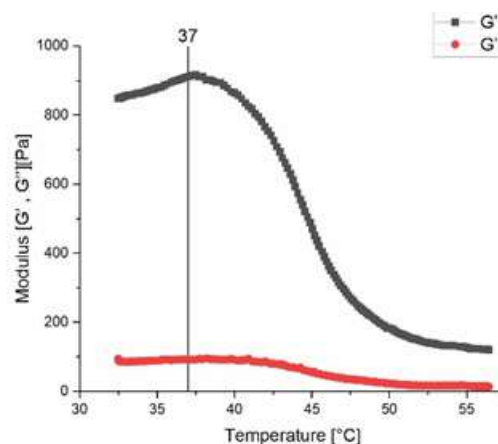


Fig. 1. Temperature sweep test results.

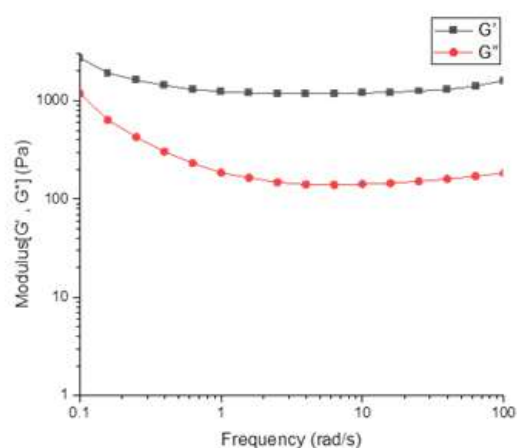


Fig. 2. Frequency sweep test results.

modulus (G') is higher than the loss modulus (G''), and then reaches its plateau region, indicating that successful hydrogel formation has occurred.

3.3 Flow Curve

Additionally, this test was conducted to determine whether the hydrogel had shear-thinning properties. With electrostatic interaction, the hydrogel's viscosity is reduced from 4200 Pa.s to below 1 Pa.s (Fig. 3). This indicates that the shear-thinning characteristic has been successfully created in the bioinks. This feature makes the bioinks suitable for extrusion 3D-printing although in the process temperature ($37\text{ }^\circ\text{C}$) the hydrogel is fully formed. It can be easily extruded from the nozzle using this feature.

3.4 Printability

After selecting the print temperature ($37\text{ }^\circ\text{C}$). In order to determine the most optimal speed and flow rate for printing the bioink mentioned above, a variety of speeds and flow rates were tested. Fig. 4 shows photos of the printed filaments and the ratio of the diameter of the printed filament to the defined diameter (U).

Fig. 4a shows the U number. The closer it reaches 1, the better the printability. The green area in the diagram represents the area close to 1. In Fig. 4b, microscopic photos of the filaments can be seen. It shows a suitable print at different speeds and flow rates.

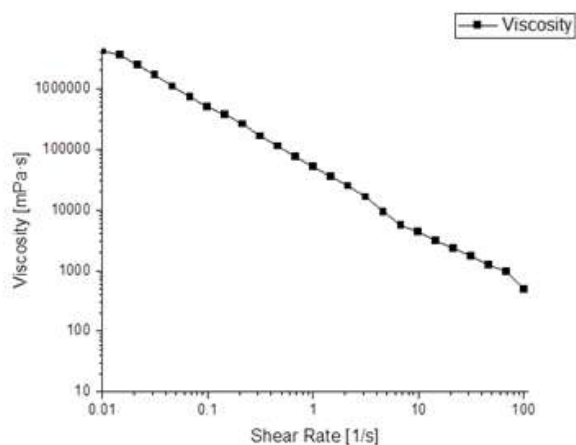
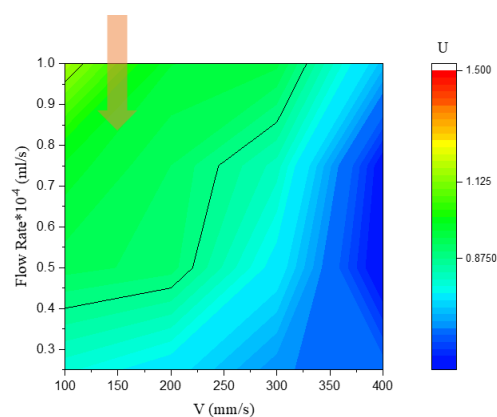
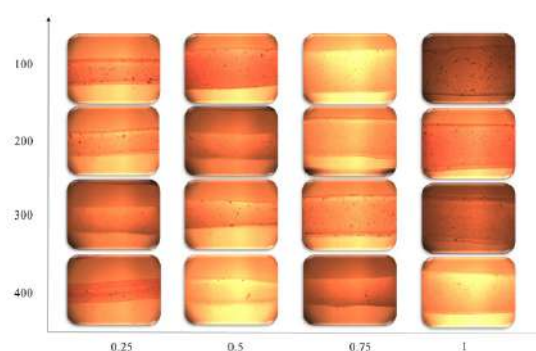


Fig. 3. Flow curve test results.



(a)



(b)

Fig. 4. Printability of hydrogel.

Conclusion

In this article, bioink printability was investigated using rheological studies, including flow curve, frequency sweep, and temperature sweep. The microscopic photograph and the U number were used to check the sample's printability. Speed of 200 mm/s and a flow rate of 0.75×10^{-4} mL/s were selected as optimal parameters.

References

- [1] Z. Zahedi-Tabar, S. Bagheri-Khoulenjani, H. Mirzadeh, and S. Amanpour, "3D in vitro cancerous tumor models: Using 3D printers", *Med. Hypotheses*, **124**, 91-94, 2019.
- [2] M. Delyanee, S. Akbari, and A. Solouk, "Amine-terminated dendritic polymers as promising nanopatform for diagnostic and therapeutic agents' modification: A review", *Eur. J. Med. Chem.*, **221**, 113572, 2021.
- [3] F. Hosseini, B. Nyström, S.A. Sande, and S. Bagheri-Khoulenjani, "Printability Study of Polyelectrolyte Bioinks Based on Chitosan, ISPST, 2022.
- [4] N. Olov, H. Mirzadeh, R. Moradi, S. Rajabi, and S. Bagheri-Khoulenjani, "Shape memory injectable cryogel based on carboxymethyl chitosan/gelatin for minimally invasive tissue engineering: In vitro and in vivo assays", *J. Biomed. Mater. Res. Part B: Appl. Biomater.*, **110**, 2438-2451, 2022.

Effect of Particle Shape on the Network Structure of Well-Dispersed Nanocomposites of Graphitic Nanoparticles in PVDF

Mohammad Babaei, Mohammad Heydarnejad Moghadam, and Fatemeh Goharpey*
Department of Polymer Engineering, Amirkabir University of Technology, Tehran, Iran

*goharpey@aut.ac.ir

Abstract

Polymer nanocomposites, comprising PVDF and graphitic nanoparticles like MWCNT and graphene, are essential for advancing high-dielectric-permittivity flexible materials. The current study explores how the shape of nanoparticles influences their network structure and consequently their electrical and dielectric performance. Nanocomposites are made using a solvent casting method with a mixture of solvents designed according to Hansen's solubility parameters. Frequency sweep measurements demonstrate both MWCNT and graphene-based nanocomposites achieve well dispersion with low rheological percolation thresholds. However, they exhibit different network characteristics. In contrast to MWCNT/PVDF nanocomposites, where carbon nanotubes are responsible for load bearing, in graphene/PVDF nanocomposites, polymer chains contribute to the formation of the load-bearing network. Also, Graphene/PVDF nanocomposites display a two-step yielding process in strain sweep measurements for storage modulus due to their possible aggregation resulting from the sheet-like shape and π - π interactions. In contrast, MWCNT/PVDF exhibits a monotonically decreasing storage modulus, indicating a more robust and strain-sensitive network. These observations are in accordance with the results of gel-fractal model calculations. The network of carbon nanotubes has a lower fractal dimension with more inter-floc elastic bonds, coming to the network of graphenes with the higher dead arms and fractal dimension and also the higher portion of intra-floc bonds. The fundamental difference of these networks originates from the entanglement ability of nanotubes, which is absent for graphene nanosheets, resulting in a more efficient and more complex network for MWCNTs, which is confirmed by the electrical conductivity measurements.

Keywords: graphitic nanoparticles, dielectric performance, network structure, gel fractal model, entanglement ability

Introduction

Polymer nanocomposites based on polyvinylidene fluoride (PVDF) and graphitic nanoparticles, (for example multi-walled carbon nanotube, MWCNT, and graphene) are of great importance due to their crucial role in the progress of flexible materials with high dielectric permittivity and energy storage applications [1]. However, the excellent performance of resulting nanocomposites for the aforementioned applications is highly dependent on the network structure and dispersion state of nanoparticles [2]. Among the various parameters, shape, dimensions, and surface chemistry of nanoparticles can strongly impress the nanoparticles network and subsequent electrical and dielectric properties. Accordingly, in the current investigation, linear and non-linear rheology are utilized to access the dispersion state of polymer nanocomposites comprising MWCNT and graphene. In continuation, the network structure of nanoparticles is quantified in terms of percolation theory and gel-fractal model for each case.

Experimental Section

For improving the interaction between polymer matrix and nanoparticles and also the achievement of well dispersion state, MWCNTs (grade NC7000 Nanocyl) and graphenes (grade N002PDR Angstrom) are subjected to the identical mild oxidation procedure. Accordingly, 1.0 g

of nanoparticles are refluxed in a mixture of concentrated HNO_3 and H_2SO_4 at 95 °C for 24 h and then are washed with excess values of deionized water. The obtained nanoparticles then are put in an oven and then in a vacuum oven each for 24 h at 60 °C. PVDF-based nanocomposites are prepared by employing a solution casting method using a mixture of DMF and DMSO (both are known solvents for PVDF). The composition of DMF/DMSO is determined based on the criterion where the dispersion of the desired nanoparticle has the most stability. Rheological measurements are performed using an Anton Paar MCR302 rheometer at 200 °C using a 25 mm parallel plate geometry. Frequency sweep measurements are conducted at a strain of 0.1% and strain sweep measurements are performed at a frequency of 1 rad/s. All samples are pre-heated for around 15 min before measurements.

Results and Discussion

As can be seen in Fig. 1, according to the frequency sweep measurements, both PVDF-based nanocomposites of MWCNT and graphene demonstrate a well-dispersion state with increasing solid-like behavior as the fraction of particles increases. Evaluating the values of G' at low frequencies using percolation theory $[G' \propto (f - f_c)^v]$ leads to the rheological percolation threshold (f_c) of 0.02 and 0.17 wt%, and critical exponent (v) of 2.07 and 1.67 for

MWCNT/PVDF and graphene/PVDF nanocomposites, respectively. The very low values of the percolation threshold confirm the ideal dispersion of both particles in PVDF. Meanwhile, according to the values of critical exponent it can be claimed that although nanotubes have a significant impact on the load-bearing network of the MWCNT/PVDF systems, in the graphene/PVDF nanocomposites, polymer chains contribute to the formation of the load-bearing network. The strain sweep results are also depicted in Fig. 1. A two-step yielding process is observable for storage modulus at high concentrations of graphene, while the trend for storage modulus of MWCNT/PVDF nanocomposites is monotonically decreasing. These observations can be connected to the possible aggregation of graphene sheets resulting from their sheet-like shape and π - π , while MWCNTs show a more robust and more strain-sensitive network [2]. The network structure of nanoparticles also can be evaluated using the modified gel-fractal model by the following equations:

$$G' \propto f^{\frac{\beta}{3-d_f}} \quad \text{and} \quad \gamma_c \propto f^{-\frac{\beta-2}{3-d_f}}$$

$$\beta = 1 + (2 + x), (1 - \alpha)$$

where d_f , x , and α are the fractal dimension of flocs, backbone fractal dimension, and a constant between 0 and 1, respectively. The modified form of the gel-fractal model is helpful when the behavior of systems does not match the strong-link or weak-link regimes behavior ($\alpha=0$ shows strong-link regime and $\alpha=1$ exhibits weak-link regime). The resulting d_f and α values for MWCNT/PVDF are 1.70 and 0.32, while they are 1.94 and 0.41 for graphene/PVDF nanocomposites. These results are in accordance with the previous observations about the network structure of nanoparticles. The network of carbon nanotubes has a

lower fractal dimension with more inter-floc elastic bonds, coming to the network of graphenes with the higher dead arms and fractal dimension and also the higher portion of intra-floc bonds. In addition, a higher constant of α for graphene/PVDF nanocomposites, demonstrates that its network is more similar to those predicted in the weak-link regime with large clusters, leading to the two-step yielding process. The fundamental difference between these networks originates from the entanglement ability of nanotubes [3], which is absent for graphene nanosheets. The existence of entangled nanotubes in the load-bearing network of MWCNT-PVDF results in a more efficient and more complex network which can be confirmed by the electrical conductivity measurements (critical exponent of 4.66 is observed for electrical percolation of MWCNT/PVDF, compared to 2.61 for graphene/PVDF).

Conclusion

In summary, this study reveals distinct network characteristics between MWCNT/PVDF and graphene/PVDF nanocomposites. While both show good dispersion and low percolation thresholds, the load-bearing network of MWCNTs primarily relies on the nanoparticles, although polymer chains assist graphene networks in the formation of the load-bearing network in graphene/PVDF nanocomposites. In addition, the high surface area and sheet-like structure of graphenes lead to a two-step yielding process at high concentrations, contrasting with the monotonically decreasing trend in MWCNT/PVDF nanocomposites. These findings align with gel-fractal model calculations and are attributed to differences in fractal dimensions and bonding characteristics, driven by the entanglement ability of nanotubes.

References

- [1] S. Sadeghi et al., *J. Rheol.*, **64**, 6, 2020.
- [2] M. Heydarnejad Moghadam et al., *ACS Appl. Nano Mater.*, **5**, 11, 2022.
- [3] K.L. White et al., *Polymer*, **84**, 2016.

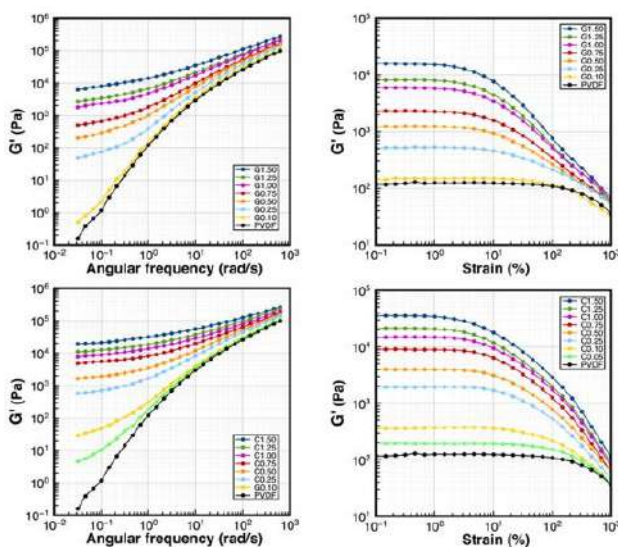


Fig. 1. Frequency and strain sweep measurements of PVDF-based nanocomposites comprising graphene (up) and MWCNT (down).



Evaluation the Effect of Multiwall Carbon Nanotube on Microphase Separation of Poly(ester-ether) Based Polyurethane Prepared via In Situ Polymerization

Babak Karimi Gobaktappeh*, Vahid Haddadi-Asl, Milad Saadat Tagharoodi, Iman Sahebi Jouibari
Department of Polymer Engineering and Color Technology, Amirkabir University of Technology,
Tehran, Iran

*karimi97@aut.ac.ir

Abstract

In this research, we investigated the effect of carbon nanotubes on microphase separation properties of polyurethane nanocomposites based on poly(ester-ether) polyol synthesized via in situ polymerization method under laboratory conditions. ATR-FTIR analysis showed successful synthesis of polyurethane nanocomposite. Time sweep analysis was used to evaluate the micro-phase separation the results showed an improvement in microphase separation between the soft and hard segments, and the acceleration of the phase separation kinetics due to the use of carbon nanotubes as a nucleating agent was observed.

Keywords: polyurethane, microphase separation, carbon nanotube, in situ polymerization

Introduction

Thermoplastic polyurethanes (TPUs) are a new class of soft materials, they have received tremendous attention due to their unique and tunable properties. TPUs represent a variety of properties thanks to the concurrent presence of hard segments (HS) with high polarity and soft segments (SS) with less polarity in their structure [1-3]. One of the most intriguing properties of TPUs is their microphase separation characteristics, arising from incompatibility between the HS and SS [2]. Due to differences in chemical structure and thermodynamic incompatibility of the HS and SS at low temperature, microphase separated domains are observed in most polyurethanes [2,3]. SS with low glass transition temperature and high flexibility acts as continuous phase and HS with high glass transition temperature and high polarity acts as dispersing phase and controlling the properties like thermal and chemical resistance [3]. The engineering properties of TPU are intensely dependent on the content of the microphase separation and morphology of the microphase separated domains. Many factors like polymerization procedures, chemical nature of the HS and SS, process parameters (melting rate, cooling rate, shear rate, temperature, etc.) affect the morphology and microphase separation of the polyurethanes elastomer [3]. The combination of nanoparticles with TPUs has attracted a lot of interest because of the selective affinity of the nanoparticles to one of the two segments. Accordingly, plenty of research has focused on the effect of nanoparticles on dynamic mechanical, rheological, electrical, and phase separation properties of the resulting nano-composites. Consequently, higher aspect ratio nanofillers are good for larger reinforcement. Carbon nanotubes (CNTs) are the best choice in this regard due to their high aspect ratio and

large interfacial area and can effectively change microphase separation in polyurethanes [1]. The aim of this work is to investigate the effect of carbon nanotube on microphase separation kinetic of polyurethane nanocomposites by rheological analysis.

Experimental

Materials: Polytetramethylene ether glycol (PTMEG) and Polycaprolactone with average molecular weight of 2000 g/mol, 1,4-Butane diol were purchased from Sigma Aldrich. DMAc as solvent, hexamethylene diisocyanate (HDI) were prepared from MERCK company, and Multiwall carbon nanotube with average diameter of 20-30 nm was purchased from Nanocyl.

Sample Preparation: Polymerization process was carried out in a two necked reactor under nitrogen gas in a heating oil bath at 80 °C. polyols and HDI were dried in a vacuum oven for 4 h at 85 °C. the molar ratio of polyol, isocyanate and chain extender were considered 1/3/2 respectively. First of all DMAc and polyols were added to the reactor and HDI was added dropwise to the solution and reacted with polyol under continuous stirring at 75 °C for 3 h until prepolymer was formed. For chain extending step, BDO was added dropwise to the content, after 3 h the high viscous liquid was poured into a preheated silicone mold and placed in an oven at 85 °C for 24 h. The last step was removing samples from silicon mold and storing at room temperature for 1 week. To prepare the nanocomposites, the nanoparticle with different weight percent (0.2 and 0.6 wt%) were dispersed in the solvent under ultrasonic conditions. The dispersion was added to the polymerization media after the addition of the chain extender. Finally, the polymerization was terminated after 2 h.

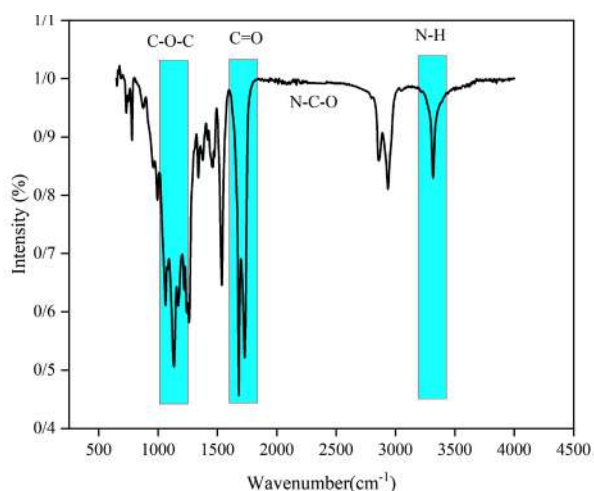


Fig. 1. ATR-FTIR spectrum of pure sample.

Results and Discussion

ATR-FTIR analysis was used to detect hydrogen bonding in this research. Fig. 1 shows the ATR-FTIR of pure sample of TPU. As it's shown, absorption peaks located at 1680 and 1730 cm^{-1} corresponding to free and hydrogen bonded of carbonyl groups (C=O stretching) respectively and peaks at 3200-3350 cm^{-1} corresponds to N-H groups of urethane linkage [2,3]. There is no peak at 2270 cm^{-1} that shows complete consumption of isocyanate groups. The characteristic peaks of synthesized TPUs are in line with the other reports in the literature and showing successful synthesis of polyurethane [1-3].

Rheometric mechanical spectrometer (RMS) is one of the best tools to study the viscoelastic behaviour of polyurethane nanocomposites in molten state. Time sweep analysis represents the rheological evolutions of a sample over time at fixed temperature. Fig. 2 shows time sweep analysis of thermoplastic poly-urethane nanocomposites with 0.2 and 0.6 wt% carbon nanotube. It has to be noted that nanocomposite with higher amount of CNT possess

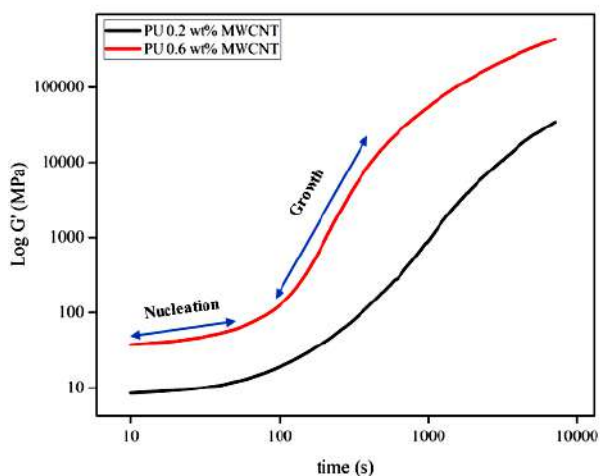


Fig. 2. Time sweep analysis of polyurethane nanocomposites.

Table I. The results of time sweep analysis.

Sample	G'_0 (Pa)	G'_∞ (Pa)	IG'
TPU 0.2 wt% CNT	25.57	185670	7260.24
TPU 0.6 wt% CNT	33.54	438870	13083.42

higher initial modulus. The first plateau is related to nucleation of microphase separation process and the sudden increase in modulus is related to the growth of microphase separated domains. As the amount of nanotube increases the first plateau gets shorter and it means by incorporation of higher amount nanotubes an acceleration in microphase kinetic has been occurred. Factors that help nucleation process decrease the first plateau and factors that aid the growth process increase the slope of the storage modulus [1]. The extent of microphase separation process, can be quantified using increment in storage modulus during time sweep analysis by following Eq. (1):

$$IG' = G'_\infty - G'_0 / G'_0 \quad (1)$$

The results are summarized in Table I as it is shown the extent of microphase separation is gradually increased because of presence of nanotubes and forming reach microphase domains.

Conclusion

Thermoplastic polyurethane/MWCNT (TPUs) have been synthesized by in situ polymerization. The analysis of microphase separation of both samples with ATR-FTIR spectra and the result showed successful synthesis of polyurethane. Time sweep analysis showed an enhancement in micro-phase separation kinetic of nanocomposites by increasing nanotube content because of nucleating effect of carbon nanotubes for hard segments.

References

- [1] I. Sahebi Jouibari, V. Haddadi-Asl, A. Esmaili, S. Shahsavari, F. Mohammadzadeh, M. Gholami, and A. Mohammadi Hatam, *Iran. Polym. J.*, **28**, 801-811, 2019.
- [2] M. Mirhosseini, V. Haddadi-Asl, and I. Sahebi, *Mater. Res. Express*, **6**, 065314, 2019.
- [3] I. Yilgör, E. Yilgör, and G.L. Wilkes, *Polymer*, **58**, A1-A36, 2015.

Investigation of Curing Behavior of SR and SEBS in the Presence of Copolymers Using Rheometer

Ehsan Alikhani and Mohsen Mohammadi*

Department of Polymer Engineering, Qom University of Technology, P.O. Box 3718146645, Qom, Iran

*mohsen.mohammadi@gmail.com

Abstract

In this work, the effect of adding small amounts of EVA and SEBS-g-MA copolymers on the cure characteristics of SEBS and SR was investigated. The polymers including 6 parts of the copolymers were prepared by melt mixing method. The moving die rheometer results showed that the presence of these two copolymers can significantly improve the crosslinking and cure behavior of SEBS. However, their improving effect seen in SEBS was not seen in SR. The presence of EVA and SEBS-g-MA caused a decrease in the curing rate and crosslink density of SR, compared to its pure state.

Keywords: chemorheology, silicone rubber, SEBS, crosslinking

Introduction

Study of crosslinking of a polymer melt compound via chemorheology reveals valuable information on curing characteristics of the materials. Various factors affect the crosslinking such as additives, compatibilizers, fillers and processing conditions. SR and SEBS, are among the most widely used polymers with unique properties such as excellent aging resistance and good thermal stability [1]. In this research, it has been tried to investigate the effect of adding EVA and SEBS-g-MA copolymers on the cure characteristics of different elastomers such as SR and SEBS.

Experimental

Materials

SR (NE-5280) having a density of 1.25 g/cm³ obtains from Djsilicone Co., Ltd. Tri-block copolymer SEBS (Globalprene-7550U), with 30 wt% styrene units and density 0.91 g/cm³, is supplied by LCY Co., Ltd. EVA (ES28005) included of 28% vinyl acetate and density 0.95 g/cm³ is from LG chem. SEBS-g-MA (FG1901) with 30 wt% styrene units and 1.8% maleic anhydride is supplied by Kraton Co., Ltd. Peroxide curing agent BIPB (Bis (tert- butylproxyl isopropyl) benzene) with a purity (percent assay) of 97% is from Rhein Chemie Co., Ltd.

Preparation of the Samples

The mixing is done at 190 °C at a rotor speed of 60 rpm for 8 min for all samples (Step-2). Formulations of all the blends are given in Table I. The blends are then mixed with peroxide curing agent for 5 min at 70 °C and 60 rpm (Step-3).

Table I. Formulation of the samples.

Name	SEBS (phr)	SR (phr)	SEBS-MA (phr)	EVA (phr)
Pure SEBS	100	0	0	0
Pure SR	0	100	0	0
SEBS/6S-MA	100	0	6	0
SEBS/6E	100	0	0	6
SR/6S-MA	0	100	6	0
SR/6E	0	100	0	6

Rheometry

The cure characteristics of the blends are studied by a moving die rheometer (SMD-200, Santam Co., Ltd.). This test is executed at a frequency of 1.68 Hz, a temperature of 175 °C, and an amplitude of 0.5° for 20 min. The cure rate of the blends is calculated as follows [1]:

$$\text{Cure rate} = (\text{Optimum cure time torque} - t_{s_2} \text{ torque}) / (\text{Optimum cure time} - t_{s_2})$$

Results and Discussion

Fig. 1 and Table II indicate the rheograms and information obtained from them, respectively. Modification of hydrogenated polymer chains such as SEBS with materials such as maleic anhydride increases chain reactivity [2]. Pavlovsky and Siegmann [2] used SEBS-MA as the main substrate to improve the curing characteristics of SEBS. Therefore, it can be expected that the addition of SEBS-MA to the blends, can have a positive effect on the cure

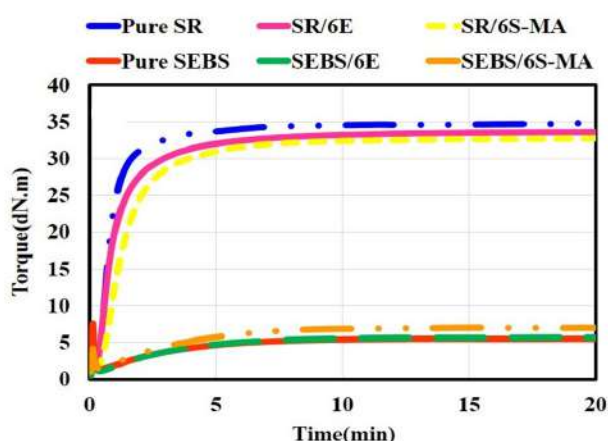


Fig. 1. Time dependency of torque for the samples during curing obtained from the rheometer.

behavior of the SEBS in the blends. Comparing the cure behavior of Pure SEBS and SEBS/6S-MA, it is clear that the presence of SEBS-MA in SEBS rises ΔM , crosslink density (CLD) and its cure rate. The improving effect of SEBS-MA on the cure behavior of Pure SEBS can be justified due to the higher reactivity of SEBS-MA compared to pure SEBS. In this way, SEBS-MA is well dispersed in the pure SEBS and with its greater reactivity, it causes better distribution and more of crosslinks in the SEBS polymer. Meanwhile, the comparison of Pure SR and SR/6S-MA shows that the addition of SEBS-MA caused a decrease in ΔM and also the cure rate of SR. The cure rate and ΔM of SR is much higher than SEBS [1]. Consequently, despite the difference in the cure rate and ΔM of SEBS and SEBS-MA, it is expected that the cure rate and ΔM of SR is still higher than SEBS-MA. Therefore, it is obvious that adding SEBS-MA to SR will decrease its cure rate and ΔM . To better understand the effect of EVA on the curing process of pure components, Pure SEBS and Pure SR compared with SEBS/6E and SR/6E blends. The chain of EVA is actually like as LDPE that has polar groups of vinyl acetate. The presence of vinyl acetate polar groups in the EVA chains makes this polymer have higher chemical activity than polyethylenes

Table II. Cure characteristics of the samples.

Name	T_{s2} (min)	T_{90} (min)	M_H (dN.m)	ΔM (dN.m)	Rate of Cure (dN.m/min)
Pure SEBS	2.50	8.01	5.53	4.18	0.35
Pure SR	0.38	2.22	34.91	33.66	15.43
SEBS/6S-MA	2.93	6.97	6.99	5.59	0.51
SEBS/6E	2.23	7.02	5.67	4.55	0.40
SR/6S-MA	0.50	3.65	32.80	31.65	4.28
SR/6E	0.37	3.20	33.60	31.91	4.02

[3]. Since SEBS, like polyethylenes, does not have polar groups, then the chemical activity and reactivity of EVA is definitely higher than SEBS. Also, the soft phase of SEBS has an olefinic nature and a structure close to LLDPE can be imagined for it. Considering the fact that the chain of EVA is also made of polyethylene, it is expected that there is a good compatibility between EVA and the soft phase of SEBS. Therefore, it is possible to consider that the addition of EVA, like as the addition of SEBS-MA to blends, can have a positive effect on the cure behavior of SEBS in the blends. Comparing the cure behavior of Pure SEBS and SEBS/6E, it is clear that the presence of EVA in SEBS causes a very slight increase in ΔM and its cure rate. It also reduces the cure time and T_{s2} of Pure SEBS. Meanwhile, the addition of EVA has caused a decrease in ΔM and also the cure rate of SR. It also increases the cure time by 1 min. This behavior has also been observed by Ganesh *et al.* [4] for SR/EVA blends cured with benzoyl peroxide (BP) and Dicumyl peroxide (DCP).

Conclusion

The use of SEBS-g-MA and EVA leads to an increase in curing time and a reduction in CLD and curing speed of SR. However, adding the copolymers to SEBS has a positive impact on the curing behavior of SEBS, reducing curing time and increasing CLD and curing speed. This effect is attributed to the increased activity of these copolymers compared to SEBS.

References

- [1] E. Alikhani, M. Mohammadi, and M. Sabzi, "Preparation and study of mechanical and thermal properties of silicone rubber/poly(styrene-ethylene butylene-styrene) triblock copolymer blends", *Polym. Bull.*, **80**, 7991-8012, 2023.
- [2] S. Pavlovsky and A. Siegmund, "Chemical sensing materials II: Electrically conductive peroxide crosslinked SEBS copolymers systems", *J. Appl. Polym. Sci.*, **114**, 1390-1396, 2009.
- [3] A.J. Peacock, *Handbook of Polyethylene: Structures, Properties and Applications* (Marcel Dekker., 2000).
- [4] B. Ganesh and G. Unnikrishnan, "Cure characteristics, morphology, mechanical properties, and aging characteristics of silicone rubber/ethyl vinyl acetate blends", *J. Appl. Polym. Sci.*, **99**, 1069-1082, 2006.

Investigating the Rheological Behavior of PA6/EVA Blend

Amin Kamkar and Hamid Garmabi*

Department of Polymer and Color Engineering, Amirkabir University of Technology, Tehran, Iran

*garmabi@aut.ac.ir

Abstract

This study has investigated the Rheological behavior of blends comprising Polyamide 6 (PA6), Polyethylene grafted with maleic anhydride (PE-g-MA), and ethylene vinyl acetate (EVA) copolymer. PA6 is a type of aliphatic polyamide with low-impact resistance. However, this characteristic can be significantly enhanced through approaches such as copolymerization, polymer blending, and the incorporation of nanoparticles and fillers. Among these, blending with EVA has proven effective by lowering the glass transition temperature and enhancing impact resistance. However, due to the inherent immiscibility and incompatibility of PA6 and EVA, the use of a compatibilizer like PE-g-MA is crucial. Experimental findings revealed notable shear-thinning behavior and increased zero-shear viscosity in PA6/EVA and PA6/EVA/PE-g-MA blends compared to neat PA6. This research underscores the importance of compatibilizers in optimizing polymer blend properties.

Keywords: polyamide 6 (PA6), Ethylene vinyl acetate (EVA), blending, rheological behavior, Frequency sweep

Introduction

Aliphatic polyamides, specifically polyamide 6 (PA6), are known for their excellent mechanical and thermal properties due to their strong hydrogen bonding and crystalline order [1]. Researchers have worked on increasing its impact resistance through methods such as copolymerization, blending with other polymers, and adding plasticizers and fillers [2]. One of the effective methods is mixing with a polymer with rubber properties such as ethylene vinyl acetate (EVA) copolymer, which lowers the glass transition temperature and improves impact resistance. In addition, the incorporation of nanoparticles, fillers, and compatibilizers with PA6 can enhance various properties. However, PA6 and EVA have shear thickening behavior. Still, they do not have the same polarity. So, these two polymers are immiscible and incompatible and require the use of a compatibilizer such as polyethylene grafted with maleic anhydride (PE-g-MA) during the process [3].

Experimental

Material

A commercial PA6 is recommended for extruder application (DuPont, Germany) with a melt flow index (MFI) of 8.1 g/10min (230 °C/2.16 Kg), a melting temperature of 220 °C and a density of 1.13 g/cm³ was used as the polymer matrix. EVA with vinyl acetate 19% and an MFI 1.8 g/10min (190 °C/ 2.16 Kg) from Hanwha company, China was used as a blending polymer. PE-g-MA from DuPont, Germany with a density of 0.954 g/cm³, an MFI of 2 g/10min (190 °C/2.16 Kg), and a melting temperature of 134 °C was used as a compatibilizer.

Preparation

Before materials were processed, PA6 was dried in a vacuum drying oven at 80 °C for 24 h. The blends containing 20 wt% EVA, were prepared in the co-rotating, intermeshing twin screw extruder (L/D=24) with a screw speed of 100 rpm and using a temperature profile that goes from 160 °C to 240 °C. The detailed blending composition is given in Table I.

Characterization

The rheological properties were recorded using the Paar Physica Rheometer. Sample were prepared by hot press at 240 °C in a mold with a diameter of 25 mm and a thickness of 1 mm. Dynamic moduli (storage modulus (G') and loss modulus (G'')) and complex viscosity were measured between the parallel plate at 240 °C. The applied strain was 1% and the angular frequency was varied from 0.1 rad/s to 700 rad/s.

Results and Discussion

Fig. 1 shows the melt viscosity for PA6 including different amounts of EVA and PE-g-MA as a function of frequency. The melt viscosity of the neat PA6 exhibits a weak shear thinning behavior. PA6/EVA and PA6/EVA/PE-g-MA

Table I. Blend compositions investigated.

Component	Blend code		
	A	B	C
PA6 (wt%)	100	80	80
EVA (wt%)	0	20	20
PE-g-MA (phr)	0	0	5

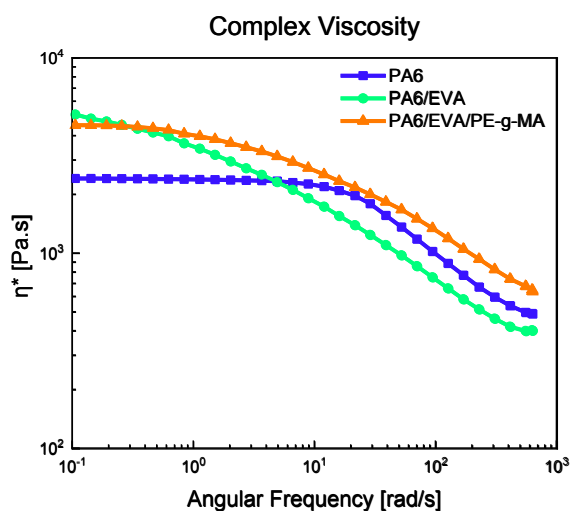
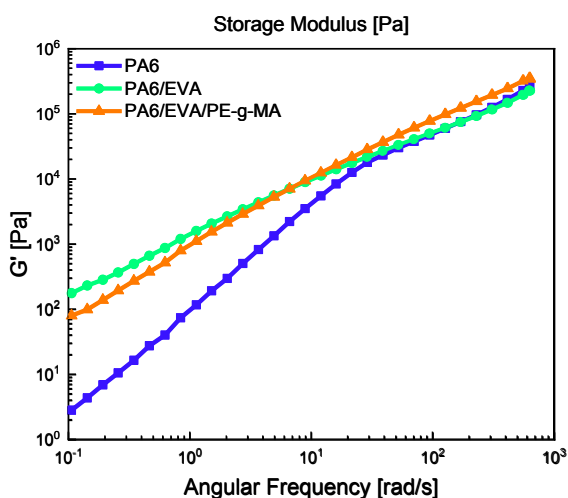
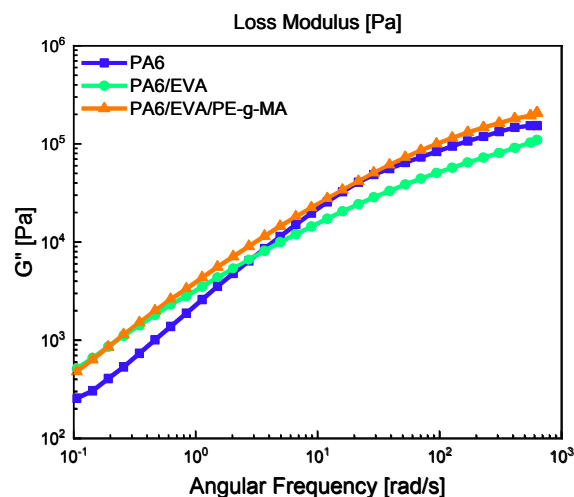


Fig. 1. Complex viscosity of neat PA6 and other blends.

compounds show eminent shear thinning behaviors over the entire frequency range and a much higher zero shear viscosity than PA6, which was calculated using the simple Carreau equation with Cox-Merz rule (Eq. (1)), where η_0 is the zero-shear viscosity, $\dot{\gamma}$ is the shear rate, τ_n is the characteristic time, and τ_n is a parameter [4]. The melt viscosity reached the highest value for PA6/EVA of which zero shear rate viscosity surprily markets almost 2 times of PA6. After that, it decreased as more PE-g-MA was added.

$$\eta(\dot{\gamma})/\eta_0 = (1 + (\dot{\gamma}\tau_n)^2)^{-(n-1)/2} \quad (1)$$

The dynamic moduli such as storage modulus (G') and loss modulus (G'') of all the studied samples are shown in Figs. 2 and 3, respectively. In linear polymer melt, a terminal-like behavior has been observed in low frequency and the storage modulus is related to the square of the frequency ($G' \sim \omega^2$) while the loss modulus is linearly related to the frequency ($G'' \sim \omega$) [4]. The storage modulus and loss

Fig. 2. Storage modulus (G') vs frequency of blends.Fig. 3. Loss modulus (G'') vs frequency.

modulus increase with increased frequency of all samples. At low frequencies, the time is large enough to open the chain of entanglements and therefore the loss and storage modulus are low. However, at high frequencies, the chains do not have enough time to open the entanglements, so the modulus increases [5]. The storage modulus is larger than the loss modulus ($G' > G''$) in the low-frequency range, all samples exhibit more solid-like behavior.

Conclusion

The aim of this study was to improve the rheological properties of PA6 by blending it with EVA and incorporating compatibilizers such as PE-g-MA. The experimental results showed that these blends exhibited significant shear thinning behavior and higher zero shear viscosity than pure PA6. In addition, all the samples tested exhibited solid-like behavior at low frequencies, with the storage modulus (G') exceeding the loss modulus (G'') in this range.

References

- [1] S. Mohanty and S.K. Nayak, *Polym. Compos.*, **28**, 153-162, 2007.
- [2] S. Aparna, D. Purnima, and R.B. Adusumalli, *Polym. Plast. Technol. Eng.*, **56**, 617-634, 2017.
- [3] A.R. Bhattacharyya, S.N. Maiti, and A. Misra, *J. Appl. Polym. Sci.*, **85**, 1593-1606, 2002.
- [4] H. Kim, K. Oh, and Y. Seo, *Polymer*, **177**, 196-201, 2019.
- [5] J.K. Mishra, K.J. Hwang, and C.S. Ha, *Polymer (Guildf)*, **46**, 1995-2002, 2005.

Investigating Depletion Forces in Nanoparticles Suspension Using Rheology Measurement

Farzane Yazdani^{1*}, Fatemeh Goharpey¹, Majid Karimi², Esmaeel Moghimi³, and Zahra Daneshfar⁴

1. Polymer and Color Engineering Department, Amirkabir University of Technology, Tehran, Iran

2. Iran Polymer and Petrochemical, Tehran, Iran

3. University of Crete, Greece

4. Yazd University, Yazd, Iran

*farzaneyazdani4@gmail.com

Abstract

In this work, we examine the effect of short-range depletion attraction on the rheology of concentrated suspensions. We use mixed suspensions of colloidal spheres with diameter D_s and colloidal rods with length L and diameter D . The depletion interaction is driven by rod particle exclusion from the space between large particles with its magnitude depending on the relative concentration of the constituents. The clustering of large particles in the samples is characterized via the thixotropic behavior and shear thickening response. Our findings demonstrate that lower rod concentrations are sufficient to induce sphere crystallization and that rod like colloidal particles prove to be highly efficient depletion agents. Additional support for these interactions in suspensions is provided by dynamic light scattering, zeta potential and NMR data.

Keywords: depletion interaction, suspensions, viscosity, shear thickening, thixotropy

Introduction

Multimodal suspensions, which have enhanced packing [1], are found in food processing and encountered in industries (e.g., slurries, concrete, ceramics). The particle size distribution affects the mixing, pumping, and transportation, for example as a tool to control the viscosity. Bimodal mixtures of spherical colloidal particles are the simplest and good model system to study the effect of size distribution. One of the most prominent interactions in bimodal colloids is the depletion attraction [2], which effects on structure [3], dynamic, and viscosity of systems [4]. One of the most prominent interactions in bimodal colloids is the depletion attraction, which effects on dynamic and viscosity of system. This interaction was first proposed by Asakura and Oosawa for colloid-polymer mixtures and later reconsidered by Vrij. Excluded volume interactions in mixtures of colloidal rods and spheres lead to mediated depletion interactions. The strength and range of this attractive interaction depend on the concentrations of the particles, the length L and diameter D of the rods, and the radius D_s of the spheres. At strong enough attraction, this depletion interaction leads to phase separation [5].

Experimental/Theoretical

Monodispersed silica particles were synthesized by Stöber *et al.*'s method (Fig. 1) [6]. CNC is natural based rod-like nanoparticles with a width of 5-10 nm and a length up to 300 nm and is produced by isolation of crystalline chains of cellulose by applying acid hydrolysis techniques [7]. Then,

suspensions with fixed mass fraction ratio are mixed with poly(ethylene glycol), PEG 400 g/mol, Daejung.

Results and Discussion

All the rheological measurements were performed using a stress controlled rheometer, UDS 200, Paar Physica (Austria). The temperature was kept at 27 °C, where the viscosity of PEG400 is about $\eta_p=0.1$ Pa.s. Oscillatory shear measurements in the predetermined linear regime (strain 0.5%) were applied to measure the storage modulus G' and loss modulus G'' as a function of angular frequency ω in the dynamic frequency sweep experiments. The dynamic amplitude sweep experiments were carried out by varying shear strain/stress at fixed angular frequency $\omega=1$ rad/s to study the yielding behavior. Fig. 2 shows the frequency

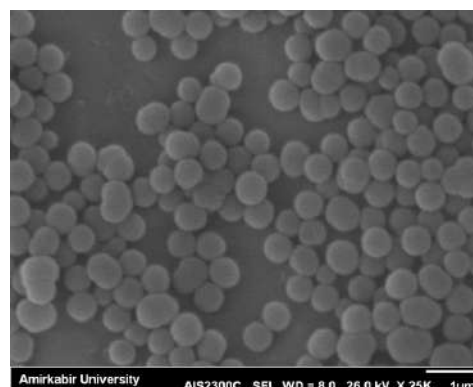


Fig. 1. SEM images of SiO_2 .

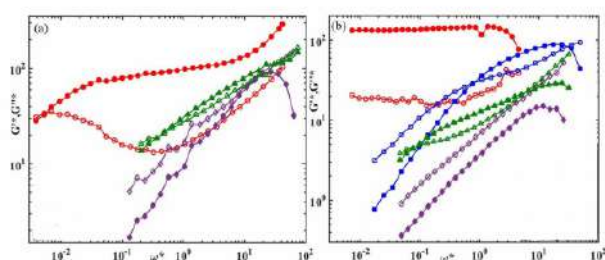


Fig. 2. Dynamic storage modulus G' (filled symbols) and loss modulus G'' (open symbols) as a function of dimensionless angular frequency ω^* .

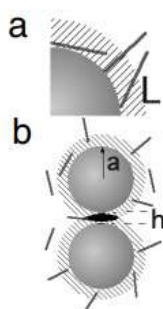


Fig. 3. The depletion attraction between two spheres. (a) Rods lose rotational degrees of freedom (and thus entropy) when their center lies in the depletion region (hashed regions) whose thickness extends $L/2$ beyond the surface of the large sphere. (b) When the large spheres approach each other, these depletion zones overlap (dark shading) and a volume, V_{overlap} , becomes accessible to the rods, increasing rod entropy and inducing an attractive force between the particles.

dependence of dimensionless storage modulus G' and dimensionless loss modulus G'' in the linear viscoelastic regime for suspensions. Fig. 3a illustrates the depletion interaction between two spheres of radius a immersed in a suspension of thin rods of length L . When the center of a rod is located less than $L/2$ from the sphere surface (i.e., in the depletion zone, the hashed regions in Fig. 3), there are fewer possible orientations available to the rod, reducing its entropy. When the separation between sphere surfaces is less than L , the depletion zones around each sphere overlap, and the amount of accessible sample volume for unconstrained rod rotation increases. The total rod entropy increases in this case, inducing a depletion attraction between the spheres.

Conclusion

We conclude from these findings that phase separation in rod-sphere mixtures can occur at very low concentrations of rods and spheres. An increase both of the sphere concentration and of the rod concentration leads to an increase of the crystallization rate. The low rod concentration needed to induce the phase separation also confirms the prediction of Asakura and Oosawa that rods are much more efficient depletion agents than small spheres. Our results showed that rod like particles are more efficient depletion agents than spherical particles. Rod like particles can flocculate and phase separate colloids at

concentrations lower than spherical depletants.

References

- [1] R.A. Lionberger and W. Russel, "Microscopic theories of the rheology of stable colloidal dispersions", *Adv. Chem. Phys.*, **111**, 399-474, 2000.
- [2] M. Laurati, S.U. Egelhaaf, and G. Petekidis, "Nonlinear rheology of colloidal gels with intermediate volume fraction", *J. Rheol.*, **55**, 673-706, 2011.
- [3] E. López-Sánchez, C.D. Estrada-Álvarez, G. Pérez-Ángel, J.M. Méndez-Alcaraz, P. González-Mozuelos, and R. Castañeda-Priego, "Demixing transition, structure, and depletion forces in binary mixtures of hard-spheres: The role of bridge functions", *J. Chem. Phys.*, **139**, 104908104940, 2013.
- [4] A Anil Kumar, "Anomalous dynamics of binary colloidal mixtures over a potential barrier: Effect of depletion interaction", *J. Chem. Phys.*, **141**, 034904, 2014.
- [5] L. Keng-hui, J.C. Crocker, A.C. Zeri, and A.G. Yodh, "Colloidal interactions in suspensions of rods. The American physical society", *Phys. Rev. Lett.*, **87**, 088301, 2001.
- [6] W. Stöber, A. Fink, and E. Bohn, "Controlled growth of monodisperse silica spheres in the micron size range", *J. Colloid Interface Sci.*, **26**, 62-69, 1968.
- [7] M.M.D. Lima and R. Borsali, "Rodlike cellulose microcrystals: Structure, properties, and applications", *Macromol. Rapid Commun.*, **25**, 771-787, 2004.

Dispersion and Rheological Properties of PLLA-graft-CNC/PLA Bionanocomposites

Amir Abbas Seraji¹, Fatemeh Goharpey^{1*}, and Jafar Khademzadeh Yeganeh²

1. Polymer and Color Engineering Department, Amirkabir University of Technology, Tehran, Iran

2. Polymer Engineering Department, Qom University of Technology, Qom, Iran

*goharpey@aut.ac.ir

Abstract

Cellulose nanocrystals (CNCs) are highly hydrophilic and their dispersion into the polylactic acid (PLA) matrix is a great challenge. To overcome this limitation, the surface grafting of nanoparticles with chains having similar chemistry as that of the matrix is an emerging technique to obtain a dispersed nanocomposite. CNCs were surface modified (M-CNCs) by the ring opening polymerization (ROP) of L-lactide (LA) monomers. Different compositions of CNCs and M-CNCs in the PLA matrix were produced by solution mixing to see the effect of the content of CNCs on dispersion and rheological results. Field emission scanning electron microscopy (FESEM) was used to observe the dispersion of M-CNCs in the PLA matrix. The rheological analysis was performed to evaluate the distribution of nanoparticles and their possible structures.

Keywords: surface modification cellulose nanocrystals, polylactic acid (PLA), dispersion, rheological properties

Introduction

Environment-friendly polymers such as poly lactic acid (PLA) and poly caprolactone (PCL) have attracted attentions in recent years due to their biocompatibility and biodegradability [1]. Cellulose nanocrystal (CNC) is a natural based additive with a whisker-like structure [2]. Kamal *et al.* added CNCs to the PLA matrix, which affected its rheological behavior. They observed a rheological percolation and the formation of a 3D structure at 3% of CNCs [3]. Goffin *et al.* reported that adding CNCs to PCL had no effect on the shear storage modulus in the frequency sweep test in the range of 0.01 rad/s to 100 rad/s. It is due to the high surface polarity of CNCs, which tend to aggregate in PCL with the hydrophobic nature, and results in a poor dispersion. To overcome this problem, they used the grafting technique to graft ϵ -caprolactone on CNCs by ring opening polymerization (ROP), using the active hydroxyl group on CNC, as initiator, and Stannous Octoate ($\text{Sn}(\text{Oct})_2$). Then, they added PCL-grafted CNCs (PCL-g-CNC) to the PCL matrix which resulted in an enormous change in the shear storage modulus in the frequency sweep test. In this procedure, percolation was observed at 2% of CNC. At higher contents of the surface grafted CNCs, the nanocomposite showed a solid elastic behavior which is the result of the formation of a physical network by the entanglement of grafted chains with matrix chains [4,5]. In this work, we tried to improve the dispersion of CNCs in the PLA matrix by grafting the L-lactide (LA) monomer on CNCs. In this way, we studied the effect of the reaction of grafted chains of nanoparticles on dispersion in the PLA matrix. After finding an optimum condition for the ideal dispersion, the rheological behavior of the PLA nanocomposites with the uniform dispersion of surface modified CNCs (M-CNCs) were studied.

Experimental

The morphology of nanocomposites was studied by the FESEM images taken by the TESCAN VEGAII (Czech) microscope. Rheological tests were performed on the MCR302 rheometer (Anton Paar) with a parallel plate fixture (diameter: 25 mm; constant gap: 1 mm) at 170 °C. CNCs were extracted from cotton by sulfuric acid hydrolysis. Active hydroxyl groups on CNCs were used as initiator for surface grafting. Chloroform (CHL) and dimethylformamide (DMF) were purchased from Merck and used as received. Sulfuric acid 98% was supplied by Sigma-Aldrich and used in the CNC production process. Stannous Octoate ($\text{Sn}(\text{Oct})_2$) was purchased from Sigma Aldrich and used as the catalyst for ROP of LA. L-Lactide monomer was purchased from Sigma Aldrich. PLA was supplied by Nature works Co. (2003-D grade). The ROP reaction was performed at 110 °C in Dimethyl

formamide (DMF). The reaction medium was under continuously stirring and purging N_2 . The soxhlet instrument was used to separate unreacted LA monomers and PLA homopolymers from the PLLA-g-CNC sample.

The Nanocomposites were prepared by the solution casting method. To prepare the samples containing nanoparticles, the required amount of each of nanoparticles (CNCs and M-CNCs), 0, 0.25, 0.5, 1, and 1.5 wt% was individually dispersed in chloroform by probe ultrasonication for 30 min; then, the dispersion was mixed with the prepared PLA solution and stirred for 24 h. The prepared solutions were then cast over a glass plate. The solvent was left for 1 week to evaporate slowly at room temperature. Then, the samples were put in a vacuum oven for 24 h at 50 °C.

Results and Discussion

The FESEM images of nanocomposites which are shown in Fig. 1, analyze the effect of CNCs and M-CNCs on their dispersion in the PLA matrix. From Fig. 1a, it can be seen that CNCs show a poor dispersion and the high levels of aggregation. According to Fig. 1b, a uniform dispersion of M-CNCs in the PLA matrix can be observed without any sign of aggregation.

In the nanocomposites of M-CNCs, aggregation is prohibited by the steric hindrance against grafted chains on M-CNCs and a reduction in strong hydrogen bonding between M-CNC particles, which causes high levels of aggregation in CNCs [6]. The dispersion and structure of the nanocomposites of M-CNCs were studied by frequency sweep tests. At first, strain sweep tests were performed on the samples with the highest contents of CNCs for the nanocomposites of CNCs and M-CNCs to see the boundary of the linear behavior of each class of samples. The nanocomposite of CNCs did not show any non-linear behavior in the range of 0.01-10% of strain, while in the nanocomposite of M-CNCs, the non-linear viscoelastic region was observed at 1% of the strain. Then, the rheological behaviors of the samples were analyzed at 0.2% of the strain which fall in the linear viscoelastic region. Fig. 2 shows the dependence of (a) the storage modulus (G') and (b) complex viscosity of various CNCs/PLA nanocomposites on frequency. The incorporation of CNCs in the PLA matrix did not affect the viscoelastic behavior of the PLA matrix for all contents of CNCs in the range of 0.03 rad/s to 628 rad/s, indicating the poor dispersion of CNCs in the PLA matrix due to the high extent of hydrogen bonding between CNCs particles and them not having any interaction with the PLA matrix [7].

Figs. 3a and 3b show the dependence of the storage modulus and complex viscosity of M-CNCs/PLA nanocomposites on frequency respectively. At low frequencies, the complex viscosity increases by increasing the content of M-CNCs, which causes the

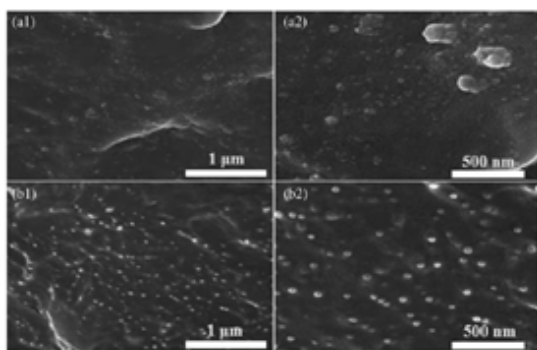


Fig. 1. FESEM images of cryofractured nanocomposites containing 0.5 wt% of (a) CNCs and (b) M-CNCs.

entanglement of grafted chains with free PLA chains in the matrix. As it can be seen from Fig. 3b, at low frequencies, storage modulus increases by increasing the content of M-CNCs. At 1 rad/s, the nanocomposite with 0.5% of M-CNCs in the PLA matrix shows a plateau. The reasons for this plateau are the entanglement of grafted chains with free PLA chains, and the good interaction of M-CNCs with the PLA matrix, which has resulted in the formation of a 3D network structure among M-CNCs. This physical network structure provides the nanocomposites with a better resistance against the applied deformation at low frequencies. By the formation of this physical structure, the relaxation time increases at low frequencies, which indicates the uniform dispersion of M-CNCs in the PLA matrix. For 1.5% of M-CNCs, a solid-like behavior is observed which indicates the formation of a strong physical network resisting against the applied deformation at all frequencies resulted from the high levels of the entanglement of surface grafted PLA chains with free PLA chains and 3D network structure [3,4,7].

In order to calculate the rheological percolation threshold (ϕ_{per}), the storage modulus of the M-CNCs/PLA nanocomposite was used for different contents of M-CNCs at a constant frequency (Fig. 4a). Eq. (1) was used and linearized to Eq. (2) to calculate the rheological percolation threshold $\phi_{per} = 0.9$.

$$G' = G_0 (\phi - \phi_{per})^m \quad (\phi > \phi_{per}) \quad (1)$$

$$\log G' = \log G_0 + m \log(\phi - \phi_{per}) \quad (2)$$

Fig. 4b represents the rheological cole-cole plot for M-CNCs/PLA nanocomposites. The semi-circular shape of neat PLA indicates the absence of any structure. Curves of 0.25 and 0.5% of M-CNCs nanocomposites show a tail, representing the formation of structures, because the interaction between free PLA chains and the grafts on the CNCs and the suitable dispersion of M-CNCs in the system result in an increase in the relaxation time of the PLA chain matrix [8]. The sample of 1% of M-CNCs did not show any tail, indicating the formation of a high physical structure between M-CNCs and considerable relaxation time.

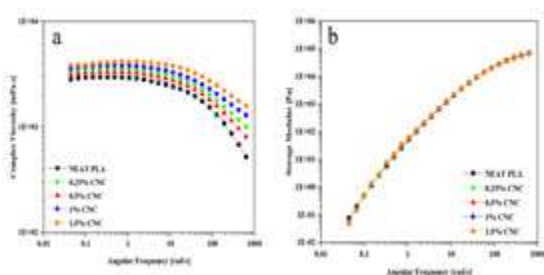


Fig. 2. Dependence of: (a) the storage modulus (G') and (b) complex viscosity of various CNCs/PLA nanocomposites on frequency.

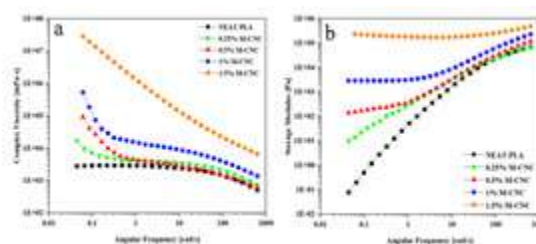


Fig. 3. Dependence of: (a) storage modulus and (b) complex viscosity of CNCs/PLA nanocomposites on frequency.

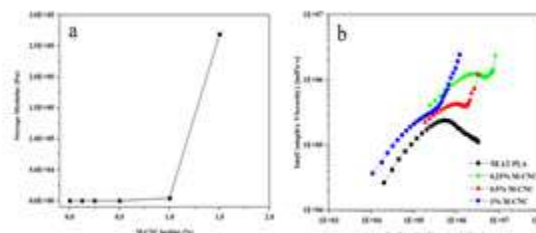


Fig. 4. (a) Storage modulus vs. the content of M-CNCs at constant frequencies and (b) rheological cole-cole plot.

Conclusion

According to FESEM images and the rheological analysis, a uniform dispersion of surface modified CNCs in the PLA matrix was obtained through the synthesis of PLA-g-CNCs by the ROP of LA monomers and the active hydroxyl groups available on neutralized CNCs. The observed plateau in Frequency sweep test of CNCs/PLA nanocomposites are the results of the uniform dispersion of M-CNCs, which is caused by an increased entanglement of grafted chains and the free PLA chain matrix and the formation of 3D network structure among M-CNCs, which both are caused by because the decreased hydrogen bonding among M-CNCs due to the steric hindrance.

References

- [1] J.M. Raquez, Y. Habibi, M. Murariu, and P. Dubois, "Polylactide (PLA)-based nanocomposites", *Prog. Polym. Sci.*, **38**, 1504-1542, 2013.
- [2] S.J. Eichhorn, "Cellulose nanowhiskers: Promising materials for advanced applications", *Soft Matter*, **7**, 303-315, 2011.
- [3] M.R. Kamal and V. Khoshkava, "Effect of cellulose nanocrystals (CNC) on rheological and mechanical properties and crystallization behavior of PLA/CNC nanocomposites", *Carbohydr. Polym.*, **123**, 105-114, 2015.
- [4] A.L. Goffin et al., "Poly(ϵ -caprolactone) based nanocomposites reinforced by surface-grafted cellulose nanowhiskers via extrusion processing: Morphology, rheology, and thermo-mechanical properties", *Polymer (Guildf)*, **52**, 1532-1538, 2011.
- [5] J.K. Muiruri, S. Liu, W.S. Teo, J. Kong, and C. He, "Highly biodegradable and tough poly(lactic acid)-cellulose nanocrystal composite", *ACS Sustain. Chem. Eng.*, **5**, 3929-3937, 2017.
- [6] V. Gollanapalli, A. Manthri, U.K. Sankar, and M. Tripathy, "Dispersion, phase separation, and self-assembly of polymer-grafted nanorod composites", *Macromolecules*, **50**, 8816-8826, 2017.
- [7] W. Zhen, "Preparation and characterization of phosphorylated graphene oxide grafted with poly(L-lactide) and its effect on the crystallization, rheological behavior, and performance of poly(lactic acid)", 2846-2859, 2019.
- [8] E.J. Dil, N. Virgilio, and B.D. Favis, "The effect of the interfacial assembly of nano-silica in poly(lactic acid)/poly(butylene adipate-co-terephthalate) blends on morphology, rheology and mechanical properties", *Eur. Polym. J.*, **85**, 635-646, 2016.

Investigating the Effect of Dioctyl Sodium Sulfosuccinate on PVC Plastisol Rheology

Hamidreza Ejraee*, Abbas Kebritchi, and Nasser Karimi

Chemical Engineering Department, Imam Hossein Comprehensive University, Tehran, Iran

*hamidejraee1998@ihu.ac.ir

Abstract

This research examines the effect of dioctyl sodium sulfosuccinate (AOT) as a wetting agent on the rheological behavior of PVC plastisol. The rheology test was conducted in order to obtain the optimal percentage composition to achieve the maximum viscosity reduction using a Brookfield rotary rheometer. For this purpose, first a sample without wetting agent was tested and then dioctyl sodium sulfosuccinate in concentration (0.2 and 0.3%) was subjected to rheology test. The obtained results show that the use of dioctyl sodium sulfosuccinate in both concentrations decreased the viscosity of PVC plastisol, but we saw a greater decrease in the concentration of 0.3%. This effect increases the loading capacity of PVC plastisol, which improves the properties of this compound.

Keywords: PVC plastisols, rheology, brookfield rotary rheometer, dioctyl sodium sulfosuccinate, wetting agent

Introduction

Polyvinyl chloride cannot be processed alone due to its very low thermal stability and high melt viscosity. Therefore, it is necessary to combine a number of suitable additives with PVC to provide a wide and varied range of properties to meet many different end applications. As shown in Fig. 1, this process is done by dispersing PVC resin particles in the softener and turning it into a product called plastisol [1]. A plasticizer is a material that is combined with another material (usually plastic or elastomer) to increase flexibility, performance, or extensibility. A plasticizer may reduce melt viscosity, second-order transition temperature, or elastic modulus. Plastisol is a liquid suspension of tiny PVC particles dispersed in a matrix of liquid plasticizer. By heating the liquid plastisol, the softener enters some of the cavities in the PVC particles and starts dissolving or swelling some of them to form a homogeneous structure [2].

The rheological properties of PVC plastisol play an important role in their load capacity and, as a result, their mechanical and functional properties. In PVC plastisol, mechanical and functional properties can be improved by increasing the solid load that includes fillers. PVC plastisol has a relatively low load capacity and therefore shows poor mechanical and functional properties in certain applications. For this purpose, in order to improve this

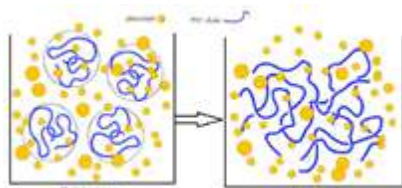


Fig. 1. Plasticizer effect on PVC resin and formation of PVC plastisol.

feature, it is necessary to increase the loadability with different methods. One of these methods is adding a wetting agent in order to reduce the viscosity of the composition and increase the fillers. One of the compounds that can be used as a humectant in PVC plastisol is dioctyl sodium sulfosuccinate [3]. The structure of this compound can be seen in Fig. 2.

The mechanism of action of the wetting agent is that the molecules of the wetting compound create empty spaces between the PVC plastisol chains, which reduces the viscosity of the PVC plastisol and increases its load capacity. The mechanism and mode of action of the wetting agent to reduce the viscosity of PVC plastisol, as seen in Fig. 3, is that the wetting molecules penetrate and are placed between the PVC molecules and create a gap between them that it reduces the viscosity of this compound [4].

Experimental

Polyvinyl chloride (PVC) has been used as resin and phthalate plasticizer to form PVC plastisol. Dioctyl sodium sulfosuccinate (AOT) as a wetting agent and liquid barium cadmium manufactured by Chem KD Korea with commercial grade LX-267 as a thermal stabilizer according to Table I were used to prepare different PVC plastisol formulations.

First, PVC powder was mixed with plasticizer and stabilizer in a planetary mixer for 15 min, and PVC



Fig. 2. Chemical structure of dioctyl sodium sulfosuccinate.

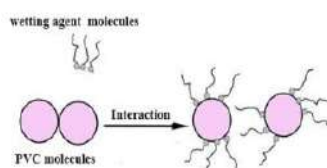


Fig. 3. Chemical structure of dioctyl sodium sulfosuccinate.

Table I. Tested formulations.

PVC (wt%)	plasticizer (wt%)	Stabilizer (wt%)	Wetting agent (wt%)		code
11	12	0.5	0		1
			AOT	0.2	2
			AOT	0.3	3

plastisol was prepared. Then, according to the formulations in Table I, we add the wetting agent agent to the plastisol and stir for another 15 min. The noteworthy point is that dioctyl sodium sulfosuccinate is in the form of wax, because this substance cannot be dissolved at ambient temperature in the composition, it must first be dissolved in the softener at 80 °C and then mixed. In the next step, the mixture was subjected to a rheology test at ambient temperature (25 °C) using a Brookfield rotary rheometer, and the viscosity was measured at different shear rates.

Results and Discussion

As can be seen in Fig. 3, the action mechanism of the wetting agent and the interfacial interactions between the polymer and the wetting agent change the rheological properties of the system. These interactions can be different depending on the type of moisturizing agent used. As can be seen in the graphs below, the incorporation of 0.2 and 0.3% of the wetting agent used in PVC plastisol has caused a significant reduction in viscosity in this composition. This decrease in viscosity has caused an increase in load capacity in PVC plastisol, which has a direct effect on the mechanical and functional properties of PVC plastisol and improves these properties [5].

The experimental results follow the power law model (Eq. (1)):

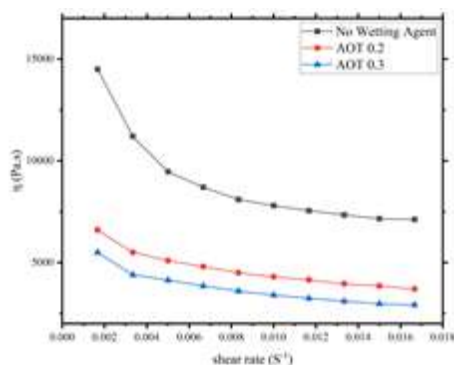


Fig. 4. Chemical structure of dioctyl sodium sulfosuccinate.

$$\eta = Kx^m \quad (1)$$

where η , x , m and K are the viscosity, shear rate, pseudoplasticity index and viscosity index, respectively. In Eq. (1), for Newtonian fluids $m=0$, in other words, the viscosity is independent of the shear rate. For dilatant fluids m is positive, while for pseudoplasticity fluids, m is between zero and -1. From the slope of viscosity vs. shear rate, pseudoplasticity index (m) and from the intercept, viscosity index (K) were determined [6].

Conclusion

This study showed the important role of dioctyl sodium sulfosuccinate on the rheological behavior of PVC plastisol. This study has shown that the type and concentration of wetting agent directly affect the viscosity of PVC plastisol. By reducing the viscosity of PVC plastisol, the load capacity has increased, which in turn improves the performance of PVC plastisol. This study not only expands our understanding of the interaction between wetting agent and PVC plastisol, but also opens a way to optimize and make PVC plastisol more efficient. Future research should focus on elucidating the underlying mechanisms of these effects and determining the extent of improvement in the functional properties of PVC plastisol. This revolutionizes PVC plastisol technology.

References

- [1] N. Nakajima and C.A. Daniels, "Plastisols of poly(vinyl chloride): particle size distribution, morphology, rheology and mechanism of aging", *J. Appl. Polym. Sci.*, **25**, 2019-2044, 1980.
- [2] N. Nakajima and E.R. Harrell, "Rheology of PVC plastisol: particle size distribution and viscoelastic properties", *J. Colloid Interface Sci.*, **238**, 105-116, 2001.
- [3] N. Nakajima and S.Y. Kwak, "Effect of plasticizer type on gelation and fusion of PVC plastisol, dialkyl phthalate series", *J. Vinyl Addit Technol.*, **13**, 212-222, 1991.
- [4] N. Nakajima and M.R. Sadeghi, "Gelation and fusion of PVC plastisols with plasticizers of varying solvent power", *Int. Polym. Process.*, **4**, 16-22, 1989.
- [5] N. Nakajima and D.W. Ward, "Gelation and fusion profiles of PVC dispersion resins in plastisols", *J. Appl. Polym. Sci.*, **28**, 807-822, 1983.
- [6] N. Nakajima, D.W. Ward, and E.A. Collins, "Viscoelastic measurements of PVC plastisol during gelation and fusion", *Polym. Eng. Sci.*, **19**, 210, 1979.

Tuning of Shear Thickening Behavior Silica Suspensions by Using Graphene Oxide by Molecular Dynamics Simulation

Mehdi Zojaji^{1*}, Seyed Hasan Hashemabadi², Amir Hydarinasab¹, and Milad Mehranpour¹

1. Department of Chemical Engineering, Science and Research Branch, Islamic Azad University, Tehran, Iran

2. CFD Research Laboratory, School of Chemical Engineering, Iran University of Science and Technology, Tehran, Iran

*mehdi.zojaji@srbiau.ac.ir

Abstract

This study uses the non-equilibrium molecular dynamics simulation to present the influences of shear value and temperature effects on shear thickening fluids. For this, the fluids were simulated with a low value of shear under constant temperature (300 K) and then the shear value increased to prepare the thickening condition of the fluid. We calculate the viscosity of fluids with precise atomic arrangement via molecular dynamics approaches. Molecular dynamics results show that, by increasing the inserted shear value the viscosity of fluids increases and then decreases dramatically. Further, the temperature of the simulated system is a prominent parameter of the viscosity of the fluid and the jamming viscosity decreases to 37.24 Pa.s by increasing the temperature to 375 K. Finally, Rheological results show that DREIDING and Universal force fields have a good ability to simulate shear-thickening fluids and correctly estimate their rheological behavior.

Keywords: shear thickening fluid (STF), viscosity, molecular dynamics (MD)

Introduction

The fluid viscosity can be considerably changed by varying the external conditions such as temperature, pressure and shear value which are implemented to them. In common cases, under low shear, the viscosity of a fluid is essentially independent of the shear value that this viscosity is Newtonian viscosity. By increasing the inserted shear, the viscosity dramatically decreases, which creates interesting mechanical and rheological behavior for these structures [1]. This extreme shear thinning develops into another shear rate regime in which the viscosity hardly diminishes a “Second Newtonian” region. A further increase in shear value can lead to an increase in viscosity, called shear thickening [2,3]. The best method for the simulation of these atomic systems is to use the molecular dynamics (MD) method [4]. MD is computer intensive and even employs the most powerful massively parallel computers as demonstrated by its ability by pioneering work [5,6]. In MD simulations, the successive configuration of the system is achieved by an atomistic description that considers atoms as geometric points whose motion is governed by Newton’s equation of motion. In the present work, we focus on the effect of these thermodynamic parameters on the rheological properties of mixture fluid which consists of Polyethylene Glycol 400 (PEG 400), SiO₂ and Graphene Oxide (GO) with different atomic ratios [7]. These MD simulations are done for the first time and we expected the results of our simulations could be modified the rheological behavior of base fluid for industrial aims.

Simulation Method

Nonequilibrium molecular dynamics (NEMD) is a powerful simulation tool. This simulation method was employed for the rheological properties study of STFs, which consist of SiO₂, PEG-400 and GO structures with 4 volume fractions (Table I) in the simulation box with 10×10×10 nm³ dimensions in X, Y, and Z axes, respectively.

These atomic dimensions have been chosen to save on computations and prevent interference. In addition, periodic boundary conditions are applied along with all directions. The simulation tool was LAMMPS, which is a classical molecular dynamics software with a focus on materials modelling. This computer software is an open-source package released by Sandia national laboratories, a US department of energy laboratory [8,9]. Further, the total number of fluid atoms was as many as 100,000 atoms (approximately) which were structured in random positions

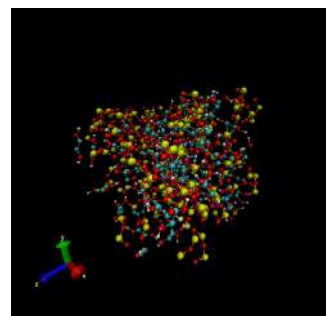


Fig. 1. Atomic structure of PEG 400-based STF with SiO₂ and GO structures.

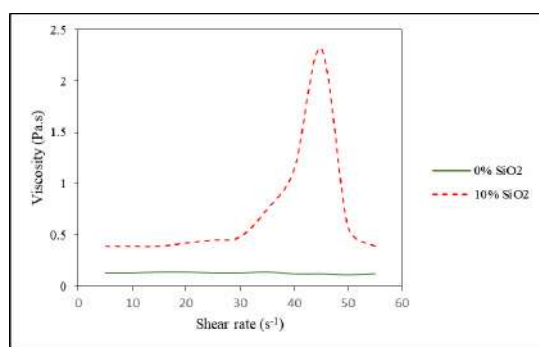


Fig. 2. The viscosity of PEG 400-based STF as a function of shear rate in S_1 atomic sample.

(Fig. 1). Furthermore, the bonded interactions consist of bond strength and bond-angle bend. The bond strength in DREIDING and Universal force fields (UFF) models are described by simple harmonic oscillator equation as [10,11]:

$$E = \frac{1}{2} kr (r-r_0)^2 \quad (1)$$

Finally, the shear rate inserted on STFs and the viscosity of the system calculated via The Green Kubo method. In this computational method, the viscosity of fluids is calculated by below equation:

$$\mu = \frac{1}{T} \int_0^{\infty} dt \int_0^V d^3x \langle \pi^{xy}(x,t) \pi^{xy}(0,t) \rangle \quad (2)$$

Results and Discussion

Atomic Ratio Effect of STFs Viscosity

In this step of our computational work, we study the effect of shear values on the rheological behavior of PEG 400 (S_0) at room temperature. The result of this simulation is represented in Fig. 2. This figure shows the viscosity of PEG 400 unchanged with the shear value increasing. From this figure, we can say that the viscosity of PEG 400 converged to 0.124 Pa.s [12]. This calculation indicates that the simulation time is sufficient for the rheological study of atomic structures. Numerically, experimental researchers estimated a 0.120 Pa.s value for the PEG 400 matrix. So, our calculated value for this parameter has a good consistency with previous reports and has only a 3.33% error rather than. After this calculation and computational method verification, SiO_2 was added to the pristine fluid structure. Numerically, when the SiO_2 atomic ratio reaches 9.95% (critical shear rate), the viscosity of fluid drops dramatically (at 45 s^{-1} shear rate).

Conclusion

The present paper offers the results of a study on the effects of atomic ratio, temperature and force field variation on the rheological characteristics of PEG 400-based STF. In all simulated models, the shear rate was enforced on the fluid atoms with 5 s^{-1} to 55 s^{-1} . Then, the results of viscosity

were reported in 1,000,000-time steps to show viscosity changes of atoms in the MD simulation box. After all, the results of different conditions were compared. Finally, the conclusions are as follows:

- 1) By increasing the SiO_2 atomic rates in PEG 400-based SFT, the potential energy of the simulated system increases and so the viscosity of the fluid increases, too. Numerically, our results show that, by SiO_2 atomic rate changes from 5% to 50% the viscosity of pristine fluid varies from 2.54 Pa.s to 132.54 Pa.s.
- 2) DREIDING and UFF force fields properly simulate the rheological behavior of PEG 400-based STFs and the results of these interatomic potentials are in good agreement with each other.

References

- [1] H.A. Barnes and H.J. Walters, *An Introduction to Rheology*, Elsevier Science, 1989.
- [2] A. Srivastava, A. Majumdar, and B. Butola, "Improving the impact resistance of textile structures by using shear thickening fluids: A review", *Critical Rev. Solid State Mater. Sci.*, **37**, 115-29, 2012.
- [3] S. Gürgen, M.C. Kuşhan, and W. Li, "Shear thickening fluids in protective applications: A review", *Prog. Polym. Sci.*, **75**, 48-72, 2017.
- [4] M.P. Allen and D.J. Tildesley, *Computer simulation of liquids*: Oxford university press; 2017.
- [5] K. Kadau, T.C. Germann, and P.S. Lomdahl, "Large-scale molecular-dynamics simulation of 19 billion particles", *Int. J. Modern Phys. C*, **15**, 193-201, 2004.
- [6] D.C. Rapaport and D.C.R. Rapaport, *The art of molecular dynamics simulation*: Cambridge university press; 2004.
- [7] M. Zojaji, A. Hydarinasab, S.H. Hashemabadi, and M. Mehranpour, "Rheological behaviour of shear thickening fluid of graphene oxide and SiO_2 polyethylene glycol 400-based fluid with molecular dynamic simulation", *Mol. Simulat.*, **47**, 317-25, 2021
- [8] S. Plimpton, *Fast Parallel Algorithms for Short-Range Molecular Dynamics*, Sandia National Labs, Albuquerque, NM (United States); 1995.
- [9] W.M. Brown, P. Wang, S.J. Plimpton, and A.N. Tharrington, "Implementing molecular dynamics on hybrid high performance computers—short range forces", *Comput. Phys. Commun.*, **182**, 898-911, 2011.
- [10] S.L. Mayo, B.D. Olafson, and W.A. Goddard, "Dreiding: A generic force field for molecular simulations", *J. Phys. Chem.*, **94**, 8897-909, 1990.
- [11] A.K. Rappé, C.J. Casewit, K. Colwell, W.A. Goddard III, and W.M. Skiff, "UFF, a full periodic table force field for molecular mechanics and molecular dynamics simulations", *J. Am. Chem. Soc.*, **114**, 10024-10035, 1992.
- [12] X.-Q. Liu, R.-Y. Bao, X.-J. Wu, W. Yang, B.-H. Xie, and M.-B. Yang, "Temperature induced gelation transition of a fumed silica/PEG shear thickening fluid", *Rsc Adv.*, **5**, 18367-18374, 2015

Characterizing of Carbon Black on Rheological and Electrical Properties Parts Prepared by FDM Method

Amirreza Eftekhari¹, Fatemeh Goharpey^{1*}, and Milad Mehranpour²

1. Department of Polymer Engineering, Amirkabir University of Technology, Tehran, Iran

2. Islamic Azad University, Science and Research Branch, Tehran, Iran

*goharpey@aut.ac.ir

Abstract

One of the emerging methods for manufacturing parts is 3D printing, among which FDM has been given more attention due to its low price and available materials. Printing polymer nanocomposites with a conductivity of at least 10^{-5} S/cm is a desirable option for applications in electrical sensors. Typically, achieving electrical conductivity in these nanocomposites involves the use of carbon nanotubes, which can be costly and challenging to print. An alternative approach is to replace part of them with cheap carbon nanoparticles such as carbon black. Utilizing a combination of carbon black and carbon nanotubes yields improved printing properties besides the cost reduction. The printability of these materials can be assessed through viscosity curves and established rheological models.

Keywords: FDM, ABS, conductive nanocomposites, CNT, 3D-printing

Introduction

3D printing (especially the FDM method) has revolutionized manufacturing by enabling the creation of complex, customized objects with precision and efficiency. This method can be used to make electronic kits. Meanwhile, electrical conductivity is considered a critical parameter. Recent studies demonstrate that ABS nanocomposites with carbon nanoparticles offer new possibilities for the 3D printing industry, providing novel capabilities in the production of intricately detailed and high-strength components. ABS and creating nanocomposites with carbon nanoparticles, the potential to fabricate electronic sensors becomes attainable. One of the carbon nanoparticles used in this field is carbon nanotubes, which, despite their excellent efficiency, have limited industrial application due to their high price. One approach is to use other carbon nanoparticles alongside these nanoparticles to reduce costs [1]. The filament of nanocomposites must be both printable and cost-effective. In this regard, the investigation of the rheology of these nanocomposites is of paramount importance. Rheology helps understand their internal structure, viscosity, and behavior during printing. These fundamental insights are essential for optimizing the printing process and obtaining high-quality components with optimal properties from these nanocomposites.

Experimental

Acrylonitrile-butadiene-styrene (ABS) was supplied by Tabriz Petrochemical Co, Iran (SD150), The MWCNT used in This Study were commercially available grade, NC7000, from Nanocyl Inc., Belgium. The multiwall

had a carbon purity of 90%, average outer diameter of 9.5 nm, length up to 1.5 μm , and surface area of 250-300 $\text{m}^2\cdot\text{g}^{-1}$. Commercially available super conductive carbon blacks, Ketjen Black EC 300J were supplied by Lion Specialty Chemicals Co., Japan. CB had a DBP absorption of 360 ($\text{cm}^3/100\text{ g}$) and BET surface area of 800 $\text{m}^2\cdot\text{g}^{-1}$. Dichloromethane (DCM) and chloroform were purchased from Dr. Mojallali Inc., Iran.

Preparation of Nanocomposites

Solution method was applied to prepare the masterbatch of nanocomposites. Then the masterbatch was added to neat ABS in Twin Screw Extruder Brabender DSE20 (L/D=40) at 230 and screw speed of 150 rpm. The nanocomposites incorporating the desired amount of nanoparticles were achieved. The Production of filaments with 1.75 0.05 mm in diameter was conducted by single screw extruder (Noztek).

Results and Discussion

Fig. 1 illustrates the DC electrical conductivity as a function of the wt% of carbon nanoparticles. Samples containing carbon black exhibit lower conductivity compared to those with carbon nanotubes due to unfavorable dispersion and formation of clusters. These clusters do not create sufficient conductive pathways. Substituting carbon black with carbon nanotubes results in an increase in electrical conductivity, indicating that carbon nanotubes lead to better dispersion of CB. This increase is significant to the extent that a synergistic effect is observed in the hyb1:1 sample, surpassing the conductivity of the CNT1.5 sample. To investigate the internal structure of printed nanocomposites

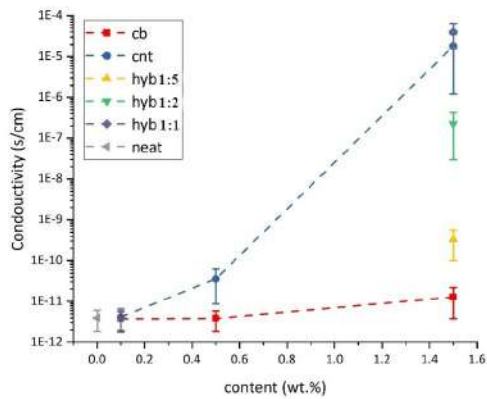


Fig. 1. Electrical conductivity versus weight percentage of nanoparticles.

containing CB and CNT (CB1.5 and CNT1.5), the fractal scaling theory developed for colloidal gels can be used (Eqs. (1) and (2)) [2]:

$$\gamma_n^c \propto \varphi^{-(1+x)/(3-df)} \quad (1)$$

$$G' \propto \varphi^{(3+x)/(3-df)} \quad (2)$$

This model correlates the composition percentage of nanoparticles with the critical strain and storage modulus at low frequencies, allowing for a better understanding of the formed structures. By conducting fractal network calculations (df) for CB and CNT nanoparticles, 2.67 and 1.25 were obtained, respectively. The CNT1.5 sample has a smaller fractal dimension than the CB1.5 due to the higher aspect ratio of nanotubes and better dispersion. A higher value in the sample containing CB indicates unfavourable dispersion and the presence of clusters, consistent with the results of the electrical conductivity test. Fig. 2 shows the behaviour of complex viscosity (a measure of fluidity) versus frequency. Replacing a part of CNT nanoparticles with CB in hybrid samples has a lesser impact on viscosity. Besides the lower viscosity observed in the hybrid samples compared to the CNT1.5 sample, the slope of the viscosity reduction has decreased. This issue also manifests in the printing process, where continuous printing and smooth

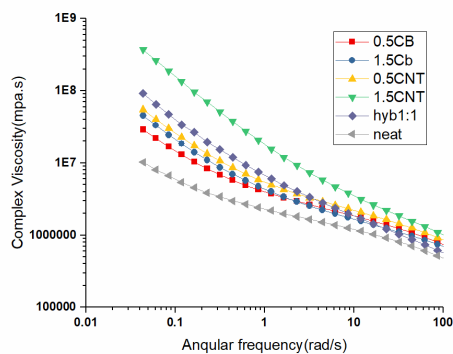


Fig. 2. Viscosity changes versus frequency using model fitting, the points are the experimental results, and the lines are the results of the fitting.

Table I. Parameters obtained using modified Carreau-Yasuda model fitting.

Sample	n	σ_0 (pa)
Neat	0.359	856702
CNT0.5	0.311	2229478
CNT1.5	0.190	15491121
CB0.5	0.321	1116740
CB1.5	0.298	1877462
Hyb1:1	0.282	3832112

printing surfaces are observed in sample hyb1:1, while nozzle blockage occurs in the CNT1.5 sample. To assess the obtained data, the modified Carreau-Yasuda model was employed for filled systems (Eq. (3)) [3]:

$$|\eta^*(\varphi, \omega)| = \frac{\sigma_0(\varphi)}{\omega} + \eta_0 \{1 + (\lambda\omega)^a\}^{(n-1)/a} \quad (3)$$

According to Fig. 2, the fitting curve aligns with the experimental data. As it is well-known, the yield stress, an essential parameter in the interaction between nanoparticles, increases with the higher percentage composition of CNT nanoparticles. Meanwhile, the Power-law power decreases as the CNT values increase, indicating the printing process's difficulty in the CNT1.5 sample (Table I).

Conclusion

In this research, viscoelastic properties were evaluated on the optimal samples in terms of electrical conductivity. Two samples, CNT1.5 and Hyb1:1, had a conductivity value in the same order of magnitude but displayed different printable behavior. The CNT1.5 sample, characterized by higher viscosity and a steeper upturn viscosity behavior at low frequency, demonstrates greater elasticity and forms a robust network, as fractal dimension theory suggests. However, this robust network adversely affects printability, leading to nozzle blockage. Furthermore, fitting the modified Carreau-Yasuda model revealed that the yield stress in the CNT1.5 sample is about four times that of the hyb1:1 sample, which indicates a strong interaction between the nanoparticles. This interaction results in incomplete printing and a rough surface. Therefore, the hyb1:1 sample proves optimal for electrical sensors due to its good conductivity and suitable printability behavior.

References

- [1] Y. Li et al., *Eur. Polym. J.*, **108**, 461-471, 2018,
- [2] J. Vermant et al., *J. Rheol. (N. Y. N. Y.)*, **51**, 429-450, 2007.
- [3] Jyoti et al., *Compos. Part B: Eng.*, **154**, 337-350, 2018.

Effect of Iranian Endemic Gums on Rheological and Tribological Properties of Non-Dairy Reduced-Fat Coffee Creamer Powder

Ferdows Pourabdollah and Seyed Mohammad Ali Razavi*

Center of Excellence in Native Natural Hydrocolloids of Iran, Ferdowsi University of Mashhad, Mashhad, Iran

*s.razavi@um.ac.ir

Abstract

Coffee creamers are commonly used to reduce the acidity and enhance the texture of coffee, but they often have high fat content. This study investigated low-fat alternatives using two types of Iranian gum: cress seed gum and Serish root gum. The creamers were tested using rheological and tribological tests, and the results indicated that as fat content decreased, dynamic viscosity also reduced. Notably, cress seed gum samples had superior viscosity than the other group. At a speed of 100 mm/s, friction coefficients were lowest for the sample without fat reduction containing cress seed gum, while the sample with 30% fat reduction and cress seed gum had the highest coefficient of friction. Overall, the cress seed gum samples performed better, while those containing Serish root gum closely resembled the commercial sample. These findings highlight the potential of Iranian endemic gums as effective thickeners in reduced-fat liquid food systems.

Keywords: tribology, rheology, fat reduction, cress seed gum, Serish root gum

Introduction

Coffee is a widely consumed beverage globally, commonly accompanied by coffee creamers to add a creamy texture and appearance to their drinks, but they're high in saturated fat [1]. High-fat diets increase health risks like cardiovascular diseases, high blood pressure, and obesity. This has led consumers to prefer low-fat products. Therefore, creating low-fat foods that mimic standard products is challenging for manufacturers [2,3]. Hydrocolloids are commonly used as fat substitutes in food and as thickeners, gel-forming agents, emulsifiers, and stabilizers [4]. Iran's endemic gums have excellent stabilizing and consistency properties in various food systems [5]. Cress seed gum (CSG) is a stable and effective food thickener with a molecular weight of 540 kDa and is a suitable alternative to xanthan gum [6]. Also, based on the recent research by Salahi *et al.* Serish root gum (SRG) has great potential for different functions in food systems [7]. Combining rheological and tribological properties can be a promising method to predict food oral perceptions [8]. Given the lack of prior research, our study investigates CSG and SRG's effects on coffee creamers' oral behavior with varying fat content (0, 10, 20, and 30%). We will analyze the product's rheological and tribological properties as an emulsion in hot water to accomplish this.

Experimental

Materials

Raw materials necessary for the basic formulation were purchased from food ingredient centers. Cress seeds and serish roots were purchased from a local medicinal market in Mashhad, Iran. CSG and SRG powder were extracted based on the method used by Karazhiyan *et al.* and Salahi

et al. [6,7]. Then, all the samples were mixed in water at 95 °C with a constant amount for each.

Methods

The samples' dynamic viscosity was measured using a capillary viscometer (Canon Ablod, Semi Micro Viscometer, No. 100, $k=0.019907 \text{ mm}^2/\text{s}^2$, Canon, USA) at 37 °C. The test was repeated three times for each sample, and the average passing time was recorded. The dynamic viscosity (η) using the following equation (Eq. (1)):

$$\eta = k \cdot \rho \cdot t \quad (1)$$

Which "t" was the sample passage time and "ρ" was the density of the samples. Samples were evaluated using a designed tribometer. AISI 52100 steel disc was used with 1 N normal force at 37 °C. Results were recorded at 100-450 mm/s rotational speeds.

Results and Discussion

Dynamic Viscosity

The findings demonstrate the influential role of CSG and SRG as stabilizers and thickeners. Analysis of Fig. 1c and Table I reveals that samples with CSG have higher viscosity than the commercial sample. Reducing fat in samples with SRG has a greater impact on dynamic viscosity than the CSG samples. The fat content reduction did not significantly impact the viscosity of these treatments ($P>0.05$). Also, Samples with SRG had a similar viscosity to the commercial sample ($P>0.05$), which indicates that samples containing CSG have acted better as a thickener.

Table I. Dynamic viscosity of all treatments with two reputation.

C-0%(b)	C-10%(b)	C-20%(b)	C-30%(b)
0.799± 0.003	0.79± 0.008	0.796± 0.004	0.787± 0.007
S-0%(a)	S-10%(a)	S-20%(a)	S-30%(a)
0.721± 0.004	0.717± 0.008	0.712± 0.003	0.712± 0.01
CC(a)		0.723±0.003	

a-b: Means followed by the same letters are not significantly different ($P > 0.05$). (CC = commercial creamer)

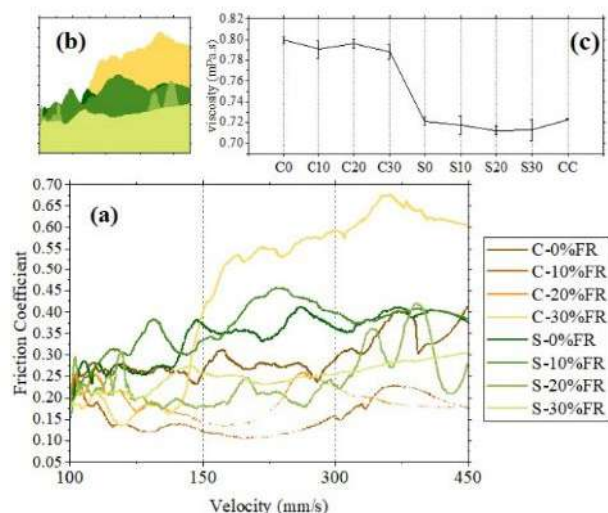


Fig. 1. (a) Tribology trend of all treatments speeding from 0 mm/s to 450 mm/s (b) area under the curve of all tribology trends (c) dynamic viscosity of all treatments.

Stribeck Curve

According to the results of the tribology test (Fig. 1a), which covered two Stribeck regimes (mix, elastohydrodynamic, until the middle of hydrodynamic) with increasing speed from 100 mm/s to 450 mm/s, the friction coefficient increased. However, the sample containing CSG with a 30% fat reduction had the highest friction coefficient values at higher speeds and in the elastohydrodynamic region, which was the opposite in the mix region (Fig. 1b). Conversely, the sample containing CSG without fat had the lowest friction coefficient values in all areas. Additionally, the friction coefficients of the samples at a speed of 100 mm/s, which was the optimal speed for oral simulation to assess creaminess, almost showed that the reduction of fat led to a decrease in friction coefficients, although this was not significant. In conclusion, the CSG samples exhibited lower friction coefficients than those containing SRG.

Conclusion

Based on the data derived from both tests, it is evident that the samples containing CSG exhibited superior performance, displaying higher dynamic viscosity and lower friction across various regions of the Stribeck curve. This suggests that creaminess can be better perceived through these

examples. Conversely, the SRG samples demonstrated favorable results that resembled the commercial sample. Consequently, it can be inferred that using Iranian endemic gums as substitutes for commercial thickeners and fat reduction has yielded commendable outcomes, thereby, the possibility of producing a healthier product.

Acknowledgment

This project was funded by the Deputy of Research and Technology, Ferdowsi University of Mashhad, Iran.

References

- [1] S. Hedayatnia et al., "Effect of different fat replacers and drying methods on thermal behaviour, morphology and sensory attributes of reduced-fat coffee creamer", *LWT-Food Sci. Technol.*, **72**, 330-342, 2016.
- [2] E. BONCIU, "Food processing, a necessity for the modern world in the context of food safety: A review, annals of the university of Craiova-Agriculture, Montanology", *Cadastre Series*, **47**, 391-398, 2018.
- [3] J. Hamilton, B. Knox, D. Hill, and H. Parr, "Reduced fat products—Consumer perceptions and preferences", *British Food J.*, **102**, 494-506, 2000.
- [4] M. Manzoor et al., "Food hydrocolloids: Functional, nutraceutical and novel applications for delivery of bioactive compounds", *Int. J. Biol. Macromol.*, **165**, 554-567, 2020.
- [5] S. Naji and S.M. Razavi, "Functional and textural characteristics of cress seed (*Lepidium sativum*) gum and xanthan gum: Effect of refrigeration condition", *Food Biosci.*, **5**, 1-8, 2014.
- [6] H. Karazhiyan et al., "Rheological properties of *Lepidium sativum* seed extract as a function of concentration, temperature and time", *Food Hydrocolloid.*, **23**, 2062-2068, 2009.
- [7] M. Salahi, S.M.A. Razavi, and E. Hasanvand, "Physicochemical, rheological and functional properties of a novel gum from *Eremurus luteus* root", *Bioactive Carbohydr. Dietary Fibre*, **27**, 100296, 2022.
- [8] F.C. Godoi, B.R. Bhandari, and S. Prakash, "Tribo-rheology and sensory analysis of a dairy semi-solid", *Food Hydrocolloid.*, **70**, 240-250, 2017.

Effect of Starch Type on the Rheological Behaviour of Custard

Razieh Kashi and Seyed Mohammad Ali Razavi*

Center of Excellence in Native Natural Hydrocolloids of Iran, Ferdowsi University of Mashhad, Mashhad, Iran

*s.razavi@um.ac.ir

Abstract

Custard is a starch-based popular dessert with a semi-solid texture. The present study aimed to investigate the changes in rheological properties of custard prepared with waxy corn starch (WCS) and high hydrostatic pressure (HHP) treated starch. All custard samples showed shear-thinning and thixotropic behaviours, which described well by the Sisko and Weltman models, respectively. The results indicated that both WCS and HHP could increase the flow behaviour index significantly from 0.04 to 0.22 in the custard samples. Using WCS and HHP-treated starch led to a significant change of initial shear stress from 1.64 ± 0.04 Pa in the control sample to 2.98 ± 0.03 and 1.36 ± 0.00 in custards, respectively.

Keywords: dairy dessert, rheology, starch, thixotropy

Introduction

Custards are generally milk starch-based desserts, with a typical texture of a semi-solid. They can be explained as a suspension of deformable starch particles dispersed in a continuous medium containing milk fat and proteins as well as a gelling agent (mostly carrageenan) that has high syneresis and phase separation [1]. Starch has a critical role in the properties of the system, including texture, flow behaviour, and viscosity, depending on the type and the concentration [2]. There are different methods to modify starch and increase the polymer flexibility with new physicochemical properties [3]. Applying high hydrostatic pressure is a physical modification method that could increase the stability, water absorption and creamy texture of the treated waxy corn starch [4,5]. There are many research reports on the effect of formulation on the rheological characteristics of custards [1,6-10]. This study aimed to determine the rheological properties of custard prepared by different starch types including waxy corn starch and HHP modified starch.

Experimental

Materials

Waxy corn starch (CAS No: 9005-25-8), sucrose (CAS No: 57-50-1), and κ -Carrageenan (CAS No: 11114-20-8) were provided by Sigma-Aldrich Company (St. Louis, MO, USA). Milk powder from Pegah Khorasan Company and corn starch from Golha Company were bought.

HHP Starch Preparation

First, a 20 w/w% suspension of waxy corn starch is prepared and stirred for 30 min at ambient temperature to disperse starch particles in the water, completely. Then the prepared suspensions are transferred to the centrifuge tubes

and every tube is subjected to a pressure of 600MPa (high hydrostatic pressure device, model S-FL-065-200-9-W, RIFST, Iran) for 20 min (pressure increase rate 10 Mpa/s to 20 MPa/s). Then, treated waxy corn starch is frozen in liquid nitrogen and dried for 24 h at -60 °C and 0.0001 Torr pressure [5].

Sample Preparation

The reconstituted milk was rebuilt by mixing the skim milk (0.1%) or whole milk (2.67%) powder in water with a ratio of 11.21 g in 89 mL. Afterwards, the prepared suspension was stirred using a magnetic stirrer at 450 rpm for 5 min at ambient temperature (about 25 °C), and 4.5 g starch, 6.5 g sugar and 0.25 g κ -Carrageenan powders were added while stirring continued. Then put in a boiling water bath (about 95 °C) for 30 min. Finally, the cooked desserts were saturated with vapour and stored at 4 °C for 24 h before the tests. Table I indicates the formulations of prepared custard desserts.

Rheological Measurements

The rheological characteristics of the prepared samples were fitted out with a viscometer (Visco 88, Bohlin Instruments Cirencester, Gloucestershire, UK). During experiments, the temperature was kept at 6 °C by applying a circulating water bath. Then, the data from both time and shear-dependent tests were fitted to the Weltman (1) and Sisko model (2) using MATLAB (R2021b, MathWorks,

Table I. Formulation of the custard desserts prepared by selected starches.

Sample	Starch	Sugar	Milk fat
C	Native	Sucrose	Whole
WSF	Waxy	sucrose	Whole
HSF	HHP	Sucrose	Whole



Table II. Weltman model parameters to describe time-dependent behaviour of custard samples at 6 °C.

Sample	A (Pa)	- B (Pa)	R ²	RMSE
C	1.64±0.04 ^a	0.12±0.00 ^a	91.12±0.08	0.025±0.01
WSF	2.98±0.03 ^b	0.33±0.01 ^b	96.55±0.04	0.05±0.03
HSF	1.36±0.00 ^c	0.13±0.00 ^a	98.20±0.00	0.021±0.00

Table III. Sisko model parameters to describe time-independent behaviour of custard samples at 6 °C.

Sample	η_0 (Pa.s)	k (Pa.s ⁿ)	n(-)	R ²	RMSE
C	0.08±0.6 ^a	119.40±18.66 ^a	0.04±0.05 ^a	99.17±0.00	0.21±0.11
WSF	0.10±0.00 ^a	24.43±1.11 ^b	0.22±0.01 ^b	99.68±0.00	0.04±0.02
HSF	0.04±0.00 ^a	39.17±1.10 ^b	0.22±0.00 ^b	99.56±0.00	0.09±0.00

USA) curve fitting toolbox:

$$\tau = A + B \ln(t) \quad (1)$$

$$\eta = \eta_{\infty} + k \dot{\gamma}^{n-1} \quad (2)$$

Results and Discussion

Using waxy corn starch could increase the time dependency and initial viscosity while similar HHP samples were weak and had lower viscosity than control. Table II demonstrates the Weltman coefficients that could investigate the time dependency well ($R^2=95.29\pm0.05$). Waxy starch led to an increase in both parameters of this model [6]. Reported similar results that using more complex starch increases the initial shear stress. An intensifying shear rate from 14 s^{-1} to 800 s^{-1} indicated a shear-thinning behaviour in all treatments. Waxy and HHP starch both decreased the viscosity. Based on the report of [11], limited changes in HHP treatment are a sign of higher stability of the structure against shear rate. Table III shows the measured parameters of the Sisko model that could explain the behaviour of the custard well with R^2 of 99.47 ± 0.00 . Adding waxy or HHP starch has led to a significant increase in the flow index which means lower molecular bond breaks and viscosity decreases slowly [12]. The consistency index decreased significantly with changing the starch type.

Conclusion

In the present study, the effects of waxy corn and HHP starches on the rheological properties of custard were investigated. HHP modified starch could increase the viscosity and shear-thinning behaviour of the dessert which is acceptable characteristics. Therefore, the proposed formulation can be used as a proper dessert with diminished syneresis. However, studying the effect of adding hydrocolloids and stabilizers is recommended to control the shear-thinning behaviour and the rate of viscosity changes.

References

- [1] R.A. de Wijk et al., "Texture of semi-solids; sensory and instrumental measurements on vanilla custard desserts", *Food Qual. Preference*, **14**, 305-317, 2003.
- [2] C. Alamprese and M. Mariotti, "Effects of different milk substitutes on pasting, rheological and textural properties of puddings", *LWT-Food Sci. Technol.*, **44**, 2019-2025, 2011.
- [3] S. Saboonchia et al., "Applications of modified starch in food", in 3rd International Congress on Engineering, Technology & Innovation, 2021.
- [4] L. Pei-Ling, H. Xiao-Song, and Q. Shen, "Effect of high hydrostatic pressure on starches: A review", *Starch Stärke*, **62**, 615-628, 2010.
- [5] A. Heydari and S.M.A. Razavi, "Evaluating high pressure-treated corn and waxy corn starches as novel fat replacers in model low-fat O/W emulsions: A physical and rheological study", *Int. J. Biol. Macromol.*, **184**, 393-404, 2021.
- [6] B. Abu-Jdayil, and H.A. Mohameed, "Time-dependent flow properties of starch–milk–sugar pastes", *Eur. Food Research Technol.*, **218**, 123-127, 2004.
- [7] J.F. Vélez-Ruiz, L. González-Tomás, and E. Costell, "Rheology of dairy custard model systems: Influence of milk-fat and hydrocolloid type", *Eur. Food Res. Technol.*, **221**, 342-347, 2005.
- [8] M. Keršienė et al., "Interactions between flavour release and rheological properties in model custard desserts: Effect of starch concentration and milk fat", *Food Chem.*, **108**, 1183-1191, 2008.
- [9] A. Tarrega and E. Costell, "Effect of composition on the rheological behaviour and sensory properties of semisolid dairy dessert", *Food Hydrocolloid.*, **20**, 914-922, 2006.
- [10] A. Tárrega, J. Vélez-Ruiz, and E. Costell, "Influence of milk on the rheological behaviour of cross-linked waxy maize and tapioca starch dispersions", *Food Res. Int.*, **38**, 759-768, 2005.
- [11] J.F. Velez-Ruiz, P. Hernandez-Carranza, and M. Sosa-Morales, "Physicochemical and flow properties of low-fat yogurt fortified with calcium and fiber", *J. Food Process. Preservation*, **37**, 210-221, 2013.
- [12] L. Rojas-Martin, S.E. Quintana, and L.A. García-Zapateiro, "Physicochemical, rheological, and microstructural properties of low-fat mayonnaise manufactured with hydrocolloids from *dioscorea* & *rotundata* as a fat substitute", *Processes*, **11**, 492, 2023.

Behavior of Dilute Viscoelastic Solution in Turbulent Pipe Flows: CFD Simulation

Mohammad Niazi^{1*}, Seyed Nezameddin Ashrafizadeh¹, Seyed Hassan Hashemabadi¹, and Hamidreza Karami²

1. Research Lab for Advanced Separation Processes, Department of Chemical Engineering, Iran University of Science and Technology, Narmak, P.O. Box 16846-13114, Tehran, Iran

2. Quality Control Department, Modalal Industrial Group, Kermanshah, Iran

*m.niazi53@gmail.com

Abstract

This study aimed to simulate turbulent pipe flow of drag-reducing fluids using RKE and RNG k-ε model. The results were then compared with Pinho simulations and some experimental data extracted from the literature. To simulate pipeline flow, CFD software was employed, incorporating a non-linear molecular viscosity and damping function to accurately account for near-wall effects. In addition to optimizing the parameters in the damping function and stress term, this research incorporated non-Newtonian terms into the k, ε and momentum transfer equations. The results showed that the model's ability to calculate essential flow parameters had significantly improved. The model's average error in calculating the friction factor of the fluids under study was determined to be 5.45%. This represents a noteworthy enhancement compared to the Pinho model, which has an average error of 32.49%.

Keywords: pipeline transportatio, drag reduction agents, turbulent flow, CFD simulation, viscoelastic fluids

Introduction

The modified GNF model which integrates an adjusted constitutive equation for the variable viscosity of the drag-reducing fluid, taking into consideration the elastic properties of DRA and initially introduced by Pinho is adopted in the present work [1]. For the CFD simulation, the RKE and RNG equations were initially selected and then modified to incorporate non-Newtonian terms. In order to enhance the accuracy of the results, certain equation parameters were optimized, leading to positive improvements.

Rheological and Transport Equations

The transport and rheological equations in the axial direction during steady-state, incompressible, and isothermal turbulent pipe flow are as follows [1]:

$$\nabla \cdot \mathbf{u} = 0 \quad (1)$$

$$\nabla \cdot (\rho \mathbf{u}_i \mathbf{u}_i) = -\nabla \bar{p} + \nabla \cdot (2\bar{\mu} \mathbf{S} - \rho \overline{u'_i u'_j} + 2\overline{\mu' s'}) \quad (2)$$

$$\bar{\mu} = f_v \bar{\mu}_h + (1 - f_v) \eta_v \quad (3)$$

$$\frac{Dk}{Dt} = \frac{\partial}{\partial x_j} \left[\left(\bar{v} + \frac{v_t}{\sigma_k} \right) \frac{\partial k}{\partial x_j} \right] + \overline{u'_i u'_j} \frac{\partial u_i}{\partial x_j} - \varepsilon + \frac{2}{\rho} \overline{\mu' s'} \frac{\partial u_i}{\partial x_j} \quad (4)$$

$$\frac{D\varepsilon}{Dt} = \frac{\partial}{\partial x_j} \left[\left(\bar{v} + \frac{v_t}{\sigma_\varepsilon} \right) \frac{\partial \varepsilon}{\partial x_j} \right] + f_1 C_{\varepsilon 1} \frac{\varepsilon}{k} P_k - f_2 C_{\varepsilon 2} \frac{\varepsilon^2}{k} + C_{\varepsilon 4} \frac{v_t}{\sigma_\varepsilon \bar{v}} \frac{\partial \varepsilon}{\partial x_j} \frac{\partial \bar{v}}{\partial x_j} \quad (5)$$

$$2\overline{\mu' s'} = \bar{c} \frac{k_v k_e}{A_\varepsilon^{p-1}} \left[\frac{v_t}{2\bar{v}} \left(\frac{\partial u_i}{\partial x_j} \right)^2 \right]^{\frac{p+n-2}{2}} \frac{\sqrt{v_t}}{L_c} \frac{\partial u_i}{\partial x_j} \quad (6)$$

In the given equations, \bar{u} is the instantaneous flow velocity, δ is the fluid density, \bar{P} is the pressure, constants k_v , k_e , n , and p are the rheological characteristics of the fluid, u'_i and u'_j the fluctuating axial and radial velocities, respectively.

Results and Discussion

The drag-reducing fluids used in this study were aqueous

Table I. Rheological parameters of the viscoelastic model.

DRA	k_v	n	k_e	p
0.2% XG	0.2701	0.4409	3.8519	1.2592
0.3% CMC	0.2748	0.6377	2.7485	1.2214
0.09/0.09% CMC/XG	0.1518	0.5783	2.1833	1.1638
0.125% PAA	0.2491	0.4250	8.2500	1.4796

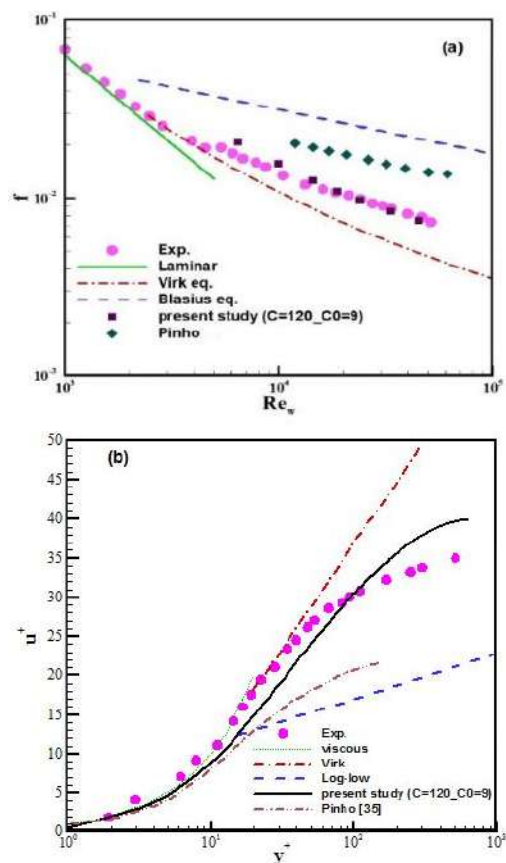


Fig. 1. Comparing the predicted and measured values of friction factor: (a) and normalized velocity (b) for 0.2% XG.

solutions of polyacrylamide (PAA), xanthan gum (XG), carboxymethyl cellulose (CMC), and a blend of XG and CMC at various weight concentrations, each with their own unique characterization, as outlined in Table I. The flow parameters under investigation are the friction factor, axial mean velocity, and Reynolds shear stress. The obtained friction factor data and mean axial velocity were compared with experimental data from references [2]. The results for 0.2% XG were shown in Fig. 1.

Conclusion

We substituted the Nagano and Hishida k - ϵ model with the RKE and RNG models, incorporating non-Newtonian fluid terms into them. We also optimized parameters like the damping function and stress terms (C and C0) for each fluid to obtain optimal values. The simulations were conducted using CFD software, and the results were compared to Pinho's model and empirical data, leading to significant findings: The friction factor profiles and normalized axial velocity profile has shown better agreement with experimental data compared to Pinho's findings.

References

[1] D. Cruz, F. Pinho, and P. Resende, "Modelling the new stress for improved drag reduction predictions of

viscoelastic pipe flow", *J. Non-Newton. Fluid Mech.*, **121**, 127-141, 2004.

[2] M. Escudier, F. Presti, and S. Smith, "Drag reduction in the turbulent pipe flow of polymers", *J. Non-Newton. Fluid Mech.*, **81**, 197-213, 1999.

Non-linear Rheological Behavior of Water in Water Emulsions

Zahra Zamani and Seyed Mohammad Ali Razavi*

Center of Excellence in Native Natural Hydrocolloids of Iran, Ferdowsi University of Mashhad,

P.O.Box 91775-1163, Mashhad, Iran

*s.razavi@um.ac.ir

Abstract

We studied the large amplitude oscillatory shear (LAOS) behavior of water-in-water (W/W) emulsions stabilized by 0.25 wt% basil seed gum (BSG) + 0.5, 1, and 2 wt% waxy corn starch (WCS) and 0.2 wt% BSG + 0.5, 1, 2 wt% high pressure treated waxy corn starch (HWCS). At each BSG level, increasing concentrations of WCS and HWCS resulted in a notable decrease in nonlinearity, while the shear thickening factors and strain stiffening values increased. Additionally, the values of G''/G'_{1st} were significantly lower than those of G''/G'_{1st} .

Keywords: Lissajous plot, non-linear viscoelastic, rheology, water in water emulsion

Introduction

The W/W emulsions are created from a binary polymeric system that uses biocompatible ingredients like proteins and polysaccharides, making them a safe and effective option for use [1]. Basil seed gum (BSG) is a new, all-natural emulsifier used in food preparation [2]. Waxy corn starch (WCS) is a widely used food ingredient used as a thickener, stabilizer, and gelling agent. The high hydrostatic pressure (HHP) process alters the functional qualities of starch sources [3]. Rheological effects have a role in W/W emulsion storage stability. According to Anvari and Joyner [4], the examination of large amplitude oscillatory shear (LAOS) characteristics in different food products is highly significant as it offers valuable insights into the micro- and macro-structural features of foods when subjected to large deformations. Our research led us to the conclusion that 0.25 wt% BSG+ 0.5, 1, or 2 wt% WCS and 0.2 wt% BSG+ 0.5, 1, or 2 wt% HWCS emulsions were stable W/W emulsions for at least a week [5]. In this study LAOS rheology of stable W/W emulsions (0.25 wt% BSG+ 0.5, 1, or 2 wt% WCS and 0.2 wt% BSG+ 0.5, 1, or 2 wt% HWCS) were investigated.

Experimental

Basil Seed Gum Extraction

Based on the study conducted by Razavi *et al.* [6].

High Hydrostatic Pressure Treatment of Waxy Corn Starch (HWCS)

According to the research conducted by Heydari and Razavi [3].

Preparation of the W/W Emulsion

Based on the study conducted by Zamani and Razavi [5].

Large Amplitude Oscillatory Shear (LAOS) Measurements
The non-linear (n-LVE) elastic and viscous properties of the emulsions were evaluated by conducting an amplitude sweep from 0.01% to 1000% at a constant frequency of 1 Hz and temperature of 25 °C. The elastic Lissajous plots, the Fourier transformed examination in the time domain, and the strain stiffening feature (S factor) and shear-thickening property (T factor) within each cycle were determined according to the methodology proposed by Ewoldt *et al.* [7] as follows:

$$S = \frac{\sigma_L^i - \sigma_M^i}{\sigma_L^i} \quad (1)$$

$$T = \frac{\eta_L^i - \eta_M^i}{\eta_L^i} \quad (2)$$

Statistical Analysis

The data was analyzed using SPSS, Duncan Multiple Range Test with significance levels set at $p < 0.05$. The rheological data were fitted using MATLAB (2013a) software's Levenberg-Marquardt technique and curve fitting toolbox.

Results and Discussion

LAOS Characteristics

The elastic Lissajous-Bowditch plots of the W/W emulsions at 1000% strain and 1 Hz frequency are shown in Fig. 1. The limited elastic Lissajous plots decrease when WCS and HWCS concentrations increase from 0.5 wt% to 2 wt%, indicating greater resilience to disruption, more elastic-dominant characteristics, stronger stiffness, and lower energy dissipation. Samples containing HWCS had lower elastic Lissajous plots due to steric stability and smaller droplet size of HHP-treated starches. In addition to visual representation, it is important to employ measurable techniques to thoroughly investigate nonlinear shear

Table I. The ratio of the third harmonic elastic modulus to the first harmonic elastic modulus (G'_3/G'_1) and the ratio of the third harmonic loss modulus to the first harmonic loss modulus (G''_3/G''_1), and strain-softening (S-factor) and shear-thinning (T-factor) parameters for the W/W emulsions.

Samples	G'_3/G'_1	G''_3/G''_1	S	T
0.25BSG +0.5WC S	0.451± 0.011 ^a	0.091±0. 010 ^a	0.378± 0.054 ^f	-0.195±0.032 ^d
0.25BSG +1WCS	0.391± 0.024 ^{ab}	0.074±0. 021 ^b	0.452± 0.068 ^d	-0.157±0.025 ^c
0.25BSG +2WCS	0.33±0 .014 ^b	0.052±0. 011 ^d	0.534± 0.088 ^c	-0.135±0.014 ^b
0.2BSG+ 0.5HWC S	0.201± 0.081 ^c	0.062±0. 001 ^c	0.402± 0.096 ^e	-0.179±0.078 ^d
0.2BSG+ 1HWCS	0.159± 0.027 ^{cd}	0.051±0. 002 ^d	0.625± 0.038 ^b	-0.144±0.041 ^{bc}
0.2BSG+ 2HWCS	0.110± 0.031 ^d	0.043±0. 001 ^e	0.801± 0.095 ^a	-0.110±0.031 ^a

stress responses. The W/W emulsions exhibited linear viscoelastic behavior when the ratio of G'_3/G'_1 and G''_3/G''_1 was less than 0.01, which fell in the strains less than 10%. This was further supported by the Lissajous-Bowditch plots, which indicated perfect viscoelastic characteristics (data not shown). For all W/W emulsions at a 1000% strain, the amounts of these ratios were higher than 0.01, illustrating the nonlinear viscoelastic characteristic of the created emulsions (Table I). In addition, the amounts of G'_3/G'_1 of the W/W emulsions were noticeably greater than the amounts of G''_3/G''_1 , indicating the predominance of nonlinear elastic behavior in the W/W emulsions. Furthermore, the extent of nonlinearity decreased as the concentration of WCS and HWCS increased (P

<0.05). High concentrations and smaller droplet sizes of starches contribute to steric stability in W/W emulsions, resulting an efficient structure resistant to large strains. All W/W emulsions showed strain-stiffening and shear-thinning characteristics. Higher concentrations of HWCS in emulsions increased T parameter values, indicating stiffening. Higher S factor values indicated greater resilience and consistency under higher strains, possibly due to increased stiffness and structural stability.

Conclusions

We examined the behavior of W/W emulsions (comprising 0.2 wt% BSG + 0.5, 1, 2 wt% HWCS, and 0.25 wt% BSG + 0.5, 1, 2 wt% WCS) under LAOS rheology conditions. By increasing the concentrations of WCS or HWCS at each BSG level, the degree of nonlinearity, exhibited a notable decrease. In contrast, the values of strain stiffening and shear thickening factors showed an increase.

References

- [1] J. Esquena, "Water-in-water (W/W) emulsions", *COCIS*, **25**, 109-119, 2016.
- [2] S. Naji-Tabasi and SMA Razavi, *Food Hydrocoll*, **73**, 313-325, 2017.
- [3] A. Heydari and S.M.A. Razavi, *Int. J. Biol. Macromol.*, **184**, 393-404, 2021.
- [4] M. Anvari and H.S. Joyner, *Food Hydrocoll*, **79**, 518-525, 2018.
- [5] Z. Zamani and S.M.A. Razavi, *LWT*, 174, 114453 2023.
- [6] S.M.A. Razavi, S.A. Mortazavi, L. Matia-Merino, S.H. Hosseini-Parvar, A. Motamedzadegan, and E. Khanipour, *Int. J. Food Sci. Technol.*, **44**, 1755-1762, 2009.
- [7] R.H. Ewoldt, A.E. Hosoi, and G.H. McKinley, *J. Rheol.*, **52**, 1427-1458, 2008.

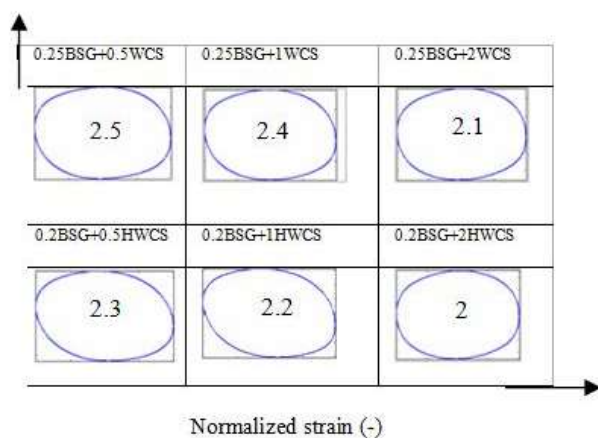


Fig. 1. Elastic Lissajous-Bowditch plots of the W/W emulsions made by BSG and WCS or HWCS at a fixed frequency of 1 Hz, 1000% strain amplitude and 25 °C.

Droplet Impact on Spherical Surfaces: Effect of Elasticity and Diameter Ratio on Behavior of Spreading and Receding

Mohammad Kazem Sheykhian*, Mohammad Hassan Kayhani, and Mahmood Norouzi
Faculty of Mechanical Engineering, Shahrood University of Technology, Shahrood, Iran

*ksheykhian@gmail.com

Abstract

In this study, experiments were conducted to investigate the spreading behavior of viscoelastic droplets on spherical surfaces. The key novelty of this research lies in analyzing how rheological properties, such as elasticity and diameter ratio, influence the impact of viscoelastic droplets on spherical surfaces. To achieve this goal, we compared the impact of viscoelastic droplets with that of equivalent Newtonian droplets, having identical viscosity and surface tension coefficients. Our findings revealed that Newtonian fluids exhibited a greater degree of spreading and retraction compared to viscoelastic fluids with equivalent viscosity, underscoring the impact of fluid elasticity.

Keywords: droplet impact, viscoelastic fluid, diameter ratio, elasticity

Introduction

In a study by Oishi *et al.* [1], droplet collisions on a solid surface were investigated using fluids with viscoelastic, and thixotropic properties. Their findings suggested that materials with lower yield stresses were minimally affected by surface tension. Another study by Xu *et al.* [2] focused on the collision of Newtonian and viscoelastic droplets on various surfaces. On hydrophilic surfaces, both elastic liquids and a Newtonian reference fluid displayed similar spreading behavior. However, on hydrophobic surfaces, the viscoelastic fluid formed branched filaments after slipping of the droplet. Singh and Dandapat [3] explored the spreading behavior of non-Newtonian fluid droplets, particularly shear-thickening and shear-thinning fluids, on uniformly uneven surfaces under conditions of complete wetting. It was observed that non-Newtonian droplets exhibited higher spreading velocities on uneven surfaces compared to smooth ones. In this research, we experimentally investigate the impact of viscoelastic droplets on spherical surfaces. We analyze the effects of rheological properties, including elasticity and diameter ratio, by comparing the impact of viscoelastic droplets with equivalent Newtonian droplets having matching viscosity and surface tension coefficients.

Materials, Equations, Experimental Setup

A high molecular weight polymer is dissolved to the Newtonian solvent to prepare the viscoelastic fluid (PAA1) adding 0.005 wt% of polyacrylamide (PAM, Mw=5×10⁶, Aldrich 181277). The Newtonian liquid was an 81.1 w/w% aqueous glycerin solution (referred to as N1).

Table I represents the required properties of the fluid used in these experiments. ρ , and λ indicate the density and relaxation time, respectively, while $\bar{\eta}$ is the equivalent

viscosity obtained from the steady shear test. Furthermore, elasticity number, dimensionless time, and diameter ratio are defined where U is impact velocity, D signifies diameter of the sphere, d is droplet diameter and x is the length of spreading. Equations are written as follows:

$$El = \frac{\bar{\eta}\lambda}{\rho d^2} \quad (1)$$

$$t^* = \frac{tU}{d} \quad (2)$$

$$D^* = \frac{D}{d} \quad (3)$$

Using a syringe, droplets were expelled from a needle and allowed to detach under the influence of gravity. The motion of the droplets was recorded using a high-speed camera operating at 8000 frames per second. Stainless steel spheres, measuring 10 and 20 mm in diameter, were utilized to investigate the effect of the ratio between sphere and droplet diameters. Fig. 1 illustrates a schematic representation of the experimental arrangement and the droplet impact process on a spherical surface.

Results and Discussion

Fig. 2. Presents the changes in the spreading factor of

Table I. Characteristics of the fluid used in the present tests.

Test liquid	Water (%)	Glycerol (%)	ρ (kg/m ³)	λ (s)	$\bar{\eta}$ (mPa.s)
PAA1	20	80	1208	0.9	84
N1	18.9	81.1	1220	-	84

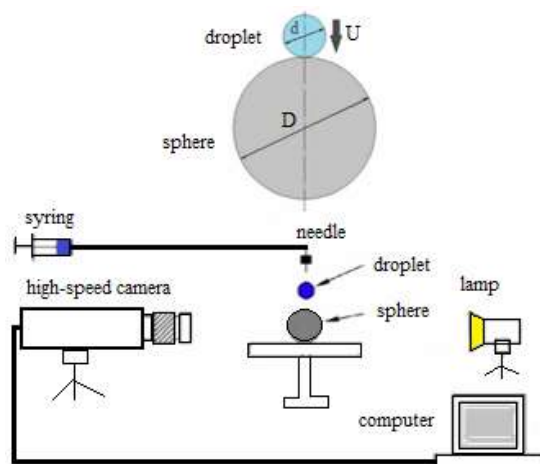


Fig. 1. Schematic plan of the experimental setup and droplet impact process.

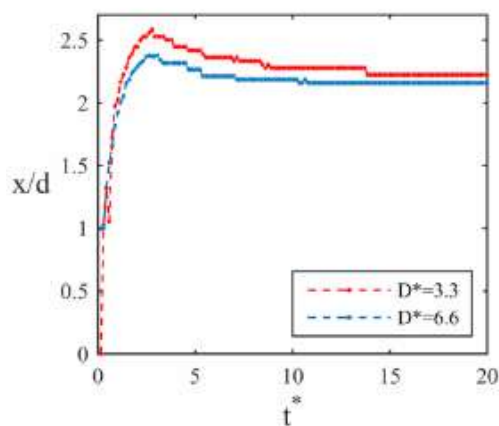


Fig. 2. Effect of Diameter ratio on spreading behavior for PAA1 droplet.

PAA50 droplets for both diameter ratios. The maximum spreading factor for a smaller ratio ($D^*=3.3$) is 2.55, while it is 2.38 for ($D^*=6.6$). With the increase in the diameter ratio of the sphere to the droplet when it reaches maximum Spreading length and the time of occurrence, it is more significant for the smaller diameter ratio. This is because of the surface curvature and the influence of the radius on the

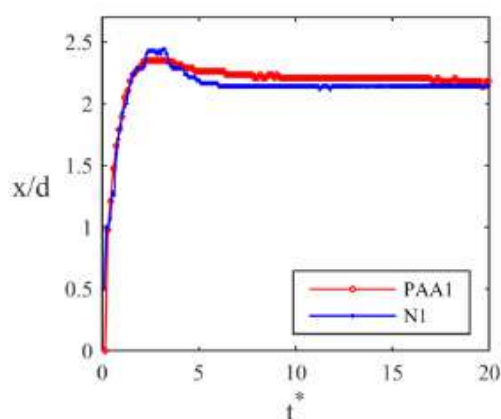


Fig. 3. Effect of elasticity on spreading behavior for PAA1 and NI droplet.

droplet spreading behavior. Fig. 3. Shows the evolution of two viscoelastic (PAA1) and Newtonian (NI) droplets for ($D^*=6.6$). The maximum spreading factor for Newtonian fluid was 2.45 while this value for viscoelastic fluid was 2.38. Also the time that maximum spreading occurred was earlier for polymeric fluid. The Newtonian fluid with the equivalent viscosity spread further. In addition, in the receding region, the non-Newtonian fluid gathered to a lesser extent than the Newtonian fluid. Therefore, the elasticity of the polymer fluid inhibits the spreading of the droplet beyond a certain point, possibly because of intermolecular forces or the entanglement of polymer chains. This behavior is distinct from Newtonian fluids, which lack such elasticity and allow for more extensive spreading.

Conclusion

- By decreasing the diameter ratio, the maximum spreading length and the time of occurrence increase. Also for smaller diameter ratio the droplet recedes more than larger one.
- The elasticity of the polymer fluid prevents the spreading and receding of droplets in comparison to Newtonian fluid with the same viscosity

References

- [1] J. Esquena, "Water-in-water (W/W) emulsions", *COCIS*, **25**, 109-119, 2016.
- [2] S. Naji-Tabasi and S.M.A. Razavi, *Food Hydrocoll*, **73**, 313-325, 2017.
- [3] A. Heydari and S.M.A. Razavi, *Int. J. Biol. Macromol.*, **184**, 393-404, 2021.
- [4] M. Anvari and H.S. Joyner, *Food Hydrocoll*, **79**, 518-525, 2018.
- [5] Z. Zamani and S.M.A. Razavi, *LWT*, **174**, 114453, 2023.
- [6] S.M.A. Razavi, S.A. Mortazavi, L. Matia-Merino, S.H. Hosseini-Parvar, A. Motamedzadegan, and E. Khanipour, *Int. J. Food Sci. Technol.*, **44**, 1755-1762, 2009.
- [7] R.H. Ewoldt, A.E. Hosoi, and G.H. McKinley, *J. Rheol.*, **52**, 1427-1458, 2008.

Investigation Rheological Properties and Phase Morphology of Poly(butylene succinate)/Poly(butylene adipate-co-terephthalate) Film

Ali Abbasi* and Mehdi Rafizadeh

Department of Polymer Engineering and Color Technology, Amirkabir University of Technology, Tehran, Iran

*aliiabassi@aut.ac.ir

Abstract

Biodegradable blends based on poly(butylene succinate) (PBS) and poly(butylene Adipate-co-Terephthalate) (PBAT) with different compositions, were prepared by melt blending and their rheological behaviors in linear viscoelastic region were studied. Except for the sample with 45 wt% PBS, the rest of the samples showed a distinct Newtonian behavior at low frequencies. Complex viscosity of blends was higher than pure polymers at low frequencies due to the interaction between two components during mixing. The Cross model was used in order to fit the experimental data and express the rheological behavior of the samples. Except for the sample containing 45 wt% PBS, all other data fitted well. The Han and Cole-Cole plots showed that the rheological behavior of the samples depends on the composition of the components and their interaction during melt blending.

Keywords: biodegradability, blending, rheology tests, complex viscosity, cross model

Introduction

In recent years, issues such as global warming and environmental pollution have caused the demand for biodegradable plastics to increase as an alternative to conventional oil-based plastics [1]. Polyesters are among the most important biodegradable polymers [2-7]. PBS is an aliphatic biodegradable polyester with suitable mechanical properties. Poly(butylene adipate-co-terephthalate) (PBAT) is an aliphatic-aromatic co-polyester. In this research, the mixture of PBS and PBAT was prepared by melt blending of them with different compositions and their rheological properties were investigated to evaluate the use of biodegradable film in the packaging application.

Experimental

Materials

Poly(butylene succinate) (PBS, MFI=4-6 g/10min) and poly(butylene adipate terephthalate) (PBAT, MFI=3.7 g/10min) used in this work were commercially grades produced by Tunhe Co. Ltd. And Kingfa Co. Ltd. (both companies were from China) under the trade name TH803S and Ecopond A400.

Preparation of Samples

Internal mixer MX21063 (IPPI, Iran) was used to prepare polymeric mixtures. The samples were mixed for 6 min at 50 rpm and 120 °C. The samples were compression molded using a Polystat 400 s machine (Servitec, Germany) at 150 °C to obtain films with 1mm thickness. To perform rheological tests, the films were cut and disks with a diameter of 25 mm were prepared from them.

Characterization Methods

The rheological analysis of the samples in the molten state

was performed using a MCR501 rotational rheometer (Anton paar, Austria) equipped with parallel plates geometry (d=25 mm, gap=1 mm). Small amplitude oscillatory shear measurements, within the linear viscoelasticity regime ($\epsilon=1\%$) were carried out in the frequency range between 0.01 and 600 rad/s and the temperature of 160 °C and the shear complex viscosity (η^*), the storage modulus (G') and the loss modulus (G'') were measured. Before performing the test, the samples were dried for 24 h in an oven with a temperature of 70 °C. The experimental results were fitted by the Cross-model:

$$\eta = \eta_{\infty} + \frac{\eta_0 - \eta_{\infty}}{1 + (\lambda \dot{\gamma})^m} \quad (1)$$

where $\dot{\gamma}$ is shear rate, η_0 viscosity at zero shear rate and η_{∞} infinity shear viscosity. λ and m are also time constants and rate constants of the Cross-model [8].

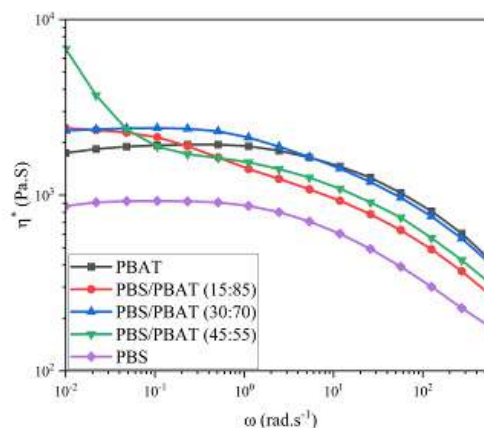


Fig. 1. Complex shear viscosity of the samples as a function of frequency.

Table I. Cross model parameters.

Pair	η_0 (Pa.s)	η_∞ (Pa.s)	λ (s ⁻¹)	m	R^2
Pure PBAT	1894.17	285.76	0.02	0.83	0.98
PBS/PBAT (15:85)	2901.48	27.56	0.83	0.36	0.99
PBS/PBAT (30:70)	2445.66	263.87	0.06	0.64	0.99
PBS/PBAT (45:55)	1.45E9	911.14	2.20E9	0.75	0.95
Pure PBS	922.92	139.98	0.04	0.80	0.99

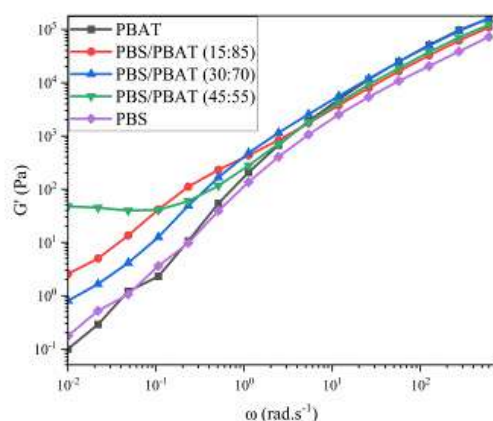


Fig. 2. Storage modulus of the samples as a function of frequency.

Results and Discussion

Fig. 1 shows the complex viscosity of the samples as a function of frequency. Except for the PBS/PBAT (45:55) sample, due to the phase separation, the rest of them showed Newtonian behavior at low frequencies [9]. Fig. 2 shows the storage modulus of samples as a function of frequency. It can be seen that the phase separation in the PBS/PBAT (45:55) has caused G' to not show terminal behavior at low frequencies and to show a plateau instead as a consequence of developing elastic responses independent from the frequency in the blend. This is while for other samples the terminal region is observed where G' tends to zero at low frequency and With the increase in frequency, all the samples showed shear-thinning behavior. The parameters

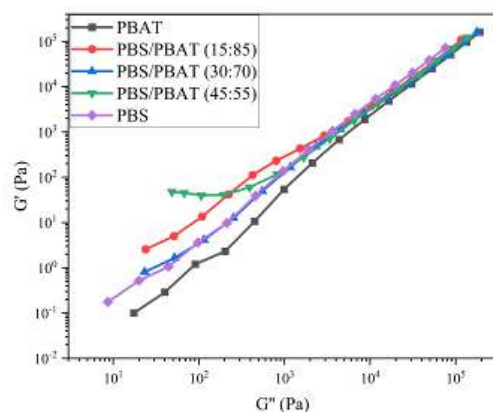


Fig. 3. Han plot of the samples.

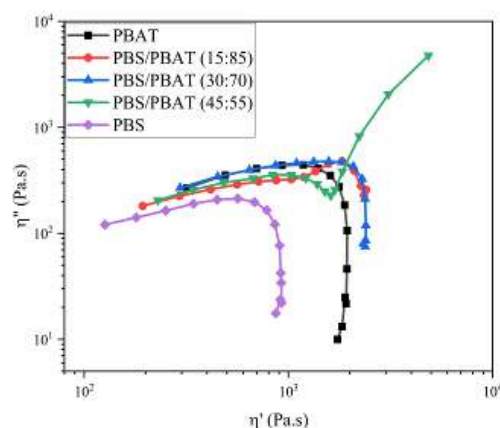


Fig. 4. Cole-Cole plot of the samples.

obtained from fitting the Cross-model to the experimental data are shown in Table I. As can be seen, the Cross-model fits the experimental results well, except for the PBS/PBAT (45:55). Fig. 3 shows the Han plot and Fig. 4 shows the Cole-Cole plot of the samples. Except for the PBS/PBAT (45:55) sample, which was nonlinear at lower frequencies, the plot of other samples was a line, but the slopes weren't the same in different compositions, which indicates a partial interaction between the phases [10]. As it is clear in the Cole-Cole plot of the samples, the diagram of the PBS/PBAT (30:70) mixture is a single arc curve that is caused by the partial interaction between the two phases during the blending [11].

Conclusion

The mixture of two biodegradable polymers, PBS and PBAT, was prepared by melt blending in an internal mixer. The evaluation of the rheological properties obtained from the parallel plate rheometer showed that all of the samples, except PBS/PBAT (45:55), had Newtonian behavior at low frequencies, and with increasing frequency, shear thinning behavior occurs in all of them. The Cross model was used to express the rheological behavior of the samples and it was observed that this model fits the samples well except for the PBS/PBAT (45:55). Han and Cole-Cole plots showed that phase separation or suitable interaction between phases can change rheological behavior of the samples.

References

- [1] R. Chandra, *Biodegrad. Polym.*, **23**, 1998.
- [2] E. Jalali Dil, *Polymer (Guildf)*, **68**, 202-212 2015.
- [3] C. de Matos, *Polymers (Basel)*, **12**, 2317, 2020.
- [4] T. Qiu, *Mech. Adv. Mater: Mod. Process.*, **2**, 2016.
- [5] R. Al-Itry, *Rheol. Acta*, **53**, 501-517, 2014.
- [6] K. Wang, *Polymers (Basel)*, **13**, 1-21, 2021.
- [7] D. Park, *Polymers (Basel)*, **15**, 2023.
- [8] T. Mezger, *The Rheology Handbook*, 135-212, 2019
- [9] A. Silberberg, *Basic Rheological Concepts*, **89**, 1977.
- [10] C. Han, *J. Appl. Polym. Sci.*, **30**, 4431-4454 1985.
- [11] I. Vinckier, *Rheol. Acta*, **38**, 274-286, 1999.

Rheological Properties, Retrogradation Behaviour and Syneresis of Native Wheat Starch-Cress Seed Gum Gel Affected by Preparation Technique

Shokufeh Taziki Shams-Abadi and Seyed Mahammad Ali Razavi*

Hydrocolloids Research Center, Department of Food Science and Technology,
Ferdowsi University of Mashhad (FUM), Mashhad, Iran

*s.razavi@um.ac.ir

Abstract

In this paper, the impact of different substitution levels of cress seed gum (CSG, 0, 5, and 10%) on the rheological properties, hardness, and syneresis, of native wheat starch (NWS, 4%) gel was investigated. Regarding these mixtures two preparation techniques were used: a mixture of the powders before addition of water (a), or separate preparation of CSG solution and subsequent mixing with starch powder (b). According to the rheological test, all the samples exhibited shear-thinning flow behavior. Increasing the CSG substitution level up to 10%, especially for preparation technique (b), elevated the consistency coefficient and yield stress. After storage, syneresis of NWS-CSG gels decreased more by technique (b); Preparation of mixtures by technique (b), greatly decreased the rate of retrogradation (hardness values) of gels during storage at 4 °C for 5 days; The results indicated that technique (b) was more effective in modifying the properties of NWS-CSG gels.

Keywords: functional properties, hydrocolloid, native wheat starch, preparation technique

Introduction

Starch is one of the most important polysaccharides which is effective in creating favorable properties in processed products. Among the commercial starches, native wheat starch (NWS) is very important due to its low price and easy availability but NWS is more sensitive to food processing conditions than other starches. Retrogradation is an undesirable phenomenon in some starch-based foods that causes syneresis, reduces the acceptability of food, and shortens the shelf life during storage and distribution [1]. Many studies have shown that carbohydrates imply an important role in improving syneresis, the rheological properties and textural attributes of starches, and retarding the retrogradation of starch gels [2,3]. Cress seed gum (CSG), as an emerging galactomannan, has shown the ability to improve the textural and rheological features of food systems based on its unique properties [4]. Also, CSG exhibited good potential to reduce the hardness of starch gels after storage for one day at room temperature [5]. Preparation techniques of the starch-hydrocolloid mixture are one of the important factors which influence the rheological properties and the behaviour of starch [6]. Therefore, the objectives of this study were to determine the impact of different substitution levels of CSG (0, 5, and 10%) on the rheological properties, retrogradation (hardness), and synthesis of native wheat starch (NWS) gel (4 w/w%) prepared by two techniques (powder-powder or powder-solution).

Experimental/Theoretical

NWS was supplied from Sigma Aldrich (Spain) and CSG was extracted from cress seeds. To produce starch gels, starch-gum mixtures (4 w/w% suspensions of NWS with

substitution of 0, 5, and 10 w/w% CSG) were prepared using two techniques: powders mixing, adding water and hydrated (technique (a), NWS+CSG-P), or adding starch powder to hydrated CSG solutions (technique (b), NWS+CSG-S) and heating samples thereafter at 95 °C and then cooled to 50 °C. After cooling at 25 °C for 1 h, the rheological properties of the gel samples were performed using a Bohlin viscometer in the range of 14 s⁻¹ to 600 s⁻¹ shear rate. The viscosity-shear rate data were fitted by the Herschel-Bulkley model. The syneresis of gels was assessed after storage at 4 °C for 1 day. The textural properties of the starch gels were determined by the back-extrusion test and using a Brookfield Texture Analyzer. The test was performed at 1 mm/s rate to 50% deformation. The Hardness parameter of gels was determined after storage at 4 °C for 0, 1, and 5 days.

Results and Discussion

1. Rheological measurement: According to the Herschel-Bulkley model, all the samples confirmed non-Newtonian shear-thinning behavior, $n_H < 1$, (Table I). No significant

Table I. Rheological parameters of native wheat starch-cress seed gum gel prepared by two techniques.

Sample	Herschel-Bulkley model parameters				
	n_H (-)	K_H (Pa.s ^{n_H})	τ_{0H} (Pa)	R ²	RMSE
1	0.66±0.01	0.69±0.01 ^c	0.27±0.07 ^c	0.99	0.00
2	0.62±0.08	0.85±0.25 ^{bc}	2.09±0.20 ^b	0.99	0.00
3	0.55±0.03	1.58±0.11 ^{ab}	3.58±0.51 ^a	0.98	0.02
4	0.62±0.01	0.97±0.08 ^{bc}	3.95±0.01 ^a	0.99	0.00
5	0.54±0.01	2.14±0.59 ^a	4.19±0.32 ^a	0.99	0.00

1: NWS4%, 2: NWS+5%CSG-P, 3: NWS+10%CSG-P, 4: NWS+5%CSG-S, 5: NWS+10%CSG-P.

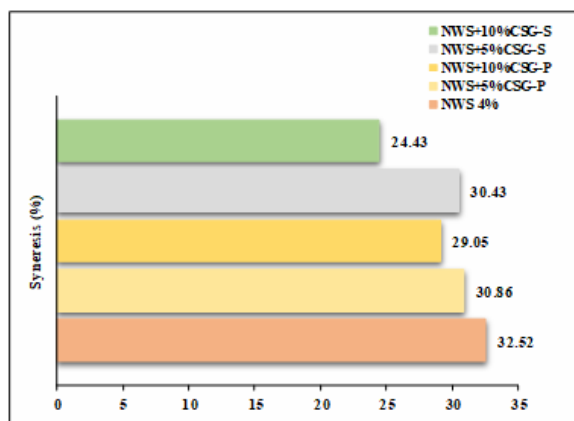


Fig. 1. Syneresis of native wheat starch-crees seed gum gel prepared by two techniques.

differences were seen between preparation techniques for the pseudoplastic behavior of the NWS gels. The consistency coefficient (k_H) and yield stress (τ_{0H}) parameters were mainly influenced by the preparation technique. Using technique (b) for preparation was more effective in increasing the k_H values rather than technique (a). It obviously increased k_H from 0.69 Pa.sⁿ to 2.14 Pa.sⁿ with increasing the substitution level of CSG from 0% to 10%. Probably, gum molecules interact with leached amylose molecules, produce a viscosity increase via synergism [6]. All samples had τ_{0H} that indicates the solid-like behavior of the fluid. With replacement of CSG, τ_{0H} of the NWS gel increased significantly. It was observed more for the preparation technique (b). In other words, the NWS+CSG-S gels had a more solid behavior than the others. In similarity, Mandala and Bayas (2004)'s results demonstrated increasing the viscosity, consistency and pseudoplasticity of the separate preparation of wheat starch and xanthan solutions and subsequent mixing technique [6].

2. Syneresis: The syneresis was measured to investigate the retrogradation of NWS gel during storage at 4 °C. In the mixed gels (technique (b)), more reduction of the syneresis was observed rather than others, which was clearly at high CSG replacement. In this regard, the syneresis decreased from 32.52% to 30.43 and 24.43% by replacing

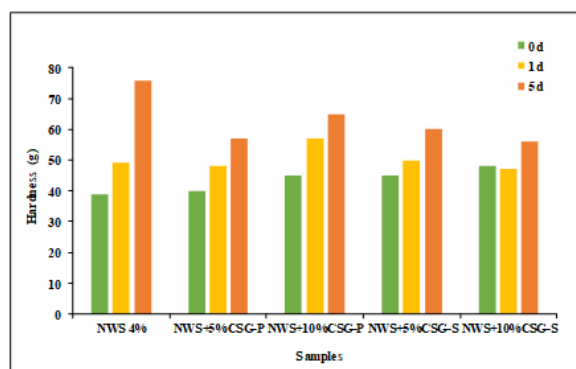


Fig. 2. Hardness parameter (g) of native wheat starch-crees seed gum gel prepared by two techniques during storage time.

NWS with 5 and 10% CSG, respectively. Hydrocolloids have high water holding capacity and probably separate hydration of CSG caused more reduction of the amount of water available for the re-crystallization of amylose and amylopectin molecules and retards the retrogradation of starch gels [7].

3. Textural properties: The evaluation of the hardness of starch gel during storage time (at 4 °C for 5 days) has shown a high correlation with the retrogradation phenomenon. As shown in Fig. 2, after storage for 5 days at 4 °C, especially in preparation technique (b), the CSG substitution with NWS reduced the rate of retrogradation. It can be stated that gum molecules inhibit leaching amylose molecules effectively and prevent retrogradation. On the other hand, it is more probable that due to the excluded volume effect of starch granules, the local concentration of CSG in continuous phase increase and phase separation of CSG–amylose polymers are promoted by preparing samples with technique (a) [6].

Conclusion

The behavior of NWS gel in the presence of CSG was affected by the mixture preparation technique. Mixtures prepared with technique (b) influenced viscosity, syneresis, and retrogradation more positively. In this regard, the viscosity and yield stress of NWS-CSG gels were increased more and its syneresis and the rate of retrogradation were decreased more.

References

- [1] K. Shevkani, N. Singh, R. Bajaj, and A. Kaur, "Wheat starch production, structure, functionality and applications a review", *Int. J. Food Sci. Technol.*, **52**, 38-58, 2017.
- [2] A.R. Yousefi, Y. Zahedi, S.M.A. Razavi, and N. Ghasemian, "Influence of sage seed gum on some physicochemical and rheological properties of wheat starch", *Starch – Stärke*, **69**, 1600356, 2017.
- [3] Y. Zhou, D. Wang, L. Zhang, X. Du, and X. Zhou, "Effect of polysaccharides on gelatinization and retrogradation of wheat starch", *Food Hydrocoll*, **22**, 505-512, 2008.
- [4] H. Karazhiyan, S.M.A. Razavi, G.O. Phillips, Y. Fang, S. Al-Assaf, and K. Nishinari, "Physicochemical aspects of hydrocolloid extract from the seeds of *Lepidium sativum*", *Int. J. Food Sci. Technol.*, **46**, 1066-1072, 2011.
- [5] S.A. Shahzad, S. Hussain, M.S. Alamri, A.A. Mohamed, A.S. Ahmed, M.A. Ibraheem, and A.A. Abdo Qasem, "Use of hydrocolloid gums to modify the pasting, thermal, rheological, and textural properties of sweet potato starch", *Int. J. Polym. Sci.*, 6308591, 2019.
- [6] I.G. Mandala and E. Bayas, "Xanthan effect on swelling, solubility and viscosity of wheat starch dispersions", *Food Hydrocoll*, **18**, 191-201, 2004.
- [7] T. Funami, Y. Kataoka, T. Omoto, Y. Goto, I. Asai, and K. Nishinari, "Effects of non-ionic polysaccharides on the gelatinization and retrogradation behavior of wheat starch", *Food Hydrocoll*, **19**, 1-13, 2005

Study of Electrical Properties and Rheological Behavior of the Nanocomposites Based on PVDF and Hybrid of Silver Nanoparticles/Graphene

Parian Garshasbi and Fatemeh Goharpey*

Polymer and Color Engineering Department of Amirkabir University of Technology, Tehran, Iran

*goharpey@aut.ac.ir

Abstract

Amidst global energy challenges and technological advancements, there is a growing interest in the electrical conductivity properties of composites. Recent advancements include hybrid nanocomposites that utilize two distinct nanoparticles, specifically carbon and metal nanoparticles. These particles, commonly used in electrically conductive nanocomposites, demonstrate complementary effects. This study specifically investigates the conductivity and dielectric behavior of PVDF-based nanocomposites incorporating graphene and silver nanowires (AgNW). Dispersion and network formation play crucial roles in electrical properties. A comparative analysis of the rheological behavior between hybrid and non-hybrid systems unequivocally illustrates how secondary particles aid dispersion and substantiates the formation of a 3D network, corroborated by conductivity measurements. G1A1, with a 1% volume content of each particle, exhibits electrical conductivity (5.22×10^{-4} S/cm), the highest dielectric constant (4148) with a low loss value (63 at a frequency of 1000), attributed to an optimal nanoparticle connection against non-hybrid counterpart. The results of frequency sweep highlight improved dispersion, evidenced by a more pronounced reduction in the frequency dependence of storage moduli at low frequencies, indicating that hybrids exhibit greater spatial constraints and fewer degrees of freedom. Additionally, strain sweep findings indicate a broader dispersion in the Graphene/AgNWs combination, establishing a correlation with electrical conductivity properties.

Keywords: conductive nanocomposites, hybrid systems, dielectric, conductivity, rheology.

Introduction

Integrating nanometer-sized conducting particles, such as metal and graphite powders, enhances polymer electrical properties, resulting in functional conductive nanocomposites. Previous research [1] notes that solely silver or graphene-based nano-composites exhibit conductivity at high volume fractions due to oxygen sensitivity and high resistance between connected AgNWs, and graphene nanosheets' stacking tendency. This study investigates network formation using rheological insights with analyzing their arrangement, electric and dielectric behavior.

Experimental

The AgNWs were synthesized with a 300 aspect ratio using the polyol method. Subsequently, nanocomposites were fabricated through solution mixing (Table I).

Results and Discussion

distinct conductivity characteristics indicates that low silver content in G1A0.2 and G1A0.5 and heightened wire-to-layer ratio in G1A1.5, exhibited increased resistance, and led to stacking of gra-phene layers, consequently, low conductivity. Con-versely, in G1A1 nanoparticle synergies improved conductivity due to a well-dispersed 3D structure. Besides, an increased dielectric constant with the addition of the second nanoparticle. In the hybrid sample (G1A1) with 2 vol% of nanoparticles, a significantly lower dielectric loss was observed compared to the non-hybrid sample (G2A0), despite the non-monotonic increase in

dielectric loss with the volume ratio of AgNW/ graphene. In Fig. 1, by strain-sweep we explore the network breakage [1] in nanocomposites. Hybrids exhibit a continuous modulus decrease with increasing strain, signaling a progressive breakdown. Conversely, non-hybrids display a two-step yielding behavior beyond a 0.75 vol% concentration, linked to large graphene ag-glomerates

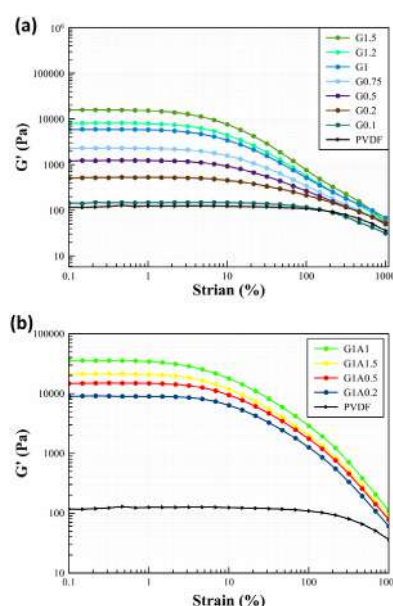


Fig. 1. Strain-sweep for: (a) graphene-based nanocomposites at various vol% and (b) hybrid nanocomposites at various compositions.

Table I. Prepared samples name and volume percent composition and their DC conductivity.

Sample name	Graphene vol%	AgNW Vol%	DC Conductivity
G0.5-G2	0.5-2	0	-
G1A0.2	1	0.2	1.77×10^{-5}
G1A0.5	1	0.5	2.04×10^{-5}
G1A1	1	1	5.22×10^{-4}
G1A1.5	1	1.5	3.58×10^{-5}

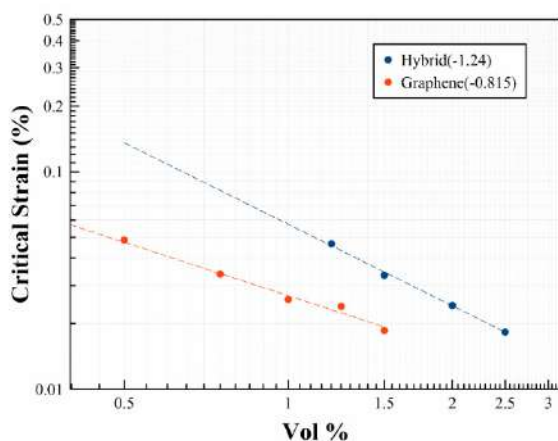


Fig. 2. Critical strain values against the composition of volume percentage in hybrid and graphene-containing nanocomposites.

which involves initial yielding from weak connections between agglomerates and subsequent yielding from the rupture of elastic connections within the agglomerates. The absence of critical strain behavior in hybrid samples (Fig. 2) indicates improved dispersion, with a more pronounced decline in critical strain compared to non-hybrids, emphasizing the heightened sensitivity of the hybrid network to strain due to superior particle dispersion and a more extensive network. A frequency sweep at low strains provides insights into the linear viscoelastic region and the particle network structure, as depicted in Fig. 3, where the system's rheological response is influenced by polymer chain dynamics at high frequencies, shifting to the influence of the nanoparticle network at low frequencies when polymer chains can relax which serves as an indicator of the system's elasticity. The rheological percolation threshold for non-hybrids (0.175 vol%) is identified, with critical exponent values of 1.67 approximating 1.88, means robust particle interactions, while lower values imply a substantial role of polymer chains in forming the load-bearing network [2]. Most polymers exhibit adherence to the Rouse model in low-frequency behavior, characterized by a storage modulus slope of 2 for unbranched homopolymers. However, the formation of particle networks deviates from Rouse behavior, resulting in time-independent features. Consequently, the frequency dependence of the storage and loss moduli reduces against frequency at low frequencies which is more pronounced in networks with greater spatial constraints and fewer degrees of freedom, indicating increased independence from frequency at low frequencies [3] that can be seen in Fig. 3c, supporting their superior ability to form 3D networks compared to non-hybrid

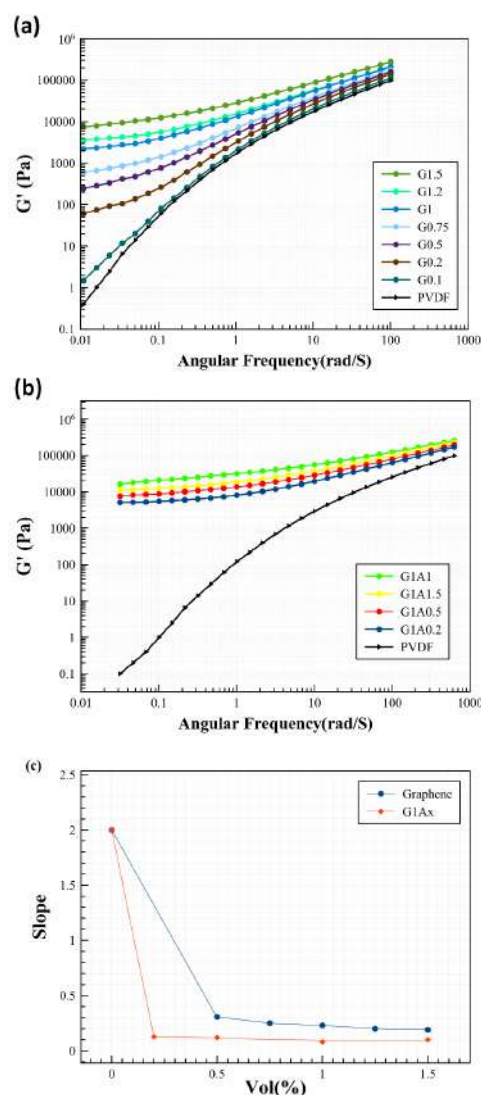


Fig. 3. Frequency-sweep for: (a) graphene-based nanocomposites and (b) hybrid nanocomposites at different compositions, (c) the slope of the log-log curve of the storage modulus against angular frequency at low frequencies for graphene-based nanocomposites.

nanocomposites. Consequently, this can be indicated that the rheological results aligned with electrical findings.

Conclusion

The hybridization of a 1:1 ratio of AgNWs and graphene in PVDF demonstrated optimal electrical conductivity and dielectric properties. This finding was corroborated by rheological investigations, employing frequency and strain sweep tests, which indicated well-dispersed and broadened network formation in hybrid systems.

References

- [1] L. He and S.C. Tjong, *Nanoscale Res. Lett.*, **9**, 1-8, 2014.
- [2] J. Goswami and V.A. Davis, *Macromolecules*, **48**, 8641-8650, 2015.
- [3] M. Sabzi, L. Jiang, F. Liu, I. Ghasemi, and M. Atai, *J. Mater. Chem. A*, **1**, 8253-8261, 2013.

Encapsulation of Blackberry Extract by Basil Seed Gum-Whey Protein Concentrate Nanoemulsion: Rheological Properties and Encapsulation Efficiency

Samin Sadeghi, Seyed Mohammad Ali Razavi*, and Shokufeh Taziki Shams-Abadi
Ferdowsi University of Mashhad, Mashhad, Iran

*s.razavi@um.ac.ir

Abstract

In this study, the effect of different mixing ratios of basil seed gum and whey protein concentrate (BSG:WPC, 25:75, 50:50, and 75:25) on physical (zeta potential and particle size) and rheological properties and encapsulation efficiency (EE) of blackberry extract O/W nanoemulsions were determined. The results showed that by increasing the BSG:WPC ratio from 25 to 75, zeta potential and particle size decreased (from -27.72 mV to -22.22 mV) and increased (from 913.52 nm to 1135.82 nm), respectively. A high ratio of BSG:WPC in nanoemulsion enhanced the consistency coefficient of nanoemulsions but reduced the EE. The EE percentage for the 25:75 BSG:WPC mixture was 90.97% and for the 75:25 BSG:WPC mixture was 81.80%. The observations indicated that the ratio of 25:75 BSG:WPC had the best potential for nano-encapsulation of blackberry extract.

Keywords: basil seed gum, blackberry, encapsulation, whey protein concentrate

Introduction

Blackberry (*Rubus sp.*) fruit contains high levels of anthocyanins (especially cyanidin-3-glycoside and cyanidin-3-rutinoside) and other phenolic compounds, which contribute to its high antioxidant capacity and other biological activities [1]. Processing can destroy and reduce the quality of natural antioxidants in fruits and vegetables. Nanoencapsulation is a more suitable procedure to enhancing bioactive compounds solubility, stability, and bioavailability [2]. In food industries, emulsion-based systems must be stabilized by some emulsifiers. Basil seed gum (BSG) is an anionic hydrocolloid and has unique properties. BSG contains substantial thickening, stabilizing and surface-active properties. Its high stability is related to the formation of a solid-like structure and the viscoelastic layer around the oil droplets, which prevents accumulation and coagulation [3]. Proteins facilitate the formation of emulsion due to the reduction of surface tension. It also stabilizes oil droplets against coalescence and coagulation by electrostatic repulsion mechanisms [4]. Whey protein has excellent emulsifying properties that can be used alone or in combination with polysaccharides within the external aqueous phase of oil-in-water (O/W) emulsions [5]. Therefore, this study aimed to investigate the potential of nanoencapsulation of blackberry extract by biopolymers mixture of basil seed gum and whey protein concentrate. In this regard, the influence of biopolymer mixing ratios (25:75, 50:50, and 75:25) on physical (Zeta potential and particle size) and rheological properties and encapsulation efficiency of O/W nanoemulsions were determined.

Experimental/Theoretical

WPC 80 (Protein content in dry matter: $\geq 80\%$) was supplied

from Sachsenmilch Leppersdorf GmbH (Germany) and BSG was extracted from basil seeds. BSG and WPC stock dispersions at 0.5 and 8 w/v% concentrations were prepared, respectively. The binary mixtures of BSG:WPC with desired mixing ratios (25:75, 50:50 and 75:25) were used. For preparing nanoemulsion samples, the 79:1 ratio of the prepared mixtures and blackberry extract were mixed. The pH of the mixtures was adjusted to 5 and then stirred for 30 min at 40 °C, simultaneously the proper amount of sunflower oil was added. At the end, they homogenized at 12000 rpm for 5 min. The mean particle size of nanoemulsions was assessed using a Vasco-3 particle size analyzer and their Zeta potentials were determined using a Zeta Compact zetameter at 25 °C. The rheological properties of the nanoemulsions were performed using a Bohlin viscometer in the range of 14 s⁻¹ to 300 s⁻¹ shear rate. The viscosity-shear rate data were fitted by the Power-law model. Encapsulation efficiency (EE) was determined as described by Robert *et al.* [6].

Results and Discussion

Zeta Potential and Particle Size: The effect of different ratios of BSG and WPC on zeta potential and particle size of BSG-WPC nanoemulsions are shown in Fig. 1. Zeta potential is an important parameter characterizing stability

Table I. Rheological parameters of basil seed gum-whey protein concentrate nanoemulsions.

BSG:WPC ratio	Power-Law model Parameters			
	EE (-)	K_P (Pa.s ⁿ)	R ²	RMSE
25:75	0.79±0.11	0.06±0.01 ^b	0.935	0.001
50:50	0.63±0.06	0.19±0.02 ^b	0.987	0.002
75:25	0.57±0.01	0.64±0.07 ^a	0.990	0.002

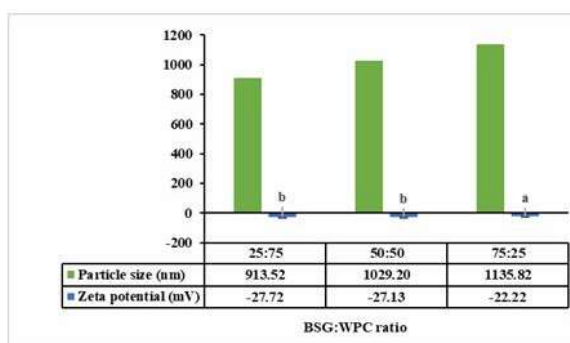


Fig. 1. Particle size and zeta potential of bail seed gum-whey protein concentrate nanoemulsions.

of colloidal dispersion. The zeta potential of all samples was less than -30 mV, indicating a great condition for protecting the oil droplets against coalescence and creating stable nanoemulsions. With the decrease of BSG:WPC ratio in nanoemulsion the amount of zeta potential was driven toward a more negative charge. The nanoemulsion containing 25:75 BSG:WPC had the highest zeta potential and the best stability (Fig. 1). According to Fig. 1, the emulsion that contained 25% BSG had the smallest particle size (913.52 nm), while the bigger particle size (1135.82 nm) belonged to the emulsions containing 75% BSG. It is well-known that the insufficient amount of the protein and/or polysaccharide for covering oil droplets in a nanoemulsion after homogenization can result in macromolecular bridging and bigger particle size.

Rheological Measurement: Table I depicts the power-law model parameters of nanoemulsions. nP values of all BSG:WPC ratios were less than 1 which confirmed non-Newtonian shear-thinning behavior of nanoemulsions. There were no significant differences in the nP of the samples but it decreased when the BSG ratio increased. The consistency coefficient (kP) of nanoemulsions was enhanced significantly by increasing the BSG:WPC ratio. Regarding kP values of all blends, 75:25 BSG:WPC showed the highest (0.64 ± 0.07) and 25:75 BSG:WPC showed the lowest values (0.06 ± 0.01).

Encapsulation Efficiency: Encapsulation efficiency was

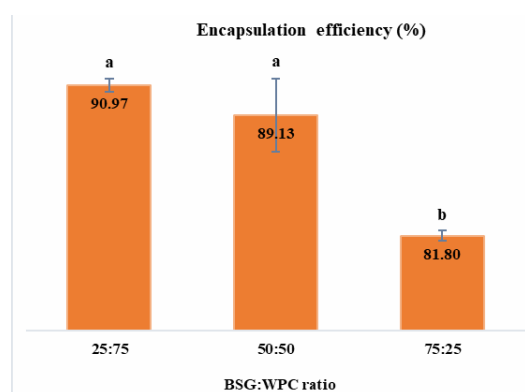


Fig. 2. Encapsulation efficiency of bail seed gum-whey protein concentrate nanoemulsions.

evaluated by measuring total phenolic content (Fig. 2). The EE of samples was significantly ($P < 0.05$) influenced by the BSG:WPC ratios. EE percentage of powders containing 25:75 BSG:WPC was the highest value (90.97%). Increasing the BSG:WPC ratio to 75:25 reduced the EE of samples from 90.97% to 81.80%. This may be due to denaturation and changes in the structure of proteins during emulsification and freeze-drying conditions, which decreased the ability to protect the core material. Similar results have been reported by Najafi *et al.* [6].

Conclusion

The present study showed that the O/W nanoemulsions prepared by using proper ratios of biopolymers mixture within the external aqueous phase were effective in nanoemulsion stability and the EE of blackberry extract. The results confirmed that capsules produced by the 25:75 BSG:WPC had the lowest particle size and the highest zeta potential which generally as an indication of the increased stability, results in more retention of bioactive compounds. Also, results revealed that encapsulation by 25:75 BSG:WPC had the lowest kp and the highest EE. Generally, we found that BSG:WPC mixtures at 25:75 ratios can be used as a well-suited mixture for encapsulating blackberry extract.

References

- [1] J.Y. Lee, S.O. Moon, Y.J. Kwon, S.J. Rhee, H.R. Park, and S.W. Choi, "Identification and quantification of anthocyanins and flavonoids in mulberry (*Morus sp.*) cultivars", *Food Sci. Biotechnol.*, **13**, 176-184, 2004.
- [2] A. Mohammadi, S.M. Jafari, E. Assadpour, and A. Faridi Esfanjani, "Nano-encapsulation of olive leaf phenolic compounds through WPC-pectin complexes and evaluating their release rate", *Int. J. Biological Macromol.*, **82**, 816-822, 2016.
- [3] S. Naji-Tabasi and S.M.A. Razavi, "New studies on basil (*Ocimum bacilicum L.*) seed gum: Part II—emulsifying and foaming characterization", *Carbohydr. Polym.*, **149**, 140-150, 2016.
- [4] N. Calero, J. Muñoz, P.W. Cox, A. Heuer, and A. Guerrero, "Influence of chitosan concentration on the stability, microstructure, and rheological properties of O/W emulsions formulated with high-oleic sunflower oil and potato protein", *Food Hydrocolloid.*, **30**, 152-162, 2013.
- [5] E. Bouyer, G. Mekhloufi, V. Rosilio, J.L. Grossiord, and F. Agnely, "Proteins, polysaccharides, and their complexes used as stabilizers for emulsions: Alternatives to synthetic surfactants in the pharmaceutical field", *Int. J. Pharm.*, **436**, 359-378, 2012.
- [6] M.N. Najafi, R. Kadkhodae, and S.A. Mortazavi, "Effect of drying process and wall material on the properties of encapsulated cardamom oil", *Food Biophys.*, **6**, 68-76, 2011.



Exploring the Impact of Chain Architecture on Morphology, Dynamics, and Viscoelastic Behavior of Ionomers

Nazanin Sadeghi¹ and Fardin Khabaz^{1,2*}

1. School of Polymer Science and Polymer Engineering, The University of Akron, Akron, OH, 78712, USA

2. Department of Chemical, Biomolecular, and Corrosion Engineering, The University of Akron, Akron, OH, 78712, USA

*fkhabaz@uakron.edu

Abstract

Ionomers are a class of polymers with a small fraction of ions in their backbone, which form ionic nanodomains and can function as physical crosslinks in polymer networks. The intensity of the physical crosslinks which in turn controls their morphology, dynamics, and rheological response, can be controlled by several factors such as electrostatic interaction strength, chain architecture, charge density, and relative size of the ions on the chains. In the context of ionomer design, the positioning of cations and anions in the form of bridged and pendant ionomers is a versatile design parameter influencing the viscoelastic properties of these polymer networks. Bridged ionomers feature both cation and anion types bound to the polymer backbone. In contrast, pendant ionomers resemble their organic cationic counterparts, with backbone-bound cations and free anions. In this study, we employed coarse-grained molecular dynamics (MD) simulations to explore the details of the morphology, dynamics, and rheology of bridged and pendant ionomers. Our results showed that the glass transition temperatures of both structures are comparable and slightly higher than the corresponding control system. The bridged ionomers exhibit a percolated ionic network, while pendant ionomers have distinct aggregates. Through analysis of the dynamics of the physical bonds and the intermediate scattering function, a direct relationship between ionic bond lifetime and structural relaxation time is established over a wide temperature range. Furthermore, the intermediate scattering function data obtained at different temperatures can collapse onto master curves, which confirms the applicability of the time-temperature superposition principle in these structures. Similarly, bridged ionomers show higher shear viscosity, and stress overshoot at steady shear simulations, suggesting its network of percolated clusters effectively transfers load when shear is applied. Overall, this study showed that incorporating ions in the backbone provides an alternative route to control the morphology, dynamics, and rheology of the ionomers.



Air-Water Interfacial Rheology of Per- and Polyfluoroalkyl Substances (PFAS)

Muchu Zhou and Reza Foudazi

School of Sustainable Chemical, Biological and Materials Engineering, The University of Oklahoma, Norman, OK 73019, USA

Abstract

Per- and polyfluoroalkyl substances (PFAS) constitute a group of partially and fully fluorinated synthetic organic compounds widely utilized in various industries, including aqueous film-forming foams (AFFFs) production, non-stick cookware, surfactants, cosmetics, and semiconductors. Their popularity arises from their exceptional chemical and thermal stability, as well as their ability to repel both water and oil. However, it is crucial to acknowledge the potential toxicity of PFAS to humans and their propensity to accumulate in organisms and the environment. Water sources have been contaminated by PFAS owing to their surfactancy and tendency of being transported through the air-water interfaces. While foam fractionation holds promise for removing surfactants and colloids from water, it currently faces challenges in PFAS removal. Understanding the interfacial rheological properties of PFAS is essential for enhancing removal efficiency through foam fractionation since correlations exist between interfacial rheology and foam properties. Nevertheless, limited research has explored the connections between the interfacial rheology of the PFAS-adsorbed interface and the properties of PFAS foams, such as foamability and stability. Therefore, this study focuses on investigating the dilatational interfacial rheological properties of various PFAS with and without additives. Additionally, PFAS adsorption behavior is assessed by measuring dynamic surface tension.



Bacteriophage Pf1 Complex Viscosity

M.A. Kanso¹, V. Calabrese², Amy Q. Shen², Myong Chol Pak³, and A.J. Giacomin^{4*}

1. Chemical Engineering Department, Massachusetts Institute of Technology, Cambridge 02139, USA

2. Okinawa Institute of Science and Technology, Tancha, Onna, Kunigami District, Okinawa 904-0495, JAPAN

3. Department of Physics, Kim Il Sung University, Taesong District, Pyongyang,
Democratic People's Republic of Korea, 999093

4. Mechanical Engineering Department, University of Nevada, Reno, Nevada 89557, USA

*giacomin@unr.edu

Abstract

Bacteriophages (phages) are viruses that attack bacteria, causing them to multiply. This attack requires phage orientation with respect to the bacterial receptor, a necessary condition for attachment. Since phages are not motile, they rely on their Brownian motion, and specifically its rotational components, to reorient. We focus specifically on Pf1 (the bacteriophage called pseudomonas phage Pf1), the phage about which much has been written, though whose rotational diffusivity determined from rheological measurements is not known. We compare general rigid bead-rod theory with intramacromolecular hydrodynamic interactions with our new measurements of the complex viscosity of an aqueous Pf1 suspension to arrive at the relaxation time. From this time, we get the central transport property for the Pf1 reorientation, the dimensionless rotational diffusivity, of $\lambda_0 Dr = 2.37 \times 10^{-6}$, which differs within one order of magnitude from the fluorescence microscopy. At low frequency, we find good agreement of our theoretical predictions with both parts of our new bacteriophage Pf1 complex viscosity measurements.

Evaluating the Processability and Rheological Behavior of Polypropylene Vitrimers

Saba Taheri and Hamid Garmabi*

Department of Polymer and Color Engineering, Amirkabir University of Technology, Tehran, Iran

*garmabi@aut.ac.ir

Abstract

Polypropylene (PP) vitrimers were prepared in two steps: First, glycidyl methacrylate (GMA) was melt grafted onto PP chains, and second, the crosslinked network was formed by reacting these active sites with dodecanedioic acid (DDDA) in the presence of zinc acetate as a catalyst. These chemically crosslinked networks are capable of undergoing transesterification exchange reactions with temperature, enabling rearrangement of network topology while maintaining a constant crosslink density. Rheological studies were conducted on samples containing various concentrations of grafting agents, and therefore, different crosslink densities, to evaluate their processability and flow behaviors. Rheological tests, including strain, time, and frequency sweeps, along with stress relaxation, show that increasing the functional groups on the polymer chains improves the melt strength and increase relaxation times in samples. Therefore, the flow and viscoelastic properties of vitrimer samples can be adjusted by the grafting agent concentration and temperature having a constant amount of catalyst.

Keywords: vitrimer, polypropylene, rheology, relaxation, transesterification

Introduction

Vitrimers, an innovative class of polymers combining attributes of both thermosetting and thermoplastic materials, offer a significant advancement in addressing the environmental issues associated with traditional polymers [1,2]. This research focuses on PP vitrimers due to polypropylene's ubiquitous presence and growing demand in global plastic production. Through the grafting of GMA onto PP chains and the utilization of DDDA as a crosslinker, vitrimers with varying crosslink densities are synthesized having dynamic covalent bonds that can rearrange through transesterification [3,4]. The study aims to evaluate the processability and rheological properties of these novel materials, and investigate the extent of network crosslinking effect on flow behavior of samples.

Experimental

PP with a melt flow rate of 25 g/10min (230° C/2.16 kg) was supplied by Marun Petrochemical Co. GMA monomers (97% purity) and DDDA were obtained from Sigma-Aldrich and Exir Co., respectively. The catalyst $[Zn(OAc)_2 \cdot 2H_2O]$ was purchased from Sigma-Aldrich Co. Melt grafting of GMA on PP with varying concentrations of 4, 6, and 8 phr was conducted in a Rheosense batch mixer at 185 °C. The vitrimers were formed by introducing DDDA with a 1:1 stoichiometric ratio to GMA and a constant amount of zinc acetate under the same processing conditions. Vitrimers containing 4, 6, and 8 phr of GMA were labeled as PP-V1, PP-V2, and PP-V3, respectively. The successful grafting and network formation were confirmed through various

characterization techniques, including FTIR, titration, and gel content measurement. To evaluate the rheological behavior, a rheometric mechanical spectroscopy (RMS) instrument (Paar Physica UDS 200) with parallel plate geometry—featuring a 25-millimeter diameter and a 1-millimeter gap—was utilized. Examination of the storage modulus, loss modulus, and complex viscosity against variables such as frequency under oscillatory conditions, along with stress relaxation tests at different temperatures and on various samples, provides valuable insights into the flow behavior and network strength.

Results and Discussion

Initially, the grafting degree and crosslinking extent in corresponding networks were measured and tabulated in Table I. The gel content, proportional to the degree of crosslinking and active sites for establishing covalent bonds, increased with higher GMA concentration in the system. Following determination of the linear viscoelastic region and evaluation of sample stability through strain and time sweeps, a frequency sweep test was conducted for all

Table I. Grafting degree and gel content for different samples.

Sample code	Grafting degree (phr)	Gel content
PP-V1	0.92	28.8
PP-V2	2.05	41.1
PP-V3	3.12	47.4

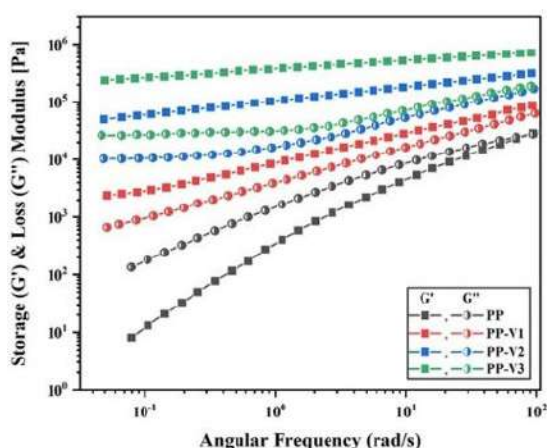


Fig. 1. Frequency sweep tests on different samples at 1% strain and a temperature of 190 °C.

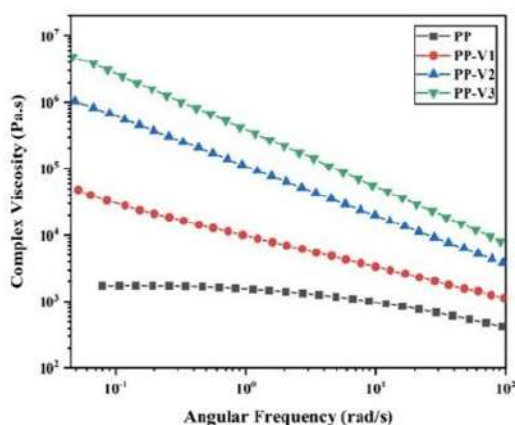


Fig. 2. The frequency dependence of complex viscosity of various samples at a strain of 1% and a temperature of 190 °C.

samples at 1% strain and a temperature of 190 °C, as depicted in Fig. 1. Neat PP demonstrated typical viscous polymer melt behavior, whereas vitrimer samples displayed notably higher storage modulus (G') exceeding their loss modulus (G'') across all measured frequencies,

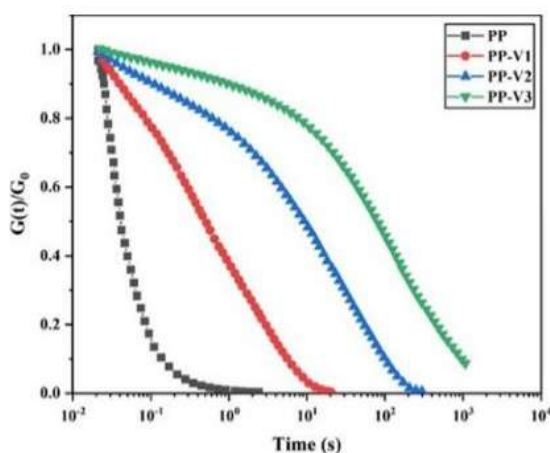


Fig. 3. Stress relaxation curve of various samples at a strain of 1% and a temperature of 190 °C.

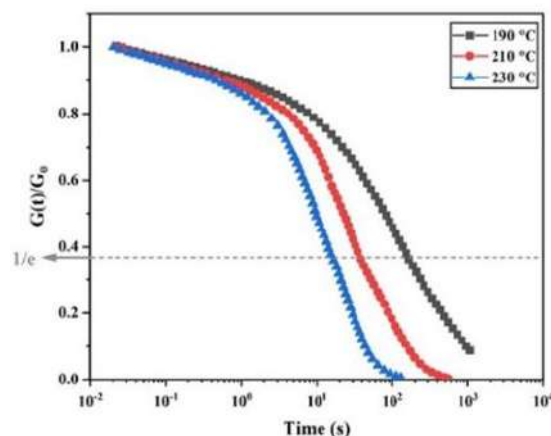


Fig. 4. Stress relaxation behavior for sample PP-V3 at a strain of 1% and temperatures of 190, 210, and 230 °C.

indicating solid-like properties. Higher crosslinking led to increased independence of G' from frequency and a more pronounced gap between G' and G'' . Moreover, Fig. 2 compares the complex viscosities of samples, with denser networks exhibiting remarkably higher values, suggesting enhanced melt strength beneficial for processing methods like foaming, blow molding, and extrusion. Stress relaxation curves in Fig. 3 reveal that despite having permanent crosslinks, vitrimers can relax applied stress via transesterification exchange reactions. However, higher crosslinking restricts chain rearrangement, resulting in longer relaxation times. Additionally, Fig. 4 demonstrates the temperature dependence of relaxation time in PP-V3. Elevated temperatures accelerate exchange reactions, causing shorter relaxation times.

Conclusion

The increased gel content with higher GMA concentrations, indicating higher crosslinking, directly correlated with enhanced complex viscosities and melt strengths, making vitrimers advantageous for diverse processing techniques. The stress relaxation tests highlighted the vitrimers' capability to alleviate stress through transesterification exchange reactions. However, the relaxation times varied depending on the crosslink density and temperature.

References

- [1] D. Montarnal, M. Capelot, F. Tournilhac, and L. Leibler, *Science*, **80**, 965-968, 2011.
- [2] N.J. Van Zee and R. Nicolay, *Prog. Polym. Sci.*, **104**, 101233, 2020.
- [3] M. Maaz, A. Riba-Bremerch, C. Guibert, N.J. Van Zee, and R. Nicolay, *Macromolecules*, **54**, 2213-2225, 2021.
- [4] G.P. Kar, M.O. Saed, and E.M. Terentjev, *J. Mater. Chem. A*, **8**, 24137-24147, 2020.

In the Name of God



The Proceedings of
3rd International Conference on Rheology

12-13 December, 2023, Tehran, Iran

www.icor-isr.ir



**The Proceedings of 3rd International Conference on Rheology
Tehran, 2023**

**Conference Office: Department of Polymer Engineering, Amirkabir University of
Technology, Tehran, Iran**

Tel: 0930 230 7582, Telfax: +9821 4478 7060

E-mail: info@icor-isr.ir, Website: icor-isr.ir

Editor: Salwa Farhangzadeh Technical Editor: Sarvenaz Alikhani

Typesetting and Layout: Ashraf Tatlari

Iranian Society of Rheology

**Office: Department of Polymer Engineering, Amirkabir University of Technology,
Tehran, Iran**

Tel: 0930 230 7582, Telfax: +9821 6454 2437

E-mail: info@ir-sor.com, Website: ir-sor.com



Welcome Message

Established in 2016, Iranian Society of Rheology (ISR) aims to expand the knowledge of rheology and enhance scientific collaboration between rheologists from industry and academia. As a member of the International Committee on Rheology (ICR), ISOR serves as a national focal point and center of excellence to achieve this goal in cooperation with higher education institutes and industry.

As ISR and ICOR president, it gives me great pleasure to address all rheologists, students, and interested in this field, 3rd International Conference on Rheology (ICOR 2023) organized by Iranian Society of Rheology on 12, 13 December 2023, Tehran, Iran. Our past experiences of organizing two international and three national conferences in Iran have demonstrated its capability of providing a highly knowledge-sharing opportunity and meeting point for scholars and industry experts in the region and throughout the world.

ICOR 2023 is open to all interested in rheology, from newcomers to established experts. We are looking forward to your valuable participation in ICOR 2023.

Fatemeh Goharpey

ISR and ICOR 2023 President



Dear All,

The 3rd International Conference on Rheology, organized by the Iranian Society of Rheology was held at the Iran Polymer and Petrochemical Institute in Tehran.

In this event, there were two plenary lectures starting in two successive days. The conference also brought together 22 international and 11 national keynote speakers. In our program we also included 20 oral presentations. In addition, there was a poster exhibition where 66 posters were presented. In the conference program three short courses were also presented two days before starting the conference.

All in all, the 3rd International Conference on Rheology in Tehran was extremely productive. The internationally known plenary speakers and keynote lecturers together with oral presenters successfully covered different topics of the conference. We extend our profound gratitude to the plenary speakers. We are also deeply grateful to the keynote lecturers and oral presenters. Finally, we are especially thankful to the panelists and all the conference participants for the willingness and courage to openly share their ideas and experiences.

Thank you all for fully participating and contributing to this conference which made it our collective success and achievement.



Hossein Nazockdast

Scientific Committee Chair



Ismail Ghasemi

Executive Committee Chair



Mahdi Salami Hosseini

Executive Committee Chair

Iranian Society of Rheology

**Office: Department of Polymer Engineering,
Iran Polymer and Petrochemical Institute, Tehran, Iran
Tel: 0930 230 7582, Telfax: +9821 6454 2437
E-mail: info@ir-sor.com, Website: ir-sor.com**